Master Thesis, Department of Geosciences

Case study of rainfall induced debris flows in Veikledalen, Norway, 10th of June 2011

Gudrun Holm

UNIVERSITY OF OSLO

FACULTY OF MATHEMATICS AND NATURAL SCIENCES

Case study of rainfall induced debris flows in Veikledalen, Norway, 10th of June 2011

Gudrun Holm

Master Thesis in Geosciences

Discipline: Environmental Geology and Geohazards

Department of Geosciences

Faculty of Mathematics and Natural Sciences

University of Oslo

June 2012

Advisers: Karen Mair (UiO) and Terje Harald Bargel (NVE)

This work is published digitally through DUO – Digitale Utgivelser ved UiO
http://www.duo.uio.no
It is also catalogued in BIBSYS (http://www.bibsys.no/english)

Cover photo: Karen Mair, 2012.

Preface

The initial plan for this thesis was to identify landslides in a study area in Veikledalen, and then to evaluate triggering mechanisms by observations, precipitation data, and sediment characteristics such as grain size analysis, firmness and thickness of sediments. Landslide type, erosion and deposition volume would be estimated by using Lidar data processed by NVE, and debris flow dynamics.

Due to adverse weather conditions during planned fieldwork in April 2012, it was too dangerous to walk in the landslide track due to snow cover, and observations of the landslides were also difficult to due to snow. A second field trip was undertaken on the 23rd of May, 2012 when the landslide tracks were safe to walk in. Due to time constraints only one landslide track was measured in detail and walked. All other landslide tracks were only measured along a road leading up to a house in the study area. Lidar data has also not been finished processed, and could therefore not be used in this thesis.

Observations have been combined with climatic data and background theory to suggest likely triggering mechanisms, landslide type, erosion volume, and deposition volume. Future work in the area can be carried out to support or refute the conclusions.

Acknowledgments

First of all I would like to thank my advisors Karen Mair from the University of Oslo, and Terje Harald Bargel from Norges vassdrags- og energidirektorat. Thank you to Terje and NVE for giving me the opportunity to work on this topic, for coming into the field with me and showing me some very interesting debris flows. Special thanks to Karen who has provided irreplaceable help and encouragement in writing this thesis, and for coming into the field with me even though you just had your tooth pulled and probably wanted to be somewhere else.

I would also like to thank my family who has supported me throughout years of studies, and to my grandfather who without knowing it made me interested in geohazards in the first place.

For me personally 10th of June 2011 was spent trying to drive from Oslo to Molde with my dad, and due to the flooding and the landslides having to drive an additional 400 kilometres by driving past Femunden. I remember that day very well and thinking that the landslides that occurred that day could be an interesting topic for a thesis, and I was right.

Gudrun Holm

Oslo, May 2012.

Abstract

On 10th of June 2011 a high amount of precipitation fell on southern Norway, the result of this precipitation in a combination with increased snowmelt cause a flood, the aspects of the flooding will not be discussed here because it has already been documented by others. The precipitation event triggered landslides in southern Norway, and caused several important roads to close.

Six landslides were identified in the study area of Veikledalen; several other landslides in the area were observed but are not part of this thesis. The landslides have been interpreted to have been triggered by precipitation, in the form of intense rainfall with or without antecedent rainfall. Rainfall thresholds were used to determine the triggering by precipitation. The landslides were determined to have started as debris slides which quickly transformed into debris flows.

Triggering zones of the six debris flows were identified and they are triggered on the western slope of the valley where the slope angle changes from a shallower angle to a steeper angle. Four debris flows were triggered at approximately the same elevation, while two debris flows were triggered at a lower elevation.

Erosion and deposition volumes have been estimated, and slope angles where deposition and erosion occurs have been measured. This can help determine the slope angle at which the debris flow transition from erosion to deposition. A possible connection between confinement of flow, by channelized flow, and erosion, and a connection between an open slope and deposition can also be observed in the study area. A combination of slope angle and confinement of flow is probably the important factors that determine the transition for a debris flow from erosion to deposition.

Debris flows are a threat to human life and property, the initial volume of the flow might be low but due to erosion the volume increases greatly. Debris flow can cause damage from impact forces, and can transport large objects for example a tractor or a car, which can cause damage due to collision with another object. Observations in the study area suggest that debris flows could transport boulder with a diameter of 4 meters, heavy tractors, and several cars. Processes that could support these objects in the debris flows are discussed.

Historical data from the area indicate that debris flows have occurred in the area previously, and with the possibility from climatic models that precipitation will increase in the study area the frequency of these events might increase.

Table of Contents

1 Background theory

On 10th of June 2011 several landslides were triggered in Veikledalen in Norway due to heavy precipitation. The precipitation in combination with increased snow melt cause flooding, this has been documented by others and will therefore not be included in this thesis.

The purpose of this thesis is to identify the landslides in the selected study area in Veikledalen, and then to determine the triggering mechanism, landslide type, erosion volume, deposition volume, and debris flow size necessary to transport large objects observed in the landslide track. The solution to these problems will be estimated from observations and data from field work, and public databases.

The thesis will conclude that the landslides in the study area are debris flows that started as debris slides; therefore information most relevant to this is included in the thesis. Theory that is used in the results or discussion chapter is included in the background theory; theory that is important for the understanding of the problem has been included in the Appendices.

1.1 Landslide types and classifications

A landslide is material moving down a slope; the material can be rock, debris or earth. Landslides can be divided into 5 main types of landslide, see table 1.1, according to their way of movement and type of material. The material in a landslide can be described as either being a soil or a rock ((Varnes, 1978) found in (Cruden and Varnes, 1996)). Rocks were in their natural location and consisted of a hard or firm intact mass, before any movement took place. Soil is generally an aggregated mass of solid mineral and rock particles. The particles are not in their natural state and have either been transported to the location, or they are a product of weathering of rocks on site. The voids in the soil can also be filled with either gases or liquids and these fluids are part of the soil (Cruden and Varnes, 1996).

Type of movement	Type of material		
		Engineering soils	
	Bedrock	Predominantly Coarse	Predominantly Fine
Fall	Rock fall	Debris fall	Earth fall
Topple	Rock topple	Debris topple	Earth topple
Slide	Rock slide	Debris slide	Earth slide
Spread	Rock spread	Debris spread	Earth spread
Flow	Rock flow	Debris flow	Earth flow

Table 1.1: Landslide types categories by the material in the landslide and the movement of the material (Cruden and Varnes, 1996).

Table 1.1 shows that soil can be divided into two different categories, debris and earth. These categories are based on the diameter of the particles in the soil. Earth is a soil where at least 80 percent of the particles are smaller than 2mm; this means that they are sand size, silt, and clay. Debris contains coarser material; between 20 and 80 percent of the soil, particles are larger than 2mm (Cruden and Varnes, 1996).

Velocity class	Description	Velocity boundary(mm/sec)	Typical velocity boundary
7	Extremely rapid	$5*10^{3}$	5 m/sec
6	Very rapid	$5*10^{1}$	3 m/min
5	Rapid	$5*10^{-1}$	1,8 m/hr
4	Moderate	$5*10^{-3}$	13 m/month
3	Slow	$5*10^{-5}$	1,6 m/year
2	Very slow	$5*10^{-7}$	16 mm/year
1	Extremely slow		

Table 1.2 Landslide velocity scale, where the velocities are the boundaries between the different classes (Cruden and Varnes, 1996).

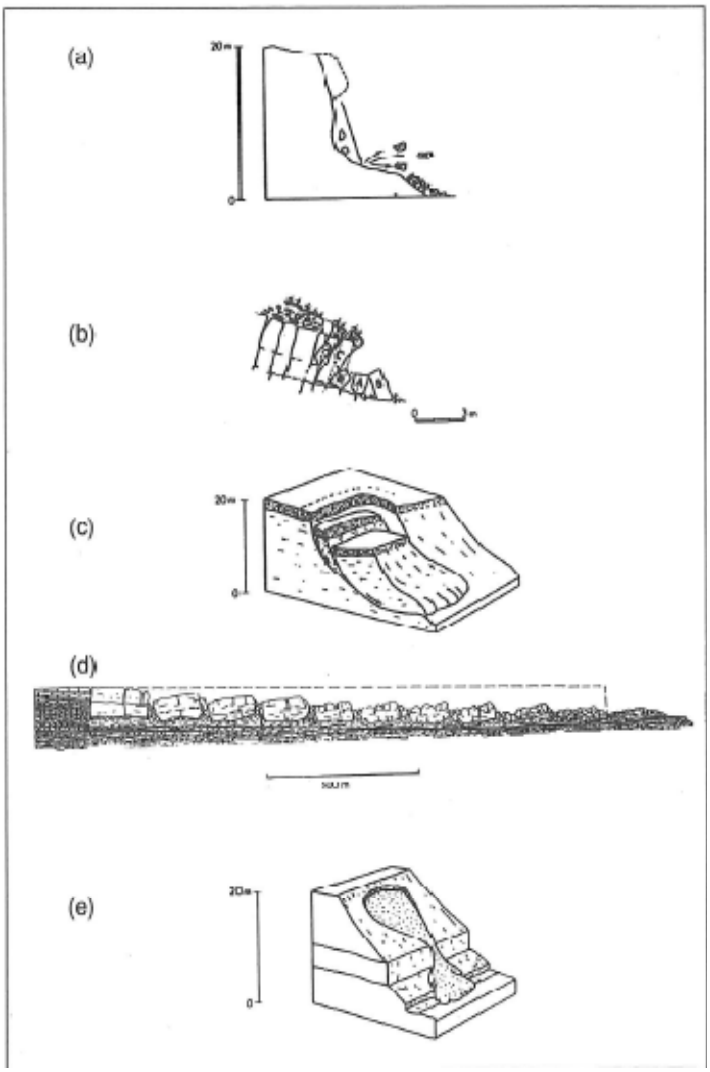

Figure 1.1 Illustrations of the landslide types classified in table 1.1 by movement. A) Fall, b) Topple, c) Slide, d) Spread, and e) flow (Cruden and Varnes, 1996).

To understand which type of landslide that exist in the study area it is necessary to know some basic information about the different landslide types, which can then be used to determine the landslide type for the landslides in Veikledalen.

1.1.1 Fall

Falls are mainly material falling, bouncing, or rolling in the air from a steep slope, where it has detached from with little or no shear deformation. This motion can be seen in figure 1.1a. The velocity of this rolling, bouncing, or falling motion is very rapid to extremely rapid, see table 2.2, which gives falls a velocity class of either 6 or 7. The separation of the displaced material from the undisturbed mass is often preceded by sliding on a small scale or a toppling movement, in an undercut slope this will not occur. The angle of the slope where the material detaches from determines if the material will fall, bounce, or roll (Cruden and Varnes, 1996).

1.1.2 Topple

The toppling motion can be seen in figure 1.1b and this movement is due to a forward rotation of the mass. This forward rotation is fixed on a point or axis below the centre of mass of the displaced mass. The mass is in a way “top heavy”, and normally a mass can only topple once. Toppling can be driven by water or ice in cracks found in the mass, or by gravity exerted on the displaced mass by material up-slope from the mass. The velocity of topples range the entire spectra from extremely slow, to extremely rapid, see table 1.2. The displaced mass can also transform into a fall or a slide (Cruden and Varnes, 1996)

1.1.3 Slide

Slides are movement of mass down a slope, the mass is mainly occurring on rupture surfaces or thin zones with intense shear strain, can be seen in figure 1.1c. The slide normally starts as a local failure that grows progressively larger in different directions. This local failure is often seen before the slide as cracks in the ground surface, these original cracks will form the main scarp of the slide. Slides can be divided into two different types, rotational slides and translational slides (Cruden and Varnes, 1996).

Rotational slides have a rupture surface that is curved and concave. There is also a possibility of very little internal deformation in rotational slides. Occur mostly in homogeneous materials where there are no clear weak zones, for example in week rocks or soils (Cruden and Varnes, 1996).

Translational slides have a rupture surface that is planar or undulating, and the displaced mass normally slides across the original ground surface. Translational slides are in most cases shallower than rotational slides and the rupture surface may occur along one or more discontinuities in the ground. Translational slides can also transform into a flow, often a landslide (Cruden and Varnes, 1996).

1.1.4 Spread

The term spread was used to describe the sudden movements on stratums of sand or silt, that are water-bearing, the stratums are then either overlain by homogeneous clays or they are loaded by fills, see figure 1.1.d. Spreads occur when a soft material is overlain by a cohesive soil or a rock mass, if the cohesive soil or rock mass is fractured and then subsides into the softer material underneath the softer underlying material might liquefy or flow. Spreads have a complex movement, for example it is also possible for the cohesive material to subside, translate, rotate, disintegrate, or liquefy and flow. The rupture surface is unidentifiable and is not a surface of intense shear (Cruden and Varnes, 1996).

1.1.5 Flows

Flows are movements that are continuous, and where the shear surfaces are brief, closely spaced, and generally not preserved, see figure 1.1e. The lower boundary of a flow is normally either a thick zone of distributed shear, or a surface along which significant differential movement has taken place. Flows distribute velocities in the same way as a viscous liquid does. The transformation of a landslide from a translational slide to a flow depends on the water content, mobility, and evolution of the movement. Debris slides can transform into a debris avalanche if the material that has been displaced loses cohesion, water is added, or the slope angle steepens (Cruden and Varnes, 1996).

Debris flows were first described by Stiny in 1910 in his book Die Muren (Stiny, 1910) found in (Hungr, 2005). He described debris flows as loads that were suspended in a mountain torrent, and that could transport masses of bed-load. With an increasing amount of sediments being transported by the flow, the flow would reach a threshold where it would transform into a viscous mass. This viscous mass would contain a mix of sediments, rocks and water and would behave as lava.

Debris flows occur when poorly sorted sediments are saturated with water and agitated the material can then surge down a slope due to gravity. The movement of a landslide is influenced by both solid and fluid forces, explaining landslide motion is therefore difficult (Iverson, 1997).

Sharpe described the difference between a debris flow and a debris avalanche, the latter was characterized by a rapid, shallow landslide, which occurred on a steep slope. The morphology of a debris avalanche was similar to a snow avalanche in the way that there was no channel or flood flow (Sharpe, 1938) found in (Hungr, 2005).The classification of debris flows that are often used today have been created and refined by Varnes several times and been completed into the classification found in table 1.1. The term debris flow can be used as a landslide type or as a landslide phase with the same properties. The most common way of using the term landslide is as a landslide type (Cruden and Varnes, 1996).

1.2 Historical Landslides in Norway

Several historical landslides have occurred in the same region as the study area, descriptions of other important historical landslides in Norway, those who are known to have been the most deadly, can be found in appendix A.

1.2.1 Storofsen

In 1789, between 21st and 23rd of July, southern Norway experienced a great flood. Gudbrandsdalslågen in Gudbrandsdalen flooded to an impressive height and multiple debris flows occurred in the area. The fall of 1788 was rainy, and the frost in the ground got unusually deep before the snow came and the winter was cold, with much more snow than normal. The spring of 1789 was warm, with a warm easterly wind, and people could start harvesting two weeks earlier than normal. The snow in the mountains started melting in large volumes in June, and the spring flood got delayed due to the ground being frozen to a great depth. Due to this deep layer of frozen soil, the spring flood was also larger than normal. The weather was warm during both June and July, up 30 degrees Celsius, and the precipitation rate was high. It has been said that from the 7th of July the rain was constant and heavy. The combination of warm weather that melted the massive amounts of snow up in the mountains, and the very high precipitation rate created a large flood in the central valley's in Southern Norway. The flood started in the smaller rivers , who transported the

snowmelt water from the mountains down to the valley below, and the flood then moved downstream (Furseth, 2006).

It has been said that the worst day was the 22th of July, when the precipitation rate was massive, there was thunder and lightning and the rivers were so great that they covered the entire valley floors. Landslides started to occur, mostly in the soil. Debris flows travelled down the valley side as a mixture of soil, rock and water. The landslides destroyed many homes and killed people and livestock. They could flee from the flooding, but it was harder to flee from the landslides. In Gudbrandsdalen there were approximately 80 landslides during these three days, and many of them were very large. But because it was in the middle of the summer, and most of the animals were up in the mountains, most of the livestock survived the floods and the landslides in this area of the country. In Gudbrandsdalen at least 60 people were killed and 889 animals. 3760 houses were completely or partially destroyed, the total cost was 300 000 riksdaler, not including roads and bridges (Furseth, 2006).

There were no measuring stations for the precipitation at the time, but at Vollan in Sunndalen it has been alleged that a barrel was filled with water in 72 hours, that is the equivalent of 320mm of precipitation per 24 hours (Furseth, 2006). This is an vast amount of water, in this area the yearly average is 740 mm (NORWEGIANMETEROLOGICALINSTITUTE, 2012a).

At the study location Brudalen there were several debris flows. The farm used to have 4921, 7m2 of fields used for agricultural purposes, but 984,34m^2 were destroyed by the debris flows. The farm also used to have a 46,45km^2 of meadows, but 27,87km^2 were completely destroyed. 10 houses of different sizes worth 80 riksdaler were destroyed. The cost of the destroyed fields and meadows were said to have been 98 riksdaler (Sommerfeldt, 1972). The combined cost was therefore 178 riksdaler, 1 riksdal is equal to 3,20 Norwegian kroner and calculated for what this would be today gives us a number of 129 761,26 Norwegian kroner in 2011(NorgesBank, 2012).

The farm could before the landslides occurred it was possible to sow 1 and a half barrel and harvest 6 barrels, after the event it was only possible to sow 1 barrel and harvest 4 and a half barrels. Before the event 3 horses, 20 cattle, and 40 sheep or goats could be fed by the farm, and after no horses, 4 cattle, and 8 sheep or goats can be fed by the farm. The value of the farm has decreased from 700 riksdaler to barely 100 riksdaler. The taxes on the farm were therefore considerably lowered for the 8 years following the event. Veikleåa was dammed up by landslides further down in the valley and the water destroyed the farm land when the soil slid out. Deep ravines were created in the valley side and the river changed its path closer to the farm (Sommerfeldt, 1972).

1.2.2 Fjærland

On May 8, 2004 a 240 000m^3 a debris flow occurred in Fjærland, which is located in western Norway. The debris flow was triggered by a glacial lake, approximately 50 000 m^3, breached a moraine ridge (Breien et al., 2008). The glacial lake normally drains in the autumn by developing a drainage system towards the ice falls in the east; the drainage system had not been created yet when the breaching occurred. The flood developed into a debris flow after travelling across a sandur, before it surged down the valley of Tverrdalen and deposited into a boulder fan 1000 meters below. The average slope gradient was 17 ° and the run out distance was roughly 3000 meters (Breien et al., 2008).

The debris flow eroded material when it flowed downstream, and the track widened to a maximum width of over 50 meters. Scouring also occurred, and the erosion was the greatest in the lower part of the track, which had a gradient of 13°. The debris flow changed the valley shape from a v-shape to a more rectangular channel with almost vertical walls. Large boulders up to 2 meters in diameter were transported by the flow. A 300m wide and 420 meter long, teardrop shaped depositional fan was created; the fan was 5 meters thick in the central area. The debris flow thickness could have been as much as 10 meters thick, and there was distinct vertical inverse grading present in the fan. A layer of mud travelled further downstream from the depositional fan and inundated farmland by up to 50 centimetres (Breien et al., 2008).

1.2.3 Historical landslides in Gudbrandsdalen

In Gudbrandsdalen excavations of sediments has been carried out to examine the debris flow history of the area. Four areas were selected close to the study area of Veikledalen, shown in figure 1.2. Sediment logs from the four locations can be seen in figure 1.3, the interpretation of the sediment logs are also shown in the figure, with a sediment description in table 1.3. The sediment logs determine that in the Gudbrandsdalen area there has been several debris flows that have occurred and they have built up colluvial fans (Sletten and Blikra, 2007).

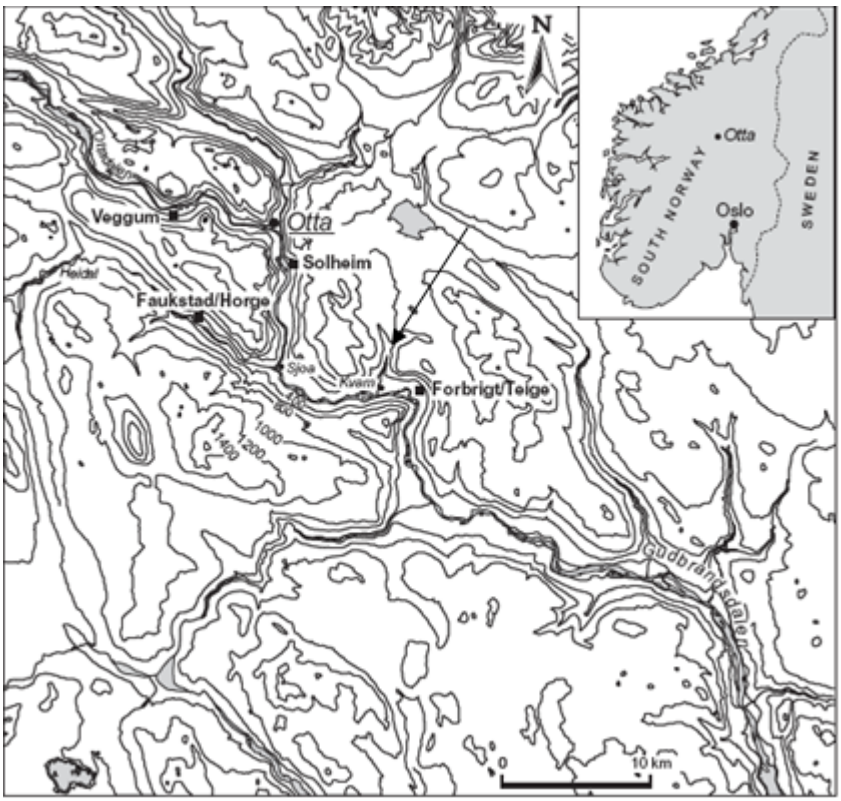

Figure 1.2 Map of the four locations Veggum, Solheim, Faukstad/Horge, and Forbrigt/Teige that were studied (Sletten and Blikra, 2007). An arrow points to Veikledalen and the study area for this thesis.

Depositional process	Sedimentological characteristics
Debris flow	Diamicton, unsorted, matrix-supported, massive
Watery debris flow	Diamicton, unsorted, more clast-supported, some grading
Hyperconcentrated flow	Massive, variable sorting
Colluvial water flow	Sorted, stratified/laminated
Fluvial flow	Sorted, stratified, thicker beds, coarser, greater rounding of clasts

Table 1.3 Sedimentological characteristics of the main sediment types and explanation to figure 1.3 (Sletten and Blikra, 2007).

All the diamict units in the sediment logs in figure 1.3 have been interpreted to have been deposited by debris flow that has originated from ravines. Clasts in the debris flows units can be up to 2 meters in diameter, the clasts are sub-rounded to sub-angular and they are often faceted. This indicate that the clasts have previously been modified by glacial transport (Sletten and Blikra, 2007).

The soil in the sediment logs was dated at certain depths and they range from 0 to about 9000 calibrated years before present. The dated sediments shows relatively high colluvial activity at ca. 8600-7400, ca. 2400-1900, and ca. 800-400 calibrated years before present. The sediment logs also show the periods when the debris flow activity was lower from ca.7100-6500, ca. 5900-5300, and 3500-2500 calibrated years before present. These calibrated dates suggest that debris flow has occurred in the Gudbrandsdalen are throughout most of the Holocene. The data seem to indicate that the colluvial activity in the area has been independent of the climatic changes in the Holocene, but this could also be due to changes in the weather situations that trigger debris flows (Sletten and Blikra, 2007).

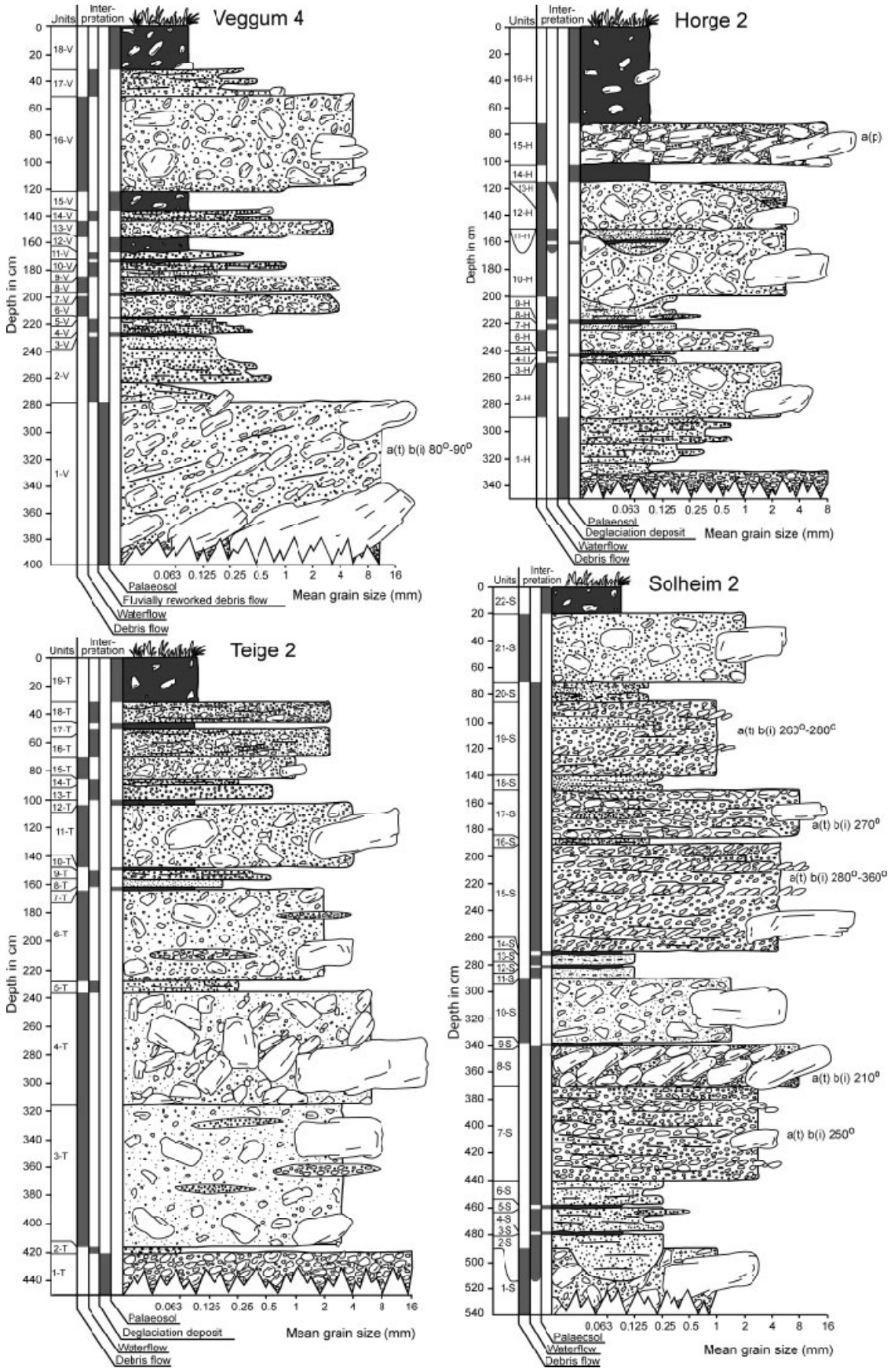

Figure 1.3: Sediment logs from the four locations Teige, Solheim, Horge, and Veggum, and interpretations of which process deposited the sediments (Sletten and Blikra, 2007).

1.3 Climate change

Precipitation, flooding, temperature, and extreme events all affect landslide potential and severity hence it is useful to consider climate and its possible affects on slides.

1.3.1Global Climate Change

IPCC states that carbon dioxide, methane, and nitrous oxide concentrations have increased in the atmosphere since 1750, because of human activities. Carbon dioxide has increased mainly through the process of burning fossil fuel, and changes in anthropogenic use of the land, in 2005 the concentration was at 379 ppm, this is illustrated in figure 1.4. Methane and Nitrous oxide concentrations have increased primarily as a result of agriculture (IPCC, 2007).

The increase in the concentration of these gases in the atmosphere is believed to be the major cause of the rising temperatures on Earth (IPCC, 2007) Figure 1.5 shows the temperature have risen since 1850 by 0,74 +/- 0,18 degrees Celsius, and the linear trend lines indicate that the warming is accelerating. Figure 1.5 also display an estimation of global temperature patterns, these patterns show that on the surface there have been greater changes in the Northern Hemisphere, compared to the Southern Hemisphere. In addition figure 1.5 establishes that the surface temperature changes relate to land and ocean, since most of the greatest changes in temperature are over land. The troposphere temperature patterns for warming illustrate a more uniform warming (IPCC, 2007).

Since 1850 the global sea level have increased by 0, 17 +/- 0, 05 meters (IPCC, 2007). The sea level rising is due to melting of glaciers and snow cover on both hemispheres, but IPCC (2007) also states that it is very likely that the ice sheets covering Greenland and Antarctica, have contributed to the sea level rise after 1993. There has also been a decrease in the sea ice extent in the Arctic. The sea level rise is also due to warming of the oceans, IPCC (2007) show that the temperatures in the ocean have increased down to 3000m below the surface and that up to 80% of the heat that has been injected into the climate system since 1961 has been absorbed by the oceans, this warming of the oceans expands the seawater and have contributed to the sea level rising.

According to IPCC(2007) the precipitation amount have increased on the land masses north of 30°N between 1900 and 2005, while on the land mass between 10°N and 30°N the precipitation amount increased between 1900 and the1950s, but have declined since the 1970s. IPCC (2007) have also observed a rise in the number of heavy precipitation events, these heavy precipitation events are the extreme-weather events that are above the 95 percentile, this has also been observed in areas where the total precipitation amount have decreased. The increase in the heavy precipitation events coincide with the warming of the climate and the significant growth of water vapour observed in the atmosphere (IPCC, 2007).

Increased water vapour in the atmosphere is a consequence of the human-induced greenhouse effects, boost evaporation in the areas where there are enough surface moisture to be able to do so, for example over the ocean or other wet surfaces. This leads to a rise in the moisture content in the air (IPCC, 2007). According to the Clausius-Clapeyron relation, for every 1°C the temperature rises, the water-holding capacity of the atmosphere is increased by approximately 7% (IPCC, 2007). This means that the water-holding capacity of the atmosphere have increased since the temperatures started to rise and if the climatic models are correct and the temperature continuous to rise, the atmosphere will be able to store even more water vapour. A consequence of this increased water-holding capacity is that there could be more precipitation than before the temperature started to

rise, since the weather systems that feed on the atmospheric water vapour are the main source for precipitation. This leads to an increase in the intensity and frequency of heavy precipitation events (IPCC, 2007).

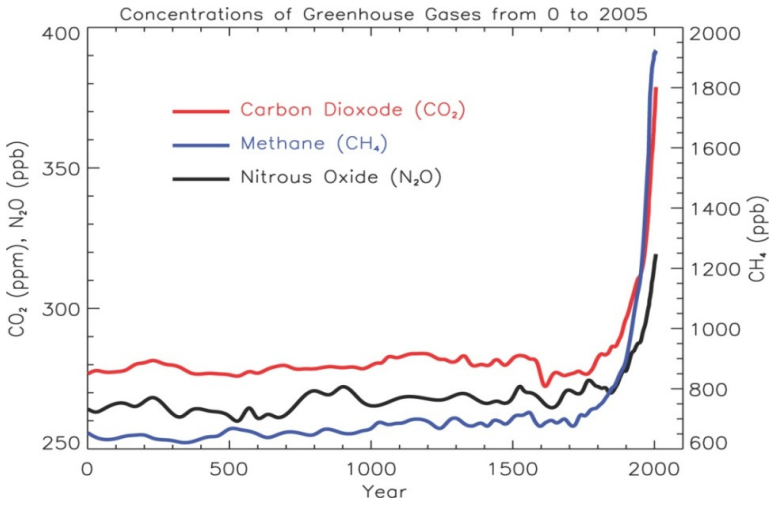

Figure 1.4 Concentrations of Carbon Dioxide, Methane, and Nitrous oxide in the atmosphere, measured values, and values calculated from ice cores. There is an increase in the concentration of all the gases after the year 1750.

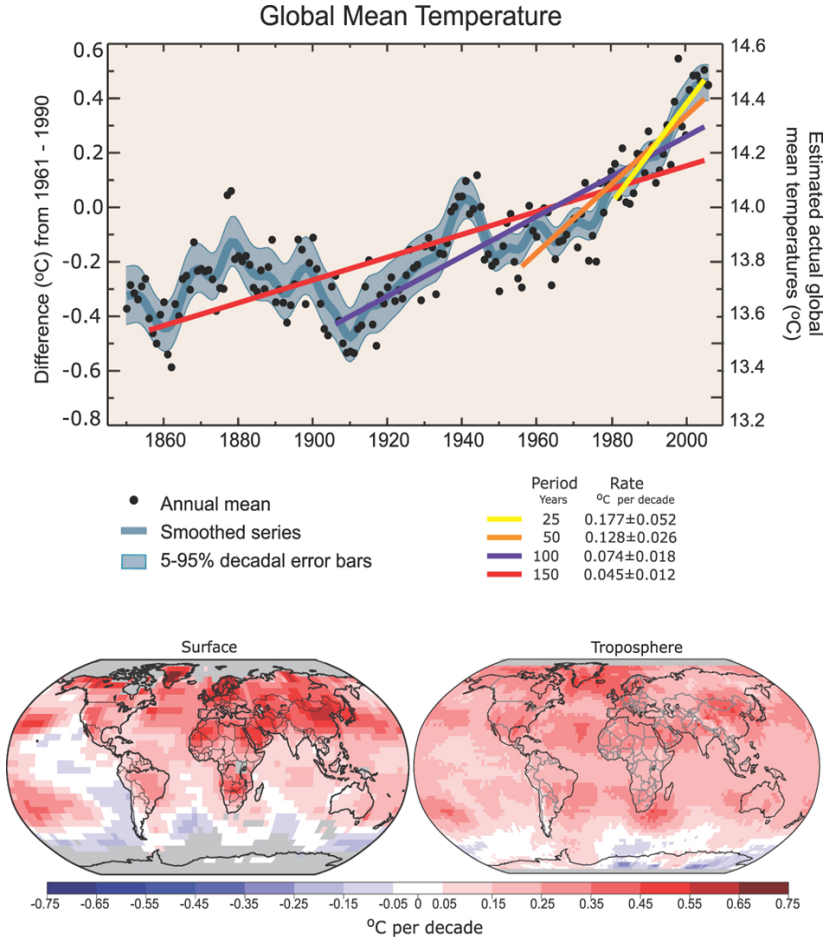

Figure 1.5 (Top) Observed global annual mean temperatures, left axis show anomalies relative to the 1961-1990 average. Linear trends to the temperature graph are also fitted. (Bottom) Linear global temperature trend patters from 1975 to 2005, estimated for the surface (left) and the troposphere (right) by satellite data, grey colour indicate areas where there is incomplete data.

1.3.2 Climate change in Norway

Climate models predicts that within the next 50 years, there will be an increase in the frequency and strength of extreme weather events in Norway (JAEDICKE et al., 2008), and IPCC (2007) have concluded that it is very likely that annual precipitation will increase in most of northern Europe. IPCC (2007) have calculated that the annual mean temperature in Europe will likely increase more than the global annual mean, and for northern Europe the greatest warming will occur in the winter, with a likely increase in the minimum winter temperature. The increase in extreme weather events will dominantly be precipitation events, and the increase in events will therefore affect all the processes that depend on precipitation.

For Norway annual precipitation will increase in all regions, but it will increase most on the western coast, see figure 1.6. Evaporation will also increase, due to a raise in temperature, figure 1.7, but there will also be an increase in runoff for most areas. The temperature will increase most in the winter season, and runoff will therefore increase during winter and winter flooding can become more common in the eastern part of the country, and on the western coast from Bergen to Trondheim (Blikra et al., 2003). Runoff in the rest of the country will increase in spring and autumn, but probably decrease in the summer months. More evaporation can lead to more precipitation and therefore more extreme weather events. Figure 1.6, 1.7, and 1.8 shows that the changes to evaporation, runoff and precipitation will be greatest on the western coast. The western coast of Norway is the area that receives the most precipitation today, and according to these models it will continue to do so.

Figure 1.9 shows that the snow cover in Norway will for coastal and northern Norway, while the mountainous and inner areas of Southern Norway will have more snow at the end of the winter in 2030-2050. The winters will be shorter and warmer than what they are today. The increase in the snow cover can generate larger spring floods in certain years and glaciers in these areas will start to grow. When the glaciers start to respond to the increase in snow depend on their response time, some glaciers , for example Briksdalsbreen, respond in just a few years, while other glaciers can take several decades (Blikra et al., 2003).

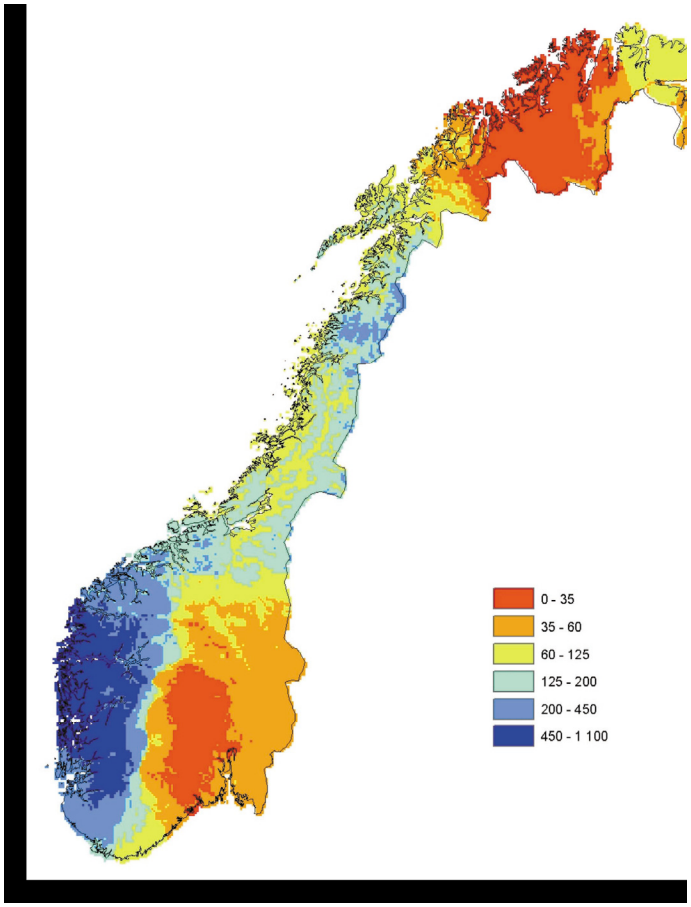

Figure 1.6: annual precipitation changes in mm/year. Difference found between control period (1980-2000) and scenario period (2030-2050) (Blikra et al., 2003).

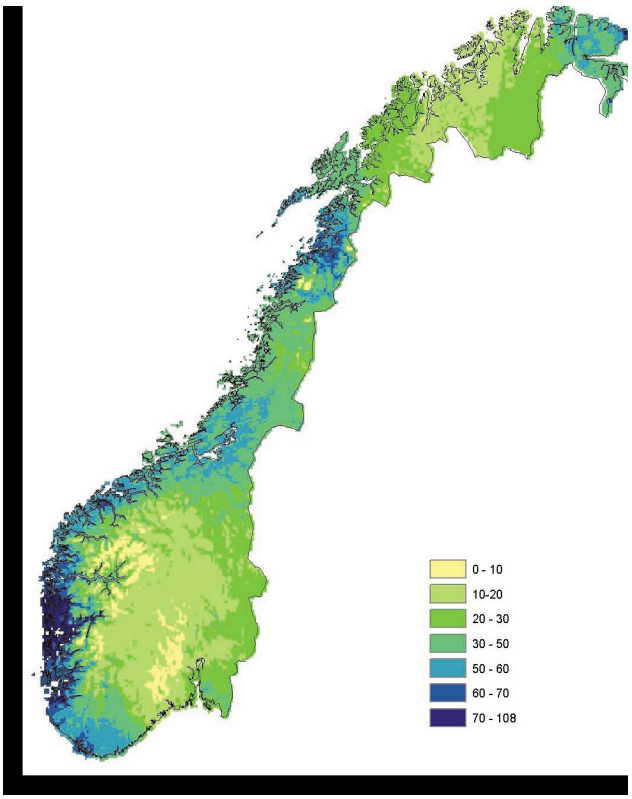

Figure 1.7: Annual evaporation changes (including contribution from vegetation in mm/year. Difference found between control period (1980-2000) and scenario period (2030-2050) (Blikra et al., 2003).

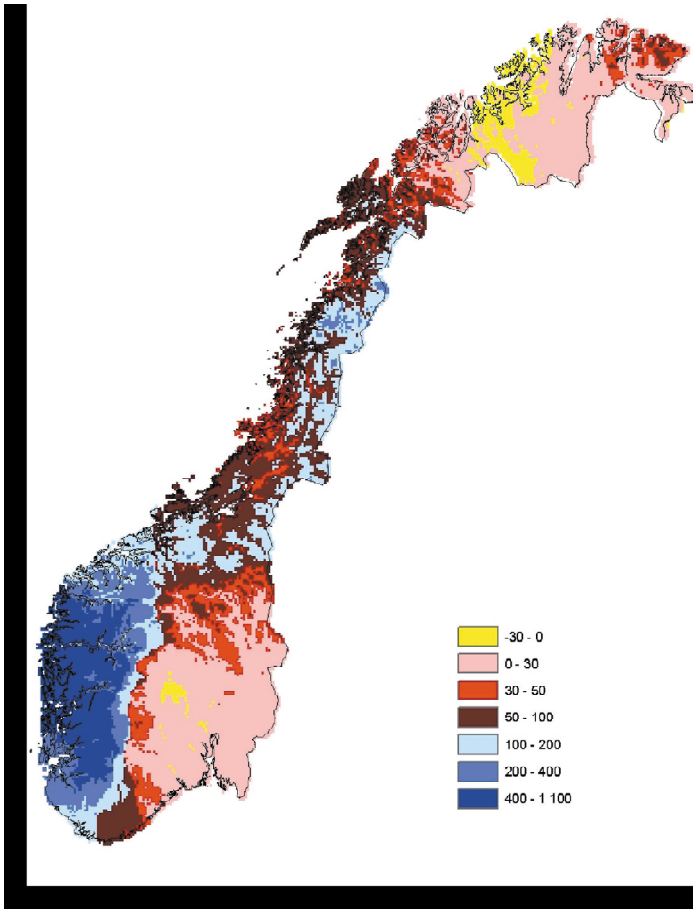

Figure 1.8: annual Runoff changes in mm per m^2. Difference found between control period (1980-2000) and scenario period (2030-2050) (Blikra et al., 2003).

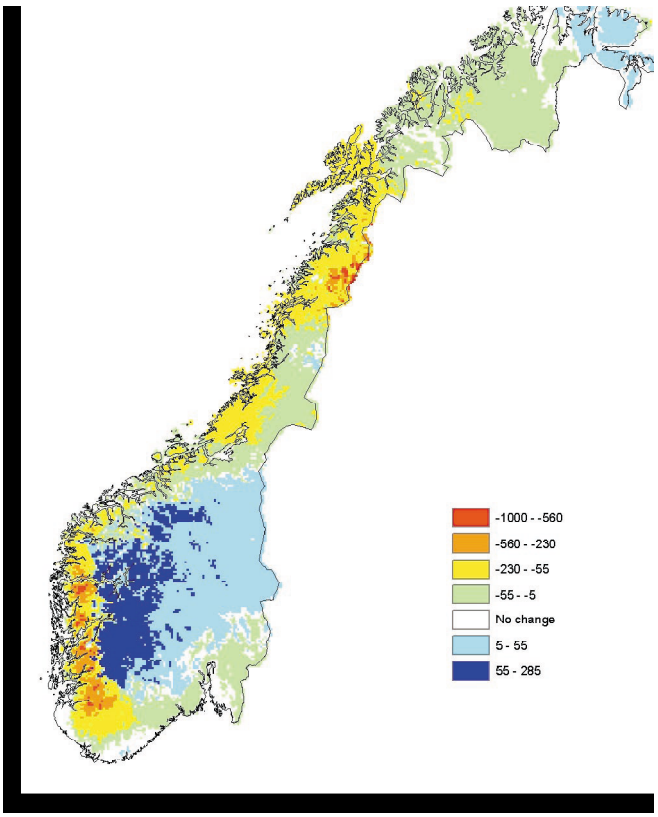

Figure 1.9: Changes in snow cover (mm of water) at the end of winter (1.april). Difference found between control period (1980-2000) and scenario period (2030-2050) (Blikra et al., 2003).

1.3.3 Consequences of climate change for landslides

Landslides are one of the most common geohazards in Norway. Triggering mechanisms for landslides are often a function of specific meteorological conditions. These conditions are normally extreme-weather events, for example intense rainstorms or rapid snowmelt. The local geological variations also play a key role in the triggering of landslides. The important meteorological factors that are used in early warning systems are precipitation, wind and air temperature. In Norway different landslide types occurs in particular parts of the country, this is due to the geology of Norway and the local weather conditions(JAEDICKE et al., 2008). In the western part of Norway landslides frequency has been the highest in the coldest and last period of the last glaciations period, this probably reflects the frequency of intense rainstorms in the area. In the eastern part of central Norway landslides often occur due to snowmelt, and the frequency of landslides has therefore been high for the entire time period since the last glaciations period. (Blikra et al., 2003).

Since the climate model illustrated by figures 1.6,1.7,1.8, and 1.9 indicate an increase in the precipitation dominated extreme-weather events, this can influence the frequency and intensity of the landslides in Norway that are triggered by intense rainstorms or longer rainfall events. The figures also show an increase in snowmelt the landslides triggered by snowmelt may also increase in frequency. The models determines that there will be an increase in runoff, which can cause landslides by erosion of material(Blikra et al., 2003). The triggering thresholds for precipitation might also change as a result of the changes in the climate, and areas that were previously thought to be safe might become unsafe in the future (JAEDICKE et al., 2008).

In Norway for similar slopes in Northern Norway and Eastern Norway the landslide frequency will be three to four times greater for the slope in Northern Norway than for the slope in Eastern Norway, and they will occur at different times. This means that the landslide frequency will change differently in different parts of the country, and the changes must be calculated on a regional scale to be accurate (Blikra and Sletten, 2002). The consequences of an increase in the frequency of landslides could be large, both socially and economically. If future landslide events occur in areas where there could be damage to people, buildings, roads etc. it could be a large economic loss for the region and for the country. The total loss depends on the scale of the event and the level of damage it causes.

1.3.4 Climate zone, Köppen-Geiger system.

The most commonly used system for climatic zones in the world is the climatic zone system developed by Wladimir Köppen (1846-1940). Rudolf Geiger (1894-1981) updated the climatic zone system into a world map. Köppen was a plant physiologist and his classifications of zones are based on five vegetation groups, the vegetation groups were determined by botanist De Candolle. He divided the world into five major zones with plants of the equatorial zone (A), the Arid zone (B), the warm temperate zone (C), the snow zone (D), and the polar zone(D) (Kottek et al., 2006).

The world map of climatic zones has been updated and the map shows that the region of Kvam is in the Dfc region. The D stand for the snow zone, where the minimum mean monthly temperature must be below or equal to -3°C , the f stands for fully humid which means that there are no dry seasons, and the c stand for cold winters and cool summers where the maximum mean monthly temperature is not above or equal to 22 °C and the minimum mean monthly temperature is greater than -38°C (Kottek et al., 2006).

1.4 Triggering mechanisms

There are several triggering mechanisms or factors for landslides, there might also be factors that are not known to us or that we still do not understand. This is an explanation on the most common triggering mechanisms of landslides, and then especially landslides that occur in Norway. For landslides triggered on forested slopes, the slopes are generally stable when the slope angle is below 30°; while on grass covered slope landslides can be triggered for slope angles as low as 25°. These are general rules and exceptions can exist (Dahl et al., 1981).

Below, only triggering mechanisms related to rainfall in some way will be presented, there are other triggering mechanisms for landslides, but they will not be covered here.

1.4.1 Intense rainstorms

There is a relationship between intense rainstorms and shallow landslides (less than 2-3 meters deep) that transform into debris flows e.g. (Caine, 1980, Wieczorek and Glade, 2005, Wieczorek, 1996). Campbell was the first to notice the relationship between high-intensity rainstorms and the triggering of shallow landslides in 1975 (Campbell, 1975) found in (Savage and Baum, 2005). The theory Campbell presented was that when sufficient antecedent rainfall had occurred before the high-intensity rainstorm, the infiltration from the rainstorm could create a temporary aquifer in the ground, illustrated by figure 1.10. The process of creating this aquifer could induce positive pore-water pressure in the ground. The increase in pore-water pressure decreases the effective strength of the surface soils, this reduction in the effective stress is then the initiator of the shallow landslide, due to the accompanying decrease in the soils shear strength (Wieczorek and Glade, 2005).

If the pore-water pressure induced by the rainstorm was not great enough to cause a landslide to be created, the water will flow down to the groundwater and long rainfall events can therefore increase the groundwater level and saturate the entire soil. Long rainfall events can cause pore-water pressure increases in deeper soil and a reduction in effective soil strength, this can lead to a deeper landslide being triggered (Wieczorek and Glade, 2005).

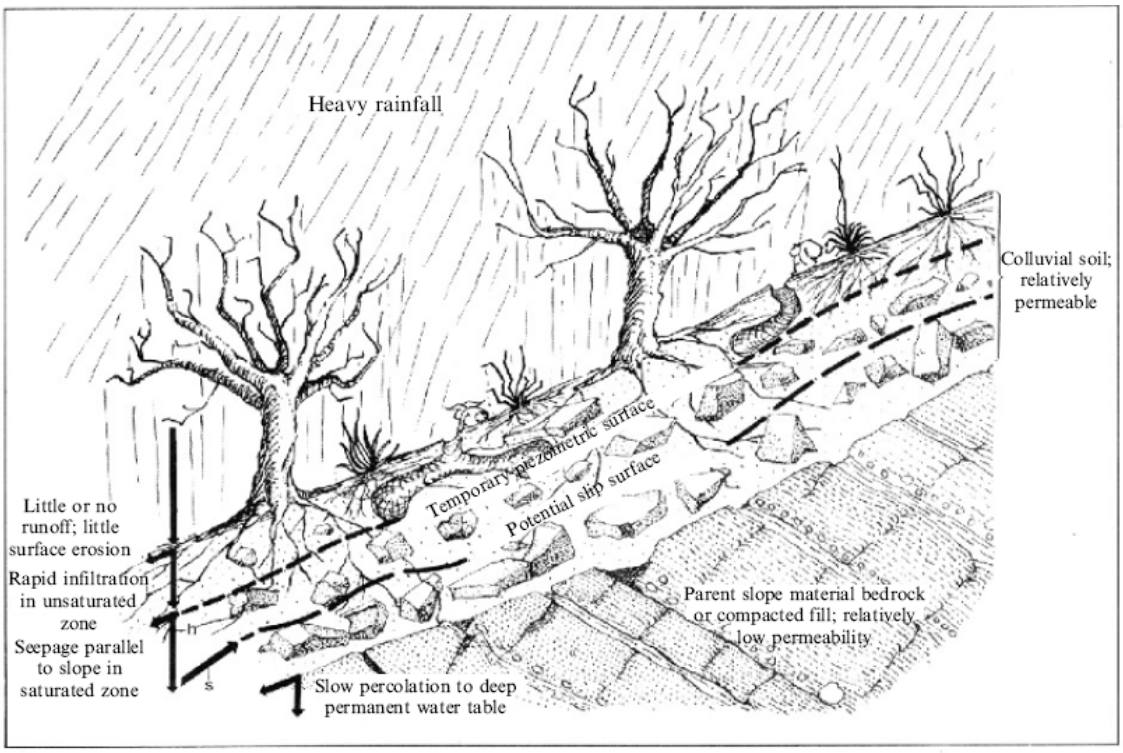

Figure 1.10 Mechanisms in Rainfall induced failure in a thin layer of colluvial soil on a steep slope (Campbell, 1975) found in (Savage and Baum, 2005).

The instability in soils due to rainfall is dependent on the rainfall intensity and the duration of the rainfall. Due to this dependency thresholds for rainfall that causes landslides have been created. For rainfall events with high intensity rainfall, but short duration, less than one hour, the infiltration rate will not be high enough to develop sufficient pore-water pressure in the soil to trigger a landslide, the surface runoff may therefore be quite substantial (Wieczorek and Glade, 2005). Very high surface runoff may erode the soil to such a degree that a landslide can be created, the probability of this increases if the soil is bare (Wieczorek, 1996). Rainfall events that last for many days, but have low intensity may increase the groundwater level, but not increase the pore-water pressure sufficiently in the near surface soil to trigger a landslide (Wieczorek and Glade, 2005).

The infiltration rate of the soil determines how fast the water can percolate into the soil and therefore also the duration of a rainfall event that will create a landslide. If the soil has a low permeability, the rainfall event needed to create an increased pore-water pressure in the soil must be longer than the rainfall event needed if the soil has high permeability. Porosity and the soil cover thickness are also important factors for the infiltration of water and triggering of landslides(Wieczorek and Glade, 2005) .

1.4.2 Other Causes related to precipitation

Water that infiltrates the soil may come from other sources than rainfall directly and these processes can decrease the water needed from a rainfall event or antecedent rainfall to trigger a landslide.

1.4.2.1 Snowmelt

Rapid snowmelt by rainfall or increased temperatures can lead to increased water infiltration. Melting snow provides a more continuous supply of water than rainfall, and normally for a greater duration than for a rainstorm. The snow need to be warm enough (above or equal to 0°) so that the rain does not freeze when it comes in contact with the snow (Horton, 1938).

1.4.2.2 Water level changes in river/lakes

Sudden lowering of the water table, for example in a river or in a lake, can trigger landslides due to a destabilization of the slope. The pore pressure in the slope adjacent to the river or lake needs to dissipate quickly following the lowering of the water level, if the groundwater level in the slope is not lowered quickly enough; the slope is then subjected to higher shear stresses and can become unstable. Prolonged water infiltration that increases the groundwater level in the slope can have the same effect on the slope and therefore also cause slope instability. Thick deposits that are uniform and have a low permeability are particularly susceptible to trigger landslides due to the process of rapidly lowering the water table (Wieczorek, 1996, Wieczorek and Glade, 2005).

1.4.2.3 Flooding

Flooding is normally due to rainfall or a combination of rainfall and snow melt. Since both flooding and landslides are due to rainfall they can occur at the same time and from the same rainfall event. Flooding can also trigger landslides by erosion of either the foot of an adjacent slope, or erosion on such a scale that the concentration of debris in the flood transforms it into a landslide (Wieczorek, 1996). In Norway there has also been Glacial Lake Outburst floods that have triggered landslides due to erosion (Breien et al., 2008).

1.6 Debris flow features

1.6.1 Debris flow material and water content

For a soil to be labelled as debris, the percentage of sand, silt and clay in the soil needs to be less than 80. Takahashi described debris as a soil where less than 20% of the particles are finer than silt size and only a very few percent of the soil particles are less than clay size (Costa, 1984, Takahashi, 1981). Debris flows normally carry a load of organic matter; the amount depends on the quantity of organic matter present at the source area of the debris flow. Debris flows in steep forested areas can consist of up to 60 % organic matter by volume (Hungr, 2005).

Water content in a debris flow has been described by Varnes in 1978, from these descriptions debris flows have a water content that is wet or very wet, or somewhere in between (Cruden and Varnes, 1996).

- **Dry:** There is no moisture visible in the material.
- **Moist:** the material contains some water, but none of the water is free water. The material can behave as a plastic solid, but it does not flow.
- **Wet:** The material contains sufficient water for the material to partially behave as a liquid, to have water flowing from the material, or for the material to support bodies of standing water.
- **Very wet:** The material contains enough water so that it can flow as a liquid, at low gradients.

Debris flow volume concentration of solid ranges from 25% to 86%, and the solids weight proportion ranges from 35% to 90%. The water content in a debris flow is normally in the range of 10% to 30% or even higher by weight (Costa, 1984).

Detail information about the transition between a debris flow and a water flood, and starting zones for debris flows can be found in appendix C.

1.6.4 Track

1.6.4.1 Erosion

Channel Shape

There are three main channel shapes circular, triangular, and rectangular. For the study area of Veikledalen the triangular channel is the most important shape, figure1.11. Detailed information on the channel shapes can be found in appendix C.

Triangular channels have a rigid plug, where there is no deformation, the assumption is that the material is a non-Newtonian fluid and it will therefore have shear strength that must be overcome before the material can flow. The dead regions in the channel can deposit into levees along the channel.

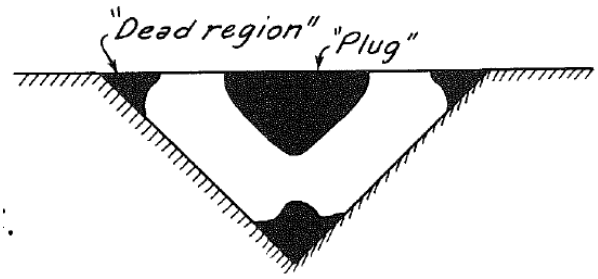

Figure 1.11 Debris flow in a triangular channel, location of dead regions and rigid plug in the triangular channel (Johnson, 1970).

1.6.4.2 Entrainment

The magnitude of a debris flow is defined as the total volume of material moved by the flow to the depositional area. The initial volume is often small; most of the mass comes from entrainment of material along the path. The total volume is therefore determined by the entrainment mechanism and the sediment supply (Hungr et al., 2005).

Information on the entrainment mechanism and bed stability can be found in appendix C.

Yield rate

The yield rate of a debris flow is the volume eroded per metre of channel length, and can be used to predict debris flow magnitude. The parameters that are relevant to the yield rate are slope angle, existing channel width and depth, bed material, bank slope angle, bank slope height, bank slope material, bank slope stability rating, and tributary drainage area or discharge. Flows that have lower solid concentrations by volume are probably more erosive, and therefore have a lower depositional angle that flow with higher solid concentrations (Hungr et al., 2005).

1.6.5 Deposition

Debris flows deposits when the gradient is low, or when it reaches an area of decreased confinement and it can start to spread out. Debris flows stop when the shear strength of the flow exceeds the internal shear stress. The exact mechanism that makes debris flows stop is not known. What is observed is that the velocity of a debris flow just before deposition must be quite low, since small vegetation on fans and in channels can divert the flow without being scarred (Costa, 1984).

The slope at which deposition occurs is still up for debate, several suggestions have been presented. The great range in depositional angles means that no general guidelines exist. It is known that smaller debris flows can deposit at steeper angles than larger events on the same path. Other important factors are mean water content of surges, and the composition and particle size of the surge front. The factors that probably influences the depositional angle are probably the same factors that affect yield rate, see chapter 1.6.4.2 (Hungr et al., 2005).

Information on debris flow as a building mechanism of alluvial fans can be found in Appendix C.

Lateral spreading

Lateral spreading could stop a debris flow because the thickness of the flow decreases to below the critical thickness needed for the flow to flow, and the shear strength of the material exceeds the internal shear stress. Lateral spreading can occur when debris flows spread out onto fan surfaces or open slopes; the debris flow follows the topography. The slope of the fan surface, the volume of the

flow, and the strength of the flow are the controlling factors for the coverage of the debris flow deposits (Costa, 1984).

Stable slope angle for deposition

Takahashi found an equation that could determine the stable slope angle for deposition for a debris flow. The equation is a function of several factors, for example the size of the particles, the depth of the flow, and the angle of internal friction. Debris flows stop flowing and starts deposits when the internal friction increases, while the slope of the channel, the volume of the flow, thickness of the flow, and strength of the flow decreases. The slope angle at which below a debris flow starts depositing is approximately 17°, for very coarse grained debris flow, deposition can start at a slope of 27° (Costa, 1984, Takahashi, 1981).

Levees and terminal lobes

When debris flows flow down a slope, larger particles are transported to the margins of the flow by dispersive forces. The plug in the centre of the flow pushes the lateral areas of the flow mass to the sides and they are then sheared from the flow. This process creates levees on the channel sides, and large boulders are often present in the levees. As the debris flow deposits mass in the levees, they will generally continue flowing until most of their mass has been deposited as levees. As debris flows stop, steep fronts and sides can be created due to the strength of the debris or the concentration of coarse clasts. The deposits are called terminal lobes, and they have a limited thickness. The deposits have a matrix, but the fine-grained matrix might be washed away in the upper parts of the levee due to rainfall or stream flows (Costa, 1984).

Lateral deposits are on the side of the debris flow channel, they are formed when the head of the debris flow move laterally, and by the fine-grained body material. If the depth of the channel is greater than the thickness of the debris flow the lateral deposits will form on the channel sides and not along the channel. Each wave of the debris flow can deposit a layer in the lateral deposits. For channels that are narrow near the apex of the fan often overtop of the channel and create lobes (Johnson, 1984).

1.6.6 Vegetation damage

A very characteristic feature of debris flows in humid areas is the complete removal of vegetation in the debris flow track. Even large trees are removed, and they are normally cut only a few centimetres above the ground surface. The removed trees leave behind small, splintered stumps that are a clear indicator that a debris flow has occurred in the area. The damage done to the vegetation is at its strongest in the centre of the flow, at the edges the velocity is lower, and the debris flow might not scar or destroy any of the vegetation in those areas. Small trees can divert the debris flow in low velocity areas of the flow, and debris can be deposited around trees without scaring the bark. The nonexistent presence of damage done to vegetation at the debris flow margins is evidence for debris flows having low velocities along the outer edges of the flow (Costa, 1984).

1.7 Stability in Water Soaked Sediments

For the stability in water soaked sediments the most important factor is the shear strength of the material, which must be exceeded before the material can fail. The presence of pore pressure in the sediments reduces the effective stress in the soil and consequently decreasing the shear strength of the material. Excess pore water pressure can be induced if the soil is under undrained conditions. So an increase in water in the sediments makes the slope more unstable.

Detailed information on the nature of soil, shear strength of soils, effective stress, permeability, and critical values for stability can be found in appendix D.

1.7.1 Infinite slope stability analysis

There are several methods used to analyze slope stability, the one explained here is the infinite slope stability analysis. The ideal case for this analysis is when the length and the width of the potential debris flow is much greater than the thickness of the debris flows; this is due to the edge effects. It is a simple limiting equilibrium method that is based on the law of static friction for a rigid block on an inclined plane, which is illustrated in figure 1.12. Failure of the block occurs when the resisting forces are smaller than the driving forces on the block and is calculated as a ratio that defines the factor of safety for the slope. The resisting forces of the slope are Coulomb friction and cohesion, and the driving force is the down slope stress created by gravity.

Friction and cohesion

The force that must be applied to cause relative movement between two particles is a shear resistance. This shear resistance is due to attractive forces from the surface atoms on particles. Chemical bonds are formed due to the attractive forces at points of contact of the surfaces. The frictional resistance between two particles is dependent on the physical and chemical nature of the particle surface, and the interaction between the particles at the point of contact. The total shear resistance, the product of the bond strength and the number of bonds present, is proportional to the normal force that pushes the two particles together; a decrease in normal force will decrease the total shear resistance. Interparticle shear resistance is therefore frictional (Lambe and Whitman, 1979).

Cohesion is the resistance to shear deformation, when a shear force is applied. (De Blasio, 2011) cohesion is more important in clay and silt soils due to electrostatic bonds between particles, while in soils without clay or silt the only cohesion is from capillary forces. For rocks the cohesion is in orders of Mega Pascal in magnitude (De Blasio, 2011)

Cohesion between particles occur when part of the total shear resistance is independent of the normal force pushing the soil particles together, this means that even if the normal force is equal to zero there is still shear resistance in the soil. If soil particles have been in stationary contact for a long time, cohesion can be developed in the contact between the soil particles. An example where cohesion is an important process is when cementation turns sand into sandstone. Normally cohesion in the soil is quite small, and the contribution from cohesion to the soil strength is therefore also small. Friction is the normal situation in soils, while cohesive behaviour of the soil is the exception (Lambe and Whitman, 1979).

Frictional resistance is normally expressed in one of two ways. First by the coefficient of friction, f or μ, where the normal force, N, across the surface is used to calculate the maximum shear force on the surface, Tmax.

$$Tmax= Nf \quad (1.1)$$

The normal force N can be expressed as the mass times the gravitational acceleration, and the maximum shear force is often expressed as F and is called the friction of the object, and equation 1.1 therefore becomes the equation used to find the resistive force that an object need to overcome before it can start to move (Lambe and Whitman, 1979).

$$F= \mu mg \quad (1.2)$$

where μ is the static coefficient of friction for rocks the static coefficient of friction has an average value of 0.85. The static friction of the debris flow is larger than the sliding friction, so when the flow has started to move less driving force is needed to keep it moving compared to getting it started (De Blasio, 2011).

The second way to express frictional resistance is to use the frictional angle, ϕ_u , which is defined as:

$$\tan \phi_u = f \quad (1.3)$$

Basic laws of Friction

Two basic laws of frictional behaviour exist:

1. The normal force between two bodies is proportional to the shear resistance between two bodies.
2. Between two bodies the shear resistance is independent of the dimensions.

The second law of friction can be explained by pulling a rectangular object on a flat surface. The pulling force does not depend on if the object is pulled on its side or on an edge, the pulling force is equal for both cases because the shear resistance is independent of the dimensions of the two bodies. The laws of friction have been found by empirical observations, they were first stated by Leonardo da Vinci in the 14^{th} century and later rediscovered by Amontons in 1699 (Lambe and Whitman, 1979).

Mechanism of Friction

Friction can be expressed by several processes. The first process is that one a sub-microscopic scale, all surfaces are rough. This surface roughness means that the contact between two solids will only be where the high points of the surface touch each other. These high points are called asperities, and this phenomenon means that the actual contact area between the two solids is much smaller than the apparent contact area. Because the actual contact area is small, the normal stress on these contacts will be extremely high, and the normal stress will reach the shear strength of the material at the asperities even under light loading. The high contact stresses between the solids can cause the two surfaces to adhere at the asperities. The shear resistance is therefore provided by the adhesive strength of the asperities. The maximum shear force Tmax can then be calculated as:

$$Tmax= sAc \quad (1.4)$$

Where s is the shear strength of the asperities that are adhered and Ac is the actual contact area which can be calculated as:

$Ac = N/q_u$ (1.5)

Where q_u is the normal stress required to cause yielding and N is the normal load.

Combining equations 1.4 and 1.5 gives the final equation for the maximum shear force.

$$Tmax = N\frac{s}{q_u} \quad (1.6)$$

This concept was first stated by Terzaghi in 1925, and they are now the starting point for almost all friction studies (Lambe and Whitman, 1979).

Cohesion and Friction can be thought of as the resistive forces in a soil and combined they show the shear strength of the soil and can be combined into equation 1.7.

$Fres = mg\cos\beta\tan\phi + cwL$ (1.7)

where w and l are the width and length of a soil sample on a slope with an angle β, and c is equal to the cohesion of the soil (De Blasio, 2011).

Factor of Safety

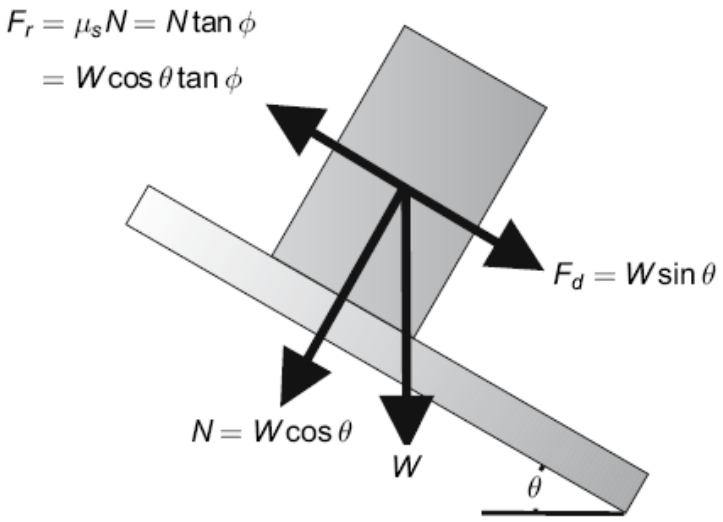

Figure 1.12 Law of static friction for a rigid block on an inclined plane, used for infinite slope stability analysis (Savage and Baum, 2005).

Figure 1.12 illustrates the law of static friction. The coefficient of static friction is μ_s and the angle of static friction is ϕ. If the resistive forces equal the driving forces, the block is in a state of limiting equilibrium and the inclination angle is equal to the static friction angle. Figure 1.12 show a simplification of the driving and resistive forces equation that can be used to calculate the factor of safety, where the resistive force is the shear strength of the material while the driving force is the shear stress of the material. A simplified equation for the factor of safety is shown by equation 1.8 (Savage and Baum, 2005).

Factor of safety= shear strength/ shear stress = $c + \sigma\tan\phi/\tau$ (1.8)

The shear strength of the material includes the resistive forces cohesion (c) and frictional forces. The factor of safety for a saturated or partially saturated soil needs to use effective shear strength instead of normal shear stress; σ can be calculated for the effective normal stress at a depth z as equation 1.9.

$$\sigma' = \gamma_s z\cos\theta - \gamma_w \Psi \quad (1.9)$$

where γ_s is the saturated soil unit weight, θ is the slope angle, γ_w is the unit weight of groundwater, and Ψ is the pressure head created by the soil water and is found by dividing the pore pressure by the unit weight of water. The first part of equation 1.9 is the normal force and when this is combined with tanϕ in the equation for shear strength it calculates the friction of the material. The shear strength of the soil for the factor of safety is therefore a combination of the friction, cohesion, and pore pressure in the soil. The pore pressure is negative in this equation and this is because increased pore pressure decreases the effective stress and therefore also the shear strength of the soil, see appendix D. The shear stress in the soil can be taken directly from figure 1.12 and adding the unit weight of saturated soil and the depth of the soil for W in the driving forces equation. When combining this into equation 1.8 we can calculate the factor of safety for an infinite slope for a slide of thickness Z (Savage and Baum, 2005).

$$F_S = \frac{c' + (\gamma_s Z \cos\theta - \Psi\gamma_w)\tan\varphi'}{\gamma_s Z \sin\theta} \quad (1.10)$$

Where c' is the effective soil cohesion and ϕ' is the effective soil friction angle. The theory says that the slope is stable when Factor of safety is >1, in a limiting equilibrium when Factor of safety is = 1, and unstable when Factor of safety is <1 (Savage and Baum, 2005).

Infinite slope stability analysis is a simplification and it does not take into account for example differences in slope or vegetation. Vegetation can contribute to slope stability by reinforcing the soil, and can be calculated as a part of the cohesion term of factor of safety. There are also problems with uncertainties in the parameters used and this will affect the results. The factor of safety can be an indicator of the slopes stability, and can be calculated as a function of the slope angle, shown in figure 1.13. The dimensionless effective soil cohesion c*, pore pressure ratio r_u, and the slope angle value ranges that has been chosen are commonly encountered in practice and are based on Bishop and Morgenstern's work in 1960(Savage and Baum, 2005).

$$C^* = c'/\gamma_s Z \quad (1.11)$$

$$R_u = p/\gamma_s Z \quad (1.12)$$

The shaded areas in figure 1.13 indicate where the factor of safety is less or equal to 1 and the slope will fail calculated by using equation 1.10. For scenario one when the effective soil cohesion and pore pressure ratio is equal to zero, the infinite slope stability model is equal to the block on an incline in a state of limited equilibrium when the slope angle θ is equal to the internal angle of friction ϕ' . Scenario 2 the internal friction angle is decreases and the stability decreases. For scenario number 3, when the pore pressure ratio is increased to 0.70, the stability is decreased in a way that is similar to lowering the effective angle of internal friction in scenario 2. For scenario number four, the dimensionless cohesion is increased to 0.05 and the stability increases. And finally in scenario five the dimensionless pore pressure is decreased to 0.35 and the stability is increased again, but not as

stable as scenario 1 when the pore pressure ratio was zero. This show that the pore pressure is important for the stability of a slope, but it can be counteracted to a degree with an increase in cohesion (Savage and Baum, 2005).

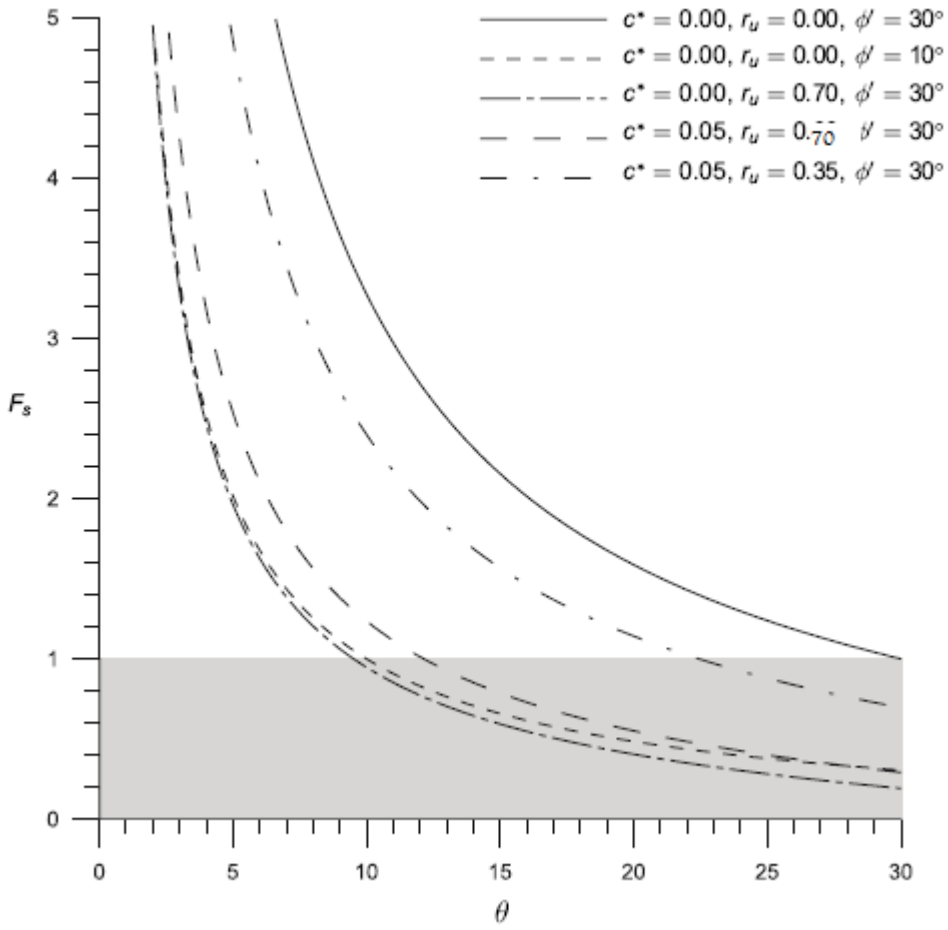

Figure 1.13 Factor of safety Fs for an infinite slope with typical values for slope angles θ, dimensionless soil cohesion c*, and pore pressure ratios ru. Shaded areas for situations when the factor of safety is less or equal to one, ϕ' is the effective internal friction angle. Figure is slightly changed from (Savage and Baum, 2005).

The factor of safety can also be expressed as

$$FS = A\frac{\tan\varphi\prime}{\tan\beta} + B\frac{c\prime}{\gamma H} \tag{1.13}$$

Where A,B are determined from figure 1.14, ϕ' is the effective friction angle, c' is the effective cohesion in the soil, β is the slope angle, γ is the unit weight of the sliding mass, and H is the vertical depth from the surface of the slope to the slip surface (Duncan, 1996).

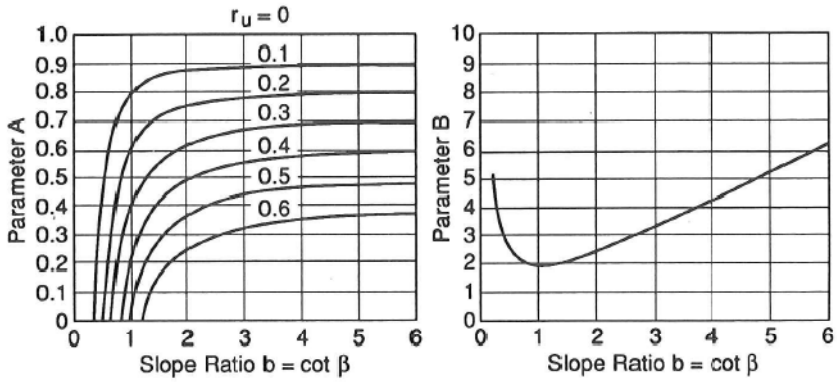

Figure 1.14 Stability charts for infinite slope stability analysis, used to calculate dimensionless stability coefficients A and B by pore pressure ratio, ru, and slope ratio (Duncan, 1996).

Ru is the pore pressure ratio and can be determined if it is known if the seepage of water in the slope is parallel to the slope or if it emerges from the slope, see figure 1.15.

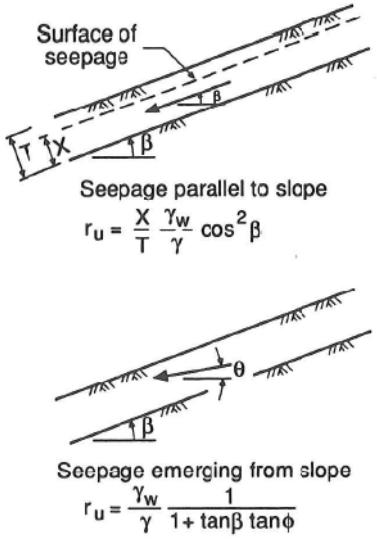

Figure 1.15 Show the seepage situation in soils on slopes, used to calculate the pore pressure ratio in the soil when the seepage is parallel to the slope, or emerging from the slope. Pore pressure ratio is used to calculate the factor of safety of slopes (Duncan, 1996).

1.8 Debris flow Motion

1.8.1 Debris flow dynamics

There are several different models that are used to explain debris flow dynamics, but the dynamics of a debris flow is not very well understood, compared to for example triggering mechanisms. The simplest way of explaining the dynamics is by assuming that the flow is a fluid, it is the possible to use fluid mechanics on the flow. Unfortunately it is clear that debris flow has a resistance to flow, and that this resistance is greater than that of water. A debris flow is therefore not a Newtonian fluid, but rather a non-Newtonian fluid (Takahashi, 2007).

If a debris flow is non-Newtonian it has shear strength that must be exceeded before the debris flow material can deform, which may result in plug flow where there is no deformation. The most common models used to explain debris flow dynamics are rheological models and Coulomb mixture theory, both will be described in detail in appendix E.

1.8.2 Runout Distance

It is important to try to predict the runout distance for debris flow, because of their importance for determining which areas will be affected, and the flow intensity. These two parameters are crucial for producing a hazard map. The runout of a debris flow is influence by many factors but the two most important are the slope angle and the lack of confinement in the runout zone(Rickenmann and Zimmermann, 1993).

There are two different methods for predicting debris flow runout, empirical-statistical and dynamic methods. Empirical-statistical methods are easy to use, but they can only be used for the same conditions as the data they were developed from. Dynamic models use the theory of energy conservation of the flow, and they are physically based. When predicting the runout it is important to decide how to measure the mass movement of the flow. The mass movement models are the mass point, lumped mass model, or continuum based models. Only a very simple empirical-statistical relationship between the runout distance and vertical displacement will be explained here (Rickenmann and Zimmermann, 1993).

Total travel distance of a debris flow

The total travel distance is the entire horizontal path length of the debris flow. A simplification used to find the travel distance is by using the Fahrböschung or the travel angle (β); it partially depends on the volume of the flow.

$$\text{Tan } \beta = H/L \tag{1.14}$$

Where H is the vertical distance between the starting point and the front of the depositional fan, and L is the horizontal distance between those two points. Channelized debris flow seems to have a higher mobility than unobstructed debris flows (Rickenmann and Zimmermann, 1993).

1.8.3 Liquefaction

Debris flows are mostly mobilized from debris flows (Iverson et al., 1997). The initial debris flow mass is transformed into a debris flow while it is sliding down a slope, in a channel, or a ravine when the material liquefies. The flow entrains eroded material while it moves down the slope and increases in size(Hungr et al., 2005). When the debris flow travels over the torrent bed deposits, high pore-water pressure can be generated within the torrent bed deposits due to undrained loading. This process

can enhance the mechanism for incorporating the deposits into the flow. This process of undrained loading of the torrent bed deposits has been shown to play a key role in the occurrence and motion of debris flows.

Liquefaction occurs when the soil rapidly loses much of the shear resistance in the soil because of high pore pressure being generated in the soil, and this can create a fluidized debris flow. Liquefaction can be triggered by for example earthquakes, or static effects such as precipitation, snowmelt etc., and the phenomenon are the topic of many studies(Wang and Sassa, 2003).

The mechanism of liquefaction is quite well known and will be explained in appendix E.

1.8.4 Transportation of material

Large boulders have been transported by debris flows, they can be found deposited on very shallow slopes surrounded by finer material (Johnson, 1970, Takahashi, 1981). When the boulders move with the flow they appear to float or tumble slightly. The boulders can sink into the flow due to gravity, and they are matrix supported. Five mechanisms have been suggested in explaining what keeps the solid load suspended and supported in the debris flow, and that prevents separation. All five mechanisms may be present during a debris flow, but only cohesive strength, buoyancy, and structural support can be present freshly deposited debris flow sediments (Costa, 1984).

Cohesion

Cohesion of clay-water slurries as an important particle support mechanism has been proposed by many (Johnson, 1970). Cohesive strength depends on the amount of clay in the debris. A clay and water slurry with a density of 1, 17 g/cm^3 can indefinitely suspends medium sand, while a clay and water slurry with density of 1, 26 g/cm^3 can support coarse sand. Since most debris flows only contain a low concentration of sand, normally below 8-10% clay, only sand-sized particle can be suspended indefinitely, but boulders with a diameter greater than 1 meter have been found in these debris flow. This means that particles that are coarser than sand in size must be supported by another mechanism (Costa, 1984).

Buoyancy

Buoyancy is an important mechanism for supporting particles in debris flows. The density difference between the fluid and the submerged solids determine the buoyancy. The buoyancy forces acting on a boulder is equal to the weight of all the displaced material, both solids and fluids. The density difference between the solids and the fluid can in many debris flows can be relatively small. The submerged weight of a boulder, decides how much of the particle weight in debris flow buoyancy can support. Costa calculated that if the particle density was 2, 65 g/cm^3, and the fluid density was 2, 0 g/cm^3, the submerged weight of the boulder would be 25% of the dry weight. If the density of the debris flow were 2, 4 g/cm^3, the submerged weight of the boulder would be 10% of the dry weight. This means that 75 to 90% of the particle weight in debris flows can be supported by buoyancy. If the pore pressure gradient is increased, due to a partial transfer of weight of solid particles to the pore fluid, the buoyancy effect can be enhanced. Dissipation of the pressure is prevented by the fine-grained matrix, and the pore pressure and buoyancy is increased. The shear strength is also reduced, and the mobility is increased (Costa, 1984).

Dispersive pressure

When high concentrations of poorly sorted grains are sheared by the debris flow, the larger particles will drift to the free surface. When particles collide, or nearly collide when they are shear over each other, forces are transmitted between them and this creates lift that transports the larger particles. Bagnold called this the dispersive pressure, and created an equation to calculate it. The dispersive pressure increases when the particle size increases, this means that the larger particles are forced away from the zones of maximum shearing. These zones are near the channel bed, the coarse particles will therefore move towards the front and the top of debris flows. This might help explain the reverse grading found debris flow deposits, called the Brazil nut effect (Costa, 1984).

Turbulence

The variation of velocity in direction and magnitude with time is known as turbulence. It is an important factor for sediment transport and entrainment. Fine-grained material in water, decrease the fall velocity of particles, 5% silt by weight decreases eddy currents and therefore also the turbulence in the flowing water. How important turbulence is in debris flows is questionable, because most debris flows appear to be laminar, and they have a high viscosity and cohesion. Debris flows can also preserve delicate clasts and brittle fragments, and this does not coincide with turbulent flow. It has been observed that when the water content of the flow increases, turbulence becomes more important for sediment transport in debris flows (Costa, 1984).

Structural support

Cohesion and buoyancy in static debris flow deposits is not sufficient to support the submerged weight of large particles. This means that some other mechanisms must support the submerged particles, other than cohesion and buoyancy, and keep the particles at their attained level. Structural support is the grain-to-grain contact, and this is the framework of the particles that are in contact with the bed and with each other. When the sediment concentrations are 35 to 58% the structural support can support 1/3 of the coarse particles weight. Cohesion, buoyancy and structural support are the mechanisms that keep large boulders suspended in debris flow deposits, structural support will not occur in dynamically moving debris flows, then turbulence and or dispersive pressure will occur in a combination with the cohesive strength and buoyancy. Since the physical properties of debris flows are varied, the importance of the difference particle support mechanisms will vary for each flow (Costa, 1984).

1.9 The Study Area - Veikledalen, Norway

1.9.1 Geology

The geology of Norway has a long and rich history leading to massively contorted rocks, hydrocarbon resources, dramatic topography and the present day soils. An extensive review is given in the excellent book The making of a Land- The geology of Norway, and a brief overview is included in appendix B.

The Quaternary period were from 2, 7 million to 11 500 years ago. This period was dominated by large inland ice sheets that covered entire continents. Almost all the soil in Norway was created in this period as an erosion product from these large ice sheets. There were several ice ages with melting in between each period of glaciation, called interglacial periods. There has been close to 50 small ice ages in the Quarternary period. The climatic cycle normally lasted either 41 000 years or 23 000 years, and were controlled by the variations in earth's axis tilt and the axis precession. The last ice age in Norway was called Weichsel and lasted from 117 000 years ago to 11 500 years ago. The ice age is then further divided into periods of warmer and colder cycles. The ice ages are what created Norway's fjords and from the shape, jagged or rounded shaped, of the mountains it is possible to see if there were underlying the ice sheet. Most of Norway is covered by the erosion product from Weichsel, but the influence of the ice sheets can also be seen in other ways, for example by glacial striations or glacial erratics. Most of the erosion products created by the last ice age were deposited on the continental shelf. In some places layers up to 3000 to 4000 meter thickness, have accumulated on the continental shelf. The continental shelf has been eroded by the ice sheets closest to shore and this has shifted the load on the crust. The landmass and the inner continental shelf have lifted, while the outer shelf has sunk in (Ramberg et al., 2007).

The last epoch is called the Holocene and is part of the quaternary period and has lasted from 11 500 years ago and until today. Most of what has happened in the Holocene has been the after effects of the last ice age. Landmasses have lifted and the ocean level has been raised due to the melting of the ice sheets. Most of the fauna and flora we have today have come in this epoch and they have been transported from areas that were less or not affected by the ice ages. Humans have also started to affect the planet, by cutting down forests and covering enormous areas with concrete or asphalt. In Norway it is the development of river deltas, erosion processes, and the landslide activity from steep valley sides that are the most noticeable geological processes. The climate has also varied in these last 11 500 years, an important reason for some of the changes were the creation of the Gulf stream (Ramberg et al., 2007).

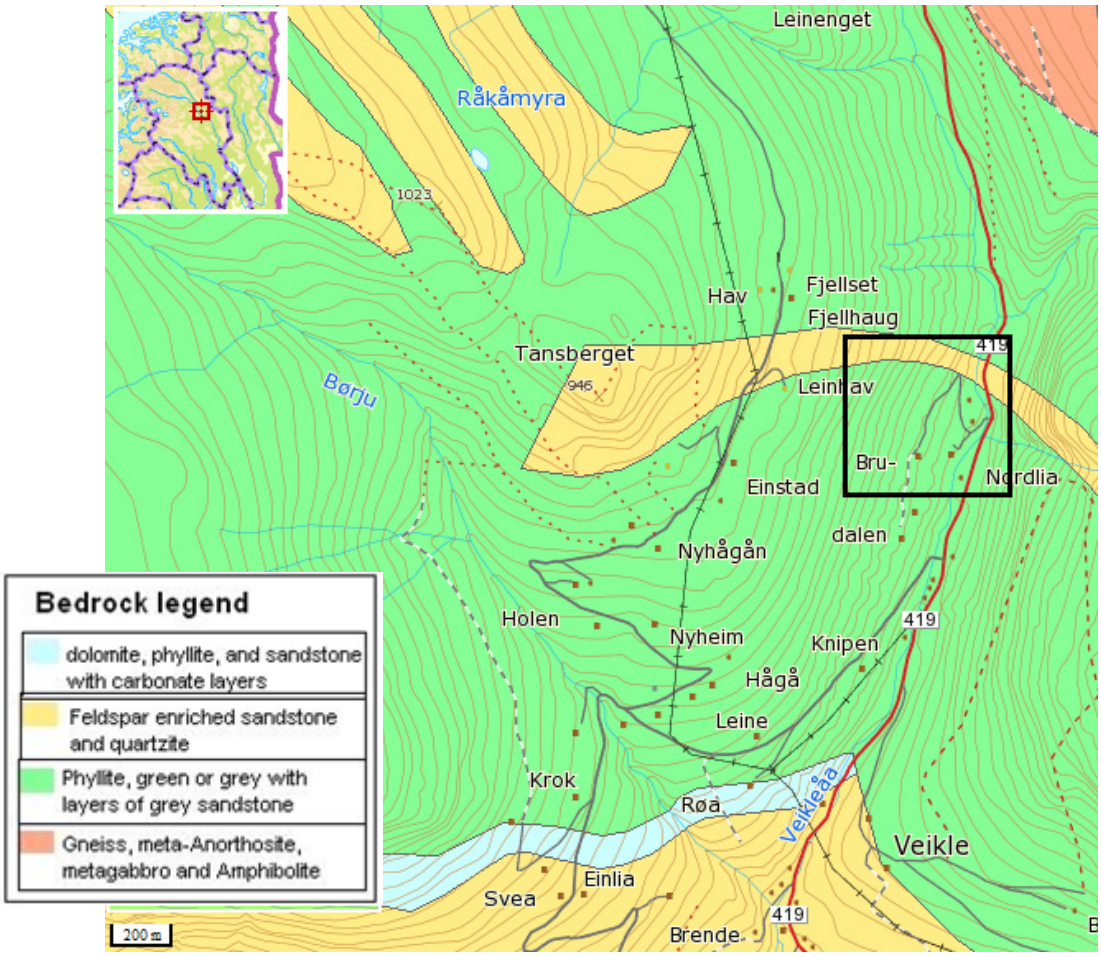

Figure 1.16 Local Geology in the Veikledalen area, the study area is marked by the black square. (NGU, 2012).

Figure 1.16 shows the local geology in Veikledalen valley. The main bedrock in the area where landslides were triggered is phyllite with layers of sandstone.

This area was affected by the Caledonian orogeny event where layers have been thrust up and over the bedrock below. A boundary between these thrust movements can be seen in the upper right corner, the boundary between the phyllite and the gneiss. The rocks are metamorphic, which means that they have undergone metamorphism, probably during the Caledonian orogeny event. Since phyllite is a low-grade metamorphic rock, and gneiss is a higher grade metamorphic rock, it is a clear indication of the rocks being created and moved to this located under different circumstances. It is evidence for the thrust movements that pushed rocks on top of the existing rocks.

- **Phyllite** is a low-grade metamorphic rock in the lower part of the greenschist facies. It is fine-grained, i.e. the diameter of the grains are less than 0,1 mm, and the parent sedimentary rocks are normally mudstones or shale's, and due to the low grade metamorphism it might be possible to partially preserve the original mineralogy and sedimentary bedding. Phyllite has a strong fissility and a surface sheen, because of the parallel orientation of phyllosilicate minerals (e.g. chlorite, muscovite, and sericite)(OxfordUniversityPress, 2003).

- **Sandstone and quartzite:**
  - ***Sandstone*** is a sedimentary rock, formed by lithified accumulation of sand-sized grains, i.e. 0,063mm to 2mm in diameter. The grains are bound together by matrix

cement that was formed during diagenesis. Main minerals in sandstone are quartz, feldspar, mica and general rock particles. Since this rock is feldspar enriched it contains more feldspar than normal sandstones (OxfordUniversityPress, 2003).

- ***Quartzite*** is a metamorphic rock that has normally been formed by the metamorphism of sandstone. By the name it is understood that in mainly consists of quartz, which makes them be predominantly white and smooth. Quartzite has a fine angular jointing and can break up due the frost. quartzite creates thin and quite barren soil, due to a slow weathering process. They can therefore protect the rocks underneath and form ridges or hills. Since this rock has both sandstone and quartzite it can be assumed that metamorphism has started in the rock, but that it was not completed, and that the metamorphism that did take place was quite low-grade (OxfordUniversityPress, 2003).

- **Dolomite, phyllite and sandstone with carbonate layers:**
  - ***Dolomite*** is a type of limestone, but it consists of the rock forming mineral dolomite (i.e. calcium magnesium carbonate [$CaMg(CO_3)_2$]). It is a sedimentary rock that can preserve its sedimentary structures if it is formed quickly after deposition. Late-diagenetic recrystallizied dolomites produce coarser- grained rocks and there is an increase in porosity. The dolomite is layered with phyllite, sandstone and carbonate layers (OxfordUniversityPress, 2003).

- **Gneiss, Meta-Anorthiosite, metagabbro and Amphibolite:**
  - ***Gneiss*** is a medium to coarse-grained, banded, high-grade metamorphic rock,. Gneiss has poorly developed schistosity and cleavage, but well- developed foliation. Banding is normally due to separation minerals, e.g. of mafic and felsic material. Banding can also be due to different grain sizes. The bandings orientation can be used to interpret the stresses that prevailed when the rock was formed. Gneiss can be classified by the parent rocks that formed the rock; orthogneiss is formed by igneous rocks, while paragneiss is formed by sedimentary rocks. Normally consist of mica, feldspar and quartz(OxfordUniversityPress, 2003).

  - ***Meta- Anorthosite*** is a plutonic igneous rock that is formed by almost only coarse crystals plagioclase feldspar (i.e. 90% or more). Are predominantly found in Precambrian shield areas, and are often found as laccoliths, lopoliths or sills. The prefix of meta means that the anorthosite has undergone metamorphism (OxfordUniversityPress, 2003).

  - ***MetaGabbro*** is a coarse grained, basic, igneous rock. The main minerals in gabbros are plagioclase feldspar (approximately 60%), and pyroxene. They are formed by slow crystallization of basaltic magmas, and can be either alkali or tholeiitic. The meta prefix implies that the gabbro has undergone metamorphism (OxfordUniversityPress, 2003).

- ***Amphibolite*** is a medium-grained, regional metamorphic rock. It is dark coloured and mainly composed of hornblende and plagioclase. They are the diagnostic rock in the amphibolites facies and show regional metamorphism. The parent rocks can be mafic igneous rocks (e.g. gabbro and basalt) or sedimentary dolomite (OxfordUniversityPress, 2003). All these rocks contain plagioclase feldspar in different percentages. All the rocks have undergone metamorphism of a higher grade than the sandstone and phyllite rocks and since it is known that the boundary between these layers are the boundary of the thrust fault movement, the classifications of these rocks confirm this theory.

1.9.2 Sediments

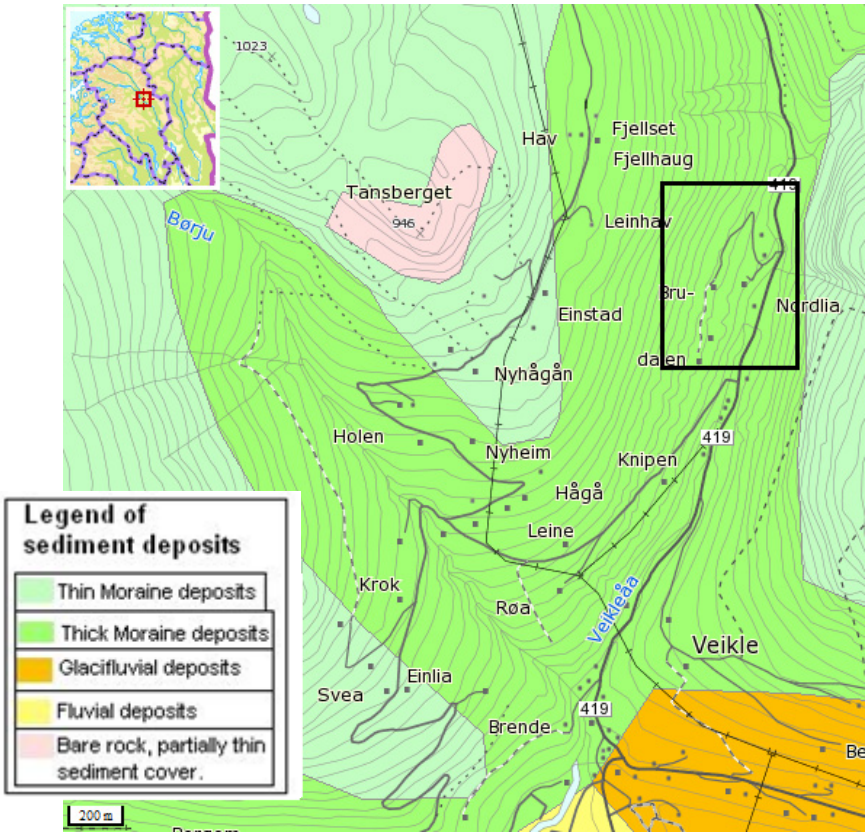

Figure 1.17: Sediment deposits in Veikledalen, the study area is marked by the black square (NGU, 2012).

The sediments that are present in Veikledalen can be seen in figure 1.17. There are moraine deposits in the valley and they are either thick or thin, the map shows a clear boundary between the thin and thick deposit zones but in reality the boundary will probably be gradual. The Moraine deposits are a result of the last glaciations period Weichsel that melted approximately 10 000 years ago and are named till. The material has been picked up or eroded, transported and then deposited by the ice sheet. Till can consist of large rocks, sand, silt or clay fraction sized grains and are therefore poorly sorted. The thick till have a thickness from approximately 0,5 meter to several ten's of meters, thin deposits are normally thinner than 0,5 meter. The top layer of the till has been affected by frost that has slowly weathered the till into a layer of loose soil, which has a high permeability. This top layer is where the water can flow and normally where landslides are triggered(Dahl et al., 1981).

Norwegian Till

The ice sheet cover and movement over Norway during the last glaciations event can be seen in figure 1.18, Veikledalen is here shown to be beneath the ice sheet divide and therefore under the area of the ice sheet where the ice thickness is at its maximum and the movement of the ice is very low (Sørbel, 1999). The material deposited in the Veikledalen area is therefore sub-glacial lodgement tills which are normally rich in fine-grained material. But the grain-size and material present in the till depends on the rocks it has been eroded from. Due to the thickness of the ice above the sediments they have been compacted has become hard (Sulebak and Sjøstrøm, 2007).

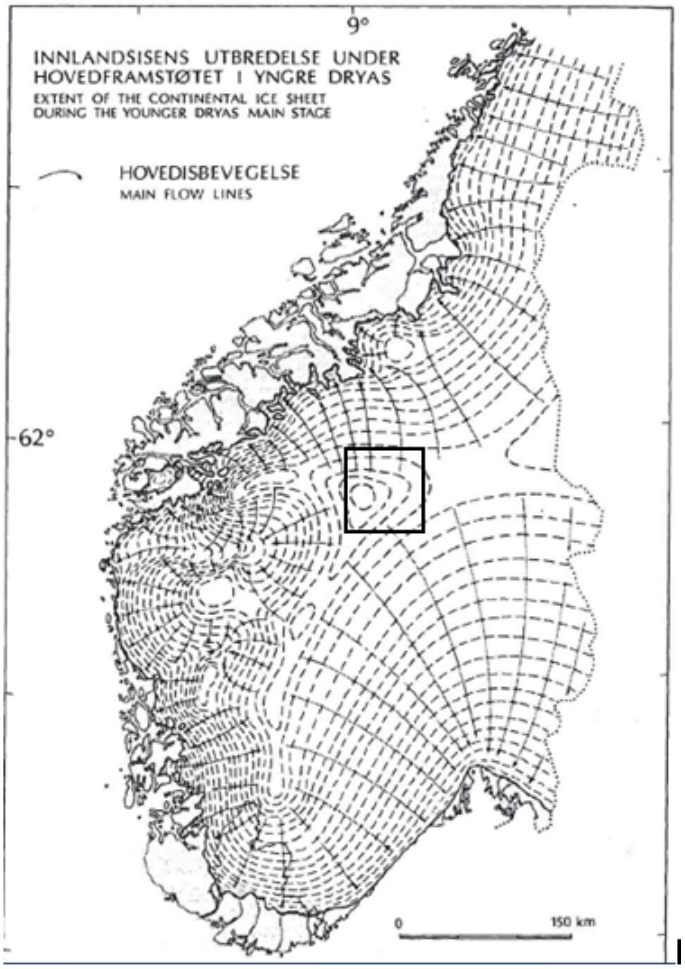

Figure 1.18 The main flow lines of the continental ice sheet during the Younger Dryas main stage (Sørbel, 1999).

In Norway till is the main Quaternary sediment in Norway and it is only covered by younger sediments along some valley bottoms and below the marine limit. The properties of tills in Norway are controlled by elevation, topography, bedrock, and the ice. The till cover in Norway is generally discontinuous and the thickness only locally exceeds 1-2 meters. The till cover in the Veikledalen area in the eastern part of Norway is thicker and more continuous, than the till cover in the western part of Norway. Eroded material was transported towards the ice margins and some of the eroded material from Norway can be found on the continental shelf. The eroded material found as sediments in Norway today has normally not been transported longer than 5 kilometres and it will therefore contain the same minerals as the bedrock in the vicinity. The uplands are covered by local material, while the valleys that were used as outlet channels for ice streams contain material that have been transported much further (Haldorsen, 1983). Norwegian tills are generally coarse grained

with a clay content below 10% (Jørgensen, 1977) , but for tills that are eroded from Cambro-Silurian sediments the tills contain more clay, see figure 1.19.

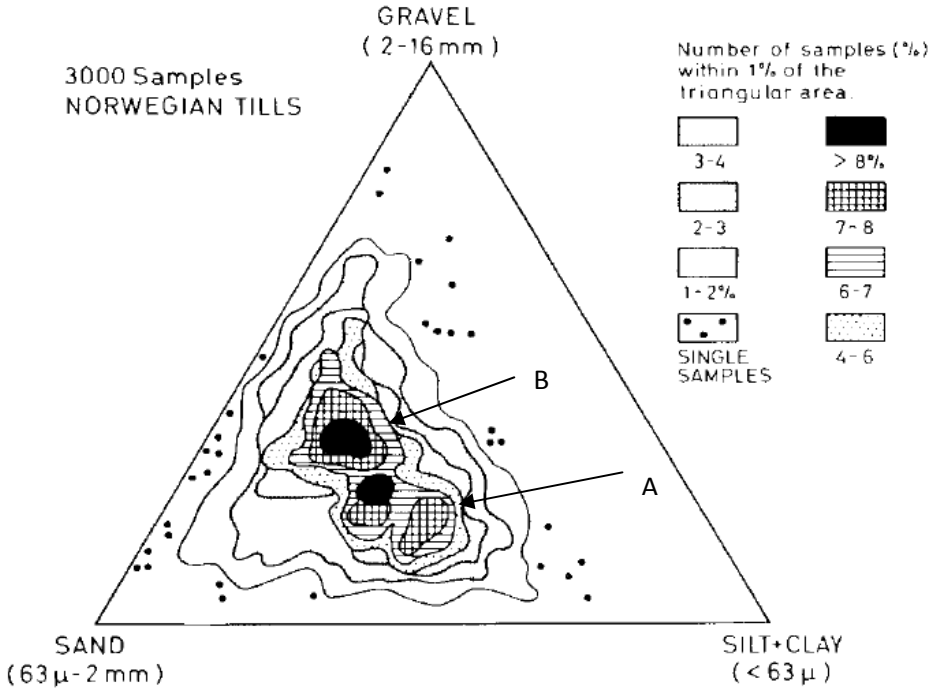

Figure 1.19 Grain-size distribution of Norwegian tills. The samples show to concentrations due to the bedrocks the till were eroded from. A= The more fine-grained concentration and are samples taken from tills from Cambro-Silurian sediments, B= the more coarse grained samples and are from all other bedrock types (Jørgensen, 1977).

1.9.3 Groundwater and infiltration of water in the soil.

Figure 1.20 shows the infiltration ability for the area, if this figure is compared with figure 1.17 that shows the sediments of this area it is clear that the thick moraine deposits have a higher ability to infiltrate water than the thin moraine deposits. This is probably due to the thin weathered top soil layer in the moraine deposits. In the thick deposits the weathered layer could be thicker than in the thin deposits and the infiltration ability of the soil will therefore be higher in the thick moraine deposit soils. The same difference can be seen for groundwater potential as well, figure 1.21. The groundwater potential for the Veikledalen area is limited or nonexistent, the limited groundwater potential coincide with the thick moraine deposits and the moderate ability to infiltrate water. This shows that the thick moraine deposits can contain more water than the thin moraine deposits.

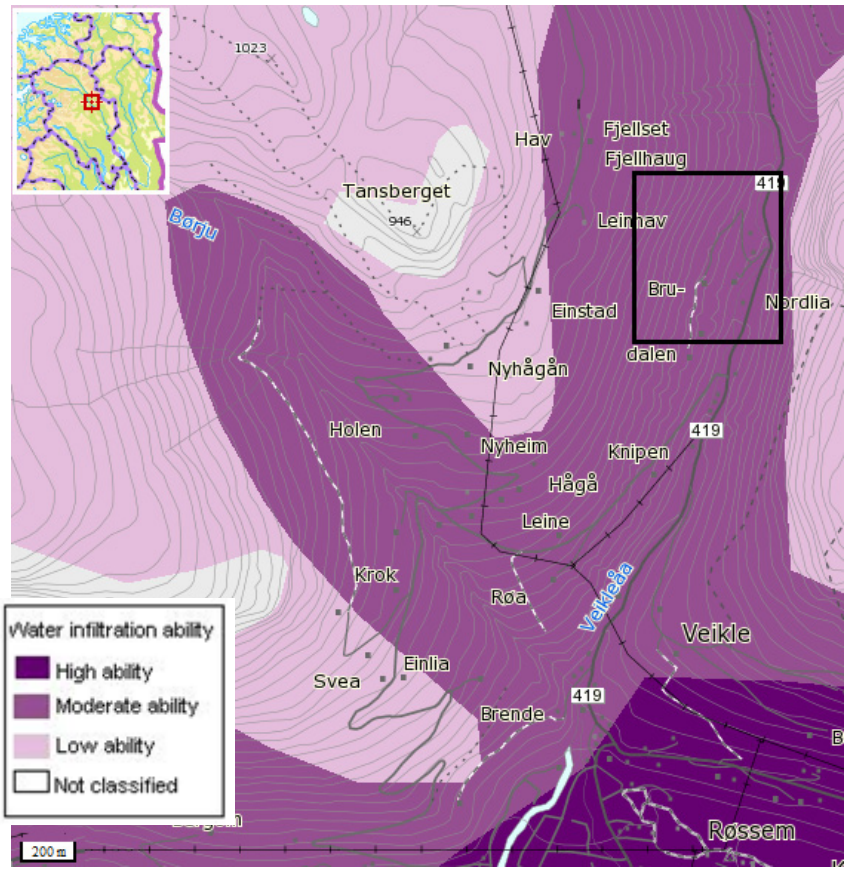

Figure 1.20 Estimated water infiltration ability of soil in the local area. Study area marked by black square (NGU, 2012).

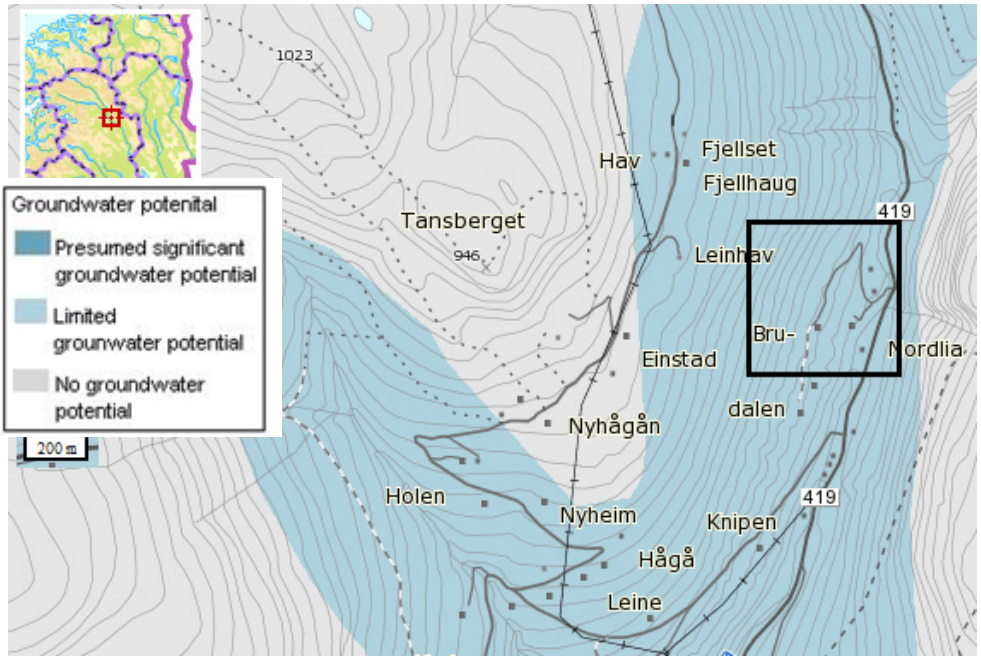

Figure 1.21 Groundwater potential in the sediments, study area marked by black square (NGU, 2012).

2 Methods

2.1 Field Work

Two fieldtrips were completed; the first was a one day field trip due to weather from the 15th to the 17th of April, 2012. The second field trip was done to find additional information and was completed on 23rd of May, 2012. On the second field trip GPS measurements of landslide tracks were undertaken with 10 meter intervals were this was possible, width and depth of the landslide track was also measured, together with the depth of the erosion and deposition. Slope angles were measured at one location at each GPS point on the surface, and the slope angle vary on the surface due to local topography so the slope angles can be inaccurate. Grain size was estimated by taking pictures of the material with a 1 meter long measuring stick, picture of approximately $1m^2$ of the material.

2.2 Precipitation data

Precipitation is collected in a collection device at a weather station, and then measured in millimetres, with an uncertainty of a tenth of a millimetre. The five chosen weather stations are different types. Sjoa, Hovdgrenda, and Espedalen are manual precipitation weather stations. Precipitation is measured once a day, at 07.00am (8 am in summertime) for the last 24 hours, the results are then sent to the Norwegian Metrological Institute every week by mail from Sjoa and Hovdgrenda weather stations, while Espedalen weather station sends the data in real time by computer to the Norwegian Metrological Institute (NORWEGIANMETEROLOGICALINSTITUTE, 2012a).

Skåbu and Venabu are automatic weather stations that measure air temperature two metres above the ground. The stations can also register the maximum and minimum temperature in the last hour. Air moisture content, and air pressure is also measured. Average wind speed and direction is measured 10 metres above the ground, and maximum average wind speed and gale wind speed is also determined (NORWEGIANMETEROLOGICALINSTITUTE, 2012b). Venabu weather station only measures precipitation every 24 hours at 7 am (8 am in summertime), while Skåbu weather station measures precipitation every hour (NORWEGIANMETEROLOGICALINSTITUTE, 2012a).

Precipitation maps presented in this thesis are created by the NVE and the Norwegian Metrological Institute using precipitation data from weather stations in Norway. The precipitation data is interpolated and then a precipitation map for the last 24 hours, or the last 7 days for an area is created (NVE et al., 2012). Precipitation data and precipitation maps are publically available.

2.2.1 Rainfall thresholds

Rainfall thresholds are used to predict if a rainfall event will trigger a landslide or not. The most commonly used threshold were created by Caine, and it has been created by collecting 73 observations of published rainfall events, where the rainfall intensity and duration was recorded. Only the rainfall events that produced a debris flow were selected. The threshold , equation 2.1, is a general equation for the entire world and it is valid for shallow (2-3 meters deep) debris flows and landslides (Caine, 1980).

$$I = 14{,}82\ D^{-0{,}39} \qquad (2.1)$$

Where I = rainfall intensity (mm/hr), D= duration of rainfall (hr). Plotted on duration vs. intensity graph, this equation creates a limiting curve. If a rainfall event exceeds the threshold, a landslide will

occur. The equation is valid for rainfall durations between 10 minutes and 10 days. Of all the 73 observations Caine used, only 8 did not match this criteria, but 7 of those observations can be explained by the observations being classified as rainfall greater than or mean intensities of rainfall for more than 10 days. The final observation was involving rainfall falling onto melting snow, and more water that was not rainfall could therefore infiltrate the soil (Caine, 1980).

A different approach to rainfall thresholds is made by Reid. He has created a simple pressure diffusion model, where the surface has flux boundary conditions. Reid's model makes it possible to compare rainfall intensity and duration, with pore pressures created in the soil. The rainfall intensity and duration for a rainfall event is classified by Reid as a sinusiudally oscillation flux over time per unit area. This is a simplification, but it explains real storms better than the average intensity for a given duration that is used by Caine, and it is easier to find peak rainfall intensity. The model starts with a simple diffusion model, the model is one dimensional, vertical, transient, and a Darcian flow. The model also assumes homogeneous soil (Reid, 1994).

$$2F_0 = p_{max} K \alpha \sqrt{2e^{\alpha z_d}} \qquad (2.2)$$

Where $2F_0$= peak rainfall intensity per unit area, p_{max}= maximum pressure head, K= hydraulic conductivity, $\alpha = \sqrt{\pi}/(Dt_0)$ D = hydraulic diffusivity. T_0= duration (oscillation period). Z_d= given depth of p_{max}.

If an increase in the pressure head that is created at a certain depth, and that causes a destabilization, is know, then equation 2.2 can find the rainfall intensity and duration that caused the increase in the pressure head. Equation 2.2 defines a rainfall stability criterion, where events that are above the curve will fail. More information is needed to use equation2.2 compared to equation 2.1 and it is therefore more useful in many cases to use equation 2.1, because even though equation 2.2 might be more accurate, the information needed might not be present. Both equations have the problem that all the rainfall that falls might not infiltrate the soil, for example due to surface runoff or interception by vegetation. These processes can affect the results because the rainfall event might not be as destabilizing as could be expected by the rainfall intensity and duration number.

2.2.2 Antecedent rainfall

Intense rainstorms might not be enough to trigger debris flows, the antecedent rainfall, the pre-storm rainfall, is important. The soil moisture content and groundwater level is largely based on the antecedent rainfall. How important it is for triggering debris flows was demonstrated in northern California by Wieczorek and Sarmiento, for the time period 1975 to 1984 they took 22 observed storms and divided them into three groups based on the antecedent seasonal rainfall and the triggering of debris flows by the storms. They found that the 10 intense storms that occurred before 280mm of seasonal rainfall, triggered debris flows. The 10 intense rainstorms that occurred after 280mm of seasonal rainfall did trigger debris flows. The low intensity rainstorm that occurred after 280 mm of seasonal rainfall did not trigger debris flows (Wieczorek, 1996).

The time period that builds up antecedent soil moisture before the event has not been agreed upon. Everything from 2 to 45 days before the debris flow is triggered, have been reported as contributing to the soil moisture content. There are also different time periods published for different countries, for example 15 days in Italy and 4 weeks in Seattle, Washington (Wieczorek, 1996).

2.3 Soil , groundwater, and runoff data

All the maps presented in this thesis use a spatially distributed version of the HBV hydrology model, also known as the Hydrologiska Byråns Vattenbalansavdelning model which is often used to analyze river discharge and water pollution. The input variables are spatially distributed air temperatures and precipitation data estimated for 1 square kilometre blocks. The data comes from the weather stations operated by the Norwegian Metrological Institute, or weather forecast models are used for prognosis meteorological data, and the data is publically available. All the maps are calculated for the conditions at 7am (8am summer time) for the selected date (NVE et al., 2012).

The “soil water deficit maps” are created by calculating the soil water storage in millimetres; this is done by finding the difference between the simulated actual water storage in the soil and the field capacity. Data are also presented as “soil water deficit map compared to normal”, which use the same model, but it compares the value with means values on the same day from 1990 to 2008. The difference between the normal value and the actual value that day is presented by percentile with the following classes: Very wet (above 95th percentile), Wet (75th - 95th percentile), Normal (25th - 75th percentile), Dry (5th – 25th percentile), Very dry (below 5th percentile)(NVE et al., 2012).

Groundwater data are presented as a “groundwater compared to normal map”. These use the same model and percentiles as the “soil water deficit compared to normal map”, but show the groundwater level which has been compared with the average groundwater level from the same day in the period from 1990 to 2008. The groundwater level is shown in millimetres of water that is stored in the saturated soil. The values are given in the same percentiles as for the soil water deficit compared to normal map. The total daily runoff also uses the HBV model and shows the total runoff which is the sum of surface and groundwater runoff given and is given in millimetres (NVE et al., 2012). These models are not very accurate on a small scale, each cell is one km^2.

2.4 Flooding

Flooding occurs when the water level in a river or a lake exceed the normal water level. There are roughly 600 measuring stations in Norway that measure the water level every hour, 365 days a year. The data that is collected is used to find the water discharge, for data to be as accurate as possible it is important to find the connection between the water level and water discharge for a river or a lake. The water level can be measured by different methods but a minimum of 12 to 20 measurements for a station at different water levels, from low water levels to flooding is needed to find a good fit between the water level and the water discharge for the station (NVE, 2012).

3 Data and Observations

3.1 Precipitation

The weather in the days and weeks before the debris flows were triggered has been collected from public databases(NORWEGIANMETEROLOGICALINSTITUTE, 2012a). The precipitation data if no other information is given have been measured at 07.00 am for the previous 24 hours. Five weather stations close to the location of the study area have been selected to show the precipitation in the area. The location of these weather stations in relation to the study area can be seen in figure 3.1.

Station name	Stnr	Operates from	Operates until	Altitude	Longitude	Latitude	distance to study area
Venabu	13420	aug 1980		930 m	61,6513	10,1087	23 km
Hovdgrenda	13450	jan 1972		666 m	61,6643	9,9744	15 km
Espedalen	13700	oct 1942		928 m	61,4167	9,5347	32 km
Skåbu new	13655	jun 2011		752 m	61,5308	9,4023	24 km
Skåbu old	13670	oct 1968	mar 2010	890 m	61,5152	9,3823	26 km
Sjoa	14050	nov 1986		330 m	61,6757	9,5562	8 km

Table 3.1 Information on all the weather stations which data is used in this thesis, the station number for each station, operation length, altitude, longitude, and latitude information is from (NORWEGIANMETEROLOGICALINSTITUTE, 2012a), distance to study has been calculated by using maps from (Kartverket, 2009).

The normal monthly precipitation values for each station has been used to compare with the precipitation data from 10th of June 2011 to see if the weather that day was abnormal. The normal monthly precipitation values for the weather stations were determined by (NORWEGIANMETEROLOGICALINSTITUTE, 2012a) as the average monthly precipitation for individual months during the period 1961 to 1990, shown in table 3.2. This means that not all the stations have the ideal number of data points to calculate normal monthly precipitation. Particular examples are Sjoa weather station where there are only three years of data, and the new Skåbu weather station that only opened in June 2011. Due to Sjoa being the closest weather station to the study area it is highly relevant and will still be included in the thesis. The precipitation data on the day are good but there are limitations in comparing the precipitation values with the normal monthly precipitation values. For Skåbu there was an old weather station that operated from October 1968 to march 2010 that can be used to calculate normal monthly precipitation. Since the two weather stations are only two kilometres apart from each other (see figure 3.2) the normal monthly precipitation data from the old weather station in Skåbu should be reasonable similar to the normal precipitation for the new weather station and it can be used as a substitute for the missing data. There are statistical methods for estimating monthly normal values for precipitation between weather stations but this will not be done here.

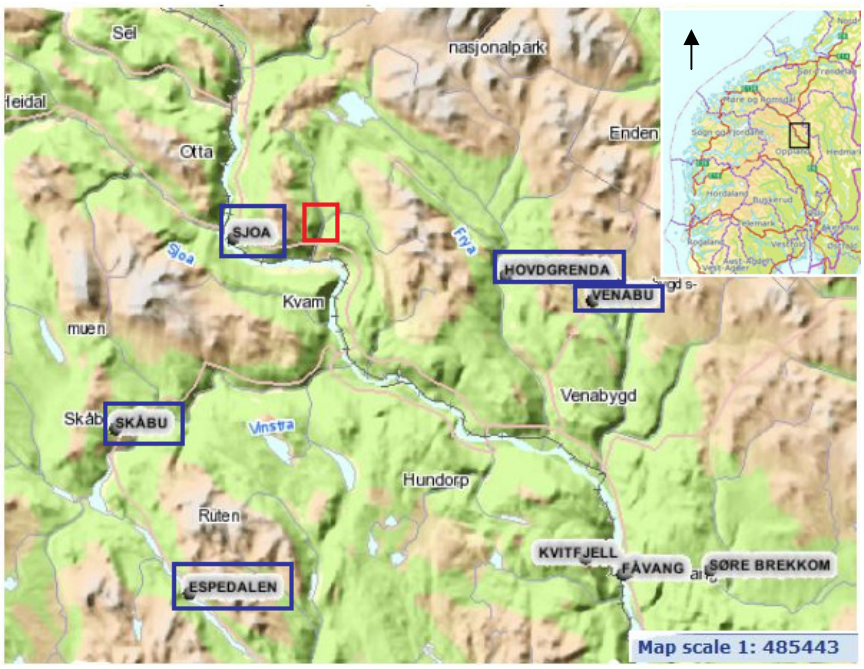

Figure 3.1 The five chosen weather stations marked in blue squares near the study area in Veikledalen marked by the red square. Weather stations Hovdgrenda, Venabu, Espedalen, and Sjoa give daily precipitation data, while Skåbu gives hourly precipitation data. Arrow show geographical north on both maps, the small map in the corner show where the area is located in southern Norway marked by the black square. The large map with the weather stations is from (NVE et al., 2012), the small map in the corner is from (Kartverket, 2009).

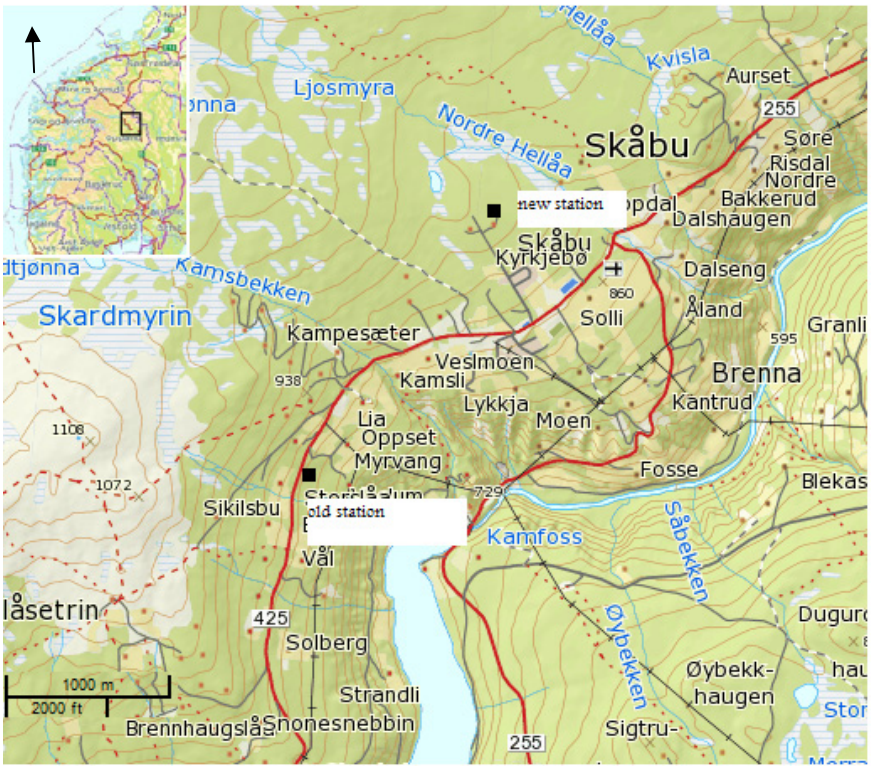

Figure 3.2 The placement of the old weather station in Skåbu number 13670 closed in march 2010, and the new weather station number 13655 opened in June 2011. The distance between the two stations is 2,3 kilometres. Arrow show geographical north on both maps, the small map in the corner show where the area is located in southern Norway marked by the black square. Maps from (Kartverket, 2009), coordinates of weather stations from (NORWEGIANMETEROLOGICALINSTITUTE, 2012a).

Station name	jan	feb	mar	apr	may	jun	july	aug	sep	oct	nov	dec	total
Venabu	36	26	32	29	48	78	87	88	70	70	52	41	660
Hovdgrenda	35	23	28	24	41	68	78	80	66	65	45	37	590
Espedalen	40	26	31	27	52	76	84	84	76	74	55	40	665
Skåbu old	34	21	27	23	44	62	74	70	54	53	45	33	540
Sjoa	28	18	20	16	32	52	56	55	46	47	34	26	430

Table 3.2 Monthly normal precipitation in mm for weather stations Venabu, Hovdgrenda, Espedalen, Skåbu, and Sjoa. Data collected from (NORWEGIANMETEROLOGICALINSTITUTE, 2012a).

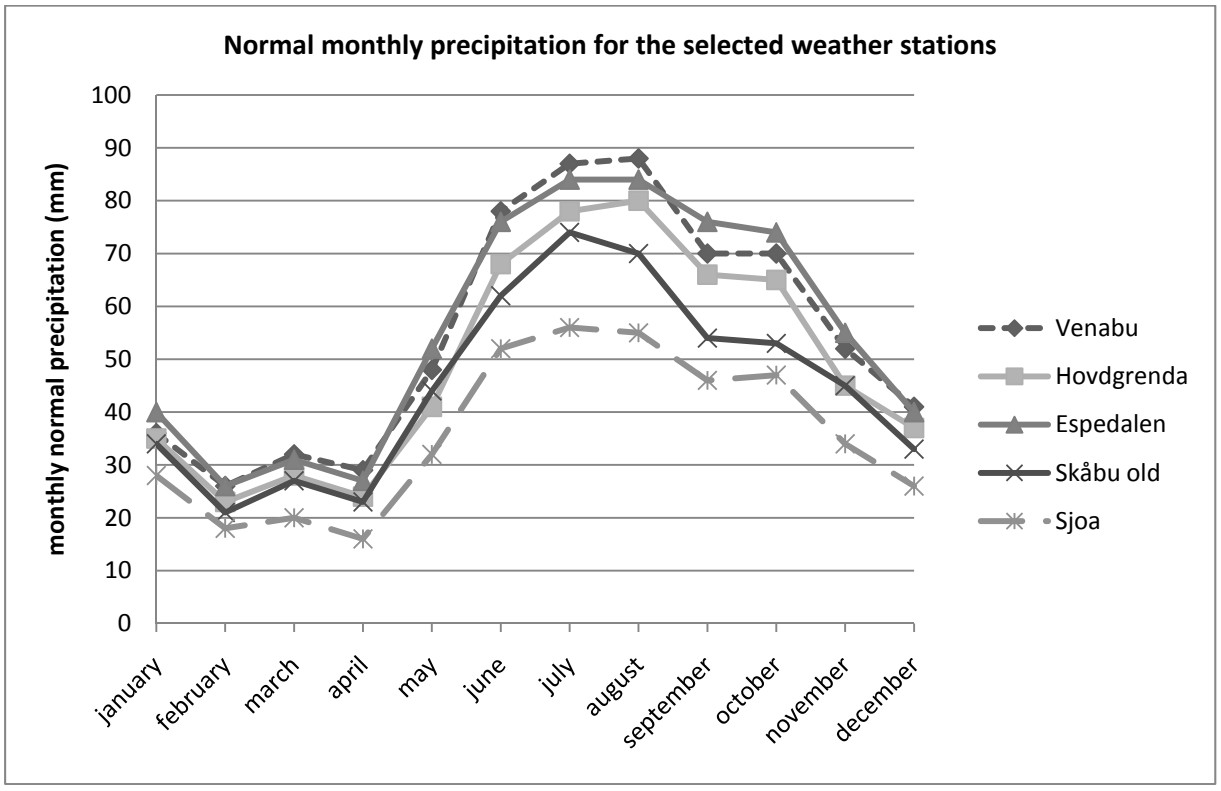

Figure 3.2b Normal monthly precipitation in mm for selected weather stations, data from table 3.2.

Figure 3.2b show that the highest precipitation for the area is in the summer months, whereas the winter months are relatively dry. The graph illustrates that Sjoa, the weather station nearest the study area, has similar pattern of precipitation during the year to the other local weather stations but that the absolute values are lower.

The precipitation measured at the five weather stations will now be presented to compare precipitation on 10th of June with the daily precipitation for the rest of the year for each station. Figure 3.3, 3.4, 3.5, 3.6, and 3.7 show daily precipitation in 2011 for Sjoa, Skåbu, Venabu, Hovdgrenda, and Espedalen respectively.

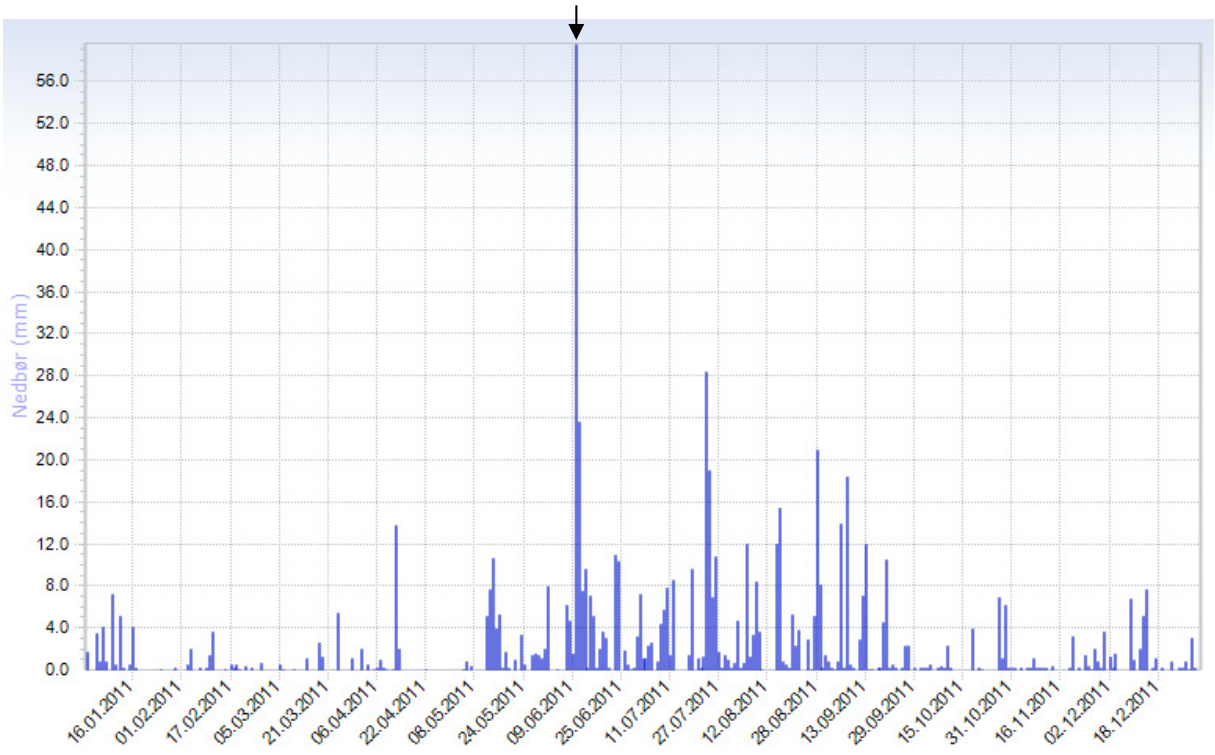

Figure 3.3 Daily precipitation values in mm for Sjoa weather station presented on the left axis vs. dates in 2011. Largest spike represent 10th of June 2011, marked by arrow (NVE et al., 2012)

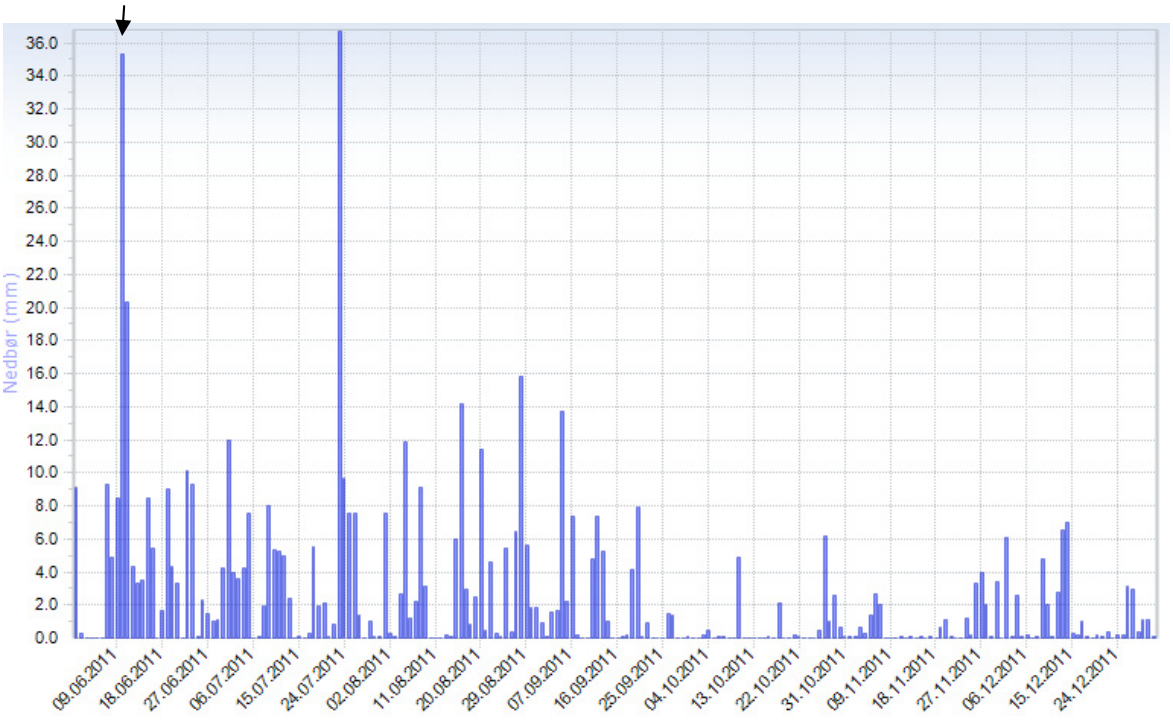

Figure 3.4 Daily precipitation values in mm for Skåbu weather station presented on the left axis vs. dates from June 2011 until December 2011. There are two large spikes for the daily precipitation for the weather station, the first represent 10th of June 2011, marked by arrow (NVE et al., 2012).

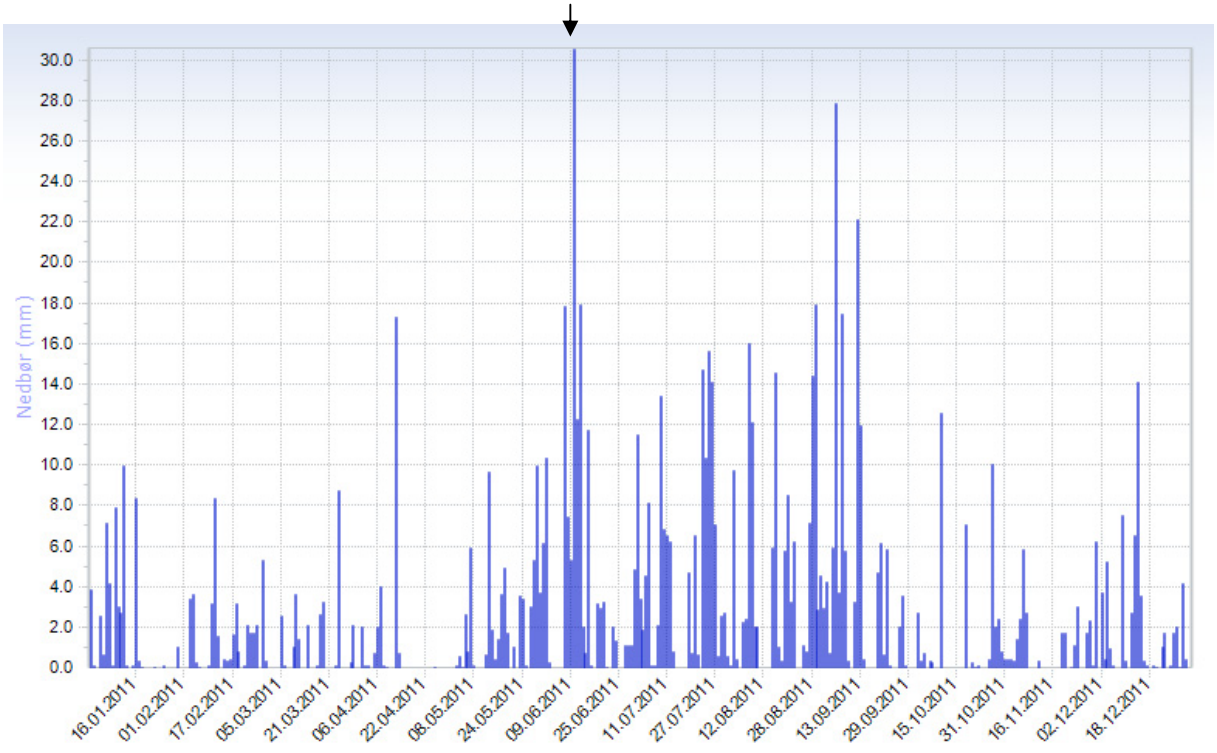

Figure 3.5 Daily precipitation values in mm for Venabu weather station presented on the left axis vs. dates in 2011. The largest spike for the daily precipitation for the weather station represent 10th of June 2011, marked by arrow (NVE et al., 2012).

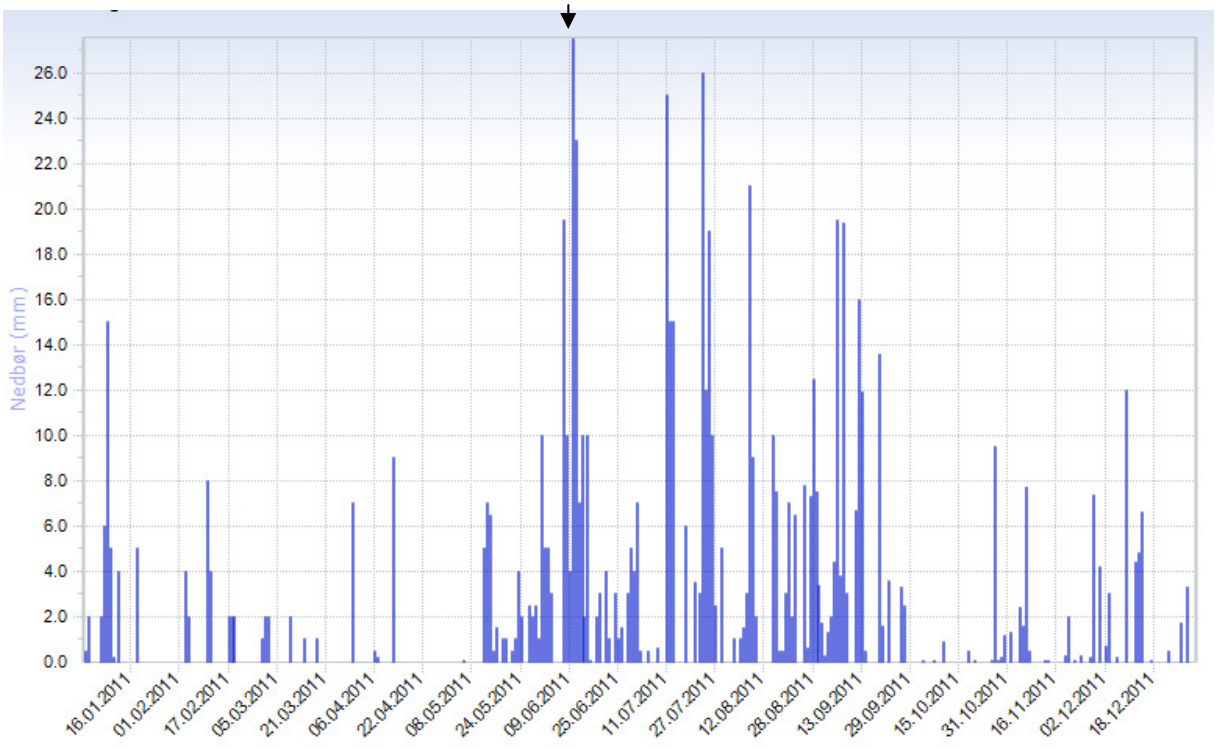

Figure 3.6 Daily precipitation values in mm for Hovdgrenda weather station presented on the left axis vs. dates in 2011. The largest spike for the daily precipitation for the weather station represent 10th of June 2011, marked by arrow (NVE et al., 2012).

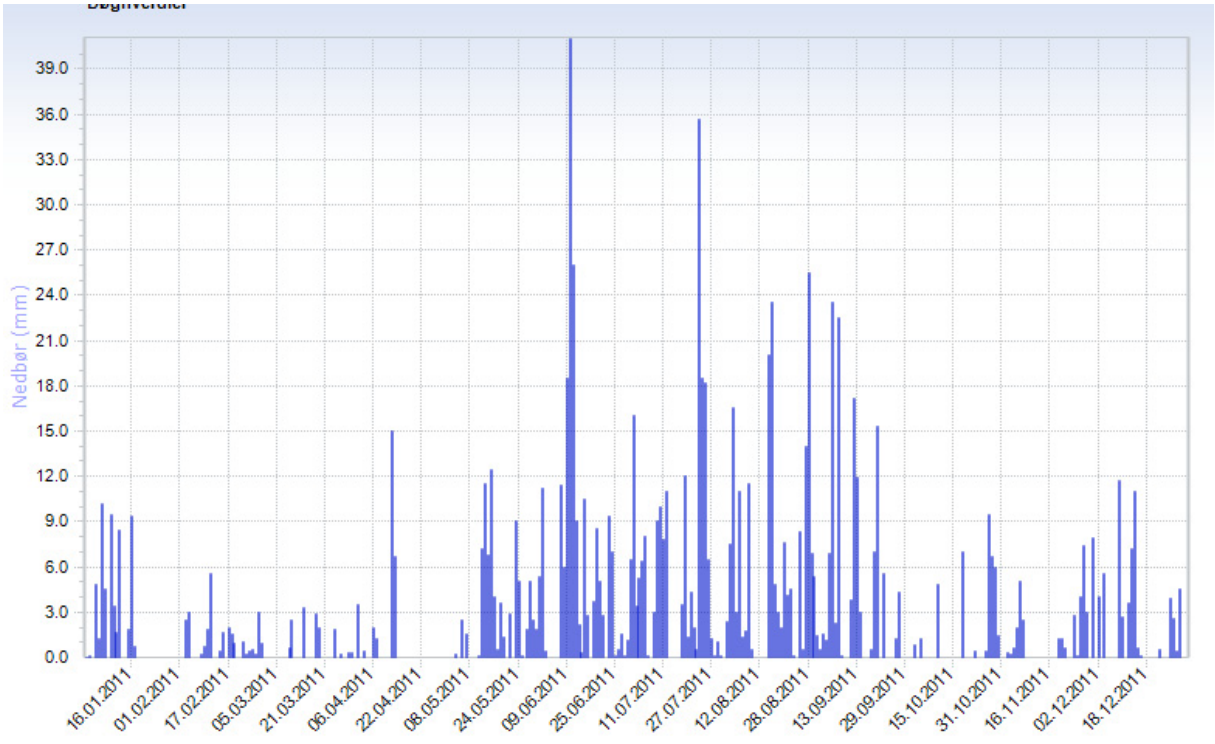

Figure 3.7 Daily precipitation values in mm for Espedalen weather station presented on the left axis vs. dates in 2011. The largest spike for the daily precipitation for the weather station represent 10th of June 2011, marked by arrow (NVE et al., 2012).

The daily precipitation from 2011 for all five weather station illustrate that 10th of June was a day with abnormally high precipitation. In fact it was the highest daily precipitation for Espedalen,

Venabu, Sjoa, and Hovdgrenda weather stations. For Skåbu weather stations 10th of June had the second highest daily precipitation value in 2011. The weather data in the month before the 10th of June are now presented in figure 3.8 to figure 3.12 for all the five weather stations to show in detail the antecedent rainfall before the debris flows were triggered. All stations show a steep rise in accumulated rainfall around 10th of June, then levelling off afterwards.

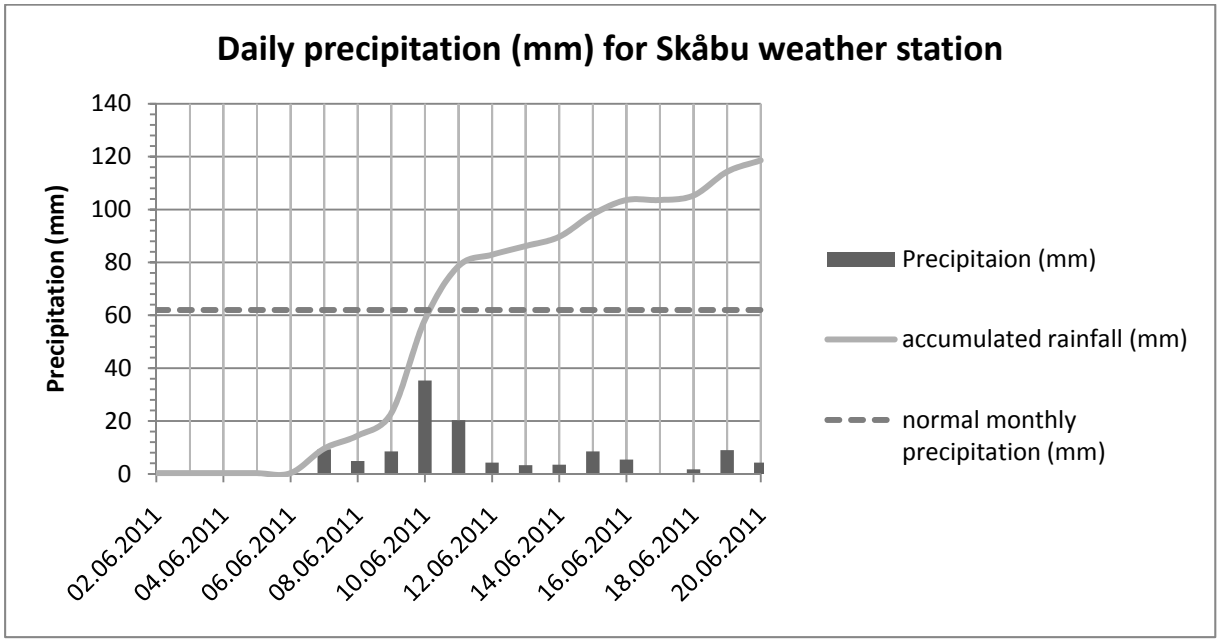

Figure 3.8 Daily precipitation values in mm for Skåbu weather station presented on the left axis vs. dates. The normal monthly precipitation for June is represented here as 62 mm, the accumulated rainfall data is calculated and plotted. The precipitation data is from (NVE et al., 2012), data for the monthly normal precipitation from (NORWEGIANMETEROLOGICALINSTITUTE, 2012a).

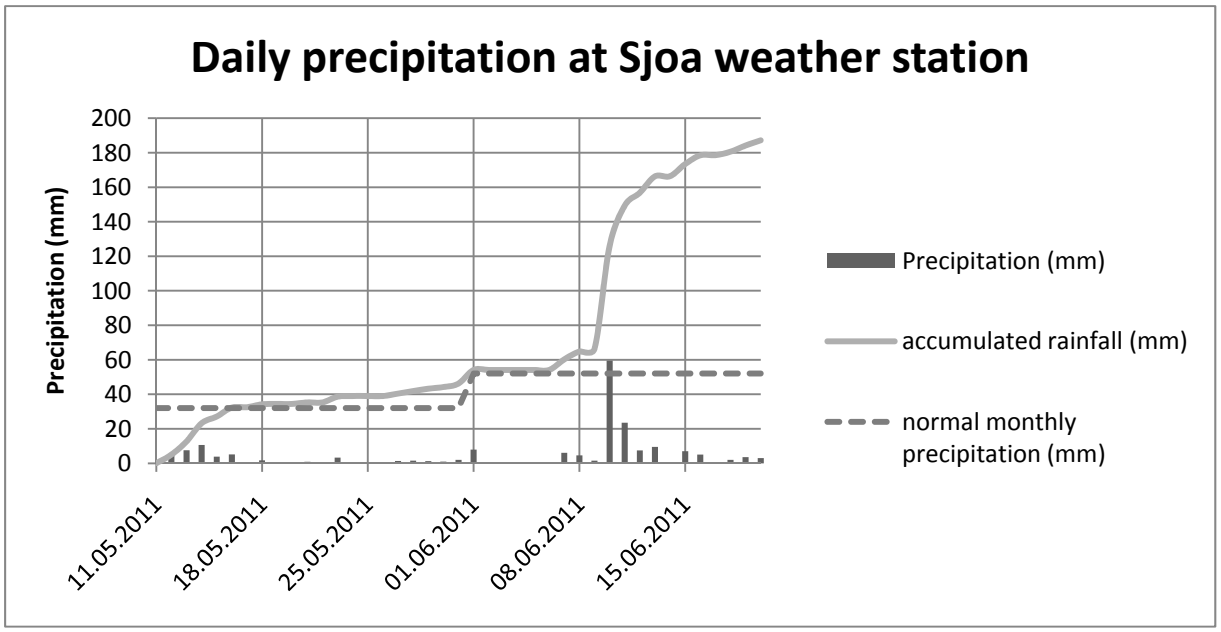

Figure 3.9 Daily precipitation values in mm for Sjoa weather station presented on the left axis vs. dates. The normal monthly precipitation for may and June is represented here as 32 mm and 52 mm respectively, the accumulated rainfall data is calculated and plotted. The precipitation data is from (NVE et al., 2012), data for the monthly normal precipitation from (NORWEGIANMETEROLOGICALINSTITUTE, 2012a).

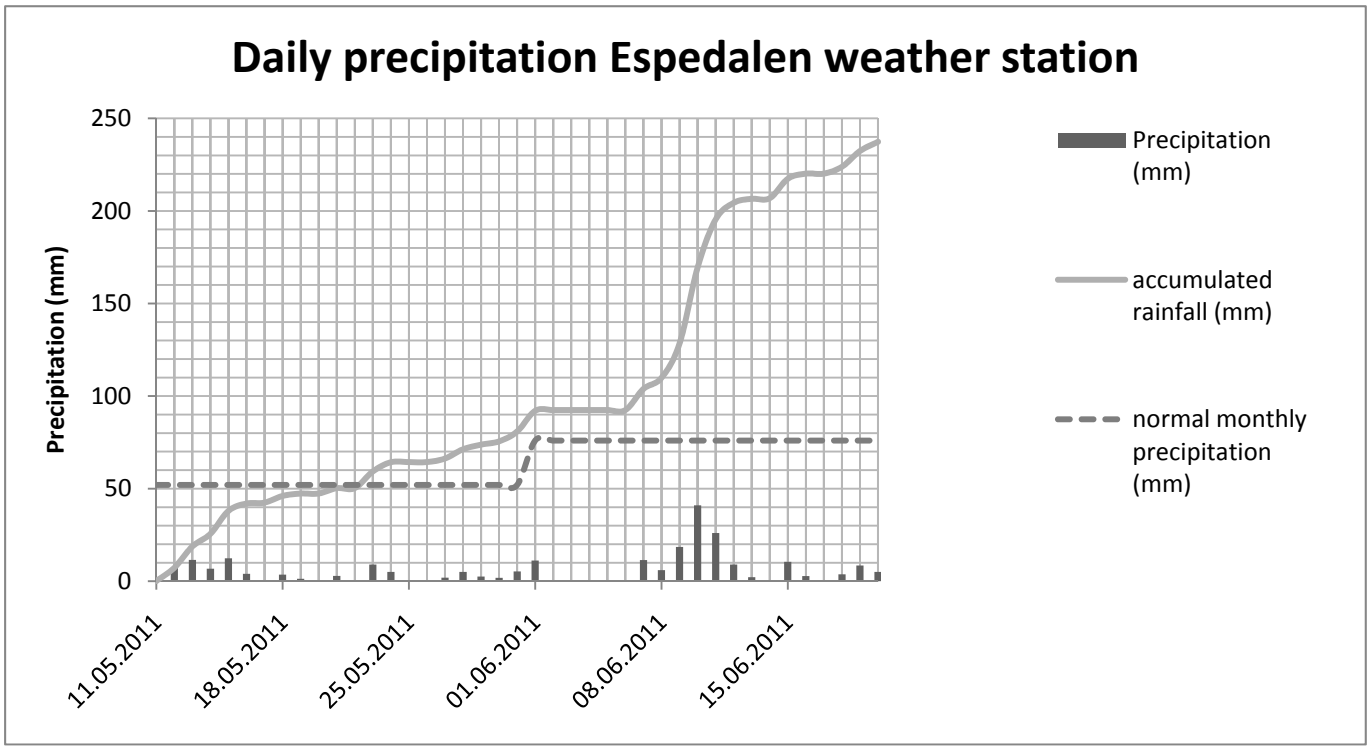

Figure 3.10 Daily precipitation values in mm for Espedalen weather station presented on the left axis vs. dates. The normal monthly precipitation for may and June is represented here as 52 mm and 76 mm respectively, the accumulated rainfall data is calculated and plotted. The precipitation data is from (NVE et al., 2012), data for the monthly normal precipitation from (NORWEGIANMETEROLOGICALINSTITUTE, 2012a).

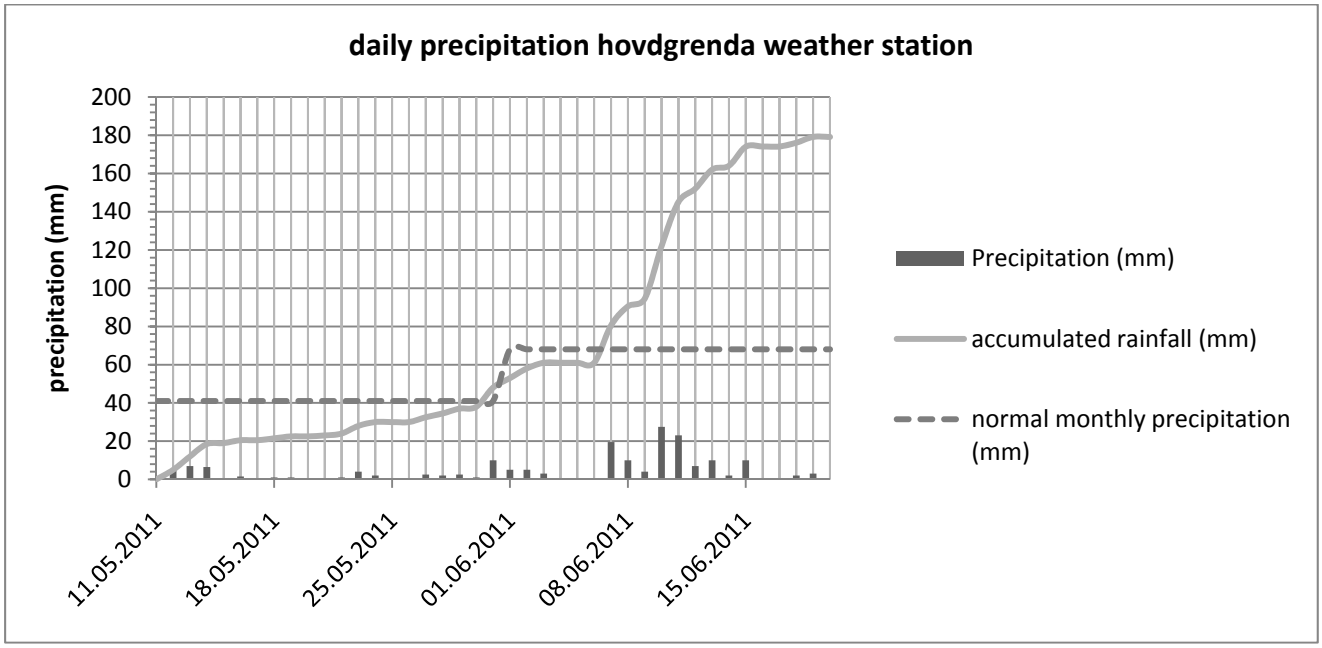

Figure 3.11 Daily precipitation values in mm for Hovdgrenda weather station presented on the left axis vs. dates. The normal monthly precipitation for may and June is represented here as 41 mm and 68 mm respectively, the accumulated rainfall data is calculated and plotted. The precipitation data is from (NVE et al., 2012), data for the monthly normal precipitation from (NORWEGIANMETEROLOGICALINSTITUTE, 2012a).

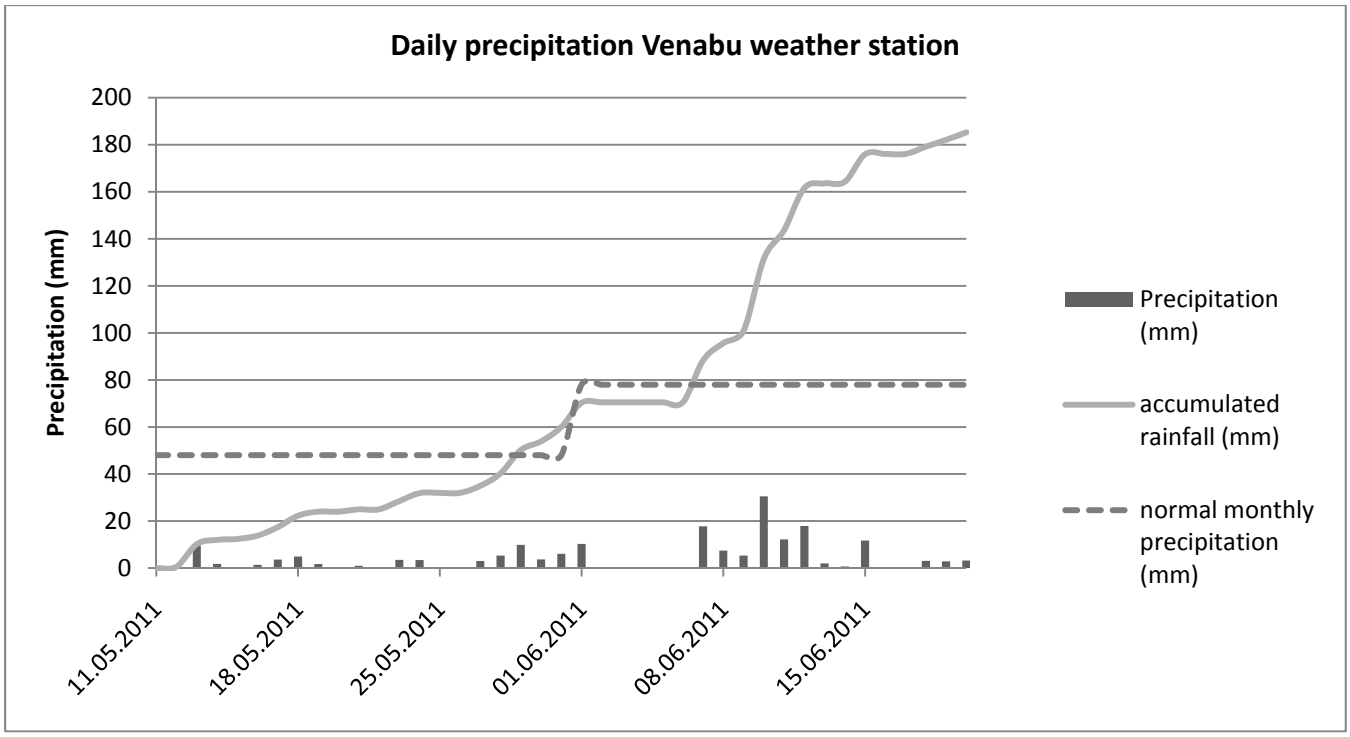

Figure 3.12 Daily precipitation values in mm for Venabu weather station presented on the left axis vs. dates. The normal monthly precipitation for may and June is represented here as 48 mm and 78 mm respectively, the accumulated rainfall data is calculated and plotted. The precipitation data is from (NVE et al., 2012), data for the monthly normal precipitation from (NORWEGIANMETEROLOGICALINSTITUTE, 2012a).

Skåbu weather station have hourly precipitation measurements, in figure 3.13 the hourly precipitation from 07.00 am on 9th of June 2011 until 15.00 pm on 10th of June 2011 is presented in combination with the calculated accumulated precipitation. For the weather station of Skåbu precipitation does not start until 14.00, shown in table 3.2b. Figures 3.14 and 3.15 are interpolations of daily and weekly weather data respectively from selected weather stations in Norway for the study area. Importantly, both figures suggest that the study area may have more precipitation than is measured at Sjoa weather station. This implies that the rainfall data from Sjoa is a lower band on the actual rainfall in Veikledalen. Note that according to these maps the area directly above the study area receives enhanced precipitation.

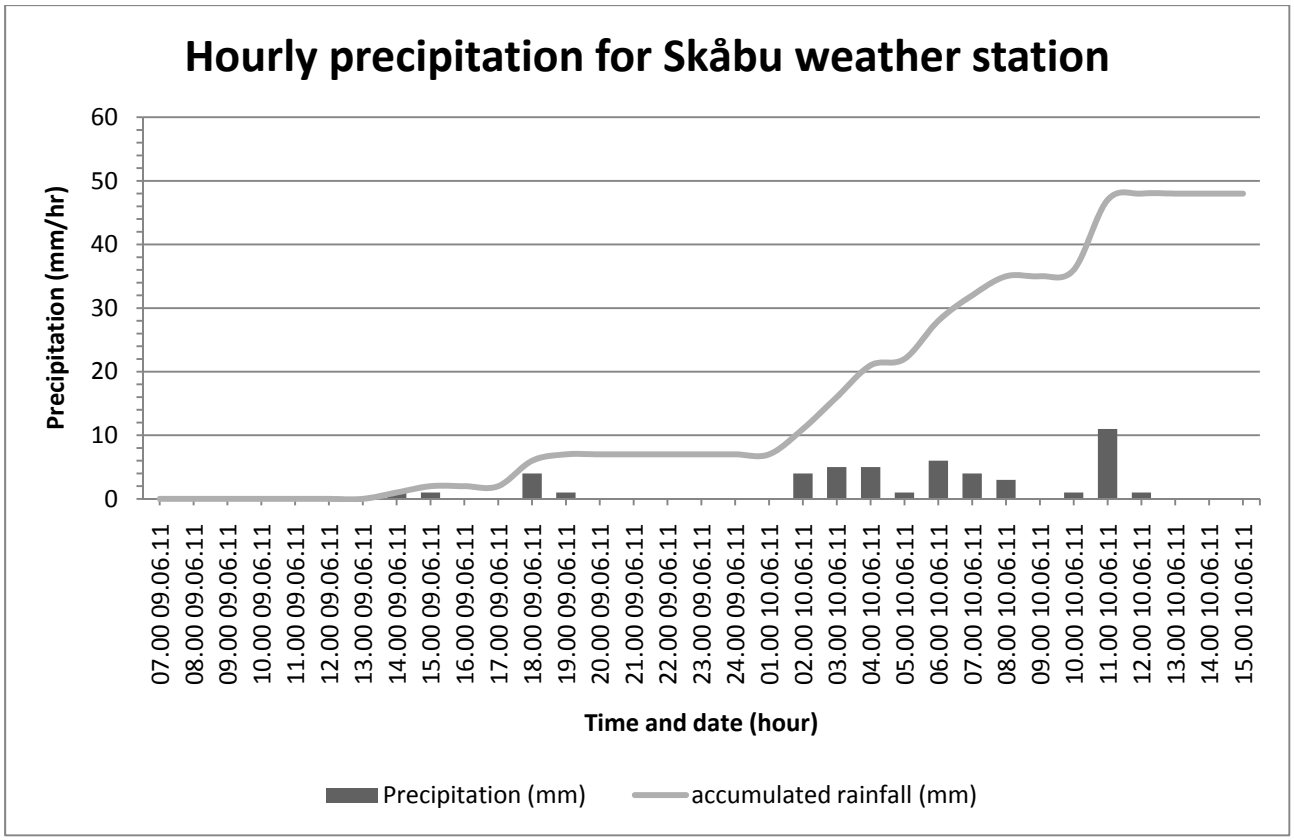

Figure 3.13 Hourly precipitation values in mm for Skåbu weather station presented on the left axis vs. dates, the accumulated rainfall data is calculated and plotted. The precipitation data is from (NORWEGIANMETEROLOGICALINSTITUTE, 2012c).

Time	Precipitation (mm)	Accumulated rainfall (mm)
07.00 09.06.11	0	0
08.00 09.06.11	0	0
09.00 09.06.11	0	0
10.00 09.06.11	0	0
11.00 09.06.11	0	0
12.00 09.06.11	0	0
13.00 09.06.11	0	0
14.00 09.06.11	1	1
15.00 09.06.11	1	2
16.00 09.06.11	0	2
17.00 09.06.11	0	2
18.00 09.06.11	4	6
19.00 09.06.11	1	7
20.00 09.06.11	0	7
21.00 09.06.11	0	7
22.00 09.06.11	0	7
23.00 09.06.11	0	7
24.00 09.06.11	0	7
01.00 10.06.11	0	7
02.00 10.06.11	4	11
03.00 10.06.11	5	16
04.00 10.06.11	5	21
05.00 10.06.11	1	22
06.00 10.06.11	6	28
07.00 10.06.11	4	32
08.00 10.06.11	3	35
09.00 10.06.11	0	35
10.00 10.06.11	1	36
11.00 10.06.11	11	47
12.00 10.06.11	1	48
13.00 10.06.11	0	48
14.00 10.06.11	0	48
15.00 10.06.11	0	48

Table 3.2b Hourly rainfall data for the rainfall event, from Skåbu weather station from 07.00 on the 9th of June 2011, until 15.00 on the 10th of June 2011. Rainfall data from (NORWEGIANMETEROLOGICALINSTITUTE, 2012c).

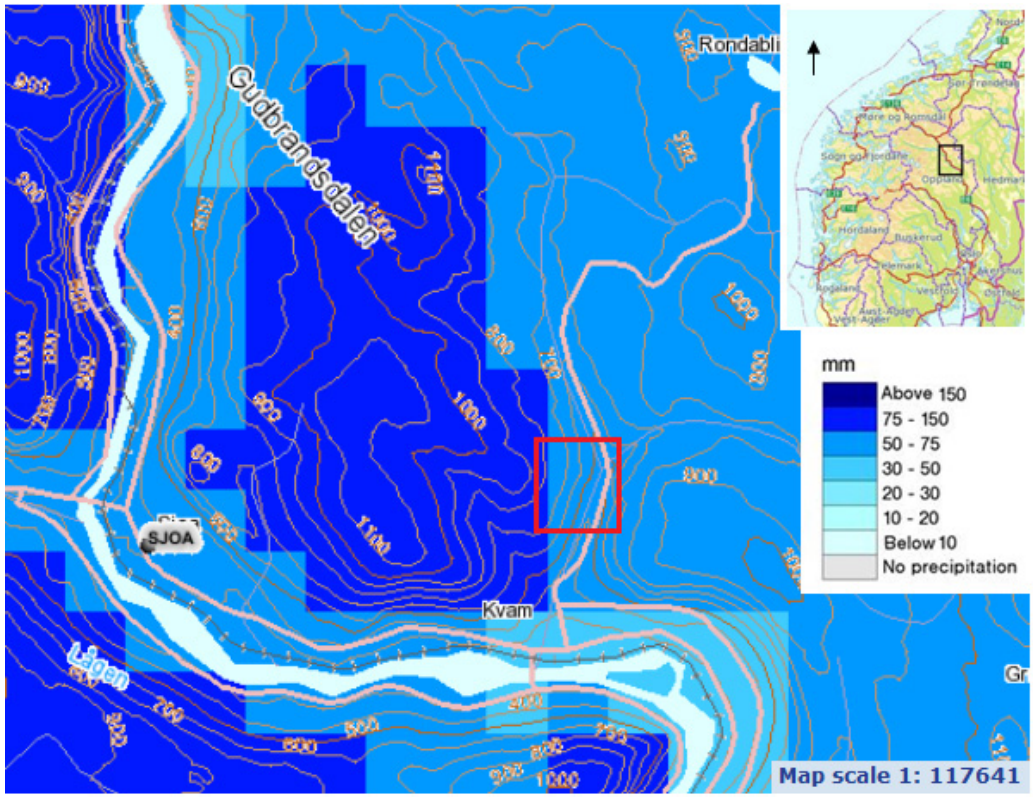

Figure 3.14 Daily precipitation in the study area for the 10th of June, 2011. Interpolated from data from selected weather stations in Norway by (NVE et al., 2012). Study area is located in the red square, the location of the figure in Norway is show in the small map as the black square (Kartverket, 2009). The arrow points towards geographical north for both maps.

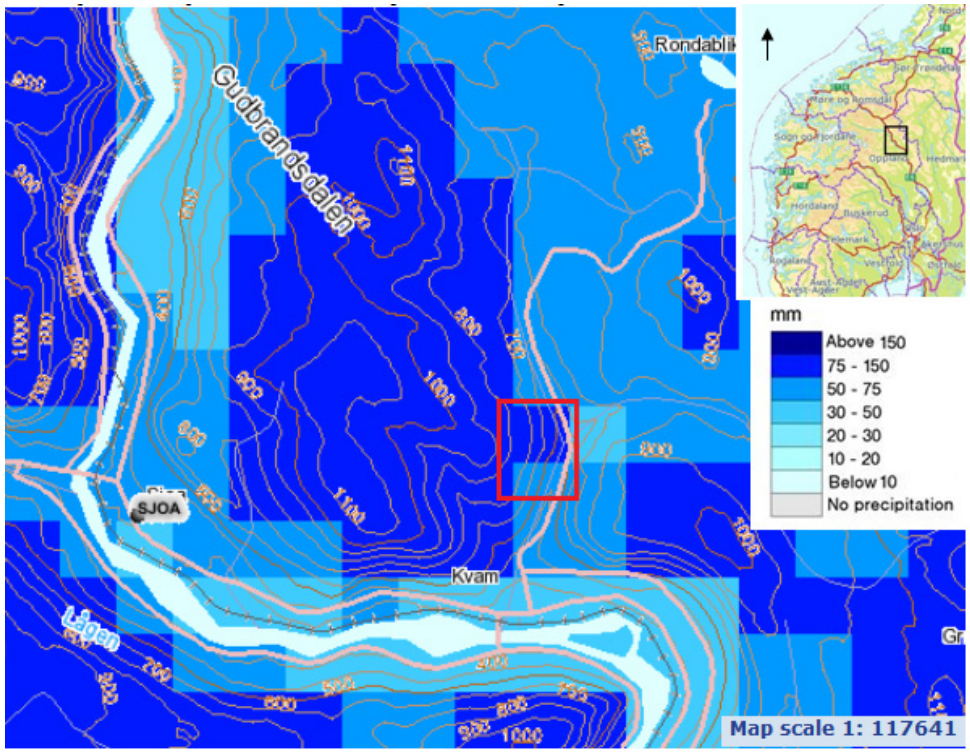

Figure 3.15 Weekly precipitation in the study area for the week before the 10th of June, 2011. Interpolated from data from selected weather stations in Norway by (NVE et al., 2012). Study area is located in the red square, the location of the figure in Norway is show in the small map as the black square (Kartverket, 2009). The arrow points towards geographical north for both maps.

3.2 Soil water, Groundwater and Surface runoff

The soil water deficit in the study area on the 10th of June 2011 is shown in figure 3.16a. The study area has a soil water deficit in the range of 20-60 mm, the map show how many mm of water is needed before the soil reaches field capacity at 0 mm, this means that the soil can still store 20 to 60 mm of water before it is completely saturated at field capacity. Figure 3.16b show the soil water deficit in the ground compared with the normal soil water deficit for the area on the same date, the normal's are calculated from data for the time period 1990-2008. The classes are given in percentiles and the percentiles for the study area are in the range of the 75th percentile and above. The soil water deficit shows that the ground was wetter than normal. The groundwater level compared to normal in figure 3.16c is for the same time period as figure 3.16b, and the percentile for the study are is above the 95th percentile, the groundwater level was very high compared to normal. Figure 3.16d show the total daily runoff in the study area on the 10th of June 2011, and the total runoff for the area is less than 5 mm, compared to normal the runoff was wetter. Figure 3.16e illustrate the total daily runoff in the study area on the 11th of June 2011, the total runoff for the area is in the range of below 5 mm to 10 mm, compared to normal the runoff was much wetter. The runoff has been compared to normal has been calculated for the date compared to the average value calculated from the period 1990-2008, is given in percentiles. The classes are: Much wetter (above 95th percentile), Wetter (75th - 95th percentile), Normal (25th - 75th percentile), Drier (5th – 25th percentile), Much drier (below 5th percentile) (NVE et al., 2012).

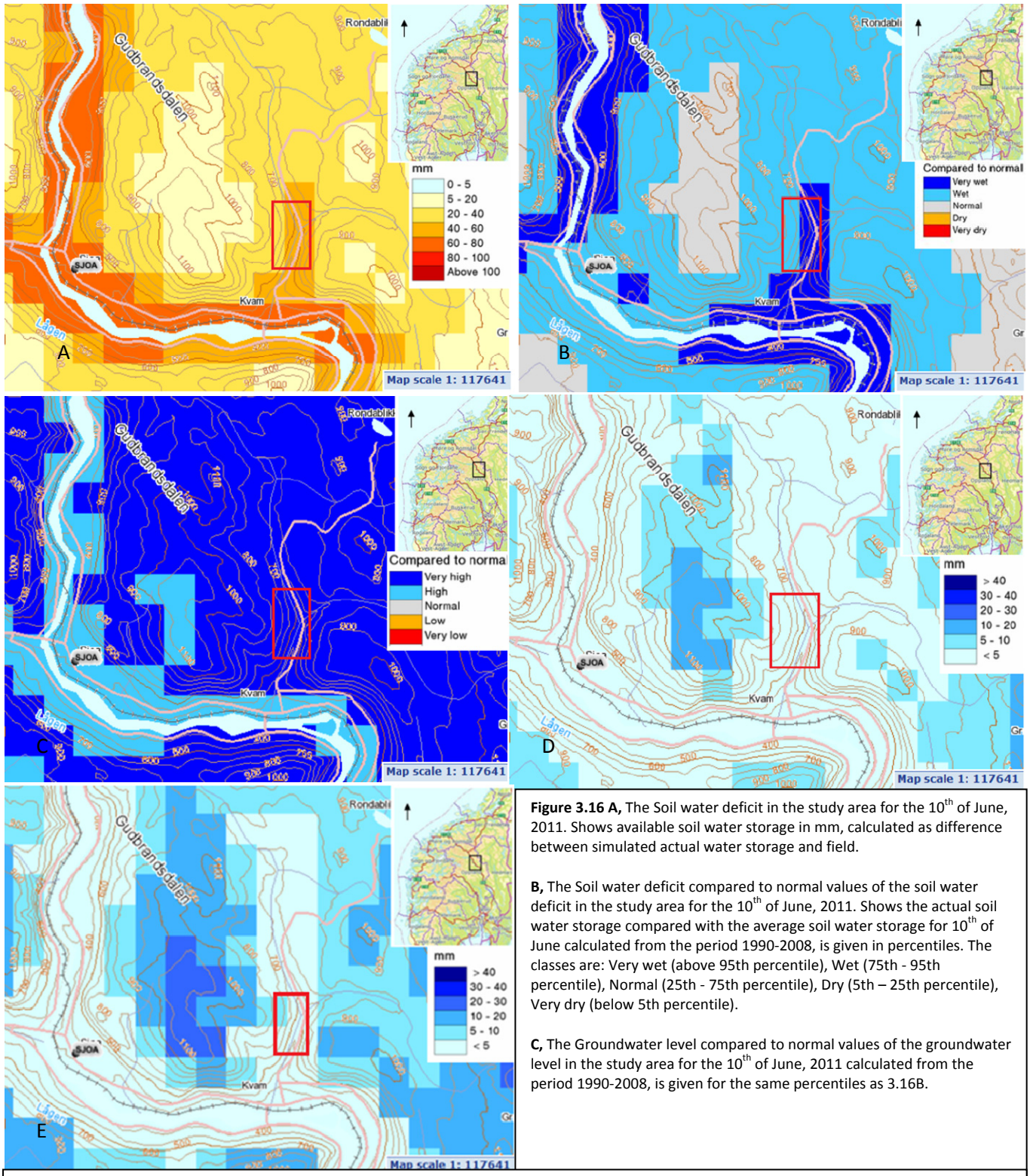

Figure 3.16 A, The Soil water deficit in the study area for the 10th of June, 2011. Shows available soil water storage in mm, calculated as difference between simulated actual water storage and field.

B, The Soil water deficit compared to normal values of the soil water deficit in the study area for the 10th of June, 2011. Shows the actual soil water storage compared with the average soil water storage for 10th of June calculated from the period 1990-2008, is given in percentiles. The classes are: Very wet (above 95th percentile), Wet (75th - 95th percentile), Normal (25th - 75th percentile), Dry (5th – 25th percentile), Very dry (below 5th percentile).

C, The Groundwater level compared to normal values of the groundwater level in the study area for the 10th of June, 2011 calculated from the period 1990-2008, is given for the same percentiles as 3.16B.

D, The total daily runoff in the study area for the 10th of June, the runoff is calculated as the sum of the surface and groundwater runoff in mm's.

E, The total daily runoff in the study area for the 11th of June, the runoff is calculated as the sum of the surface and groundwater runoff in mm.

For all the figures the following information is similar:

Study area is located in the red square, the location of the figure in Norway is show in the small map as the black square (Kartverket, 2009). The arrow points towards geographical north for both maps.

The maps have been created by NVE (NVE et al., 2012).

3.3 Flooding

The flood on June 2011 has been documented by NVE (Kleivane, 2011), the flooding affected large parts of southern Norway with Gudbrandsdalen, Driva, and the inner parts of Western Norway were affected the most by the flood, location is shown in figure 3.17A. On a regional scale in early spring there was not that much snow in the mountains and much of the snow melting phase occurred in early April, but there was still snow in the mountains in May and there was an unusual high amount of precipitation in May. The precipitation was infiltrated into the soil and started to fill up the soil and groundwater potential in the soil. The precipitation before 10th of June was significant in the region and high temperatures melted snow in the mountains. Locally there were also high precipitation rates, and this increased the water level in areas where there was no snow, as in the Veikledalen area. In several places the flood was a 100-year flood at its maximum, for example in Driva, Losna and Vågåvatn. In Gudbrandsdalen the flood was in places almost as high as the flood in 1995 and Mjøsa had a maximum elevation of 124, 24 meters above sea level (6,73meters on the local scale). For the maximum water discharge levels in the Otta area the flood frequency was measured to be < 100 year flood for all stations except one that was a 50 year flood (Kleivane, 2011).

Figure 3.17b show the flooding in Veikelåa and the consequences of the flood. In the centre of the picture there is a house that has been washed away and the river banks has clearly been eroded. The river is white and looks quite large, especially since these pictures were taken on the 12th of June 2011. Two landslides can be seen on the right side of the picture as well. Figure 3.17c show that the river might have created a new channel for itself and that is has transported large timbers a certain distance. There is also the possibility that a small slide has occurred in the scar area in the central part of the picture. Figure 3.17d shows that part of the road that lead into the valley was destroyed by the river and this means that the river must have been larger than normal and must have had enough force to erode the road. Figures 3.17e and f show the flooding in the town of Kvam.

The flooding in Veikledalen occurred lower in the valley than the slides, so it probably did not initiate the landslides, but flooding can affect the groundwater conditions in slopes. The flooding in Veikledalen and the landslides were caused by the same precipitation event, and are not known to have been connected in any other way in the Veikledalen area.

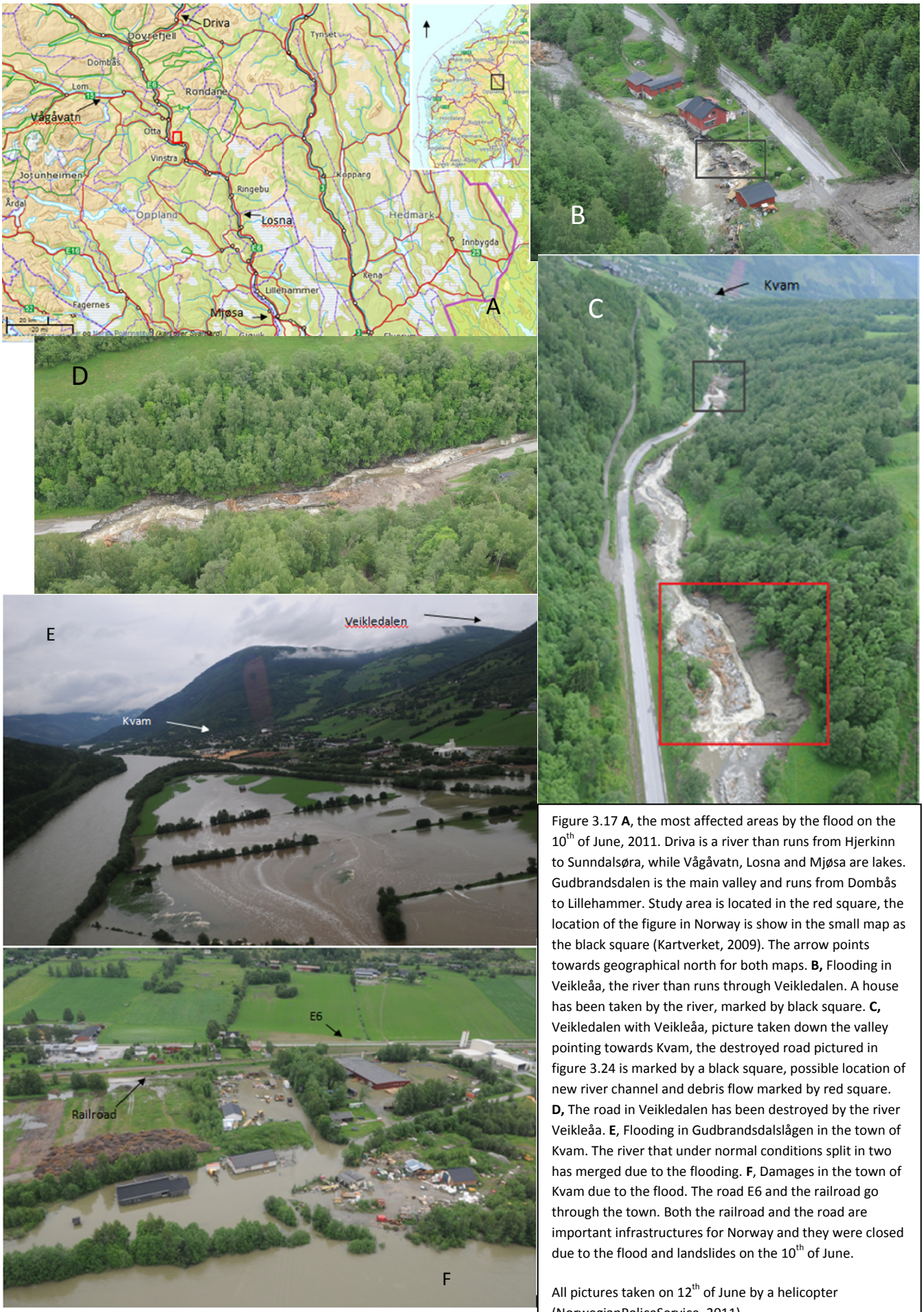

Figure 3.17 **A**, the most affected areas by the flood on the 10th of June, 2011. Driva is a river than runs from Hjerkinn to Sunndalsøra, while Vågåvatn, Losna and Mjøsa are lakes. Gudbrandsdalen is the main valley and runs from Dombås to Lillehammer. Study area is located in the red square, the location of the figure in Norway is show in the small map as the black square (Kartverket, 2009). The arrow points towards geographical north for both maps. **B,** Flooding in Veikleåa, the river than runs through Veikledalen. A house has been taken by the river, marked by black square. **C,** Veikledalen with Veikleåa, picture taken down the valley pointing towards Kvam, the destroyed road pictured in figure 3.24 is marked by a black square, possible location of new river channel and debris flow marked by red square. **D,** The road in Veikledalen has been destroyed by the river Veikleåa. **E**, Flooding in Gudbrandsdalslågen in the town of Kvam. The river that under normal conditions split in two has merged due to the flooding. **F**, Damages in the town of Kvam due to the flood. The road E6 and the railroad go through the town. Both the railroad and the road are important infrastructures for Norway and they were closed due to the flood and landslides on the 10th of June.

All pictures taken on 12th of June by a helicopter (NorwegianPoliceService, 2011).

3.4 Landslides in Veikledalen

On the 10th of June 2011 up to 20 to 30 landslides were triggered in Veikledalen, probably in the morning before noon. Most of the landslides occurred on the steep western side of the valley. The material from some of the landslides reached the river and was transported downstream. Trees and bushes were also transported by the river and this caused the river to dam up (Lyche et al., 2011). The study area contains seven landslides in a small area called Brudalen. The six landslides were identified in the field, and the track of landslide two was documented in detail. Landslide two will be described, and then the other landslides will be compared to landslide two to find similarities and differences. Given the proximity of the slides and the consistency of the topography, soil cover and geology of the area, the main features and dynamics are assumed to be similar for all the landslides. The study area before the landslides occurred can be seen in figure 3.18 a. Ancient sub-parallel ravines running from north-west to south-east can be identified on the valley side to the west of the houses, and vegetation cover is complete before the landslides occurred. Figures 3.18b, c, and d show the landslide tracks and the proximity to the houses. The landslides have been numbered from 1 to 6, and they are sub-parallel going down the same slope. Landslides 1,4,5,and 6 start at a similar elevation , while landslides 2,4 a start at a similar but lower elevation than the other four landslides. There are some basic characteristics that can be identified immediately. Landslides 1 are 3 are single tracks, landslides 2 and 6 split, and landslides 4 and 5 merged. A summary of the observations for all six landslides can be found in table 3.10.

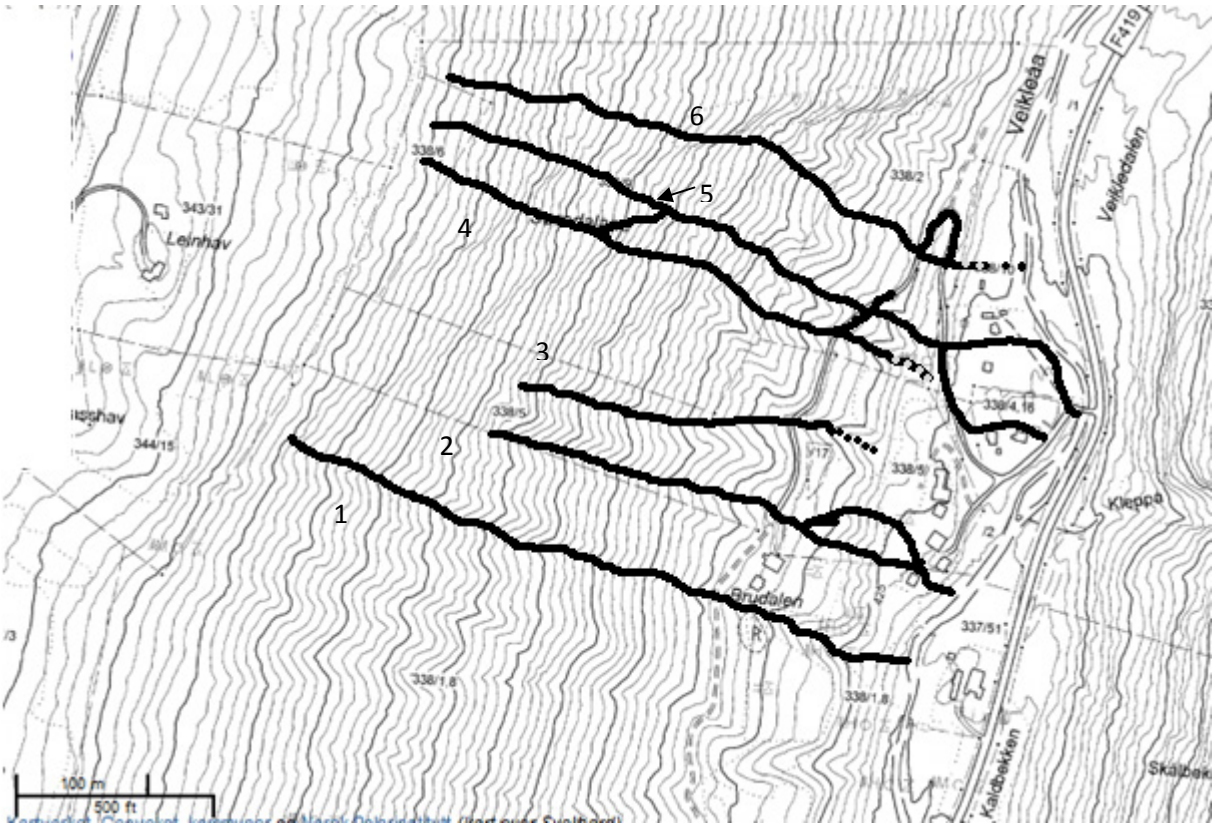

Figure 3.17G The six identified landslides in the study area of Veikledalen, numerous other landslides were observed in the valley but they are not part of this thesis. The slides have been numbered from 1 to 6, and most of the pictures from landslides 1,3,4,5, and 6 have been taken at the location where the landslide cross the upper road. Dotted lines represent probable landslide tracks that could not be identified from archive photos. Map from (Kartverket, 2009).

Figure 3.18 **A**, the study area before 10th of June, 2011. Red square mark the farms in the study area, the landslides occurred in valley side above these farms. The direction towards Kvam is shown; the location of the figure in Norway is show in the small map as the black square. The arrow points towards geographical north for both maps. (Kartverket, 2009).

B, The landslides in the Brudalen area, landslides 4 and 5 is partially in the picture, and landslides 6 is not present in the picture and are to the right of the picture. The two landslides in the left part of the picture is not part of the study area.

C, Landslides 4, 5, and 6 has been marked on the picture. Pictures B and C taken by helicopter on the 12th of June, 2011 (NorwegianPoliceService, 2011).

D, the six landslides have been marked by arrows in the picture to show the distance to the houses they affected (Bargel, 2011).

3.4.1 Landslide Two

The track of landslide two has been walked and documented by measurements of widths, erosion depth, boulder sizes, tree deposition, bedrock exposure, local slope angle, deposition grain sizes, channel shape etc. GPS measurements were taken to find the track location and elevation. The landslide track has been divided into five sections based on observed changes in the track, see figure 3.19. Landslide two starts at the an elevation of 617 meters this is at a lower elevation than landslides 1,4,5, and 6. The landslide has been calculated to have a run out of 335 meters and a height different of approximately 197 meters, this gives the landslide an apparent friction angle of 30,4°. The landslide started as two strands that merged together, and then deposited on the road at an elevation of 460 meters, before it split when it met a small ridge at an elevation of 453 meters. The landslide merged again and was ultimately deposited in the river, see figure 3.19A. Yellow scale bar in some pictures is 1 meter long. Observations are summarizes in tables 3.3, 3.4, 3.5 and 3.6.

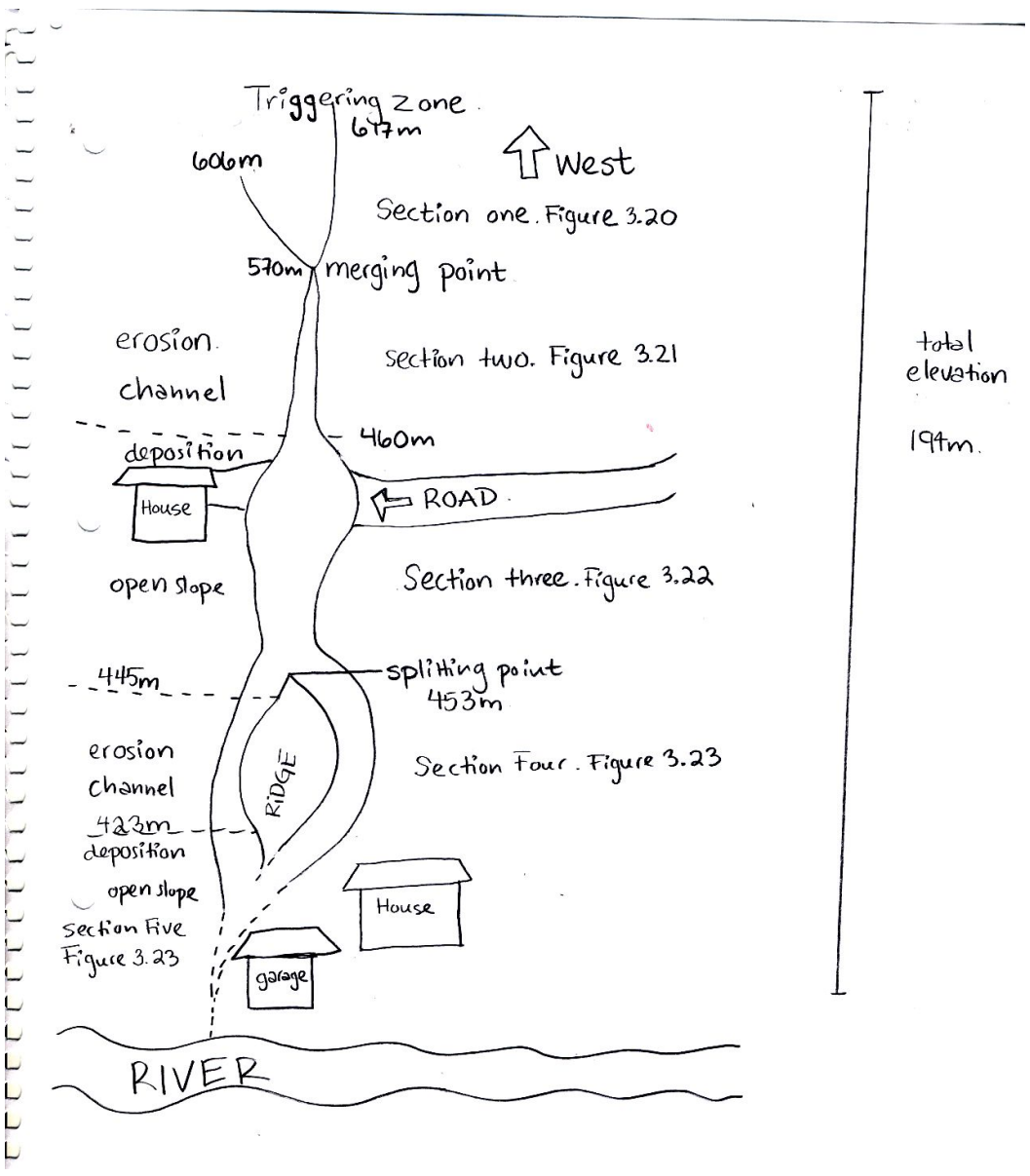

Figure 3.19A Simple schematic sketch of landslide two, not to scale.

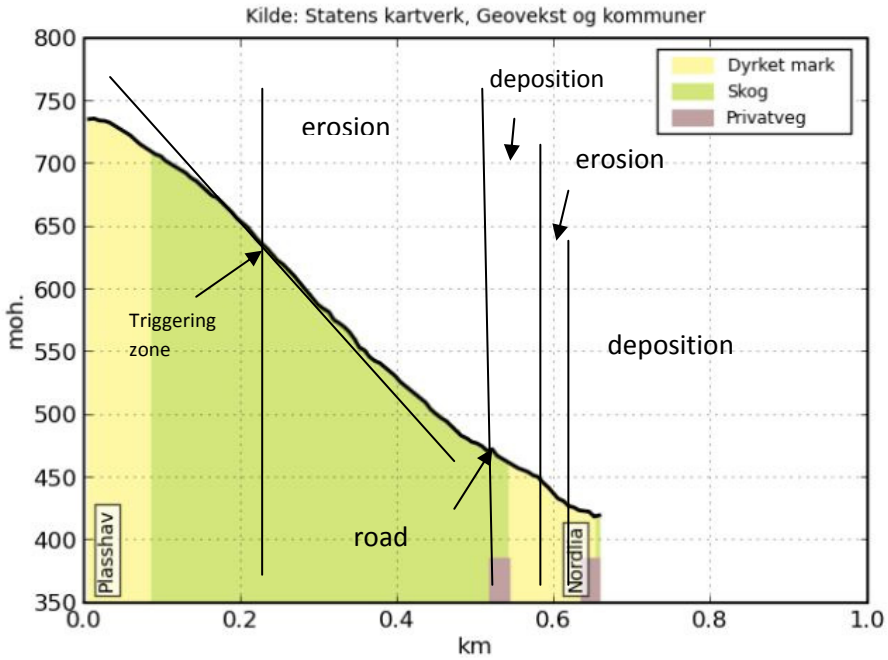

Figure 3.19b Profile of the track of landslide two, showing areas of erosion and deposition. Tangent at triggering zone show change in slope angle. Map from (Kartverket, 2009).

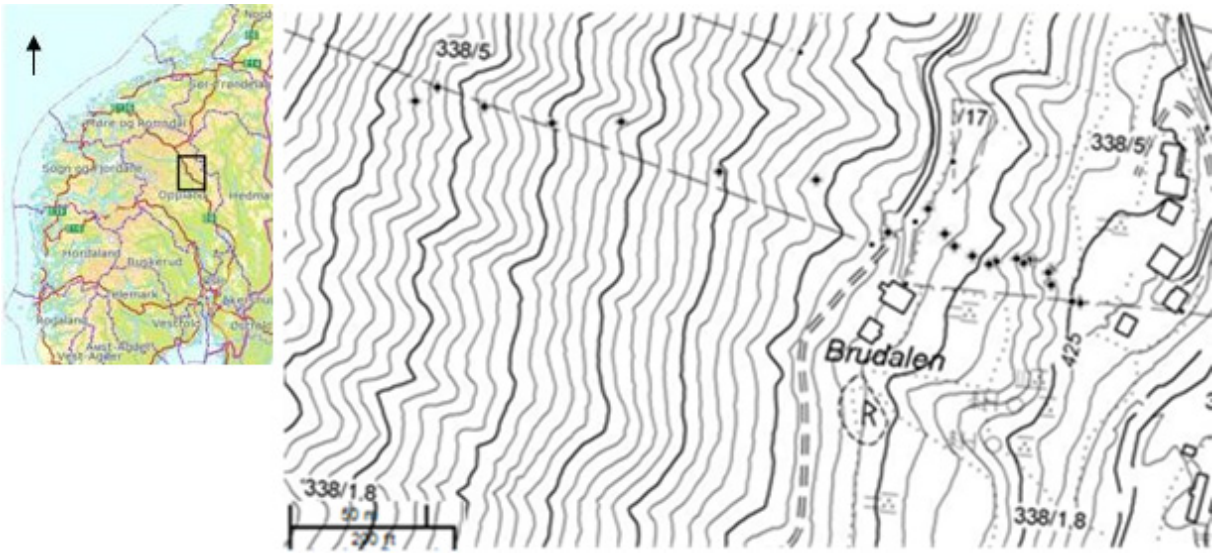

Figure 3.19c GPS measurements taken of the track of landslide two, presented in a map of the study area. The GPS points range from 12 at the bottom of the slope, to 33 at the triggering zone at the top. Map is from (Kartverket, 2009), black square marks study area, and arrow points to geographical north.

Section one

Section one includes the track from the triggering zone of the landslide, point 32 at an elevation of 617 meters, and down to the point where the two landslide strands merge together, point 31 at an elevation of 595 meters. Landslide two is triggered at two strands, see figure 3.20 a and b, where the northern strand is wider and at a higher elevation than the southern strand. Above the triggering zone trees are bent down towards the east, see figure 3.20c, but the rest of the vegetation is intact. The scar is distinct and sharp and almost vertical and has a height of approximately 0,5 to 1 meter. The material has coarser angular blocks in a fine-grained matrix that is clay and silt rich, see figure 3.20a. The material was waterlogged, unstable and loose when they were observed in may 2012. The northern strand has a wider triggering zone of 15 meters, compared with the southern strands width of 10 meters. The northern strand has exposed the bedrock beneath the soil with an erosion depth of no more than 0,5 to 1 meter, this indicates that the soil cover in the triggering zone is thin, this also gives the track a u-shape. The southern strand has been triggered immediately in front of a cliff face which is 1m high. The southern strand does not expose the bedrock, but the erosion depth is approximately 0,5 meter. The channel shape is more triangular than the northern strand but it is still u-shaped , see figure 3.20 e and f. The slope angle in the triggering zone is determined to be 40°, and the slope angle lessens above the triggering zone.

Between the two landslide strands there is a wedge of mostly undisturbed material where a few trees near the merging point of the two strands have been pushed over, but mostly the trees are not disturbed. A block of soil looks to have been pushed on top of this undisturbed soil wedge and the contact between the block of soil and the soil wedge is sharp, where the soil block has exposed soil on the sides of the block the top of the block has undamaged vegetation, see figure 3.20 f.

When the two strands merge together the erosion depth increases to 3 meters, and the width is 10 meters. The slope angle remains 40° and the channel becomes v-shaped. Large blocks have been exposed in the channel, with a length up to 2 meters. All the vegetation has been removed by the landslide, and trees on the side of the channel have been pushed over parallel to the channel. Just below the merging point a small slide 5 meters wide, has been triggered from the side of the channel, it is 0,5 meters high and show the same features as the triggering zone higher up, see figure 3.20d. The scar is sharp and almost vertical; the vegetation above the small slide is intact. From observations in the area, the landslide has been triggered in an old ravine with a ridge on each side. On the other side of these ridges are landslides one and three.

Figure 3.20 Landslide 2 section one, triggering zone**. A**, Triggering zone of northern strand, looking west. **B**, triggering zone of southern strand, looking West. **C,** vegetation cover and pushed over trees above the triggering zone of the southern strand, looking north-west. **D,** small slide along the channel after the two strands have merged, looking west. **E,** track of southern strand, looking south-west. **F**, track of northern strand and wedge marked by red square between the strands of the landslide, looking west.

All pictures by (Mair, 2012).

Section two

Section two includes the track from the merging point of the two strands of the landslide in the triggering zone in point 31, down to point 26 where the landslide crosses the road, the landslide has eroded in this section of the track. The track is triangular in shape at the top with an inner channel with almost vertical walls, with a width of 2 meters and an erosion depth of 1, 5 meters, see figure 3.21A. These vertical walls are indications that the landslide has eroded into the overconsolidated sediment layer. This inner channel has been observed almost along the entire track in this section, other than in the areas where the landslide has eroded down to the bedrock, see figure 3.21 C. When the landslide has exposed the bedrock the shape of the channel also changes from a triangular shape to a more u-shaped track, the track has been confined by the bedrock. The channel width is between 6 and 4 meters in the upper track, but at point 27 just before the landslide track crosses the road the track is 13 meters wide. The erosion depth does not show the same changes it remains approximately 2, 5 meters down the entire section of the track, but for the parts of the track that has an inner channel part of the total erosion depth has been done by the inner channel. The local slope angle is steep for this section of the landslide track, it starts at 40° and decreases to 20° at point 27 just above the road. The slope angle increases in the middle of this section, at point 28, but at this location the track moves over a 3 meter high and 4 meter wide cliff face, so the track was confined at that location, see figure 3.21D.

All along the edge of the track numerous trees have been pushed over and uprooted, and they have been deposited parallel to the track. In some instances the trees have been deposited together with soil or large rocks, and they have created levees along the track. The difficulty of pushing these trees over is not known, but when the location was visited several trees very close to the track were pushed over by accident using very little force, other trees would not move. If these rotten trees are similar to the trees that were pushed over by the landslide, or if they have rotted later is not known. But all pictures from June 2011 and August 2011 only show trees that are alive.

The vegetation in the track has been removed completely, though some moss has started to grow. At location 28 several mud marks were observed on the side of the trees that faced the landslide track, see figure 3.21B. At the bottom of the tree they could be up to a cm thick, and they were observed several meters from the track. Mud marks extended to 3 meters above the ground, more than 3 meters away from the landslide track.

When the landslide track on 23rd of May 2012 is compared with pictures from 23rd of June 2011, it is clear that the track has changed, see figure 3.21E and 3.21F. This is probably due to 11 months of weather, with snow and rain. The inner channel in May 2012 still contains a small creak, and the inner channel compared with June 2011 has been eroded more. The coarse grains are also more prominent in the pictures of the track, so apparently the fine-grained material has been removed from part of the landslide track.

Figure 3.21 Section two of Landslide two**. A**, Upper track of landslide, looking west. **B,** 1 cm thick mudmarks on trees close to landslide track at point 28. **C,** Landslide track confined by bedrock into a u-shaped channel, looking east. **D,** Cliff face exposed by landslide track at point 28, looking south-west. **E,** Landslide track just above point 26, looking west, on 23rd of June, 2011. **F,** Same location as Picture F, but taken on 23rd of may, 2012.

All Pictures except E is from (Mair, 2012), Picture E from (Bargel, 2011).

Section three

Section three of the landslide includes the track from when it crosses the road at point 26, at an elevation of 459 meters above sea level, to when it starts eroding again at point 24, at an elevation of 451 meters above sea level. The horizontal travel distance for this section of the landslide track has been calculated to be 8 meters. The landslide has deposited significant debris in this part of the track, see figure 3.22F, and it splits into two strands at point 25, see figure 3.22E. The slope angle at the road is 4°, and it increases to 26° just below the road at point 25,5, before it decreases again to 16° at point 24. The width of the deposits are the greatest for the entire landslide track in this section, with the deposition on the road having a width of 32,5 meters and forming a tear shaped depositional fan. The width of the deposit decreases to 25 meters before the landslide splits into two before the width decreased further to 8,3 meters and finally to 5,3 meters at point 24. The topography for this section is all open slope, and the landslide has started to deposit at the point where the slope angle decreases to 4°, and the slope changes from a channelized flow to an open slope. At the road the material is coarse grains in a fine-grained matrix, see figure 3.22B. The material just below the road has coarser grains than the deposition on the road, and the difference in the grain size is clear, see figure 3.22C. All the deposits have angular grains, and they are poorly sorted. Large blocks up 1 meter in diameter are found in the deposit on the road, while a block of 1,8m in length is found in the deposit at point 25, see figure 3.22D.

The thickness of the deposit decreases down slope, it is 3 meters thick at the road and at point 25,5, before it decreases to 2 meters at point 25, and up to 1 meter at point 24. The deposits include numerous trees oriented in all different directions, but some are parallel to the track and these trees are normally along the edge of the track. Along the southern part of the deposit on the road several trees have been deposited in a curve shape which has confined the deposition in that location, see figure 3.22A. Other items that have been affected by the landslide deposit are a fence at point 25,5 that has been pushed over and destroyed, and a tractor at the road, see figure 3.22C. The tractor was partially buried by the deposits and moved by the landslide, it has later been moved by humans from the northern side of the depositional fan at the road to the southern part of the deposit. The topography of the deposit varies and has clearly been eroded after it was deposited; there is also a stream that flows through the northern part of the deposit. The landslide track splits before a small ridge before it continues down slope towards a house.

Figure 3.22 Section three of Landslide two**. A**, Trees deposited along the edge of the depositional fan at point 26, looking south-west. **B,** Grain sizes in the depositional fan at point 26. **C,** Fence that has been destroyed by the landslide at point 25,5. **D,** Large 1,8m in diameter block deposited by the block at point 25, looking north-west. **E,** Landslide track just above point 25, looking east down the slope of the southern strand of the landslide after it has split into two strands at point 25. **F,** Looking down the deposition on the slope before the landslide splits in two, looking east from point 26.

Picture 3.22 F is from (Mair, 2012), the rest belongs to the author.

Section Four

Includes the landslide southern strand of the landslide track from point 23 at an elevation of 448 meters to point 16 at elevation of 421 meters, the horizontal travel distance for this section is 33 meters. The landslide track changes from deposition to erosion and from open slope to a channelized slope with an inner u-shaped channel with increased erosion, see figure 3.23 B. The width of the main channel remains relatively constant in the entire section, it varies between 3,4 meters and 4,3 meters. The inner channel width and erosion depth changes in the section, the greatest inner channel width occur at the highest slope angle at 28°, and the smaller inner channel width occurs when the slope angle decreases. This is not always the case due to exposed bedrock the channel is confined at certain locations, for example point 17,5 where the slope angle is 28° the inner channel width is at its lowest value of 0,5 meters. The erosion depth is also often confined by large blocks of bedrock in the bottom of the track, and the greatest erosion depth of 0,6 meters occurs when the slope angle is at its lowest of 20°.

Trees have been deposited along the slope, see figure 3.23A, at point 20 at elevation 436 meters a tree has been uprooted and deposited upslope, this might not be a result of this landslide but of other processes, trees have also created a levee at point 17 at elevation 423 meters. There are also terraces in the inner slope at an elevation of 440 meters. The vegetation in the track has also been removed by the landslide, but moss has already started to grow in the soil.

Section Five

Section five includes the landslide track from point 15 at a registered elevation of 420 meters to point 12 at a registered elevation of 423 meters. The track does move down slope, so the measured elevations might differ from the actual elevation. At the point where the channelized slope changes to open slope and the slope angle decreases by 4° ,from 20° to 16°, the landslide deposited material, see figure 3.23C. The width of the landslide track increases down slope from 6 meters at point 15, to a width of 10 meters at point 12. The deposition depth is 0,1 to 0,2 meters and decreases down slope where there might have been very thin deposits or very little erosion. This bottom part of the section has been disturbed by humans and is therefore difficult to interpret. The depositional material is a coarse gravel with a fine-grained matrix of sand and silts, see figure 3.23D. The blocks are angular and the length of the largest blocks found in the deposit were 0,5, 0,2, 0,25,0,3, and 0,15 meters, this is much smaller than the largest blocks found in the other deposits for this landslide, but the deposit is still poorly sorted as the other deposits. The vegetation has been removed down the slope, but the vegetation in this area was only grass, see figure 3.23E.

The northern strand of the landslide track has also eroded in section 4 and merges with the southern strand in section five. The northern strand was stopped from reaching the house by a small ridge no higher than 30 centimetres. After the two strands merge together the landslide has flowed past a garage and into the river.

Figure 3.23 Section four and five of Landslide two**.**

A, Trees deposited along the edge of the channel at point 22, looking south-west.

B, Erosion in the inner channel of the landslide track, looking west at point 17.

C, Start of deposition in section five, and the bottom of the channel in section four, looking west from point 14.

D, Grain sizes in the deposition at point 14**.**

E, Landslide track below the deposition, looking west from point 12.

All Pictures belong to the author.

Data from landslide two

Observations that have been documented for all the sections in landslide two are presented in tables 3.3, 3.4,3.5, and 3.6. Some of the data is then presented in figures 3.24, 3.25 a and 3.25 b, and the figures show the measurements of the slope angle, landslide width, and deposition and erosion depth along the landslide track.

point name vista hcx	Latitude and Longitude (WGS 84)	elevation from GPS (m)	point name Oregon 300	Latitude and Longitude	elevation from GPS (m)
33	N61 41.295 E9 41.082	617	20	N61 41.295 E9 41.082	617
32	N61 41.298 E9 41.093	606	19,5	N61 41.298 E9 41.093	606
31	N61 41.294 E9 41.119	570	19	N61 41.296 E9 41.115	595
30	N61 41.291 E9 41.157	549	18	N61 41.292 E9 41.159	562
29	N61 41.293 E9 41.193	525	17,5	N61 41.293 E9 41.188	549
28	N61 41.283 E9 41.256	490	17	N61 41.284 E9 41.268	520
27	N61 41.282 E9 41.302	476	16	N61 41.277 E9 41.309	489
26	N61 41.270 E9 41.344	460	15	N61 41.273 E9 41.347	476
25,5	N61 41.277 E9 41.364	454	14	N61 41.275 E9 41.372	467
25	N61 41.271 E9 41.373	453	13	N61 41.265 E9 41.375	469
24	N61 41.268 E9 41.380	451	12	N61 41.265 E9 41.384	468
23	N61 41.267 E9 41.390	448	11	N61 41.264 E9 41.389	466
22	N61 41.264 E9 41.399	445	10	N61 41.264 E9 41.402	467
21	N61 41.265 E9 41.403	439	9	N61 41.269 E9 41.409	460
20	N61 41.266 E9 41.414	436	8	N61 41.271 E9 41.411	450
19	N61 41.265 E9 41.418	433	7,5	N61 41.269 E9 41.426	453
18	N61 41.265 E9 41.424	433	7	N61 41.267 E9 41.427	448
17,5	N61 41.266 E9 41.423	431	6,5	N61 41.268 E9 41.431	442
17	N61 41.263 E9 41.432	423	6	N61 41.266 E9 41.437	436
16	N61 41.264 E9 41.433	421	5	N61 41.264 E9 41.446	433
15	N61 41.260 E9 41.434	420	4	N61 41.263 E9 41.442	427
14	N61 41.261 E9 41.433	420	3	N61 41.260 E9 41.441	428
13	N61 41.256 E9 41.446	421	2	N61 41.258 E9 41.447	426
12	N61 41.256 E9 41.451	423			

Table 3.3 GPS points measured for the track of landslide two in Veikledalen. Two GPS' were used an calibrated to the an equal elevation at the same location. The GPS point were measured by two different GPS models by the same manufacturer, a Garmin Vista Hcx and a Garmin Oregon 300.

point name Vista Hcx	Distance from triggering zone(m)	Local slope dip°	dip direction	main channel width (m)	main channel erosion depth(m)	inner channel width (m)	inner channel erosion depth(m)	deposition depth (m)
33	0	40		15	0,5			
32	5	40		10	0,5			
31	31	40		10	3			
30	66	30		6		2	1,5	
29	99	25	110	6	2,5			
28	149	35	94	4	2,5			
27	195	20	108	13	1,5	1,3	1	
26	238	4	108	32,2				2,50
25,5	249	26	114	25				3
25	251	16	142	8,3				1,5
24	266	16	98	5,3				1
23	274	12	92	3,4	0,6			
22	277	28	108	4,3		1,8	0,3	
21	284	28	109	3,4		1,2	0,25	
20	289	26	124	3,7		1,5	0,15	
19	297	22	116	3,5		0,55	0,45	
18	298	28	90	4		0,5	0,55	
17,5	304	22	80	4,1		1,2	0,3	
17	308	21	110	4,1		0,7	0,6	
16	313	20	98	4		0,6	0,6	
15	315	16	110	6				0,2
14	320	15	120	7				
13	331	12	112	9,5				
12	335	11	128	10				

Table 3.4 Observations of the track of landslide two. Information gathered by walking the track of landslide two. Corresponding latitude and longitude coordinates for the GPS points are found in table 3.3.

point name Vista Hcx	grain sizes	tree orientations	largest boulder (m)	bedrock exposed	vegetation removed	channel shape	open slope
33	fine grained matrix, coarse clasts			yes	yes	u-shaped, confined by bedrock	
32	fine grained matrix, coarse clasts			yes	yes	u-shaped	
31			2	yes	yes	triangular	
30			1		yes	triangular	
29				yes	yes	u-shaped, confined by bedrock	
28				Yes, cliff exposed 3m high, 4m wide	yes	u-shaped, confined by bedrock	
27				yes	yes		
26	poorly sorted, medium coarse, less coarse than further down the slope, angular rocks	080,110, 064,190, 045,063, 042					yes
25,5	angular, coarse, poorly sorted- fine material is sandy.	60	2				yes
25	angular, coarse	128,080, 104,128	1,8				yes
24	angular, coarse						yes
23					yes		yes
22		108, 106			yes		yes
21				rocks exposed	yes		
20				rocks 1m	yes		
19					yes		
18					yes		
17,5					yes		
17					yes		
16	angular blocks, fine: clay to silt. Coarse gravel		0,7, 0,4, 0,4, 0,25, 0,2		yes		
15	angular blocks, fine: clay to silt. Coarse gravel		0,5, 0,2 , 0,25, 0,3, 0,15		yes		
14					yes		yes
13					yes		yes
12					yes		yes

Table 3.5 Observations of the track of landslide two. Information gathered by walking the track of landslide two. Corresponding latitude and longitude coordinates for the GPS points are found in table 3.3.

point name Vista Hcx	side deposits	special features
33		triggering zone
32		triggering zone, no erosion on top but trees are bent. Clear scar.
31	trees	two landslides merge into one. Large trees have been pushed over.
30	trees	erosion into overconsolidated material.
29	trees	stream in the middle of the channel.
28	trees	several mudmarks 3m high, 3m from channel, 1cm thick at the bottom of tree on the side facing the channel, stream in the channel.
27	trees deposited and/or pushed over	bottom of upper channel, stream in the channel
26	trees range orientation from 060 to 120	depositional fan
25,5		stream 1m in the middle, pushed a fence over, large trees deposited, deposional topography varies possibly erosion after deposition.
25		large blocks deposited, splitting point.
24		large trees deposited, levee.
23	trees and material	
22	trees and material	top of channel
21		terraces in the inner channel
20	trees bent on side of channel	
19		
18	trees, 0,15 m diameter	
17,5	trees	
17	trees, soil, rocks and moss	bottom of channel
16		
15		
14		
13		
12		

Table 3.6 Observations of the track of landslide two. Information gathered by walking the track of landslide two. Corresponding latitude and longitude coordinates for the GPS points are found in table 3.3.

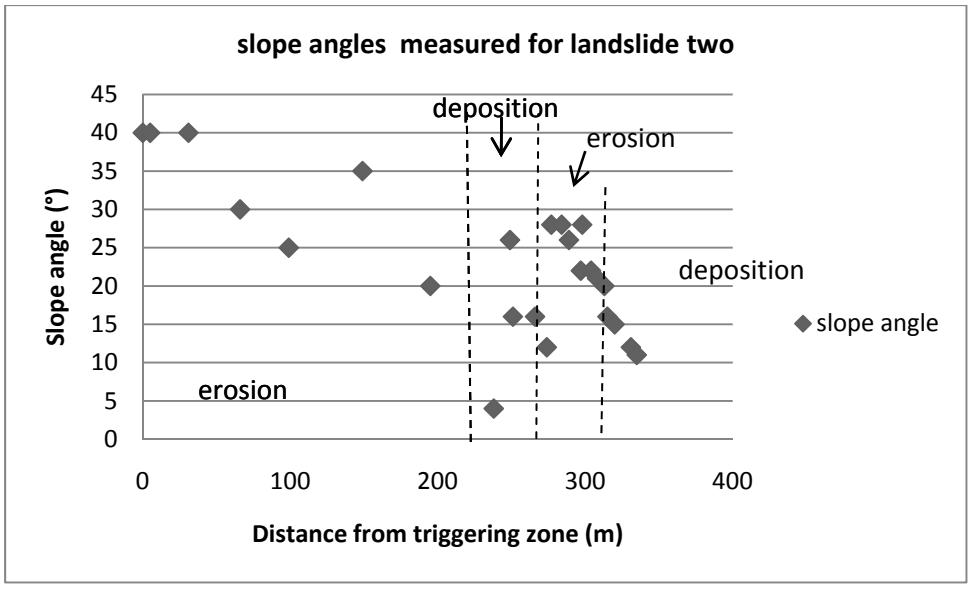

Figure 3.24 Measure slope angles for the track of Landslide two. The slope angle decreases down the slope. areas of erosion and deposition has been marked in the figure.

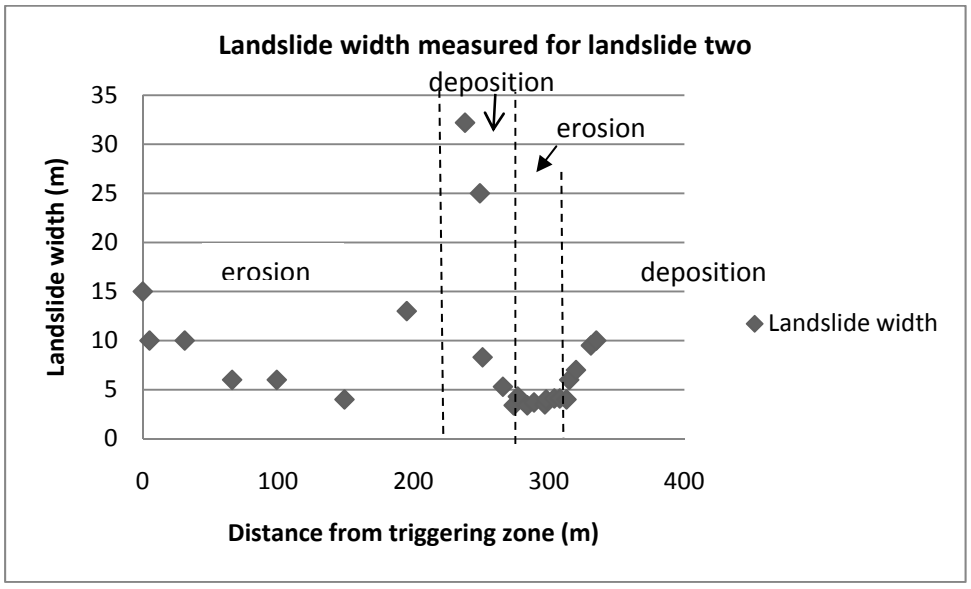

Figure 3.25a Measured landslide widths in landslide two from the triggering zone down to the final deposition, landslide width is the greatest at the locations where the landslide has deposited. areas of erosion and deposition has been marked in the figure.

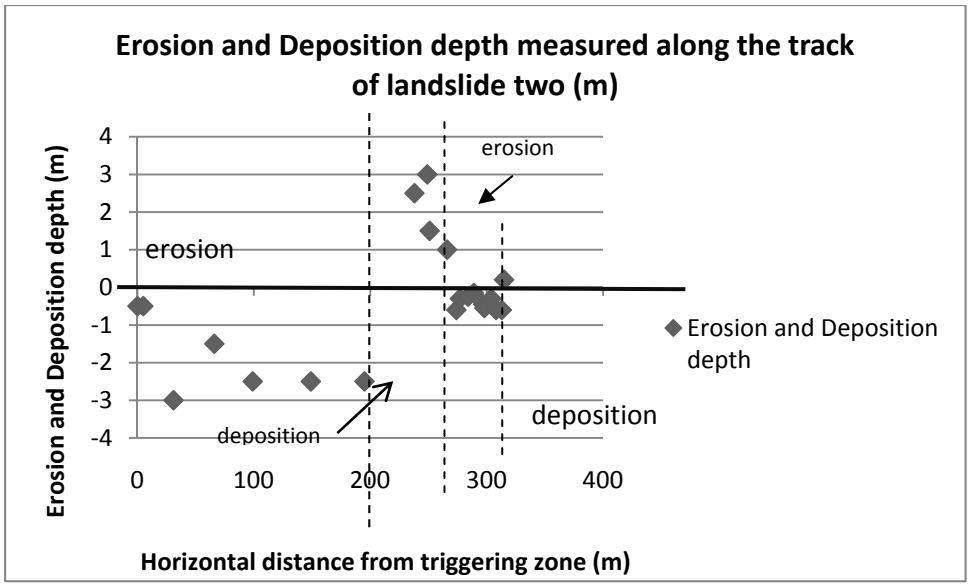

Figure 3.25b Erosion and deposition depth measured along the track of landslide two, negative numbers represent total erosion depth in meters, and positive number represent deposition depth in meters. Data is presented in table 3.4, and areas of erosion and deposition have been marked.

The other landslides in the study area will now be presented, and the differences or similarities with landslide two will be determined.

3.4.2 Landslide one

From figure 3.18B, the starting zone of landslide one is interpreted to be where the slope angle changes to a slightly steeper angle similar to landslides 4,5 and 6 in the study area. At the same elevation as the triggering zone of landslide 2 and 3, see figure 3.26 A and B, landslide one continues up the slope and has therefore been triggered at an higher elevation that landslides two and three. The landslide has a run out of 400 meters, calculated from figure 3.19, and a height difference of approximately 275 meters. This gives the apparent friction angle of the landslides to be approximately 34, 5°. The landslide has moved down an old ravine and down towards the valley floor. The channel is slightly triangular in shape, see figures 3.26 A, B, D, and E. The landslide has removed all the vegetation in the track and transported it down slope; the conditions before the landslide occurred can be seen in figure3.18A. In figure 3.26C a broken tree stump can be seen, as well as several trees that have been deposited parallel to the landslide track. An approximate width of the channel is 10-15 meters with a maximum erosion depth of 1-2 meters, see figure 3.26D. The landslide has eroded down to the bedrock in locations and a has possibly eroded into the overconsolidated sediment to a depth of 0,2-1 meter, shown in figures 3.26D and 3.26E. The grain sizes in the sediment the landslide has eroded is quite fine-grained in figure 3.26D with no visible large boulders present. On the 23rd of June, 2011 when figures 10.20 and 3.33 were taken there was still water present in the channel. The landslide does not deposit when it crosses the road at the same elevation as landslide two, it continues to erode. The landslide reaches to and has been deposited in the river. The consequences of this landslide for the people living in the areas were not great since it narrowly missed the house.

3.4.3 Landslide three

Landslide three start at approximately the same elevation as landslide two as seen in figure 3.18B. From figure 3.19 the landslide has a runout of around 200 meters and a height difference of 210 meters, this gives the landslide an apparent friction angle of 37,4°. Figure 3.27 A and E show that the channel has a triangular shape, and that it follows and old ravine. The landslide deposits into a fan when the slope angle becomes close to zero at an elevation of 435 meters above sea level, when the landslide cross the road, this is similar to landslide two. The slope angle decreases abruptly, and the track goes from a channelized slope to an open slope when the landslide deposits, see figure 3.27D. The upper track of landslide two is similar to landslide two at the same elevations, see figure 3.27 a, b, and C, landslide three is not as wide with a width of 3 to 5 meters, and has not eroded as deep as landslide two, the erosion depth can be approximated to 0,5 to 1 meters. The landslide has removed the vegetation in the track and has transported several trees down the slope and deposited them parallel to the track or at the road, see figure 3.27C and D. Figure 3.27D show the deposition of the landslide, and it has a thickness of roughly 1,5 meters and a width of 10 meters, the depositional fan has been partially stopped by a metal structure that has stopped the trees from moving in that direction, this has confined the landslide flow, see figure 3.27D. Figure 3.27E show that the landslide continues to flow down the slope after it deposited, but the landslide is small compared to the original landslide with a width of 1m. From figure 3.27 D and E the grain size of the landslide does not show any large boulders, but the tress are at least 5 meters long and 20 cm wide. The landslide has deposited on a road, and has therefore destroyed part of the road leading up to the upper most house in figure 3.26E.

Figure 3.26 Landslide one**.**

A, Landslide track of landslide one at the same elevation as the triggering zone of landslide two, looking south-west up the track.

B, Landslide track of landslide one at the same elevation as the triggering zone of landslide two, looking south-east down the track.

C, Broken tree on the side of the track at the same elevation as the triggering zone of landslide two, looking east.

D, Landslide track at the same elevation as landslide two cross the road, looking south-west up the track.

E, Landslide track at the same elevation as landslide two cross the road, looking east down the track. .

Pictures 3.26 a, b, and c are from (Mair, 2012), and Pictures 3.26 d and 3e are from (Bargel, 2011).

Figure 3.27 Landslide three**. A**, Landslide track of landslide three at the same elevation as point 30 for landslide two, looking north-west up the track. **B,** Landslide track of landslide three at the same elevation as the point of 28 of landslide two, looking north-west up the track. **C,** Landslide track of landslide three at the same elevation as the point of 28 of landslide two, looking east down the track.. **D,** Landslide track and deposition at the same elevation as landslide two cross the road, looking south-west up the track, metal barrier that stopped the landslide in the front of the Picture. **E,** Landslide track at the same elevation as landslide two cross the road, looking east down the track.

Picture 3.27 D belongs to the author, all the other pictures are from (Mair, 2012).

3.4.4 Landslide four

Landslide four starts at the same elevation as the landslides 1,5 and 6, as seen in figure 3.18B. The landslide has a run out of 435 meters and a height difference of 260 meters, this gives an apparent friction angle of 31, 45°. Part of landslide four has merged with the track of landslide five, figure 3.28D show deposition on the road 15 meters from the track of landslide five, the track of landslide four is on the other side of the track of landslide five than the deposited material. This deposited material cannot be from landslide five, because landslide five has only eroded when it crosses the road. Landslide four has split into two parts when it crosses the road, one part has gone straight down the slope while the other strand has followed the road. This deposit is therefore a clear indication that it was from landslide four, and that means that landslide four must have occurred before landslide five, since landslide five cuts through the deposited material on the road. Landslide four has therefore deposited when it crosses the road, similar to landslide two. Figure 3.28Adisplays that the landslide has a triangular channel, width of 4-5 m and it follows an old ravine. The vegetation has been removed by the landslide and transported down the slope. When the landslide meets the low slope angle of the road, and the track changes from channelized to open slope it deposits, much of its material. The matrix is fine-grained with coarse grains, blocks up to 2 meters in diameter were observed. The depositional fan on the road is 15 meters wide and 3 meters thick, see figure 3.28B. the landslide continues past the road and deposits further down the slope, see figure 3.28C. The erosion depth of the landslide is 2 meters.

3.4.5 Landslide five

Landslide five has a starting zone that is roughly at the same elevation as the other six landslides studied, the starting point has been measured by GPS, see appendix F. The runout of the landslide has been determined from figure 3.19 to be 450 meters with a height difference of 260 meters, this gives an apparent friction angle of 30°. The channel is triangular in shape and follows an old ravine. A large boulder with a diameter greater than 4 meters have been moved by the landslide in the track, this can be seen in figure 3.29a. The track is 25 meters wide just before it crosses the road, then it increases to 35 meters, and decreases to 10 meters below the road, the erosion depth is 8 meters, see figures 3.29b and c. The landslide has eroded into the overconsolidated sediments to a depth of 2-3 meters, see figure 3.29d. All the vegetation has been removed from the track and the landslide has deposited into a depositional fan when the slope angle decreased and the slope changed from channelized to open slope. Landslide five did not deposit when it crossed the road, as landslide two did, but it did deposit into a fan at the same elevation as the deposits in landslide two at point 14.

The landslide material in has a relatively fine-grained matrix with coarse grains. The landslide has deposited in a tear-shaped fan before it ended up in the river, seen in figure3.29d, e and f. The depositional fan has a width of roughly 100 meters and a maximum thickness of 3 meters that decreases with increased distance from the slope. Figure 3.29f show the depositional fan of the landslide being stopped by a fence. On the side where the depositional fan is, the thickness of the sediment is 70 cm, while it is only a few cm on the other side of the fence. The depositional fan contains large rocks with a diameter up to 1 meter. The landslide has crossed the road in two locations and the erosion depth into the overconsolidated sediment has increased each time the landslide has crossed the road. The landslide moved two cars that were parked in the area, and destroyed a garage that contained two additional cars. The landslide eroded the road at two points which completely destroyed the road in those locations, the landslide also deposited into a depositional fan that almost reached a house.

Figure 3.28 Landslide four**.**

A, Landslide track of landslide four when the landslide cross the road, looking west up the track.

B, The landslide has deposited on the road, looking North.

C, Landslide track of landslide four after it has crossed the road, looking east down the track, black square marks depositional fan of landslide four.

D, Deposits from landslide four on the road, approximately 15 meters from the track of landslide five, marked by blue sqaure.

All pictures belongs to the author.

Figure 3.29 Landslide five **A**, Large block with a diameter of approximately 4 meters in the upper part of the track of landslide five **B,** The track of landslide five just before it crosses the road, looking west up the track.

C, Landslide track of landslide five after it has crossed the road, looking east down the track,

D, Depositional fan of landslide five, looking west up the track.

E, depositional fan of landslide five, looking east.

F, depositional fan of landslide five, looking east.

Pictures a, d, and f are from (Bargel, 2011)

3.4.6 Landslide six

Landslide six starts at the same elevation as landslides 1,4, and 5, and it splits into two parts. The runout is determined from figure 3.19to be 350 meters with a height difference of 250 meters, this gives the landslide an apparent friction angle of 35,5°. The channel has a triangular shape, see figure 3.30a, and a levee has been deposited on the road in figure 3.30b.The vegetation has been removed by the landslide and several trees have been deposited on the road, see figures 3.30c and d. The channel has a width of 2 meters and an erosion depth of 2 meters, just above the road, when it crosses the road the width increases to 50 meters and a depositional depth of 0,5 meters, after the landslide has crossed the road the width decreases to 3 meters and an erosion depth of 1 meter . When the landslide crosses the road and deposits the slope angle decreases, and the slope changes from channelized to open slope, similar to landslide two. The landslide follows the road when it deposits, and it also continues straight down the slope; see figure 3.30 c and d. The part of the landslide that moves straight down towards the river erodes down into the overconsolidated sediments by approximately 0,5 meters. The landslide deposits contain rocks that have a diameter between 0,5 meter to 1 meter, and the grain size of matrix in the deposits on the road are relatively fine-grained with coarse grains. The landslide has ultimately been deposited in the river, but it deposited on the road in two location.

Figure 3.30 Landslide six **A**, track of landslide six, looking west up the track

B, deposits from landslide six when it crosses the road, looking south.

C, Deposition from landslide six on the road, looking north.

D, Erosion and deposition from landslide six when it crosses the road the second time.

Pictures a and d are from (Bargel, 2011), all the other pictures belongs to the author.

3.4.7 Comparison of the landslides when they cross the road.

GPS measurments of the point where the landslides crosses the road		
Landslide	GPS measurments	elevation
Landslide 1	N61 41.242 E9 41.304	465 m
Landslide 2	N61 41.270 E9 41.344	460 m
Landslide 3	N61 41.316 E9 41.357	472 m
Landslide 4	N61 41.353 E9 41.379	469 m
Landslide 5	N61 41.366 E9 41.405	465 m
Landslide 6	N61 41.397 E9 41.464	452 m

Table 3.7 GPS measurements of the point where the landslides cross the access road to the house.

Landslides width for the landslides (m)						
Landslide number	1	2	3	4	5	6
above the road (m)	15	13	3	2	25	2
at the road (m)	15	32,2	10	15	35	50
below the road (m)	15	25	1	2	10	3

Table 3.8 Landslides width of the landslides at the point just before they crosses the road, at the road, and below the road, illustrated by figure 3.31.

Erosion depth or deposition depth for the landslides (m)						
Landslide number	1	2	3	4	5	6
above the road (m)	-2	-2,5	-1	-2	-6	-2
at the road (m)	-2	2,5	1,5	3	-8	0,5
below the road(m)	-2	3	-0,5	-2	-6	-1

Table 3.9 Erosion depth, represented by negative numbers, in meters, and deposition depth, represented by positive numbers, in meters, for the when the landslides cross the road, illustrated by figure 3.32.

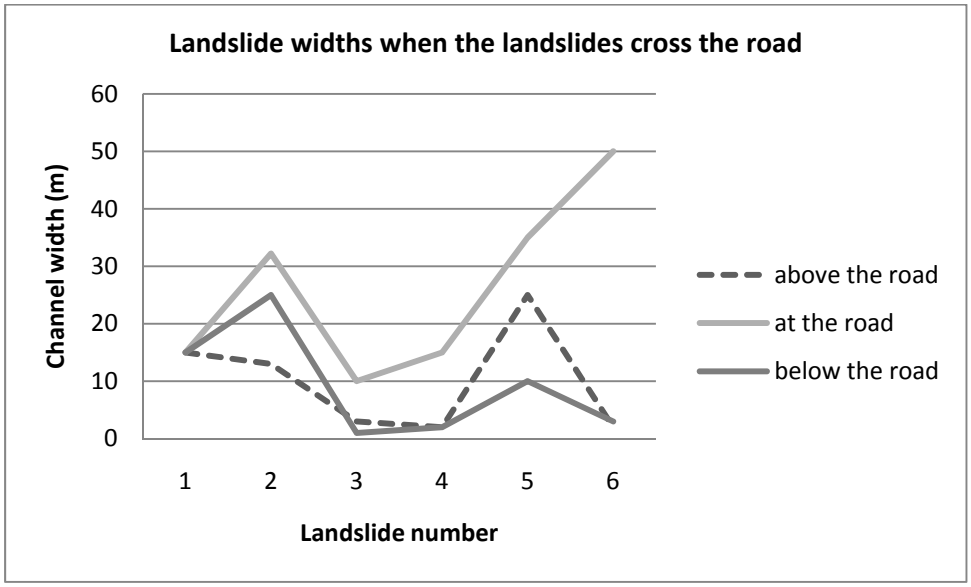

Figure 3.31 Landslide width of the six landslides when they cross the road, the elevation when the landslides cross the road is similar, but the elevation ranges from 472 meters to 452 meters.

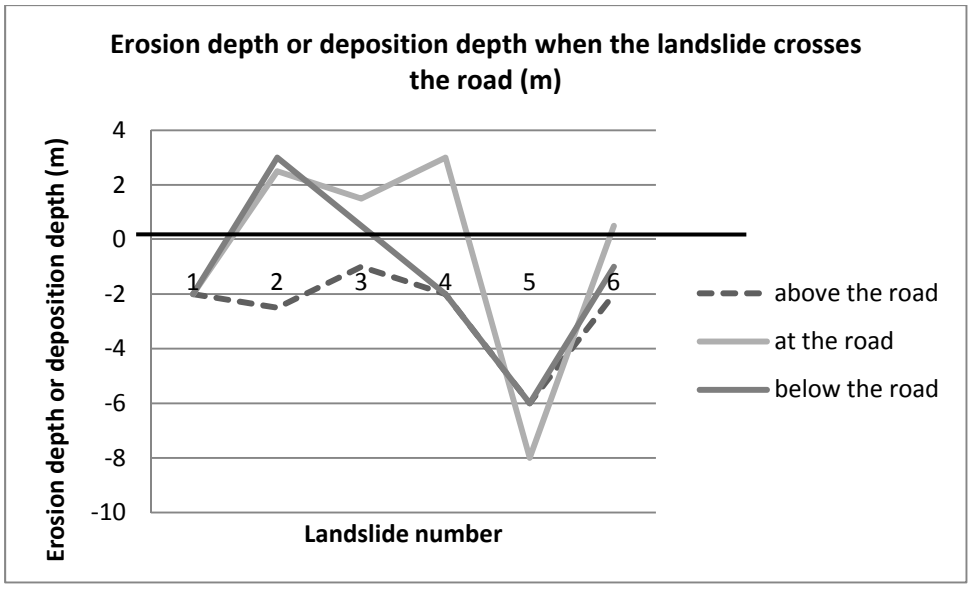

Figure 3.32 Erosion depth, represented by negative numbers in meters, and the depositional depth, represented by positive numbers in meters, when the landslides crosses the road. Landslides 2,3,4 and 6 all deposit on the road, while landslides 1 and 5 continues to erode when it crosses the road.

Table 3.7 show the longitude and latitude of the landslides when they cross the road, and the differences between the landslides when they do cross the road can be seen in tables 3.8 and 3.9, and figures 3.31 and 3.32.

Figure 3.31 show that for all the landslides except landslide 1 the width of the landslide increases when the landslide crosses the road, and from figure 3.32 it is clear that landslides 2,3,4, and 6 deposits when they cross the road. Landslides 1 and 5 does not deposit when they cross the road, but continues to erode.

3.4.9 Summary

Landslide	1	2	3	4	5	6
Height difference	275m	270m	210m	260m	260m	250m
runout	400m	425m	200m	435m	450m	350m
apparent friction angle	34,5°	32,4°	37,4°	31,45°	30°	35,5°
Runout ratio H/R	0,6875	0,635	1,05	0,598	0,58	0,714
channel shape	triangular	triangular	triangular	triangular	triangular	triangular
channel width	10-15m	5, 10-15, 20-30	3,10, 0,5	2,15,2	25,25,10	2,50,2
erosion depth	1-2m	2m	0,5-1m	2m	4-8m	0,5-1m
eroded overconsolidated sediments	yes	yes			yes	yes
deposition depth		2,5, 3, 0,2	1,5m	3m	1,5m	0,5m
deposition width		20-30m	20-30m	15m	100m	50m
levees		yes				
grain-size estimate of matrix	fine-grained	fine-grained	fine-grained	fine-grained	fine-grained	fine-grained
largest block		1,8m		2m	4m	0,5-1m
bedrock exposed	yes	yes	yes		yes	yes
crossed the road	yes	yes	yes	yes	yes	yes

Table 3.10 Summary of key features for the six landslides in the study area of Veikledalen.

Summary of key observations:

- All weather stations show spike in rainfall on the 10th of June 2011.
- All weather stations measured rainfall in the days before the landslides were triggered.
- Rainfall intensity (mm/hr) from Skåbu weather station at 11.00am was 11mm/hr.
- Soil water deficit on the 10th of June, 2011 was 20-60mm.
- Total runoff on 10th of June, 2011. Below 5mm.
- Total runoff on 11th of June 2011, between below 5mm to 10mm.
- The flood was locally a 100 year flood.
- Summary of landslide features in table 3.10.

4 Results and analysis

4.1 Grain size and friction angle

The material in the triggering zone of landslide two was observed in the field to have a fine-grained matrix and coarse grains. Even though the matrix is fine-grained, the weight percentage of the coarse grains means that the average grain size of the sample is medium to well-graded sand.

Since the top layer of the soil is relatively loose, the friction angle of the soil at ultimate strength can be estimated from empirical tables (Lambe and Whitman, 1979) to be in the range 26° to 30°. Considering the coarse grains in the soil, the friction angle is most probable closer to 30° so for the calculations in this chapter a friction angle of 30° will be used. Cohesion forces have been assumed to be zero for this result section. This is a simplification based on an estimate that the soil contains 10-20% clay or silt-sized material and hence will not cause significant cohesion. Note that this simplification may contribute to an error in the calculations.

A future quantitative grain-size analysis (not possible in this study) would allow more confidence in the friction angle, and how large the cohesive force in the soil is likely to be.

4.2 Factor of Safety

The soil in the study area has two layers, a lower overconsolidated layer at the bottom of the soil and a top layer that has become loose due to thawing and freezing processes over numerous years. The overconsolidated layer has a low permeability and groundwater will therefore most likely flow along the border between the top layer and the overconsolidated layer. The overconsolidated layer is much stiffer and has higher shear strength. The weaker top layer is potentially where the landslide has most likely failed. The thickness of this loose top layer can be estimated from the height of the back scar in the triggering zone which for landslide two is measured to be 0,5 meters. This thickness can vary along the slope, but the important number for determining the factor of safety calculation is from the triggering zone.

To calculate the factor of safety of the soil equation 1.13 will be used, see chapter 1.7 for definitions:

$$FS = A\frac{\tan\varphi'}{\tan\beta} + B\frac{c'}{\gamma H} \qquad (4.1)$$

If we assume the cohesive forces in the soil are negligible, and that the cohesion force due to vegetation is also insignificant, the second term in the equation becomes zero and only the first part of the equation is needed. The factor of safety will now be calculated for the triggering zone of landslide two for two scenarios: firstly the situation when the soil is completely dry; and secondly when the soil is completely saturated.

4.2.1 Completely dry soil

The local slope angle in the triggering zone has been determined from field observation (table 3.4) to be 40° and the friction angle in the triggering zone has been estimated (chapter 4.1) to be 30°.

When the soil is completely dry, the pore pressure ratio ru is zero and the dimensionless stability coefficient A is equal to 1, shown in figure 1.14.

The factor of safety for the soil when it is completely dry can therefore be determined.

$\mathrm{FS} = \mathrm{A}\frac{\tan\varphi'}{\tan\beta} + \mathrm{B}\frac{c'}{\gamma H}$ = 1*(tan 30/ tan 40) + 0 = 0,688

This gives us a factor of safety that is below 1 and is therefore unstable. Since the slope is standing and has not failed under dry conditions, it suggests either that there must be cohesive forces in the soil, the friction angle estimated for the soil is too low, and/or the slope angle measured in the landslide track was higher than average (it is noted in chapter 2.1 that the slope was generally variable).

4.2.2 Completely saturated soil

Here the factor of safety are calculated for the same friction angle and slope angle as for wet conditions. The cohesion is still assumed to be zero so the second term disappears but due to the soil containing water, the pore pressure ratio will no longer be zero, and constant A will therefore no longer be equal to 1. A can be determined by calculating the pore pressure ratio, because the sum of A and the pore pressure ratio is equal to 1. The pore pressure ratio can be calculated for seepage parallel to the slope:

$$r_u = \frac{X}{T}\frac{\gamma_w}{\gamma}cos^2\beta \qquad (4.2)$$

The information needed is X, the thickness of the seepage water, which for a completely saturated soil it is equal to the soil thickness, hence here 0,5 meter. T is the thickness of the soil the water seeps through, which for the triggering zone is estimated to be 0,5 meter. The unit weight of water, γw is constant at a value of 10 kN/m^3. The unit weight of the soil, estimated from published values for wet sand with gravel is 20 kN/m^3 (De Blasio, 2011).

The pore pressure ratio for a completely saturated soil can be calculated from figure 1.15:

$r_u = \frac{0,5}{0,5}\frac{10}{20}cos^2 40$ = 0,29.

A is then equal to 1-0,29 =0,71.

The factor of safety can then be calculated for a completely saturated soil:

$\mathrm{FS} = \mathrm{A}\frac{\tan\varphi'}{\tan\beta} + \mathrm{B}\frac{c'}{\gamma H}$ = 0,71*(tan 30/ tan 40) + 0 = 0,488.

This shows that the factor of safety for a completely saturated soil is below one and the soil is unstable. The factor of safety decreases compared to that for a completely dry case, suggesting that the soil is more unstable when the soil is completely saturated. Although the absolute values computed may have error due to the simplifications made but the relative values are thought to be correct.

4.3 Deposition volume

The volume of the deposits in the landslides can be estimated, if the deposition is assumed to have the simple geometric shape of a rectangle. The data are presented in table 4.1. In landslide two (L2), data are presented for immediately above (section3a) and below road (section 3b) and section 5.

Landslide	Length of landslide (m)	Width of landslide (m)	Thickness of deposit (m)	Estimated Volume (m^3)
L2 (section3a)	10	32,2	2,5	805
L2 (section3b)	24	25	3	1800
L2 (section5)	2	6	0,2	2,4
L2 TOTAL	-	-	-	2602,4
L3	8	10	1,5	120
L4	5	15	3	225
L5	100	70	1,5	10500
L6	22	50	0,5	550

Table 4.1 Deposition volumes calculated for landslide two.

The total deposition for landslide two is calculated to be 2602,4m^3. The depositional volume of landslide three on the road is 120m^3. Landslide four deposits on the road with a volume calculated to be 225m^3 This slide also deposits further down the slope, but that depositional fan was not been measured and can therefore not be calculated. Landslide five deposits at the same elevation as section five of landslide two, the dimensions are estimated from figure 3.29F giving a depositional volume of 10 500m^3. The deposition volume of landslide six based on the road deposit is calculated to be 550m^3.

From these simple calculations of the depositional volume, with the assumptions that were made, show that landslide five is the landslide that has deposited (and presumably eroded) the greatest amount of material. The landslide with the second largest deposition is landslide two, then landslide six, landslide four, and finally landslide three. The deposition of landslide one was not observed, and part of the deposition from landslide four was not measured so the volume is underestimated here.

The erosion is also a lower bound to a possibility of 11 months of erosion of the deposited material.

4.4 Erosion Volume

The erosion volume of landslide two can be estimated from the measurements of the track made in the field. Assumptions used are: i) that the erosion depth measured in the field is the height to the previous surface, ii) that the track has a constant slope angle and landslide track width between each measuring location, and iii) that the horizontal distance measured using the GPS is accurate. The track has been assumed to be a triangular prism. For point 27 the channel has an observed inner channel so the volume calculation has been divided into two parts. Importantly, we measured the track shape in May 2012 and have assumed that all the erosion is due to the landslide, However, photographs taken in June 2011, see figure 3.21, indicate that additional erosion has taken place between June 2011 and May 2012. Unfortunately we do not have constraints on the extent of the subsequent erosion and our estimate will be an upper bound, however, future work processing lidar

data collected in June 2011, or detailed comparison of photographs at key points could help indicate the intermediate erosion.

The volume of a triangular prism is calculated using the height of the prism, length, and width and then multiplying the number by 0,5. To find the lengths of the prisms the slope angle and the horizontal distance between each point is used to calculate the length in the following manner.

For the right strand of the triggering zone: horizontal distance is 31m, slope angle is 40°, length is equal to= 31m /cos 40° = 40,5 meters. The total erosion depth is then added for the height of the prism, here 0,5 meter, and the width of the channel, 15 meters. Total erosion volume for the right strand of the triggering zone is then: 152m^3.

The same method is then used for all the sections of the landslide, see table 4.2, for section four an average slope angle and channel width have been used to estimate the erosion volume of the entire section with the entire horizontal length of section four, due to the erosion in this section being very small compared to the erosion in sections one and two. The Total eroded volume is 2179,3 m^3.

point	horizontal distance to next point (m)	slope angle °	length of track (m)	width of track (m)	depth of track (m)	Estimated volume m^3
33	31	40	40,5	15	0,5	152
32	26	40	34	10	0,5	85
31	35	40	40,4	10	3	606
30	33	30	36,4	6	2	218,4
29	50	25	61	6	2,5	457,5
28	46	35	56,2	4	2,5	281
27 main channel	43	20	45,8	2	1,5	68,7
27 inner channel	43	20	45,8	13	1	297,7
Section four	47	23	51,1	1,2	0,42	13
Total Volume:						2179,3 m^3

Table 4.2 Erosion volumes calculated for landslide two.

4.5 Rainfall thresholds

For calculating rainfall thresholds in Veikledalen, the hourly rainfall measurements at Skåbu weather station, figure 3.13 and table 3.2b, were used. The maximum hourly rainfall was measured to be 11mm/hr, this can be compared to figure 4.1 (from Caine, 1980) of the rainfall thresholds expected for shallow landslides.

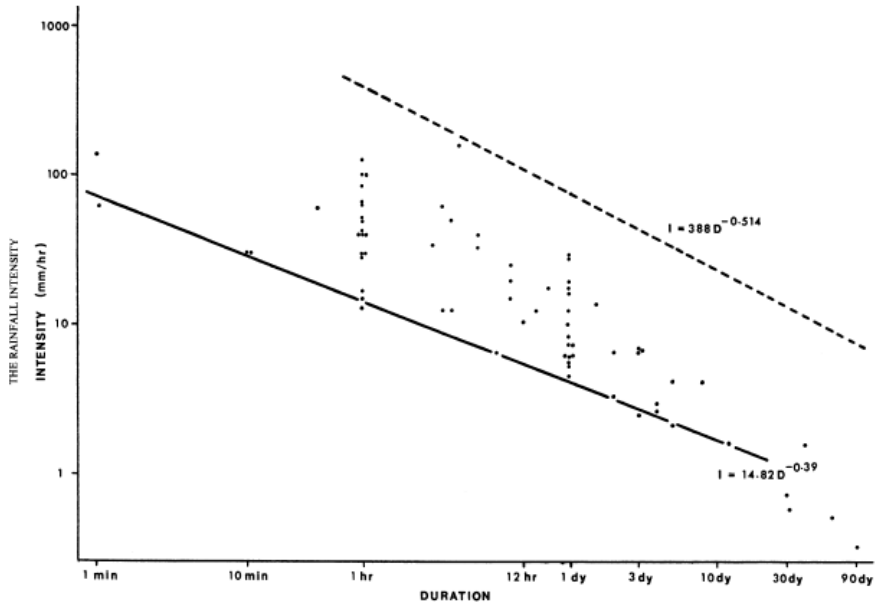

Figure 4.1 Rainfall thresholds for slope failure from rainfall intensity and duration. The lower threshold is for the equation I= 14.82D$^{-0,39}$, where I is the rainfall intensity in mm/hr, and D is the duration of the rainfall in hours. The upper curve will not be used here but is the global maximum precipitation intensities: I = 388 D$^{-0.514}$ (Caine, 1980).

Weather station	Total precipitation (mm/24hr)	Rainfall Duration (hr)	Average hourly precipitation (mm/hr)
Sjoa	59,5	24	2,48
Hovdgrenda	27,5	24	1,146
Venabu	30,5	24	1,271
Espedalen	41	24	1,71

Table 4.3 Average hourly precipitation for Sjoa, Hovdgrenda, Venabu, and Espedalen weather station, used in figure 4.2 for rainfall threshold calculations.

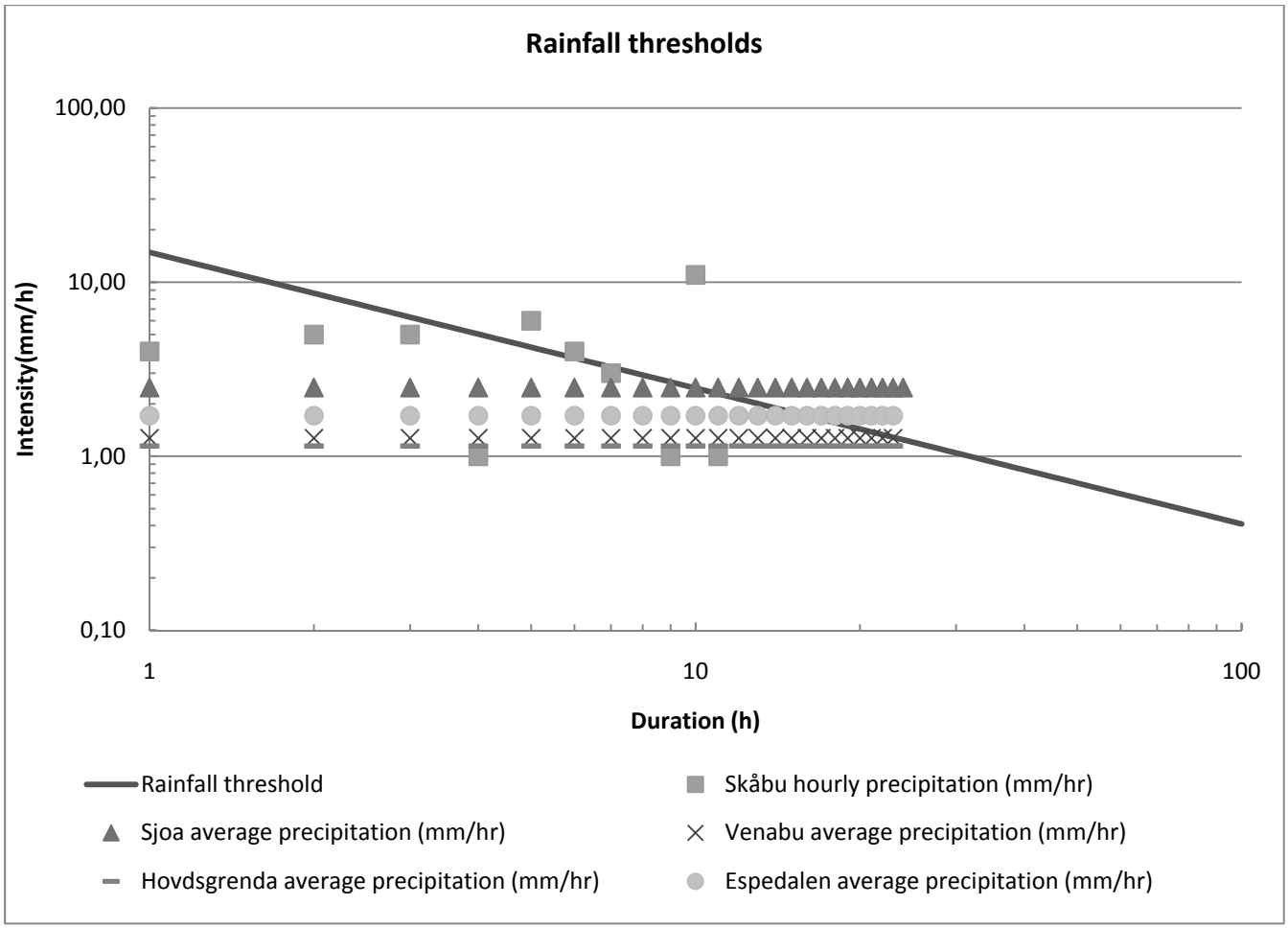

Figure 4.2 Rainfall thresholds calculated with hourly precipitation data from Skåbu weather station, table 3.2b, for a rainfall that started at 02.00 on 10th of June 2011. The duration of this rainfall was 11 hours. Average precipitation values from Sjoa, Venabu, Hovdgrenda, and Espedalen weather stations are also presented.

For duration of 11 hours, whit a maximum hourly rainfall intensity of 11mm/hr the rainfall event crosses the rainfall threshold created by Caine, figure 4.2. From table 3.2b rainfall occurred before 02.00 am, but the rainfall stopped and is therefore not part of the rainfall event used to calculate the rainfall thresholds. This means that the duration of the rainfall event was 11 hours, and an accumulated rainfall of 41mm, this gives an average rainfall intensity of 3,73 mm/hr. The rainfall threshold in figure 4.2 is exceeded after duration of five hours at 06.00 am in the morning. The landslides have been reported to have been triggered in the early morning on 10th of June and the rainfall data support this. The rainfall in the local area of Veikledalen might be slightly different from Skåbu weather station, and the rainfall event might therefore have crossed the rainfall threshold at a different time or not at all.

If the rainfall data from the other four weather stations at was used, the weather station only measured precipitation every 24 hours, and it is therefore necessary to assume that the rainfall event lasted for 24 hours, the average precipitation for every hour can then be calculated, see table 4.3. The average rainfall intensities for all weather stations except Hovdgrenda exceed the rainfall threshold, but the rainfall data from Hovdgrenda is very close to the threshold. This indicates that the rainfall event could trigger shallow landslides, based on this rainfall threshold. The rainfall event probably did not last for 24 hours, and the rainfall intensity could therefore be higher or lower for the weather stations.

The antecedent (accumulated) rainfall is an important aspect to consider in the triggering shallow landslides due to rainfall events. The soil moisture content before the rainfall event (9th of June 2011) that apparently triggered debris flows in Veikledalen on the 10th of June 2011, was normal, but the soil moisture conditions at 7am on the 10th of June 2011 were wet or very wet compared to normal (NVE et al., 2012). In the 10 days before the debris flows were triggered 20,1mm of rain had fallen in the area, see figure 3.9.

4.6 Transport of boulders and cars, and vegetation damage.

The transportation of large boulders by debris flows is observed in the landslides in the study area. The diameter of the largest boulder that can be transported is dependent on the average flow depth (Oliferov, 1970) found in (Costa, 1984). The buoyancy, e.g. of the large transported boulder in figure 3.29A, can be calculated, see chapter 1.8.4, to show how much of the object can be supported by the buoyancy force.

The bulk density of the debris flow depends on the amount of solids that are present in the water. Bulk density has been measured from effluent fluids in debris flow flume experiments (Iverson, 1997) giving a range of bulk fluid densities from 1030 to 1110 kg/m^3 for a sand-gravel mix. The bulk densities for a debris flow, have been calculated from bed stress in the experiments range from 1400 to 2400 kg/m^3 for a sand-gravel mix (Iverson, 1997). 2400 kg/m^3 will therefore be used for the calculations below since it reasonably well fits the material in the triggering zone in the study area. These bulk densities have been calculated with the assumption that debris flow solids and fluid constituents interact, and have distinct properties.

The correct bulk density depends on whether the debris flow is assumed to be a Newtonian fluid, like water, or a non-Newtonian fluid which has shear strength. If the boulder is assumed to be a sedimentary rock, the bulk densities generally range from 2200 to 2800 kg/m^3, the mean of this density range is 2500 kg/m^3, which will be used here. The submerged weight of the boulder can then be calculated, where ρ_s is the solid density, and ρ_f is the fluid density.

Thickness of Flow required to move boulder assuming buoyant forces

Fluid density: $\frac{\rho_s - \rho_f}{\rho_s}$=(2500kg/m^3-1100 kg/m^3)/2500kg/m^3= 0,56.

This means that the submerged weight of the boulder is only 56% of its dry weight, which means that a volume approximately twice as large as the volume of the boulder is needed to move the boulder. This can be shown by the following equation.

The boulder has an estimated volume of 4m*4m*2m= 32m^3.

The mass of the boulder can be calculated from the density and the volume to be:

32m^3*2500kg/m^3= 80 000kg.

To find the volume that is needed to transport a boulder with that weight the same equation is used.

80 000 kg= 1100kg/m^3 *Volume.

Volume= 80 000 kg/ 1100 kg/m^3= 72.7m^3.

This means that the volume needed to displace the weight of the boulder is 72,7m^3. To find how deep the debris flow must be, the area beneath the boulder must be found. The area has been estimated to be 4m*4m=16m^2. The thickness of the debris flow is therefore:

16m^2*X= 72,7m^3 , X= 72,7 m^3/16m^2= 4,54 meter.

The thickness of the debris flow needed to move the boulder is 4,54 meters, which landslide five does have in certain locations, but it is not known if the thickness of the flow were that great in that location. Other forces than buoyancy can influence this number and lower it, for example the impact force, then the boulder will not be buoyant in the debris flow but rather pushed by the debris flow.

Solid density: $\frac{\rho_s - \rho_f}{\rho_s}$=(2500kg/$m^3$-2400 kg/$m^3$)/2500kg/$m^3$= 0,04

This means that the submerged weight of the boulder is only 4% of its dry weight, which means that the submerged weight of the boulder is much lower than the dry weight and it is therefore easier to transport. The thickness of the material needed to transport the boulder can be calculated.

The boulder has an estimated volume of 4m*4m*2m= 32m^3.

The mass of the boulder can be calculated from the density and the volume to be:

32m^3*2500kg/m^3= 80 000kg.

To find the volume that is needed to transport a boulder with that weight the same equation is used.

80 000 kg= 2400kg/m^3 *Volume.

Volume= 80 000 kg/ 2400 kg/m^3= 33,3m^3.

This means that the volume needed to displace the weight of the boulder is 33,3m^3, this is almost equal to the volume of the boulder at 32m^2. To find how deep the debris flow must be the area beneath the boulder must be found. The area has been estimated to be 4m*4m=16m^2. The thickness of the debris flow is therefore:

16m^2*X= 33,3m^3 , X= 33,3 m^3/16m^2= 2,08 meter.

The thickness of the debris flow needed to move the boulder is 2,08 meters, which is almost equal to the height of the boulder at 2 meters. Other forces than buoyancy can influence this number and lower it, for example the impact force, then the boulder will not be buoyant in the debris flow but rather pushed by the debris flow.

These calculations on buoyancy show that a non-Newtonian debris flow which has a high bulk density can transport large boulders more easily than a Newtonian fluid, for example water which has a low bulk density. Since the debris flow does contain percentage of solids, that have been deposited down the slope, for the rest of the calculations that need bulk density the bulk density of 2400 kg/m^3 will be used for the debris flow.

Thickness of flow required to move a tractor and a car

The landslides transported several cars, and a tractor. The thicknesses of the flow necessary to transport these items have been calculated and are shown in table 4.4.

item	weight	Area beneath the item	volume necessary to transport the item	thickness of flow
car	1500 kg	2,5m *1,5m = 3,75m2	1500/2400= 0,625 m3	0,625/3,75= 0,17m
tractor	7000 kg	2m *3,5 m= 7m2	7000/2400= 2,92m 3	2,92/7=0,42m

Table 4.4 Thickness of flow necessary to transport a car and a tractor.

Table 4.4 show that the thickness of the flow does not need to be very thick, and since the deposition in the area where the cars were transported were at least 70 cm, this should be sufficient to transport the cars. The deposition depth where the tractor is located on the depositional fan at the road for landslide two, the thickness of the deposit is 3 meters thick.

Impact Force of the debris flow

The impact force of the debris flow can also be calculated.

$$P = \alpha \frac{\gamma v^2}{g} = 0{,}41v^2 \quad (4.3)$$

Where P is the impact pressure, α is the velocity-head coefficient (which is 2.0 for laminar flow), γ is the unit weight, v is the mean velocity, and g is the gravitational acceleration. The equation can be simplified to $0{,}41v^2$ by assuming the flow is laminar, and that the unit weight is 2000 kg/m^3, which are common values for debris flows (Costa, 1984). This impact force can destroy trees and push objects, for example cars or boulders. If you assume the velocity of the landslide was 50 km/h or 14m/s, then the impact force will be 80N/m^2.

Shear stress on the bed

The shear stress the debris flow can exert on the stream bed can be found:

$$\tau = \rho g R S \quad (4.4)$$

where τ is the total shear stress, ρ is the fluid density, g is the gravitational acceleration, R is the hydraulic radius(can be approximated as the average flow depth in wide channels), and S is the friction angle (can be estimated to be the slope angle for uniform flows).

If we assume that the flow depth is equal to the erosion depth, and the fluid density is 2400 kg/m^3, the total shear stress can be calculated for the landslide at different points. For point 27 the erosion depth is 2,5 meters, and the slope angle is 20°, the total shear stress is then:

τ= 2400 kg/m^3*9,81m/s^2*2,5m*20°= 1 177 200 Pascal.

5 Discussion

The interpretation of how the landslides were triggered, and insights into possible debris flow dynamics from erosion, transport and deposition along the track is now presented. Most information is landslide two, which was studied in detail but it is thought that this can be used as a generic example of all six landslides. Information from the other landslides is added where appropriate.

5.1 Material and landslide

The soil material in the area has a fine-grained matrix of clay and silt, with coarse grains, see for example figure 3.20B or 3.22B for the material in the triggering zone of landslide two, and the material has angular grains and is poorly sorted. This is due to the soil being an erosion product from the last glaciation period in Norway, which started approximately 115 000 years ago and had the ice had melted about 9000 years ago. Veikledalen was close to the ice divide and the ice thickness was probably a few kilometres thick, see figure 1.18. The material is interpreted to be a sub-glacial lodgement till that has been transported for maximum five kilometres. The rocks in the area are sedimentary rocks, figure 1.16, and the moraines that are a product of these rocks have been shown to be fine-grained, figures 1.17 and 1.19. This indicates that the type of landslide material that is present in the area would be debris, and not earth since 20 and 80 percent of the soil has a particle size that is greater than 2mm.

The glaciation period in Norway overconsolidated the soil in the study area, but due to freezing and thawing of water in the soil for the last 9000 years the top layer of the overconsolidated soil has become loose. The overconsolidated soil is hard and has a low permeability; the permeability, or ability for the soil to infiltrate water, in the study area can be seen in figure 1.20. The overconsolidated soil is also stable, this can be seen when the landslides have eroded into this overconsolidated layer of soil, the channel walls are almost vertical and has apparently stayed that way for 11 months. Due to the overconsolidated layer being stable (and having higher shear strength), the loose top layer is the probable material associated with the initially triggered landslide. The thickness of this top layer has been estimated to be 0,5 meter, from the back scar of landslide two.

When determining the type of movement for the landslide, fall and topple can be quickly rejected, because the material has clearly been transported down the slope and has not fallen down or toppled in free fall. The landslide cannot be classified as a spread since unlike a spread. The softer material is in the top layer, and the bottom layer has not spread out and liquefied beneath the top layer, as would be expected. This means that the two remaining possible landslide types are slides and flows.

From figure 3.20A and B, the starting zone is shown to have an almost vertical back wall. Flows rarely have a preserved initiation shear surface; therefore it is unlikely that this event started as a flow. On the other hand, the landslide is clearly not a coherent slide which would be expected to move along a rupture surface or failure plane when it moves down the slope. This points to that the landslide was initiated as a debris slide and then transformed into a debris flow. The transformation into a debris flow is probably greatly dependent on the water content in the soil. It is common for many landslides that they start as one type then transition into other types.

The precipitation in the area in the days before the debris flows were initiated were high, especially in the 24 hours before the event occurred, table 3.2b show the hourly precipitation data on 9th and 10th of June, 2011. Figures 3.14 and 3.15 are precipitation maps created by NVE for the study area, the area received between 75 to 150 mm of precipitation in the week before 10th of June, 2011. The soil water deficit in the area was low which means that not much water was needed before the soil would be completely saturated. Figure3.16A indicates that the amount of water in the area was high. This water was surface runoff and since the top layer has a high permeability this must mean that the soil must be almost fully saturated due to the water. Figure 3.16A shows the soil water deficit estimated by a model on the 10th of June at 7am, the soil water deficit in the study area is between 20 to 40mm. Figure 3.16B shows that the soil water deficit compared to normal is wet or very wet. This suggests that there is probably enough water in the area for the initiated landslide to be transformed into a debris flow, which is also indicated by the channels. The starting zones for debris flows explained in appendix C are not applicable to these flows.

5.2 Triggering mechanisms

Due to the intense rainfall in the days before the events and the watermarks on the trees ,it is likely that the debris flows in Veikledalen were rainfall induced, however we first rule out other possibilities e.g. flooding and snow melt, then present the supporting evidence.

Since there was no snow in the local area, the soil cannot have become saturated by melting water from snow. The river in the valley was flooded during this enhanced rainfall (and before the debris flows were initiated). It is possible that the flood may have affected the groundwater levels in the adjacent areas and may have contributed to the event but it is thought to be too far from the starting location to have contributed significantly to the triggering. The river may have eroded the river banks, but again they are thought to be too far away to have caused the slope to become unstable due to erosion. This leaves antecedent rainfall and intense rainstorms as the most probable triggering mechanisms for these debris flows. The true triggering mechanism is most likely a combination of these two mechanisms.

5.2.1 Antecedent Precipitation

The area had experienced rainfall in the days before the debris flows were triggered, and this would have increased the soil water content, figure 3.15 shows that the area has gotten at least 75 mm of precipitation in the week before the event, possibly over 150 mm in the slopes above the study area. The soil water content on the 9th of June was normal, and the soil water deficit was between 40 to 60 mm, and 24 hours later it was 20 to 40 mm, but the groundwater level in the soil compared to normal was high. 24 hours later the groundwater level was very high compared to normal. This clearly indicates that the precipitation that fell on the area in those 24 hours has been infiltrated into the soil and made it more saturated. The groundwater potential, and infiltration ability of the soil are shown in figures 1.20 and 1.21, and they show that the soil had a moderate ability to infiltrate water, and a limited groundwater potential. This means that the soil can infiltrate the rainwater at a sufficient level and that not all the rainwater will become surface runoff. The groundwater potential show that the amount of water needed to completely saturate the soil is less than for a soil with a significant groundwater potential. By changing the groundwater conditions, the antecedent rainfall may have increased the likelihood of debris flows being initiated, because together with the precipitation from the intense rainstorm it makes the water content in the soil reach critical levels. Studies of debris flows have shown that antecedent rainfall is an important contributing factor and

that insufficient antecedent rainfall may cause no debris flows to be triggered, see chapter 2.2.2. Further investigation is required to determine how important the antecedent rainfall was for this particular event. Figures 3.3 to 3.12 show the antecedent rainfall in the local area before the debris flows were triggered.

5.2.2 Precipitation Intensity

The intense rainstorm on the 10th of June, 2011 precipitated between 50 and 75 mm of rain on the study area, figure 3.14, measurement from the closest weather station Sjoa gives a precipitation value for the 24 hours before the events occurred to be 59,5 mm. Hourly precipitation data from Skåbu weather station, table 3.2B and figure 3.13, show that the maximum hourly rainfall intensity for the areas was measured to be 11mm/hour. The total precipitation measured for Skåbu weather station at 7am on 10th of June was only 32mm, this indicates that the precipitation in the study area was likely greater than what was measured at Skåbu weather station.

The duration of the rainfall at Skåbu weather station has been estimated to be 11 hours, and the rainfall event did exceed the rainfall threshold, see figure 4.2, after 5 hours of rainfall. The average hourly rainfall from Sjoa, Espedalen, and Venabu weather stations also exceeded the rainfall threshold, Hovdgrenda weather station is very close to the rainfall threshold. Due to the numbers being average hourly precipitation, the hourly precipitation might have been higher, and the duration of the rainfall event could have been shorter than 24 hours, this would affect the point at which the rainfall event exceed the rainfall threshold. The crossing of the rainfall threshold of the rainfall event can be interpreted to mean that the landslides were triggered by the intense rainstorm, possibly in a combination with antecedent rainfall.

5.2.3 Triggering Zone

It is possible that the intense rainstorm precipitation coupled with the antecedent precipitation created a temporary aquifer in the soil in the triggering zone. Figures 3.19b, 3.19c, and 3.18 show that debris flows 1,4,5 and 6 start at similar elevations, and debris flows 2 and 3 start at similar elevations, and this corresponds to the point where the slope angle changes from a shallower to a steeper slope angle. This bend in the slope can create a confinement because the thickness of the soil is greater above the bend but may be reduced in the steeper part since the increased slope angle makes the soil more likely to slide, due to an increase in the gravitational force which increases the driving force of the soil and decreases the factor of safety, see chapter 1.6.

Because the permeability in the underlying overconsolidated layer of the soil is low, the infiltration rate of water (and hence rainwater) into that layer is less than in top layer. This leads to undrained conditions and the upper layer can become more and more saturated by the rainwater. It is likely that this may have occurred before the debris flows were triggered. Alternatively, groundwater could also flow along the boundary between the two layers and be injected into the area in that way. Because of the transition in the slope, the amount of water being infiltrated into the soil above the bend may be greater than the amount of water that can move past the bend in the slope. This means that the amount of water above the bend would increase and a confinement of the temporary aquifer could have been created. Figure 3.16 indicates significant surface water present in the area, which means that the precipitation rate must have been higher than the infiltration rate of the soil, or that the soil is completely saturated. Which of these occurred here is not known, but it is more probable that the surface water was due to the infiltration rate than the soil being completely

saturated, because surface runoff was measured in the days before the debris flows were triggered, and the soil water deficit had not reached field capacity, see figure 3.16A.

5.2.4 Excess pore pressure

The significant increase in water in the soil may induce an excess pore water pressure in the soil if it is not allowed to drain away (i.e. undrained conditions exist),the pore water taking the additional vertical stress on the soil due to the extra weight of the water. The increase in stress cannot be accommodated by the soil skeleton because the soil grains cannot rearrange and must therefore be supported by the pore water. The increase in pore water pressure decreases the effective stress in the soil which in turn decreases the shear strength in the soil, because the shear stress can only be resisted by the soil skeleton. Loose sand can also withstand lower shear than Dense sand , see appendix D, and this could explain why the overconsolidated soil does not fail; only the top loose layer initially fails. Given the conditions, the materials and the geomorphologic situation, it is reasonable to suggest that this is how the debris flows in the area were triggered: by an intense rainstorm (following an accumulation of rainfall) that due to a confined undrained soil induced an excess pore water pressure in the soil, which decreased the effective stress in the soil and hence the soil strength in the soil. When the soil strength decreases below the value of the shear stress in the soil the soil will fail and initiate a debris slide that turned into a debris flow.

5.3 Debris flow track

5.3.1 Channel

The debris flow channels follow old ravines that were thought to be created by debris flows during the flood in 1789, see chapter 1.2.1. Since houses were built at this location between the debris flow channels it is reasonable to assume that debris flows do not occur very frequently in the area, if they did people would have tried to protect their homes. The debris flow channel is both triangular, figure 3.21A, and u-shaped (rectangular or circular) where the track has been confined by bedrock, figure 3.21C. Both triangular and circular or rectangular channels have a rigid plug where there is no deformation, in the centre of the flow, see chapter 1.6.4 and appendix C, Triangular channels also have the presence of dead regions along the edges of the channel, where there is no internal deformation. These dead regions can create levees, which have been observed for landslide two as a combination of trees and soil, or only soil, for example figure 3.23A. This strengthens the theory some sort of plug flow with dead areas occurred in the channel.

5.3.2 Vegetation removal

Prior to the debris flows, the area was covered in vegetation, figure 3.18A, especially quite high birch trees and possible Alder trees. The debris flow tracks are now completely void of any vegetation indicating that the energy in the slide/flow was sufficient to uproot and move the trees. Along some of the edges of the debris flows the trees have been bent, but not removed, this indicate that the flow has a lower velocity along the edges of the flow, as would be expected for a triangular channel, see chapter 1.6.4 and appendix C. In the steeper parts of the debris flow track, at a slope angle of 40° in section one and two of landslide two, chapter 3.4.1, all the vegetation has been removed, but when the debris flow reaches areas where the slope angle is less or when the slope opens up, for example the deposition of landslide six on the road in figure 3.30C, the vegetation is spared. In some places, figure 3.29F, the trees seem to help stop the debris flow, or at least stop it partially. This means that the debris flow must have a certain amount of energy to be able to remove the

vegetation, and the removed vegetation, size and diameter of trees, can therefore be used as a estimation of energy between the debris flows. The larger the trees the debris flow is able to uproot or break in half, the more energy the debris flow must have, this energy could for example be an impact force of large boulders in the debris flow, see chapter 4.6.

5.3.3 Erosion

The debris flow channels show erosion of the sediments by the debris flow. Erosion can only occur when the slope angle is great enough for the debris flow to have sufficient energy to transport the material down the slope. Much of the debris flows show erosion into the overconsolidated sediments, table 3.10, these layers are stiff and much more energy is needed to erode into these sediments compared to the loose layer on top. The overconsolidated sediments can be seen as almost vertical walls of soil, figure 3.29 B and 3.29D, and the shear strength needed in the soil for it to be able to remain vertical for a long period of time is high, and this indicates that this soil layer is very stable. The erosion into the overconsolidated layer seems to occur in the areas where the slope angle is steeper, and these are the areas in theory where the debris flow has the highest energy, the erosion depths confirms this theory, see figure 3.29B and table 3.9. The debris flow with the greatest erosion depth and the observed greatest amount of erosion into the overconsolidated sediments is the fifth debris flow. This means that debris flow five in theory should be the debris flow with the highest energy, and it is the debris flow with the largest depositional fan and has therefore also entrained the most amount of material.

For debris flow two, which is the one that has been studied in detail, the channel of the debris flows becomes wider when the slope angle becomes shallower, see table 3.4, and the debris flow is more spread out, and the erosion depth has decreased. The width and erosion depth of the landslide is also influenced by the possible confinement by bedrock, see figure 3.21.

The bed material has become entrained into the debris flow, and this process was probably helped because the sediments were at least partially saturated due to the weather, see chapter 1.6.4 and appendix C. The channel material can also become more unstable due to undrained loading, impact loading, and liquefaction of the material because of the debris flow moving over the channel bed material, see appendix D and E. When the debris flow erodes into the material, the channel bank material may become undercut and slide into the channel. For these debris flows erosion has clearly been present and the starting volume of landslide two is much smaller than the depositional volume of the flow.

The erosion volume has been estimated, see chapter 4.4, but the upper track has continued to erode in the 11 months since debris flow two were triggered, this can be seen by comparing figures 3.21E and 3.21F. The calculation of erosion volume involves numerous assumptions and it is therefore an upper bound. By using lidar data (collected in June 2011 but not yet processed) the number of assumptions could be decreased and a more accurate estimate made. However, given current methods, the total erosion volume for debris flow two was calculated to be 2179,3 m^3.

5.3.4 Deposition

Figures 3.22B, 3.22C, and 3.23D of the deposited material of landslide two illustrate that the soil material is coarser for the depositional fans of landslide two than in the triggering zone of landslide two. This indicates that the more coarse material must have been eroded from the slope and entrained into the landslide. The grain sizes of the coarse grains, figure 3.22B, in the depositional fan

on the road, see figure 3.19A are smaller than for the deposition just below the road, figure 3.22C, and in the last deposition area of the landslide in section five, figure 3.23D. This change in relative grain size of the coarse grains corresponds with a change in slope angle for the deposition. The depositional fan on the road is deposited on the lowest slope angle at 4°, which means that the landslide could not have supported finer-grains that could possibly have been supported at higher slope angles. The deposition just below the road has the highest slope angle at a range of 16° to 26°, this means that the landslide had a greater velocity in this area and could probably have suspended more coarse grains than for areas where the slope angle and velocity is lower.

The debris flows deposited when the slope angle became lower when the debris flows crossed the road, and this coincided with when the debris flow could start to spread out because it was no longer confined by a channel. This can be seen for the depositional fan for debris flow five, debris flow two, debris flow three, debris flow four, and debris flow six, see table 3.9 and figures 3.30, 3.29, 3.28, 3.27, 3.25, 3.23 and 3.22. Debris flows one and five did not deposit when they crossed the road this indicates that the energy in debris flows one and five were greater than for the other debris flows. The depositional volume of each debris flow has been calculated, see chapter 4.3, and debris flow five is clearly the largest observed debris flow, and this fits the theory that debris flow five has the greatest amount of energy, since debris flow five eroded and entrained the greatest amount of material. The depositional volume calculated for landslide two is greater than the erosion volume, this indicates that the depositional volume calculated is too high since the erosion volume is the upper bound. The mostly likely error is in the deposition thickness, due to the topography before the material was deposited is not known. Lidar data from the area, or detailed comparison of photographs could help estimating the earlier topography.

The debris flow stops when the shear strength exceeds the shear stress from gravity, see chapter 1.6.5, and since the gravitational component of the flow decreases when the slope angle decreases the theory supports the findings of localities where the debris flows started to deposit. For the debris flows in this case that did deposit into fans, and did not deposit most of their material into the river, lateral spreading into a fan have probably been one of the main reasons for the debris flows stopping where they did.

5.3.5 Transport of boulder and cars

A large boulder with a diameter greater than 4 meters has been found in the track of debris flow five, the boulder shows signs of being transported by the debris flow. In the depositional fan boulders up to 1 meter in diameter is found, and they are shown to still be floating in the upper layers of the depositional fan. The size of the boulders that have been transported by the debris flow indicates that the energy and forces in the debris flow must have been great enough to support the boulders and move them. Debris flow two managed to move a large heavy tractor that weighed approximately 7000 kg. Debris flow five moved two cars, which weighed roughly 1500 kg.

The weight of the objects that have been transported by the debris flow might not have been completely supported by the debris flow, but rather pushed down the slope. In chapter 4.6 the thickness of the debris flow needed to transport boulders, tractor and cars have been calculated, and only a debris flow with a thickness of 0,17 meters is needed to transport a car. Since the depositional fan of debris flow five in the area where the cars were transported to were at least 0,7 meters, debris flow five should be able to transport the cars relatively easy.

The large boulder in debris flow five has been calculated; chapter 4.6, to need a debris flow with a thickness of approximately 2 meters to transport the boulder, and this number depends on the contribution of additional forces other than buoyancy. To move the tractor in debris flow two the debris flow thickness must be 0,42 meters, and the depositional fan in the area is 2,5 meters thick so this should be sufficient.

Five possible mechanisms that can support debris flow loads in the depositional fan and during a movement have been described in this thesis, in chapter 1.8.4 , The actual mechanisms that occurred in the debris flows is difficult to determine with the data that is available, but some constraints can be offered. The debris flow material is relatively fine-grained, but the clay content is normally below 10 percent and cohesion can therefore be present as a mechanism for suspending grains, but the boulders are too large for the clay content to be able to suspend the boulders indefinitely. Cohesion is therefore possibly a mechanism that suspends the smaller grains, and could help suspend the larger boulders but it cannot be the only mechanism present.

Buoyancy can support large boulders due to differences in densities between the particles and the fluid. Buoyancy is enhanced when pore pressure increases in the debris flow, and because of the fine-grained material in the flow the pressure dissipates slowly. The densities of the debris flow material and the fluid is not known, but the material should have a greater density than the fluid and buoyancy should therefore be present in the flow. The debris flow material is relatively fine-grained and could therefore sustain excess pore pressure which could enhance the buoyancy in the flow. The generation of excess pore pressure in the flow could have occurred, but even if it did not occur buoyancy was probably an important mechanism in supporting the boulders.

If there was dispersive pressure in the flow the larger grains would move to the top of the flow, and a reverse grading could be found in the deposits. Reverse grading is often found in debris flow deposits so dispersive pressure was probably present in these debris flows as well, but the evidence of it occurring was not directly observed in the field (at least in the areas studied in detail). Turbulence in the debris flow becomes more important when the water content in the flow increases, and the water marks above the starting zone indicates that the water content has been quite high (e.g. greater than 3m) in the area. However, many debris flows seems to be laminar in nature, and fine-grained material in the flow decreases the fall velocity of the particles, so because the material is relatively fine-grained turbulence is probably not a very important grain transporting mechanism for these debris flows. When the debris flow material has been deposited and it still supports boulders, only cohesion, buoyancy, and structural support can support the material. Structural support must be present because cohesion and buoyancy alone is not enough to support submerged boulders in the deposits, and keep them from sinking down into the depositional fan. Structural support must therefore be present in the depositional fans that support boulders; this can be seen in the deposition of landslide two, figure 3.22D.

5.3.6 Runout ratio

The runout for all six debris flows have been calculated, see table 3.10, but they are not very accurate. Mainly because the debris flow tracks that have been estimated are based on pictures, topographical maps, and a few GPS measurements. Almost all the debris flows flowed into the river. Because the debris flows flowed into the river the true total travel length that the debris flows could have achieved if the river was not present in the valley is not known, but because the river is at the

bottom of a the valley and the other side of the valley starts close to the other side of the river the true travel length of the debris flow would not have been very much longer.

5.4 Impacts on Humans living in the area

The houses in the study area were not destroyed, but the access road to the upper house was completely destroyed, and by May 2012 it has still not been fixed. Cars and a tractor were also moved and possibly destroyed by the debris flows. People are now living in the lower houses, but it is not known if the people in the upper house have been allowed to come back. In the days following the debris flows people were evacuated, and part of the valley was declared inhabitable. The access road into the valley was also destroyed and was reopened on the 28th of November, 2011. Several news reports were made from the area and can be accessed from the websites of NRK and TV2, the flooding is also covered in these news stories.

6 Conclusion

From the data available, that has been collected either in the field or from public archives; conclusions can be made for the landslides that were initiated in Veikledalen 10th of June, 2011.

The triggering mechanism has been interpreted to be an intense rainstorm; antecedent rainfall might also have played an important role in the triggering of the landslides. The rainfall event was shown to exceed the rainfall threshold for initiating shallow landslides, for four out of five weather stations. Precipitation is a common triggering mechanism for shallow landslides, and if climatic models are correct in predicting more precipitation in Norway in the future, the frequency of landslides triggered by precipitation might increase for certain areas of the country. From observations in the field the landslides have been interpreted to have been triggered as a debris slide, and then transformed into a debris flow shortly after initiation.

Six landslides were identified in the field, but numerous landslides were observed. The triggering zones of the debris flows were interpreted from photographic archives, and observations in the field. Debris flows two and three were triggered at a lower elevation than debris flows one, four, five, and six. The reason for this inconsistency is probably local conditions, for example slope angle or sediment thickness, future work in the area is needed to determine the exact reason for the triggering zones of debris flows two and three to occur at a lower than debris flows one, four, five, and six.

The debris flow tracks were interpreted to be located in the areas were complete vegetation removal had occurred, and the topography of the track was determined to be ravines. The interpretation is therefore that the debris flows moved down old ravines, probably due to these areas being the paths of least resistance when compared to the local ridges in the area. The debris flow channels are interpreted to be triangular; this is supported by the actual shape of the channels and the presence of levees along the track.

Removal of vegetation was observed in all six debris flow tracks, and numerous large trees were deposited along the side of the debris flow track, indicating that the energy in the debris flows must have been sufficient to uproot and move trees. In locations where trees have only been bent, but not removed the energy and the velocity can be interpreted to be lower than for areas where the trees have been completely removed. Observations show that trees in areas where the slope angle was low could be preserved and vegetation was not damaged, while at higher slope angles more trees were observed to be broken and removed.

Erosion in the debris flow tracks were observed for all six debris flows. Debris flow two had two main zones of erosion, in the upper track above the road, and in the channelized slope of section four. Zones of erosion coincide with the areas that had the highest slope angles, which indicates that the energy was high enough in those areas to erode the bed material. Erosion also occurred in locations of the track where the debris flow channel was confined into a channel, for example by ridges or bedrock. Deposition occurred immediately when the slope angle decreased, and the channel opened up to an open slope. When debris flow two deposited on the road the slope angle decreased from 20° to 4° and the second area of deposition occurred when the slope angle decreased from 20° to 16°. A transition angle between erosion and deposition has been suggested to be around 17°, and the data from debris flow two support this theory. The areas of deposition in all six debris flows

indicate that a combination of confinement of the debris flow track, and slope angle is important for determining areas of erosion and deposition.

Future work in the area could be determining the actual erosion and deposition volumes of all debris flows, for example by using Lidar data from before and after the event occurred. Walking all the tracks with a GPS and taking measurements of widths, changes in grain sizes, largest blocks, vegetation removal, mud marks, and sediment thickness. Determining the reason for why debris flows two and three were not triggered at the same elevation as the other four debris flows, by comparing local information of the triggering zones, for example grain size analysis from soil samples, sediment thickness, slope angles, or shear strength test of soil sample from the triggering zone. Determining why debris flow five was so much greater than the other debris flows, were there more material available, was the grain size distribution different, the water content higher due to differences in the soil, etc. Information that could possibly prevent the consequences of future events to be as unfortunate ass they were on 10th of June. 2011.

7 References

BAGNOLD, R. A. 1954. Experiments on a Gravity-Free Dispersion of Large Solid Spheres in a Newtonian Fluid under Shear. *Proceedings of the Royal Society of London. Series A, Mathematical and Physical Sciences,* 225**,** 49-63.

BAGNOLD, R. A. 1956. The Flow of Cohesionless Grains in Fluids. *Philosophical Transactions of the Royal Society of London. Series A, Mathematical and Physical Sciences,* 249**,** 235-297.

BARGEL, T. H. 2011. Veikledalen.

BLIKRA, L. H. & SLETTEN, K. 2002. Klimaendringer kan påvirke skredfaren. *Cicerone***,** 27-30.

BLIKRA, L. H., ØYGARDEN, L., MATHEUSSEN, B., ASVALL, R. P., BELDRING, S., BOGEN, J., ENGESET, R., JENSEN, T., L'ABÉE-LUND, J. H., JENSEN LUND, P. T., ROALD, L. & SKAUGEN, T. 2003. Vannlandet i 2050. Vann, natur og samfunn i et endret klima. *In:* BERTHLING, I. (ed.). Oslo: Norges vassdrags- og energidirektorat.

BOGGS, S. 2006. *Principles of sedimentology and stratigraphy,* Upper Saddle River, N.J., Pearson Prentice Hall.

BREIEN, H., DE BLASIO, F., ELVERHØI, A. & HØEG, K. 2008. Erosion and morphology of a debris flow caused by a glacial lake outburst flood, Western Norway. *Landslides,* 5**,** 271-280.

CAINE, N. 1980. The Rainfall Intensity: Duration Control of Shallow Landslides and Debris Flows. *Geografiska Annaler. Series A, Physical Geography,* 62**,** 23-27.

CAMPBELL, R. H. 1975. Soil slips, Debris flows, and Rainstorms in the Santa Monica Mountains and Vicinity, Southern California. *USGS Professional paper***,** 51.

COSTA, J. E. 1984. Physical Geomorphology of Debris Flows. *In:* COSTA, J. E. & FLEISHER, P. J. (eds.) *Developments and Applications of Geomorphology.* Berlin: Springer.

CRAIG, R. F. 2004. *Craig's soil mechanics,* Abingdon, Oxon, E & FN Spon.

CRUDEN, D. M. & VARNES, D. J. 1996. Landslide types and Processes. *In:* SCHUSTER, R. L. & TURNER, A. K. (eds.) *Landslides: Investigation and Mitigation.* Washington D.C.: National Academy press.

DAHL, R., BERG, K. & NÅLSUND, R. 1981. *Stabilitetsforholdene i skråninger med morene og lignendejordarter: sluttrapport vedrörende et NTNF-stöttet prosjekt,* Trondheim, Instituttet.

DAS, B. M. 2008. *Advanced soil mechanics,* London, Taylor & Francis.

DE BLASIO, F. V. 2011. *Introduction to the Physics of Landslides: Lecture notes on the dynamics of mass wasting,* Dordrecht, Springer Science+Business Media B.V.

DUNCAN, M. J. 1996. Soil Slope Stability Analysis. *In:* TURNER, A. K. & SCHUSTER, R. L. (eds.) *Landslides, Investigation and mitigation.* Washington D.C.: National Academy Press.

FETTER, C. W. 2001. *Applied hydrogeology,* Upper Saddle River, N.J., Prentice-Hall.

FURSETH, A. 2006. *Skredulykker i Norge,* Oslo, Tun.

HALDORSEN, S. 1983. The characteristics and genesis of Norwegian tills. *In:* EHLERS, J. (ed.) *Glacial Deposits in North-West Europe.* Rotterdam: A.A.Balkema.

HERMANNS, R. L., BLIKRA, L. H., NAUMANN, M., NILSEN, B., PANTHI, K. K., STROMEYER, D. & LONGVA, O. 2006. Examples of multiple rock-slope collapses from Köfels (Ötz valley, Austria) and western Norway. *Engineering Geology,* 83**,** 94-108.

HORTON, R. E. 1938. Phenomena of the contact zone between the ground surface and a layer of melting snow. *Association Internationale d'Hydrologie Scientifique,* 244**,** 545-561.

HUNGR, O. 2005. Classification and terminology. *In:* HUNGR, O. & JAKOB, M. (eds.) *Debris-flow Hazards and Related Phenomena.* Chichester, UK: Springer.

HUNGR, O., MCDOUGALL, S. & BOVIS, M. 2005. Entrainment of material by debris flows. *In:* HUNGR, O. & JAKOB, M. (eds.) *Debris-flow Hazards and Related Phenomena.* Berlin: Praxis- Springer.

IPCC 2007. The physical science basis: Contribution of Working Group I to the Fourth Assessment Report of the Intergovernmental Panel on Climate Change, 2007 *In:* SOLOMON, S., QIN, D., MANNING, M., CHEN, Z., MARQUIS, M., AVERYT, K. B., TIGNOR, M. & MILLER, H. L. (eds.). Cambridge, United Kingdom and New York, NY, USA.

IVERSON, R. M. 1997. The Physics of Debris flows. *Reviews of Geophysics,* 35**,** 245-296.

IVERSON, R. M. 2003. The debris-flow rheology myth. *In:* RICKENMANN, D. & CHEN, C. L. (eds.) *Debris-flow Hazards Mitigation: Mechanics, Prediction, and Assessment.* Rotterdam: Millpress.

IVERSON, R. M. & DENLINGER, R. P. 2001. Flow of variably fluidized granular masses across three-dimensional terrain 1. Coulomb mixture theory. *J. Geophys. Res.,* 106**,** 537-552.

IVERSON, R. M., REID, M. E. & LAHUSEN, R. G. 1997. DEBRIS-FLOW MOBILIZATION FROM LANDSLIDES1. *Annual Review of Earth and Planetary Sciences,* 25**,** 85-138.

JAEDICKE, C., SOLHEIM, A., BLIKRA, L. H., STALSBERG, K., SORTEBERG, A., AAHEIM, A., KRONHOLM, K., VIKHAMAR-SCHULER, D., ISAKSEN, K., SLETTEN, K., KRISTENSEN, K., BARSTAD, I., MELCHIORRE, C., HØYDAL, Ø. A. & MESTL, H. 2008. Spatial and temporal variations of Norwegian geohazards in a changing climate, the GeoExtreme Project. *Natural Hazards and Earth System Sciences***,** 893-904.

JOHNSON, A. M. 1970. *Physical processes in Geology,* San Fransisco, Freeman.

JOHNSON, A. M. 1984. Debris flow. *In:* BRUNSDEN, D. & PRIOR, D. B. (eds.) *Slope Instability.* John Wiley & Sons.

JØRGENSEN, P. 1977. Some properties of Norwegian tills. *Boreas,* 6**,** 149-157.

KARTVERKET. 2009. *Norgeskart* [Online]. Available: www.norgeskart.no [Accessed 06.05 2012].

KLEIVANE, I. 2011. Flaumen i Sør-Noreg, juni 2011. *In:* NVE (ed.). Oslo: Norges vassdrag og energidirektorat.

KOTTEK, M., GRIESER, J., RGEN, BECK, C., RUDOLF, B. & RUBEL, F. 2006. World Map of the Koppen-Geiger climate classification updated. *Meteorologische Zeitschrift,* 15**,** 259-263.

LAMBE, T. W. & WHITMAN, R. V. 1979. *Soil mechanics: SI version,* New York, Wiley.

LYCHE, E., TAURISANO, A. & SKAUGE, J. 2011. Oversikt befaringsobjekter 14.06-17.06.2011. Norges vassdrag og energidirektorat.

MAIR, K. 2011. *RE: Notes from Geo 4130 Engineering geology and Geomechanics*

MAIR, K. 2012. Veikledalen Pictures, may 2012.

MAJOR, JON J. 1997. Depositional Processes in Large-Scale Debris-Flow Experiments. *The Journal of Geology,* 105**,** 345-366.

NGU. 2012. *Kart of Data* [Online]. NGU. Available: http://www.ngu.no/no/hm/Kart-og-data/ [Accessed 01.03 2012].

NORGESBANK. 2012. *Priskalkulator* [Online]. Norges Bank. Available: http://www.norges-bank.no/no/prisstabilitet/inflasjon/priskalkulator/ [Accessed 23.04 2012].

NORWEGIANMETEROLOGICALINSTITUTE. 2012a. *eKlima* [Online]. NORWEGIANMETEROLOGICALINSTITUTE

Available: www.eklima.no [Accessed 06.03 2012].

NORWEGIANMETEROLOGICALINSTITUTE. 2012b. *Helautomatiske værstasjoner* [Online]. Available: http://met.no/Meteorologi/A_male_varet/Observasjoner_fra_land/Varstasjoner/Automatiske_varstasjoner/ [Accessed 18.05 2012].

NORWEGIANMETEROLOGICALINSTITUTE. 2012c. *yr.no* [Online]. Norwegian Metrological Institute

Norwegian Broadcasting Corporation. Available: http://www.yr.no/sted/Norge/Oppland/Nord-Fron/Sk%C3%A5bu/almanakk.html?dato=2011-06-10 [Accessed 14.05 2012].

NORWEGIANPOLICESERVICE 2011. Helicopter pictures taken on 12th of June 2011.

NVE. 2012. *Norges vassdrags- og energidirektorat* [Online]. Available: www.nve.no [Accessed 20.05 2012].

NVE, NORWEGIANMETEROLOGICALINSTITUTE & NORWEGIANMAPPINGAUTHORITY. 2012. *senorge.no* [Online]. Available: www.senorge.no [Accessed 04.02 2012].

OLIFEROV, A. 1970. Transport of large rocks by mudflows. *Soviet Hydrology,* 2**,** 121-123.

OXFORDUNIVERSITYPRESS 2003. *Oxford, Dictionary of Earth Sciences,* New York, United States, Oxford University Press.

PICARELLI, L. 2009. Understanding to Predict. *In:* SASSA, K. & CANUTI, P. (eds.) *Landslides - Disaster risk reduction.* Berlin: Springer.

RAMBERG, I. B., BRYHNI, I. & NØTTVEDT, A. 2007. *Landet blir til: Norges geologi,* Trondheim, Norsk geologisk forening.

REDFIELD, T. F. & OSMUNDSEN, P. T. 2009. The Tjellefonna fault system of Western Norway: Linking late-Caledonian extension, post-Caledonian normal faulting, and Tertiary rock column uplift with the landslide-generated tsunami event of 1756. *Tectonophysics,* 474**,** 106-123.

REID, M. E. 1994. A Pore-Pressure Diffusion Model for Estimating Landslide-Inducing Rainfall. *The Journal of Geology,* 102**,** 709-717.

RICKENMANN, D. & ZIMMERMANN, M. 1993. The 1987 debris flows in Switzerland: documentation and analysis. *Geomorphology,* 8**,** 175-189.

SASSA, K. 1985. The mechanism of debris flow. *Proceedings of XI International Conference on Soil Mechanics and Foundation Engineering, San Fransisco.* Rotterdam: A.A. Balkema.

SASSA, K. 2000. Mechanism of flows in granular soils. *Proceedings of GeoEng2000, Melbourne, 19-24 November.* Pennsylvania: Technomic Publishing Company, Inc.

SASSA, K. & WANG, G. H. 2005. Mechanism of landslide-triggered debris flow: Liquefaction phenomena due to undrained loading of torrent deposits. *In:* JAKOB, M. & HUNGR, O. (eds.) *Debris-flow Hazards and Related Phenomena.* Berlin: Praxis-Springer.

SAVAGE, S. & HUTTER, K. 1991. The dynamics of avalanches of granular materials from initiation to runout. Part I: Analysis. *Acta Mechanica,* 86**,** 201-223.

SAVAGE, S. B. & HUTTER, K. 1989. The motion of a finite mass of granular material down a rough incline. *Journal of Fluid Mechanics,* 199**,** 177-215.

SAVAGE, W. & BAUM, R. 2005. Instability of steep slopes. *In:* JAKOB, M. & HUNGR, O. (eds.) *Debris-flow Hazards and Related Phenomena.* Berlin: Praxis-Springer.

SHARPE, C. F. S. 1938. *Landslides and Related Phenomena,* New York, Columbia University Press.

SLETTEN, K. & BLIKRA, L. H. 2007. Holocene colluvial (debris-flow and water-flow) processes in eastern Norway: stratigraphy, chronology and palaeoenvironmental implications. *Journal of Quaternary Science,* 22**,** 619-635.

SOMMERFELDT, W. 1972. *Ofsen i 1789: og virkninger av den i Fron,* Otta, Fron historielag.

STINY, J. 1910. *Die Muren,* Innsbruck, Verlag der Wagner'schen Universitäts-buchandlung.

SULEBAK, J. R. & SJØSTRØM, K. H. 2007. *Landformer og prosesser: en innføring i naturgeografiske tema,* Bergen, Fagbokforl.

SØRBEL, L. 1999. *Siste istid i Fennoskandia: noen hovedtrekk,* Oslo, Unipub.

TAKAHASHI, T. 1981. Debris flow. *Annual review of fluid mechanics,* 13**,** 57.

TAKAHASHI, T. 2007. *Debris flow: mechanics, prediction and countermeasures,* Boca Raton, FL, Taylor & Francis.

VARNES, D. J. 1978. Slope Movement Types and Processes. *In:* ECKEL, E. B. (ed.) *Special Report 29: Landslides and Engineering Practice.* Washington D.C.: National Research Council.

WANG, G. & SASSA, K. 2003. Pore-pressure generation and movement of rainfall-induced landslides: effects of grain size and fine-particle content. *Engineering Geology,* 69**,** 109-125.

WIECZOREK, G. F. 1996. Landslide triggering mechanisms. *In:* SCHUSTER, R. L. & TURNER, A. K. (eds.) *Landslides: Investigation and Mitigation.* Washington D.C.: National Academy Press.

WIECZOREK, G. F. & GLADE, T. 2005. Climatic factors influencing occurence of debris flows. *In:* HUNGR, O. & JAKOB, M. (eds.) *Debris-flow Hazards and Related Phenomena.* Berlin: Praxis-pringer.

WU, T. H. 1996. Soil Strength Properties and their Measurment. *In:* TURNER, A. K. & SCHUSTER, R. L. (eds.) *Landslides: Investigation and Mitigation.* Washington D.C.: National Academy Press.

YANO, K. & DAIDO, A. 1965. Fundamental Study on Mud-flow. *Bulletin of the Disaster Prevention Research Institute,* 14**,** 69-83.

Appendices

Appendix A Historical Landslides in Norway

Gauldal

From September 21st through 24th of 1345; the largest natural disaster in Norwegian history took place. Very little is known about the event because few details have been passed on to later generations, possibly due to the Black Plague that hit Norway only four years later in 1349, which killed half the population of Norway (Furseth, 2006). What is known about the event comes from Icelandic books and they tell a story of a valley where there was much farming due to the fertile marine clay that was deposited there. The summer and autumn before the event had been rainy, possibly continuous rain for quite some time with some flooding (Furseth, 2006). Gauldal River had become large and brown due to smaller landslides higher up in the river system. There were also stories about rivers that disappeared or changed directions. The ground was so filled with water that it bounced in many places when walked on, and there were numerous small clay slides along the river banks.

The consequences of the quick clay slide occurred in stages, the quick clay slide itself was released on the 21th of September at the narrowest point of the valley. The slide was very large, 3-5km of the side of the valley slid out and travelled across the valley over to the other side, this dammed up the river to a 14km long lake. The height of this dam has been estimated to be 33 meters, while the water volume is thought to have been between 150-200 million m^3 (Furseth, 2006). On the 24th of September the dam broke and a flood of water and debris moved quickly downstream, destroying everything in its path. It killed approximately 500 people, and in a country that only had 300 000 inhabitants at that time, this would have been a massive catastrophe. It is estimated that 0.17% of the population died in that one event (Furseth, 2006).

Verdal

On May 19th, 1893, there was a large quick clay slide in Verdalen in the Trondheim region in Norway. The valley is dominated by the Verdal River, and there are clay deposits up to 200 meters thick. There had been previous clay slides in the same area in both 1747 and in 1822 and numerous smaller slides, but nobody imagined that a slide of this size could happen (Furseth, 2006) . There were few warning signs before the event. One of the known signs was in the autumn of 1892, when a farmer was making holes in the ground for a fence, and his crowbar sunk down into the ground. There were also an unusual number of small clay slides from the river banks in the spring of 1893 and some houses' basements were flooded with water (Furseth, 2006).

The day before the landslide occurred, on the 18th of May, a well known phenomenon before large clay slides was sighted; the river was full of sediments and had turned a grey colour. This normally only happened after a large rainfall, and it hadn't rained for some time. The slide began 30 minutes after midnight, and lasted for about an hour. It came in three or four distinct waves, causing many farms and people to be swept away by the slide as it progressed, while others fled to safety. There was an abundance of smaller after-slides, which did not help the rescue efforts. In the end, 111 people were killed along with hundreds of animals. The slide's volume was approximately 65 million cubic meters and it was deposited on about 9 000 000 m^2 in up several meters in thickness. It is currently ranked as the second largest landslide disaster in Norwegian history (Furseth, 2006).

Tjelle

On February 22, 1756, the largest rock fall in Norwegian history took place at Tjelle in the western part of Norway. 15,7 million m^3 of rock were released into the fjord from approximately 400m above sea level and created three 40 meter high tsunamis killing 32 people (Redfield and Osmundsen, 2009, Furseth, 2006). The people living in the area recalled seeing a crack form, and that the crack grew progressively larger in the years leading up to the event. In the previous spring and autumn there had also been an infinite number of small rock falls from the same mountain side. There were reports of an unusual amount of rain before the rock fall occurred, and this could have been a triggering factor (Redfield and Osmundsen, 2009, Furseth, 2006). There has also been thoughts about the possibility of a seismic event being the trigger of the landslide due to the shaking and noises felt before the landslide, which may be valid due to the presence of a fault system in the region (Redfield and Osmundsen, 2009).

Loen

The Loen rock fall can be divided into two events, one on the January 15th 1905, and the second, on the 13th of September 1936. The mountain consists of gneiss with zones of amphibolites and a set of fractures that extend into the mountain side, the amphibolites are according to (Hermanns et al., 2006) weak planes. Before the rock falls in 1905 and in 1936 , there were numerous small rock falls leading up to the events (Furseth, 2006).

The rock fall in 1905 a block of about 50 000m^3 fell from Ramnefjellet at about 500m above sea level, onto a talus, which mobilized the it and the volume increased to 350 000m^3 , before sliding into the lake Loenvatnet and creating a tsunami (Furseth, 2006). 61 people were killed by the tsunami that had a maximum run-up height of 41m. The tsunami wave destroyed the two villages of Bødal and Nesdal. The people living there later rebuilt, after the geologists had said it was safe to do so (Furseth, 2006).

Before the 1936 event, a large crack developed up in Ramnefjellet. When the people living there applied for the government to decrease the water level in the lake in case of a new rock slide, no answer was ever given. In the summer and autumn of 1936, an infinite number of smaller rock falls took place, and on September 13th, a one million m^3 block fell from about 800 meters above sea level into the lake, creating another tsunami, this one with a maximum run-up of 74m. The tsunami killed 73 people. The villages of Nesdal and Bødal were again destroyed but were not rebuilt after geologists had thoroughly investigated the mountain and found several fractures and weak zones that dipped towards the lake (Furseth, 2006). A monitoring program was initiated and it did not detect any changes from 1936 to 1946. In 1947 a new crack developed, causing a several hundred thousand m^3 block to fail on June 22 1950. Due to the lake being so full of deposits from previous events, only a tsunami with a 15m run-up was created. The last event in 1950 opened up a deep-seated fracture, and it is a potential sliding surface for future events (Hermanns et al., 2006, Furseth, 2006).

Tafjord

On April 7th, 1934 there was a large rock fall with a volume of 1, 5 million m^3 from Langhammeren in Tafjord. The rock fall mobilized a talus that was below the mountain and the material entered the fjord. This caused a tsunami with a maximum height of 62 meters. There were several signs that a large rock fall was going to occur; from around 1870, people from the village of Fjørå saw a crack develop on top of the mountain. The crack continued to grow each year and in 1930 it was 1,5m wide. The growth then accelerated until the block failed in 1936 (Hermanns et al., 2006, Furseth, 2006). There were a great number of smaller rock falls which took place along the mountain and they increased in frequency until April of 1934. The people fishing in the fjord avoided the mountain and they were aware of its possible failure, but since no one lived directly under the mountain, they didn't believe that a tsunami would be able to reach them (Furseth, 2006).

At 03.10 am on April 7th, 1934 the rock fell from around 730 meters height , resulting in 3 million m^3 of rocks sliding into the fjord. It took only 2-3 minutes before the villages around Tafjorden were hit by the tsunami (Furseth, 2006). It created three large waves that destroyed everything in their path. People survived by running up the steep sides of the valley, but still 40 people were killed (Furseth, 2006). Since the event, geological mapping has revealed that there are deposits and scars from approximately ten previous large rock falls in the same area (Hermanns et al., 2006).

Appendix B Geological History of Norway

Geological history of Norway

The geological history of Norway started 2900 million years ago. The oldest rocks, gneisses, found in Norway are in the most northern part of Norway and are from the Archean eon, in the meso-archean era, as can be seen in figure 1 as a light peach colour. Most of Norway's bedrock is younger, from between 1700 to 900 million years ago. The archean gneisses are tonalite, Trondhjemite and Granodiorite dominated gneisses, also called TTG gneisses. Gneisses that crystallized in the eons after the archean are more potassium rich (Ramberg et al., 2007).

The Precambrian bedrocks in Norway are part of the Fennoscandian shield, often referred to as the Baltic shield. The Fennoscandian shield has grown and developed in periods of volcanism, deformation, orogenesis, and periods of erosion and sedimentation. In the neoproterozoic era, in the eon of proterozoic, from between 1000 to 542 million years ago, the supercontinent of Rodinia, which was a product of the even older supercontinent named Columbia, split into multiple smaller continents. Norway was on the edge of the continent named Baltica, numerous sedimentary basins were located on the north-western edge of Baltica. The rocks deposited in these sedimentary basins have either been preserved directly on the bedrock they were deposited on, or they have in some areas been pushed onto the bedrock by the later Caledonian Orogeny event. These thick layers of sedimentary rocks consists of sandstone, conglomerate, slate, and carbonate rocks. The areas on which the rocks cover are called the Sparagmite area of Southern Norway. During the neoproterozoic era, the edge of the continent of Baltica experienced fracture periods of the crust and melted mantle was pushed into the cracks that developed (Ramberg et al., 2007).

From 542 million years ago to 416 million years ago, in the the Cambrian, Ordovician and Silurian periods, Norway had been eroded down to a low-lying flat landscape. In the Cambrian period this flat landscape was flooded by the ocean and life on earth flourished in what is known as the “Cambrian explosion”. Only thin sediment layers were deposited on the old bedrock ,and in many localities these thin layers have later been eroded away . A shallow ocean, called the Iapetus, closed when Baltica collided with the continent named Laurentia. This orogeny process lasted from 500 to 405 million years ago, and created the mountain ranges we today have in Norway. The rocks that already existed in Norway were recrystallized into metamorphic rocks, for example into gneiss or slate, or folded during the collision. Large sheets of rock were ripped from the crust and transported over the existing bedrock onto the continents (Ramberg et al., 2007).

There was a subduction zone between Baltica and Laurentia, and the volcanic material ejected from the island volcanoes created in the subduction zone can be found in the geological layers from this time period. The large granite batholiths in Norway were created by this collision at around 450-430 million years ago. The western part of Norway was pushed deeper down by the sheets of rock that were transported on top of them and the pressure and temperature were so great that eclogite was created. There has also been found micro diamonds in the gneisses at Fjørtoft in Møre and Romsdal, this is especially interesting because among geologists many believe that the depth needed to create diamonds is more than 100 kilometres. These high pressure rocks and minerals were pushed onto the continent in the last part of the collision between Baltica and Laurentia (Ramberg et al., 2007).

The collision between the continents Baltica and Laurentia created the larger continent Euramerica. The Caledonian mountain range was as tall as the Himalayas are today, but the mountains started to erode immediately after they were created. In Norway this occurred in the Devonian period from 416 million to 359 million years ago. There was also a period where the large rock sheets that had been pushed onto the continent started to glide back west. This gliding occurred when the forces from the collision were gone and the two continents started to move away from each other. This stretching of the rocks created multiple fault complexes with these extension zones. The extension zones started when the rocks were deep down in the crust, and there was plastic deformation. The deformation continued when the extension zones were raised to shallower depth and cooled, but the deformation was now brittle. This transformation from ductile to brittle deformation occurred at different times in different parts of the country, all depending on how deep the rocks had been pushed and how fast they were rising. The rocks on the Møre and Romsdal coast were the last to start brittle deformation and were probably therefore the deepest rocks, this also coincide with the findings of eclogite and diamonds in this region (Ramberg et al., 2007).

In the Carboniferous and Permian periods, at around 359 to 251 million years ago, Euramerica collided with Gondwanaland, and this collision created the super continent of Pangaea. The mountain range that was created as a result of this collision now exist deep in the crust in today's central Europe. Norway was at the time located at the equator, but plate tectonics were moving the continent northward. This movement through different climatic zones made a distinct impression in the sedimentary rock layers deposited in the sedimentary basins at that time. The fauna and the flora on land was rich, due to the warm climate, and they were deposited as organic- matter rich layers in the sedimentary basins. These layers are the source rocks for the unique coal rich mountains on Svalbard. When Norway moved further north, into colder and drier climates, the material was deposited in progressively deeper and cooler water. From deposition in rivers, sumps and narrow rift basins in early carbon, to a large inland sea in late carbon and early Permian, and finally in a deeper and cooler ocean in the late Permian (Ramberg et al., 2007).

Late in the carboniferous period the area which is Oslo today started to break apart into the Oslo Graben. This process lasted for 70 million years and was dominated by volcanism and large pluton and batholith intrusions. The Oslo graben has many rare minerals and unusual rocks, which were created by crystallization of melts. The two most famous of these unusual rocks are rhomb porphyry and Larvikite. There are also sedimentary rock layers created erosion material from the Caledonian mountain range. Most of the rocks on what is the landmass of Norway today were created by the end of the Permian (Ramberg et al., 2007).

In the Triassic period from 251 to 200 million years ago, Norway was mostly dry land. The only exception is the most northern part of Norway where fossils have been found in the sedimentary rocks from this period. Pangaea tried to break up between Norway and Greenland along the weak zone where the Iapetus ocean had at one time been closed. The climate was still warm, but became more moist towards the end of the Triassic period, and this warm climate caused a strong chemical weathering and oxidation on land. This process resulted in discoloured sand and gravel, and red mud to be deposited in the sea and in sedimentary basins on land (Ramberg et al., 2007).

In the early and middle Jurassic period from 206 to 160 million years ago the basins in the North sea, the Norwegian sea, and in the Barents sea were flooded when they started settling. Thick layers of

sandstone and mud stone were deposited in the sea, due to increased erosion on land as a result of the climatic change from a dry climate into a subtropical climate. The sandstones that were deposited are very porous and are therefore the most important reservoir rock for oil and gas in the North sea. Rocks from the Jurassic period are generally not found on land, except for a few special locations, for example on Andøya or Svalbard (Ramberg et al., 2007).

In the late Jurassic period from 161 to 146 million years ago, the source of Norway's oil was created, either directly or indirectly. The crust offshore Norway started to rip apart and a large rift structure was created on the continental shelf. The structure is similar to today's Riff Valley in Africa. Thick layers of organic rich mud were deposited on the continental shelf and the large sedimentary basins from the middle Jurassic period were broken up into multiple smaller basins. In these smaller basins the water circulation was poor and this caused the organic rich material to not be oxidized. These organic rich layers were covered by kilometre thick layers of sediments and they were in places buried at the correct depth for the organic material to transform into oil and gas. There were also deposited fine-grained layers that acted as a capping rock for the oil and gas. This in a combination of the dipping of the porous sand layers that were created in the Jurassic created the perfect combination for preserving and trapping oil and gas (Ramberg et al., 2007).

The Cretaceous period lasted from 146 to 66 million years ago. The breakup of Pangaea now finished and the spreading of the Atlantic ocean started. The climate was at its warmest in geological history, 10 degrees Celsius warmer than today, and the ocean level was at its highest, but in large areas there were shallow oceans . It has been calculated that the ocean level might have been as high as 350 meters above today's level. The warm climate was due to the lack of deep ocean currents, relatively flat continents, and a higher concentration of CO2 in the atmosphere. The higher concentration of CO2 was a product of an increase in the volcanic activity due to rapid sea floor spreading. Thick layers of limestone and mudstone, in places also marlstone, were deposited in large sedimentary basins created by a thinning and stretching process of the crust. In places the crust thinned down to 20-25% its original thickness, but it did not thin enough for oceanic spreading to start. The limestones were mainly created from the skeletal fragments of marine organisms with calcium carbonate rich shells, mostly coccoliths (Ramberg et al., 2007).

The Tertiary period, also known as the Paleogene and Neogene periods lasted from 66 million years ago to 2,7 million years ago. The continental plate Norway was a part of continued to drift further north and all the continents in the world moved to the location they have today and received the shape they have at the present time. The northern part of the Atlantic ocean started to open up and new seafloor was created, the continental spreading in the southern part of the Atlantic ocean started in the Triassic period. The alps and the Pyrenees were created and with the opening of the Norwegian sea the climate in Norway changed. Polar winds from the north and warm tropical winds from the south were stopped by mountains and this was the beginning of a cooling period. The continents were raised from flat planes up to what we see today, with high mountains and valleys (Ramberg et al., 2007).

Appendix C Debris flow features

Difference between a water flood and a debris flow

The most important difference between a water flood and a debris flow is that a debris flow cannot transform into a water flood by deposition, while a water flood can vary the sediment concentration in the flow by deposition and erosion. A debris flow can only deposit the coarsest particles selectively; this is called the condition of irreversible sediment entrainment. Water floods carries small concentrations of sediments (normally between 1-40% by weight) and most of the damage done by the flood is caused by the water. Water flood bulk densities range from 1,01 to 1,3 g/cm^3. Mud floods are water floods that carry a greater concentration of sediments (about 40-70% by weight), and the damage caused by the mud flood is due to both the debris and the water. Bulk densities of mud floods range from 1,3 to 1,8 g/cm^3. For water floods, the solids in the flow separate from the fluid phase when they deposit (Costa, 1984).

The boundary between debris flows and mud floods occur at sediment loads of 400-500 kg/m^3 of water. Debris flows can have a sediment concentration of up to 90% of the flow mass by weight (Johnson, 1970), and the bulk densities are generally 1,8 to 2,5 g/cm^3 but can be lower if the flow has a high concentration of fine grained material. How deposition occurs is explained in chapter 1.6.5. Damage by debris flows are caused by the debris and impact forces, chapter 4.6 (Costa, 1984).

A critical value for the sediment load used to distinguish between water and mud floods, and debris flows is a function of many factors, but it seems to occur when the fluid density is 1,5 to 1,8 g/cm^3. Below these values, the flow transport the sediments by turbulence, shear, lift and drag. The fluid is still almost Newtonian, so hydraulic formulas still apply to the fluid. Above this threshold however, the shear strength of the fluid increases exponentially. The transport of sediments is due to cohesive strength, buoyant forces, grain interactions, structural support, and possibly turbulence. This rapid increase in shear strength above this threshold in fluid density means that there must be a simultaneous rapid transition from water flood to debris flow landforms and deposition, and therefore also a transition from Newtonian fluids to non-Newtonian visco plastic fluids. Water and mud floods, and debris flows deposits and landforms are distinct and can be used to determine which process occurred (Costa, 1984).

It is important to recognize the difference between a water flood and a debris flow because the mitigation procedures that work for water floods, may not work for debris flows. Peak discharges measured from debris flows can unknowingly be used to estimate floods in small basins and therefore create a number that is too high. Indirect-discharge estimates have sometimes been used to determine rainfall amounts from storms, and this may lead to inaccurate numbers used for rainfall and flood discharges when working with flood mitigation structures (Costa, 1984).

Starting Zone

Zimmermann identified four different starting zone types for debris flows, this is a simplification, but it is useful when trying to identify potential starting zones. The four starting zone types can be divided into two groups, according to the location of the starting zone. Debris flows from pre-existing debris beds in gullies are called the valley type , and debris flows that occurs due to a sliding mass are called slope type (Rickenmann and Zimmermann, 1993).

- **Slope type starting zone:**
    - ***Type 1:*** The starting zone is located in a steep talus slope, which is often weakly consolidated. The talus slope can be quite new or older and have been created by moraine or slope debris. Retrogressive erosion often leads to the formation of the initiation scar. Primary factor for initiating debris flows of this type is normally water availability. Slope gradients ranges from 27 to 38° (Rickenmann and Zimmermann, 1993).
    - ***Type 2:*** The contact zone between a rock wall and a steep talus slope is the starting zone location. The triggering factor is often runoff in the rock wall that causes water infiltration into the talus slope on a large scale. The debris flow is then initiated in a channel in the talus slope, close to the rock wall. In the channel there is normally some progressive erosion. Slope gradients ranges from 27 to 38° (Rickenmann and Zimmermann, 1993).
- **Valley type starting zone:** Rainwater will normally follow gullies after a rainfall event. If the slope is steep enough, the debris bed can slide due to the rising seepage flow level. But because there is not a sufficient amount of water present in the soil, it will not turn into a debris flow. For intermediate slopes, the debris will only slide when the seepage flow has reaches the surface of the bed. When runoff increases, more water will flow on the surface of the bed sediments, and the acting shear stress of the static weight of the surface and seepage water will exceed the resistance in the near surface debris. This can initiate a debris flow, and it will continue for as long as the slope is adequate (Takahashi, 1981).
    - ***Type 3:*** Starting zone is in a rock gully filled with debris. Erosion is limited due to the rock bed and rock walls. Debris can often have previously been covered by ice. The gradient normally ranges from 24 to 35° (Rickenmann and Zimmermann, 1993).
    - ***Type 4:*** Increased runoff conditions suddenly mobilize large temporary debris accumulations in the channel. Erosion is often progressive and the starting volume of debris is often small compared with the final volume of the event. The slope varies from 13 to 33° (Rickenmann and Zimmermann, 1993).

It is clear from these four types that the slope gradient is an important factor for debris flow initiation. Takahashi determined that the theoretical limiting slope is about 15°(Takahashi, 2007)

Channel shape

Debris flows will often flow in a channel or down a ravine, it is therefore useful to look at what happens to the flow as a Bingham fluid moves through the channel. There are numerous assumptions, for example that the channels have a simple geometrical shape and that the fluid is a Bingham fluid and the only velocity that is not zero is the velocity parallel to the surface.

Circular channel

Natural debris flows are seldom observed and it is therefore often more common to analyze debris flow velocity profiles and properties by creating artificial debris flows in the lab. The channel shape that can best determine the properties of the material has been found to be circular channels , and surface velocities can be measured accurately. Because the channel has a simple geometry, the pattern of steady flow of the Bingham fluid in the channel is relatively simple. The velocity distribution in the channel for a steady flow assumes that the velocity may change with respect to distance from the sides of the channel, so for equal distances from the sides the velocity is constant. Shear stress acting parallel to the cylinder is independent of the position along the length of the cylinder. These assumptions means that it is possible to analyze the equilibrium of a small portion of the flow and it will represent any part of the flow. The forces acting on the flow that are part of the equilibrium equation are the normal force, shear force and the weight of the flow, the equilibrium equation is then combined with the rheological model of a Bingham fluid to find the velocity profile in the flow (Johnson, 1970).

The equations show that a rigid plug of material must be present in the centre of the flow because the shear stress vanishes at the centre of the channel and increases with distance from the centre of the channel, see figure C.1. The shear stress in the plug is therefore less than the shear strength of the material and there will therefore be no deformation in the plug, but it will flow down the slope on top of the moving flow. The radius of this plug can be calculated and it depends on the unit weight of the material, slope angle and the yield strength of the material. The equations for a circular channel can be altered to give a solution for flow in a wide channel (Johnson, 1970).

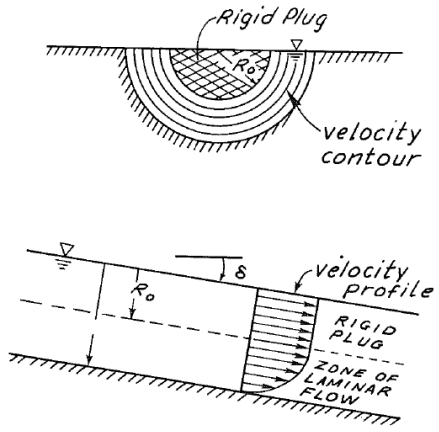

Figure C.1 Debris flow in a cylindrical channel, the velocity contours and velocity profile in the debris flow is shown. Ro is the thickness of the rigid plug, and δ is the slope angle (Johnson, 1970).

Rectangular channel

Bingham fluids flowing down a rectangular channel uses Bingham rheology theory and can be calculated for two-dimensional flow. The velocity profile is found much in the same way as for a circular channel, the difference is in the geometry of the channel and it is more complicated to calculate. The boundary conditions are the most difficult to define, in the corners of the channel there will be regions of no flow due to the shear stress being less than the yield strength of the material. The edges of the regions must be found before the velocity distribution can be calculated. In comparison with a circular channel where shear stress increased linearly from the centre of the channel, in a rectangular channel shear stress increases with increasing distance from the centre, then the shear stress goes through a maximum value before if decreases to zero again at the corners of the channel. This creates dead regions in the corners of the channel and a rigid plug in the centre of the channel. The size of these dead regions and the rigid plug increases when the shear strength of the material increases, see figure C.2. To find the velocity distribution in a rectangular channel is quite difficult and a computer is needed. Velocity is highest at the edge of the rigid plug and decreases towards the edges of the channel (Johnson, 1970).

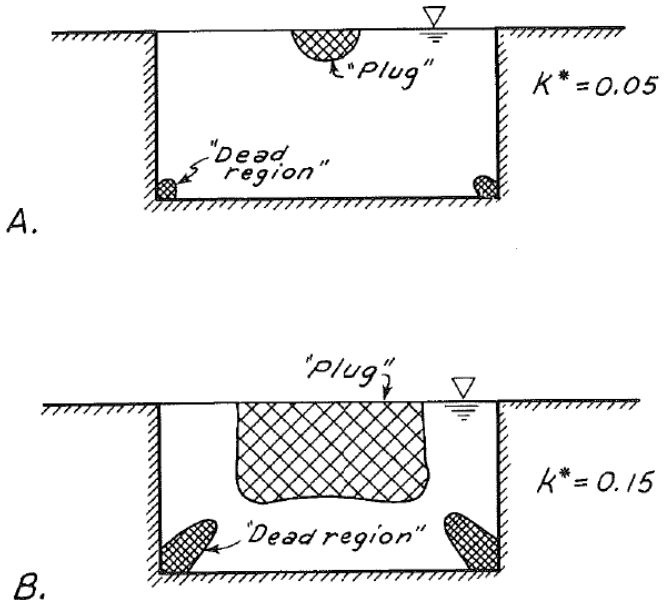

Figure C.2 Debris flow in a rectangular channel, and how the size of the dead regions and the rigid plug in the debris flow changes with changes in the shear strength. A) low shear strength, B) high shear strength (Johnson, 1970).

Triangular channel

Flow of a Bingham fluid in a Triangular channel is interesting because the theory of dead regions in a rectangular channel means that the dead regions will be at the surface of a flow in a triangular channel. This means that it should be possible to see these dead regions in small scale experiments. Natural channels and valleys also often have a triangular shape. For a triangular channel, the theory is that it is a rotated closed rectangular channel; nothing changes except the coordinate system. If the flow pattern is unchanged by rotating 45 degrees, then the dead regions and velocity contours must also remain unchanged by the rotation. A triangular channel is therefore half of a closed square channel, and the velocity distribution and dead regions are therefore known. Dead regions are present at the bottom of the flow and at the edges of the flow, see figure 1.13. These dead regions at

the edges should be present in experiments; photographs show that they can be seen in flows moving down triangular channels. The rigid plug in the centre of the flow is still present and the velocity decreases from the edge of the rigid plug and towards the edges of the channel (Johnson, 1970).

The Entrainment Mechanism

Transport of bedloads in a stream channel occurs by suspension, rolling, sliding, or saltation. Experiments show that when the slope angle is higher than 10°, the bed sediment itself can become unstable due to gravity and drag forces imposed by the over-riding water flow. When the fluid flowing over the bed sediments are saturated debris, even greater drag forces are created and the material can be mobilized and entrained into the debris flow. Surges in the debris flow can probably increase the drag forces even further and increase entrainment (Costa, 1984).

Destabilization of bed material causes entrainment, and it is a product of drag forces acting at the base of the flow, but can also be helped by strength loss in the sediments as a result of undrained loading, impact loading, and liquefaction of the saturated channel material. Bed destabilization affects any erodible bed substrate (Costa, 1984).

The second mechanism comes from instability of stream banks that have been undercut by bed erosion. Channel and gully banks are often being actively carved into, and they exist in a state of marginal equilibrium that can be affected by lowering of the bed, which often occurs during a debris flow surge. Shallow debris flows can then be initiated from the banks either during the surge or it's delayed and the material can be remobilized by the next surge or the next event (Hungr et al., 2005).

Bed stability

The process of destabilization of the bed during a debris flow can be represented by an extension of the infinite slope stability theory. The assumptions made for the pore-water pressure in the bed material is important, and the normal assumption is slope-parallel seepage in a saturated bed. This assumption was first made by Takahashi in 1978. The bed becomes unstable due to the added tractive force of the debris. It is theoretically possible to calculate the depth below the original surface that becomes unstable, but several assumptions are needed and some of the information needed is not very well known (Hungr et al., 2005).

Alluvial fans deposition

Debris flows are important in building alluvial fans. For a long time they were not recognised as such, probably due to debris flow long recurrence intervals. The recurrence interval depends not only on rainfall, but also very much on sediment availability. It is rare that debris flows are the only process that builds up an alluvial fan, water-flooding is also very important. Some alluvial fans only consists of water-laid sediments, this is normally due to sediment availability. There are also some observations that show that an increase in the annual precipitation, decrease the number of mudflows that make up the alluvial fan, while other observations show the opposite. Debris flows that have been deposited on an alluvial fan are normally reworked and sorted by later water flows, it is therefore possible that evidence of debris flows in the alluvial fans have been removed and this could affect the observations. This affects decreases when the grain size increases, coarser material are tougher or impossible for the water flow to rework. Water-laid deposits are more common in the middle and

lower parts of the alluvial fan, deposits near the head of the fan are dominated by debris flows overtopping channel banks. This can explain the observed decrease in maximum, minimum, and mean size of grains when you move down an alluvial fan. When a debris flow flows onto a fan it is possible for the debris flow not to spread laterally, but to be contained in a channel. They normally shift course quite frequently due to clogging of the channels by sediments (Costa, 1984).

Appendix D Stability in water soaked sediments

The nature of soil

Soil can be seen as an assemblage of soil particles that are arranged in a certain way that creates voids between the grains. To understand soils it is important to know the basic structure of the soil.

Weight-Volume relationship

Soil normally consist of three phases, solid, gas, and liquid. The solid phase is the mineral particles, the gas is normally air, and the liquid is usually water. Figure D.1 show the three phases in a normal soil that is partially saturated, if the soil is fully saturated the gas phase will not be present in the soil. For the volume of the soil there are three important relationships: porosity, void ratio, and degree of saturation, and they can be calculated using figure D.1. Porosity and void ratio indicate the relative void volume in a soil, the void volume can be filled with a fluid. The degree of saturation indicate the percentage of the void volume that is filled with water, if the soil is completely saturated the degree of saturation is 100% , while a dry soil has a degree of saturation of 0 (Lambe and Whitman, 1979).

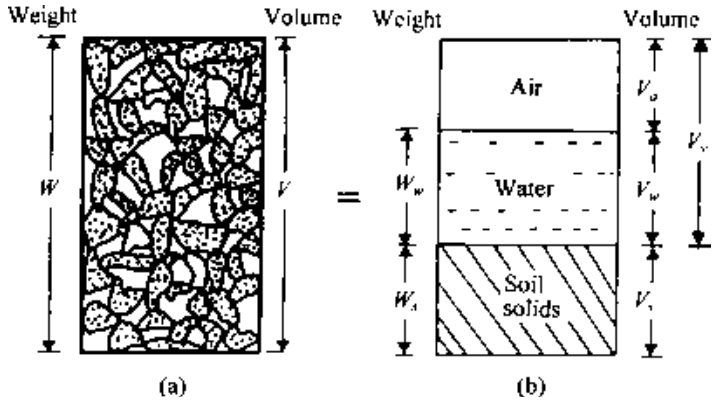

Figure D.1 Weight-volume relationship for soil aggregate (Das, 2008) W is the weight of the soil, V is the volume of the soil. Ww is the weight of the water, Ws is the weight of the solid. Va is the volume of the air, Vw is volume of the water, Vs is the volume of the solid, and Vv is the volume of the water and the air (voids).

The water content is one of the most useful relationships that can be calculated from figure D.1. The water content of the soil is found by weighing the sample while it is wet, then drying it and weighing it again, the difference in weight divided by the dry weight is the water content of the soil. The unit weight is the weight of a given volume, it can be either dry or wet. Several equations can be used to find important information about the soil from these phase relationships shown in figure D.1,only the most important and general equations are shown here. There is also the possibility to find more equations by using the special case when the volume of the solid is unity and equal to 1 (Lambe and Whitman, 1979).

Volume

- ***Porosity*** $n= V_v/V$, $n=e/1+e$ (D.1)
- ***Void ratio*** $e= V_v/V_s$, $e= n/1-n$ (D.2)
- ***Degree of saturation*** $S=V_w/V_v$ (D.3)

Weight

- ***Water content*** $w=W_w/W_s$ (D.4)

Unit weight

- ***Total*** $\gamma= W/V$ (D.5)

Grain size distribution

To understand a soil it is important to know the grain size distribution of the soil, and this is determined by sieve analysis. The sieve analysis is then expressed as a plot of percent finer(cumulative percentage by weight) versus diameter in mm. The percentage of clay, silt, sand, and gravel can then be estimated for the soil using the grain size distribution curve (Lambe and Whitman, 1979). Other soil parameters can also be found, for example the uniformity coefficient also called the effective size of the soil. The effective size is the diameter at which 10% of the soil passes through the sieve, this is called the D_{10}. D_{60} is where 60% of the soil mass passes through the sieve, and D_{30} is where 30% of the soil mass passes through, they are used to find the uniformity coefficient Cu, and the coefficient of gradation Cc (Das, 2008).

$Cu= D_{60}/D_{10}$. (D.6)

$$C_c = \frac{{D_{30}}^2}{D_{60}D_{10}} \quad \text{(D.7)}$$

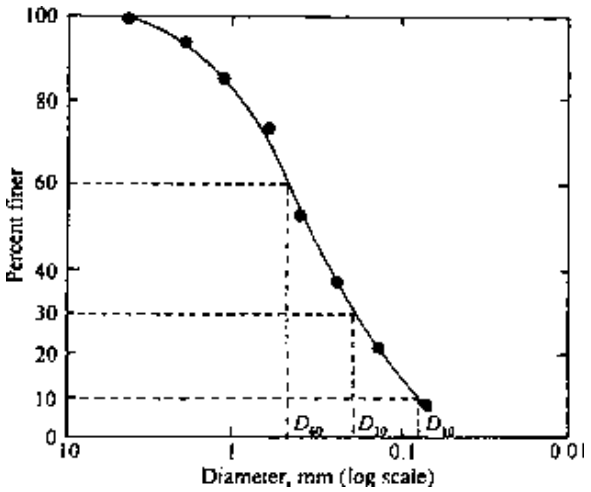

Figure D.2 Grain size distribution of a sandy soil. Found using U.S. standard sieve sizes (Das, 2008).

The soil is well graded if the distribution of the grain sizes extends over a large range of grain sizes, this means that the uniformity coefficient is large. A soil is thought to be well graded if Cu is larger than 4-6, and Cc is between 1 and 3. When most of the grains in a soil are close to equal in size, Cu is close to 1 and the soil is poorly graded, if a soil is a combination of two or more well graded soil fractions, the soil can be a gap-graded soil (Das, 2008).

Sorting in a soil is a measure of the range of grain sizes present in the soil, and the magnitude of the spread of the grain sizes around the mean grain size. Standard deviation can be used to calculate if a soil is well or poorly sorted, but is also possible to determine the sorting of a soil visually. A well

sorted soil will have grains that are of similar size, while a poorly sorted soil will have grains that differ greatly in size (Boggs, 2006).

Atteberg limits

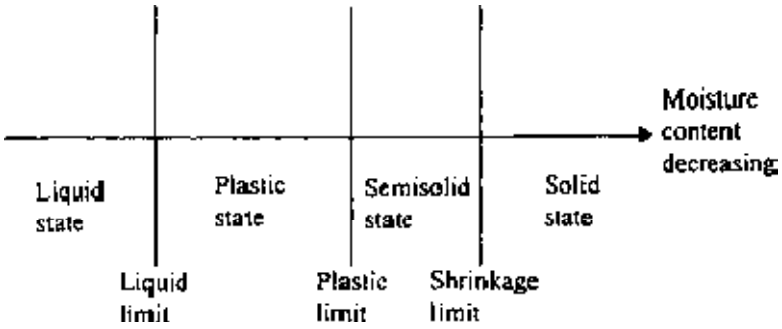

Figure D.3 Atteberg limits and related indices (Das, 2008).

Atteberg limits are useful characteristics of assemblages of soil particles, and have been found through the work of Atterberg and Casagrande. The limits, shown in figure D.3, are based on a theory that fine-grained soil can exist in four different states, depending on the water content in the soil. When the soil is dry it is solid, and then when the water content increases the soil proceeds through the semisolid, plastic, and liquid states. The water content needed to pass the thresholds between the phases are called the shrinkage, plastic and liquid limit. The limits can be found by different testing methods. The concept of a soil existing in the different states is a sound one, because when the water content increases the interaction between grains decreases and the soil should behave more like a liquid. Several indices can be calculated when the atteberg limits have been found for a soil. An important index is the plasticity index, which is the liquid limit minus the plastic limit (Lambe and Whitman, 1979).

Soil classification

Major divisions	*Group symbols*	*Typical names*	*Criteria or classification**
Coarse-grained soils (< 50% passing No. 200 sieve)			
Gravels (< 50% of coarse fraction passing No. 4 sieve)			
Gravels with few or no fines	GW	Well-graded gravels; gravel–sand mixtures (few or no fines)	$C_u = \frac{D_{60}}{D_{10}} > 4$; $C_c = \frac{(D_{30})^2}{(D_{10})(D_{60})}$ Between 1 and 3
	GP	Poorly graded gravels; gravel–sand mixtures (few or no fines)	Not meeting the two criteria for GW
Gravels with fines	GM	Silty gravels; gravel–sand–silt mixtures	Atterberg limits below A-line or plasticity index less than 4† (see Figure 1.38)
	GC	Clayey gravels; gravel–sand–clay mixtures	Atterberg limits about A-line with plasticity index greater than 7† (see Figure 1.38)
Sands (≥ 50% of coarse fraction passing No. 4 sieve)			
Clean sands (few or no fines)	SW	Well-graded sands; gravelly sands (few or no fines)	$C_u = \frac{D_{60}}{D_{10}} > 6$; $C_c = \frac{(D_{30})^2}{(D_{10})(D_{60})}$ Between 1 and 3

Major divisions	Group symbols	Typical names	Criteria or classification*
	SP	Poorly graded sands; gravelly sands (few or no fines)	Not meeting the two criteria for SW
Sands with fines (appreciable amount of fines)	SM	Silty sands; sand–silt mixtures	Atterberg limits below A-line or plasticity index less than 4† (see Figure 1.38)
	SC	Clayey sands; sand–clay mixtures	Atterberg limits above A-line with plasticity index greater than 7† (see Figure 1.38)
Fine-grained soils (≥ 50% passing No. 200 sieve)			
Silts and clay (liquid limit less than 50)	ML	Inorganic silts; very fine sands; rock flour; silty or clayey fine sands	See Figure 1.38
	CL	Inorganic clays (low to medium plasticity); gravelly clays; sandy clays; silty clays; lean clays	See Figure 1.38
	OL	Organic silts; organic silty clays (low plasticity)	See Figure 1.38
Silts and clay (liquid limit greater than 50)	MH	Inorganic silts; micaceous or diatomaceous fine sandy or silty soils; elastic silt	See Figure 1.38
	CH	Inorganic clays (high plasticity); fat clays	See Figure 1.38
	OH	Organic clays (medium to high plasticity); organic silts	See Figure 1.38
Highly organic silts	Pt	Peat; mulch; and other highly organic soils	

Table D.1 Soil classification from grain size analysis. Figure 1.38 in the figure represent figure D.4 (Das, 2008).

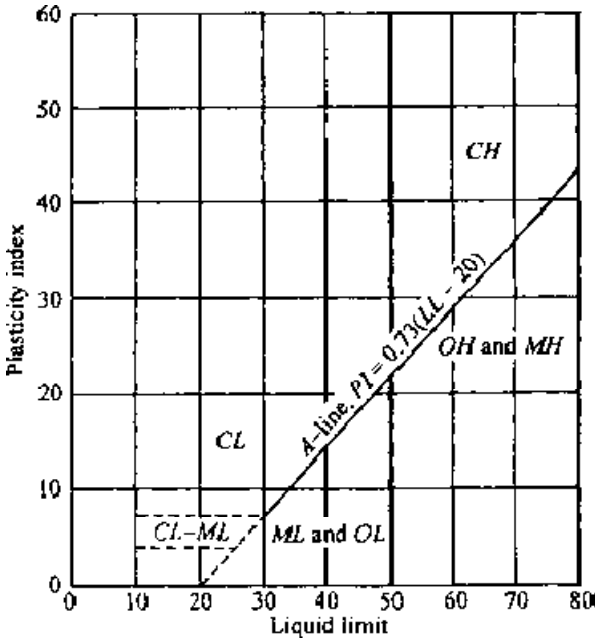

Figure D.4, plasticity chart, in table D.1 describes as figure 1.38.

Soil classification is to arrange soils into groups to express the general characteristics of the soil without a detailed description. There are two major soil classification systems used today, the unified system, which is the system used here, shown in figure D.4 and table D.1, and the AASHTO system. Both systems are based on simple index properties, for example grain size distribution, liquid limit, and plasticity index of soil. The unified system was created by Cassagrande in 1948, and then revised in 1952 by the U.S. using the U.S. standard sieve sizes (Das, 2008).

Soil particles

A soil consists of numerous soil particles with air and/or liquid filling the voids between the particles. The differences between the soil particles themselves will now be presented.

Particle size

The particle size depends on the dimensions that was recorded and how they were recorded, because the size of a particle that isn't a sphere or a cube cannot be individually defined by a single linear dimension. Sieve analysis is a common way of finding the particle size for coarse to fine-grained grains, and a hydrometer analysis for very fine-grained particles. In a hydrometer analysis the size of the particle is equal to a sphere settling with the same velocity in the water. Particle sizes ranges extensively and are distinguished by size and name, table D.2 show the common particle sizes (Lambe and Whitman, 1979).

Particle classification	Particle size (diameter in mm)
Boulder	> 300 mm
Cobble	150 – 300 mm
Gravel	2,0mm (or 4,76 mm) to 150 mm
Sand	0,06 (or 0,076 mm) to 2,0 mm (or 4,76 mm)
Silt	0,002 to 0,06 mm (or 0,076 mm)
Clay	< 0,002 mm

Table D.2 Particle sizes in diameter and the corresponding classification (Lambe and Whitman, 1979).

Particle shape

Soil particles can have many different shapes and they are normally described with a term such as disk, sphere, blade, and a rod, based on the basis of the dimension ratios of the particle. As with the size of the particle it is difficult to explain the shape with only one number if the particle is not a cube or a sphere. When working on an entire soil mass as an engineer it can be impractical to characterize numerous particle shapes because of the size of the particle compared to the entire soil mass, but for a geologist this is quite common (Lambe and Whitman, 1979).

Degree of roundness, surface texture, and colour of the soil particle.

The sharpness of the edges and corners of a particle explains the degree of roundness the particle has, it can also be used to find the transport distance of the grains. If the grains are very sharp and

not very rounded they are often immature and have not been transported very far, but if they are round then they are often transported for quite some time. The surface texture of a particle is the features on the surface that are independent of the size, shape, and roundness of the particle. Terms that are often used to explain surface texture are dull or polished, smooth or rough, frosted, etched, or pitted. The colour of a soil particle is important in a mining perspective, but not very important for a soil engineer (Lambe and Whitman, 1979).

Saturated and partially saturated soils

Below the water table in a soil the soil is assumed to be fully saturated with a degree of saturation that is close or equal to 100%. If there is an unsaturated zone in the soil, the soil is partially saturated and capillary tension can make water have a negative pressure. The capillary tension is not constant but changes with the changes in pore sizes in the soil. When water percolates from the surface down to the water table some water may be held around the contact points between grains due to surface tension. The negative pressure created by the capillary tension results in attractive forces between soil particles, this process is known as soil suction, and is a function of the pore size and water content. If there is no unsaturated zone in the soil and the water table reaches the surface the soil is completely saturated (Craig, 2004).

In a soil that is partially saturated with a dry zone and a saturated zone, a negative fluid pressure can be measured above the water table. This is known as the tension and occurs due to water molecules at the water table being subjected to an upward attraction from the surface tension of the air-water interface, and by molecular attraction between the liquid and solid phases in the soil. This phenomenon is known as the capillarity and it can draw water up from the saturated zone and into the unsaturated zone and create a capillary fringe above the water table. This process is more pronounced in fine-grained soils due to greater tensions being created by smaller pore spaces, and the capillary water does not rise to the same level everywhere due to the size difference in the pore spaces. If the water table is close enough to the surface so that the capillary fringe reaches the surface, direct evaporation of the ground water can take place. It is also possible for the water to evaporate drop by drop from the capillary fringe (Fetter, 2001).

Shear Strength of soils

Before the shear strength of the soil has been exceeded, deformation or flow of the soil cannot occur. The shear strength is also one of the parameters that can stop a debris flow on a slope. The shear strength is provided by cohesion from the fine-grained matrix of the soil, and by the internal friction from the coarser clasts. Debris flows are not cohesionless, the very small amounts of clay (less than 10 %) is still able to provide cohesive strength to the soil. This cohesive strength holds the debris together when the debris flow flows. The internal friction is due to the interlocking of grains, and the sliding friction in poorly sorted material (Costa, 1984).

Mohr-Coulomb Failure Criterion

Mohr presented in 1900 a theory for ruptures in a material. Mohr's theory is due to a critical combination of normal and shear stresses, failure can occur along a plane. This relationship between normal and shear stresses is given by D.8 (Das, 2008).

$$s = f(\sigma) \tag{D.8}$$

Where s is the shear stress at failure and σ is the normal stress(stress is calculated as Force/Area) on the failure plane. Coulomb defined in 1776 f(σ) as equation D.9 (Das, 2008, Wu, 1996).

$$s = c + \sigma \tan \varphi \quad \text{(D.9)}$$

Where c is cohesion and ϕ is the internal friction angle of the soil, they are known as the shear strength parameters and can be obtained from the failure envelope, but the shear strength parameters are normally obtained by one of two methods; either the direct shear test or the triaxial test.

Equation D.9 is better known as the Mohr-Coulomb failure criterion(Das, 2008, Wu, 1996). This equation creates a failure envelope in a normal stress versus shear stress graph. On the failure envelope, failure will occur along that plane. If the stress situation is below the failure envelope, failure will not occur. Conditions where the stresses are above the failure envelope cannot exist, this is because shear failure would have occurred before the normal or shear stresses reached those values (Das, 2008).

The shear stress in a soil can only be resisted by the soil skeleton of solid particles, so for a saturated soil the shear stress carried by the soil skeleton is known as the effective stress. The total stress in the soil is therefore a combination of the effective stress carried by the soil skeleton and the pore water pressure from the pore water. Equation D.9 then becomes equation D.10(Das, 2008).

$$s = c + (\sigma - u) \tan \varphi = c + \sigma' \tan \varphi \quad \text{(D.10)}$$

Where u is the pore water pressure and σ' is the effective stress on the plane. For sand, inorganic silts, and normally consolidated clays, cohesion is ≈zero, cohesion is greater than zero for overconsolidated clays.

Shear strength parameters

The shear strength parameters differ in loose and dense sand. In direct shear test for cohesionless soils it is clear that denser sands can withstand a higher shear stress than loose sand before they fail, but that the ultimate final shear stress of both sands are equal and remains constant. This means that it takes more to shear denser sand and looser sands will therefore be more prone to failure. The volume of the sand also changes with horizontal shear displacement, dense sands will eventually increase in volume while loose sands will decrease in volume. It is off course also very important if the soil is dry or not, if the sand is dry then the pore water pressure, u, is equal to zero.

The shape of the grains are also important when it comes to internal friction angle, angular grains have a higher internal friction angle than round grains, this is due to the dilatency of the grains. When the results from the test are plotted in a effective normal stress vs. Shear stress graph, a Mohr failure envelope can be drawn and the angle of the envelope is the internal friction angle. If there is cohesion in the soil, the intercept between the Mohr failure envelope and the vertical axis of shear stress is the cohesion of the soil. For unconsolidated undrained tests with cohesion, the internal friction angle is equal to zero, because the failure envelope is a horizontal line, formed by the total stress because the deviator stress (the difference between the major principal stress and the minor principal stress) is constant (Das, 2008).

For the shear strength test of a soil to be correct it is important that the test sample is a representative sample of the material, and this can be difficult because of the possible presence of very large clasts, and that fine-grained material might have been removed from the deposits due to water etc.

Estimating shear strength from the debris flow deposits

Measurements of shear strengths of natural debris flows while they are flowing are very rare, because then the measuring equipment must be placed at the location before the debris flow was initiated. The only way to find the shear strength of the soil in a debris flow is normally to measure it after the event has happened. Three methods of estimating shear strength for natural debris flows has been developed by Johnson, all using the deposits from the debris flow (Johnson, 1970) .

- ***Thickness of unconfined lateral deposits.***

  The unconfined lateral deposits were deposited when their thickness were at the critical thickness for the soil, by measuring the thickness of the deposited material it is possible to estimate the shear strength.

- ***Dimensions of channels plugged by debris.***

  If the cross-section of a channel is known, and the debris flow has plugged that channel, the dimensions of the channel can be used to estimate shear strength.

- ***Size of the largest deposited boulders.***

  This method assumes that unusually large boulders are transported by the small density difference between the boulders and the debris fluid, and that consolidation after deposition has been minimal. Shear strength can then be estimated for the soil, by looking at the volume fraction of the boulder that is submerged in the debris .

Undrained shear strength

Undrained conditions occur when an external load changes at a rate that is much faster than the rate at which the pore water pressure can dissipate. The material is important for how quickly the pore water pressure dissipates from the soil, pore pressure dissipates relatively slowly from a clay and relatively quickly from a sand (Lambe and Whitman, 1979). This process is explained in the chapter on effective stress in Appendix D.

Undrained shear strength is more important in clays than in sands due to the dissipation time of pore water pressure for the two materials. Undrained shear strength depends on several factors, some of which are included here. Undrained strength increases when the water content in the soil decreases, the consolidation stress increases, and when the maximum past consolidation stress increases (Lambe and Whitman, 1979). Undrained shear strength is lower than the drained shear strength and will therefore be more likely to fail if all other factors are the same.

Positive or negative pore pressure can be induced in saturated sands, this depends on if the sand decrease or increase in volume during drained shear, this process is the same for all soils. Tests show that loose sand induces positive pore pressure, while dense sand induces a negative pore pressure.

Effective stress paths can be produced for undrained shear tests of a soil and they depend on the tendency of the soil to either expand or contract during shear. Loose soils decrease in volume, while dense soils initially decrease in volume but increases in volume quite rapidly following the small decrease in volume. It is not the water content in the soil that determines the shear strength, but the density or tightness of packing of the mineral skeleton. This was shown by Lambe and Whitman, in sand the pore water pressure cannot be less that 1 atmosphere, if the pore pressure is below this limit the pore water will cavitate. If a soil cavitates the samples volume does not remain constant even if the sample is undrained. The pore pressure remained constant after the cavitation, and the behaviour of the soil was the same as for drained shear (Lambe and Whitman, 1979).

Effective Stress

A soil is built up of a skeleton of solid grains, and the voids between the grains. The voids between the grains contains air if the soil is dry, and water is the soil is completely saturated, if the soil is partially saturated the voids contain a mixture of water and air. The volume of a soil can change due to a rearranging of the grains by rolling or sliding since the grains and the water are considered incompressible, while air is highly compressible. Shear stress can only be resisted by the soil skeleton, due to forces between the grains. Normal stress can be resisted by the soil skeleton with an increase in the grain contact forces ,the water can resist normal stress with an increase in the pore water pressure if the soil is fully saturated (Craig, 2004).

Principle of effective stress

Terzaghi presented in 1923 the principle of effective stress and the importance of particle to particle forces, and how these forces were transmitted through the soil skeleton was shown. Terzaghi's principles only apply to fully saturated soils and consist of three stresses (Craig, 2004).

- ***Total normal stress (σ)*** acts on a plane within the soil. It is the force per unit area that is transmitted in the normal direction across the plane.
- ***Pore water pressure (u)*** is the pressure from the water in the soil voids.
- ***Effective normal stress (σ')*** acts on a plane, it is the stress that is transmitted through the soil skeleton.

The equation for combining these three stresses is that the total stress in the soil is the product of the pore water pressure and the effective normal stress, equation D.11 (e.g.(Lambe and Whitman, 1979)Craig, 2004, Wu, 1996).

$$\sigma = \sigma' + u \qquad \text{(D.11)}$$

The effective stress is calculated from a sum of interparticle forces over certain cross sectional area A. Because A is much larger than the actual contact area for each grain contact, the true contact area is normally between 1-3% of the cross sectional area, the true effective stress between particles is very much higher than the calculated average effective stress (Craig, 2004).

Effective vertical stress

The total vertical stress is equal to the weight of the material per unit area above a certain depth. The material is both water and soil, and the total vertical stress (σ_v) can therefore be found (Craig, 2004).

$$\sigma_v = \gamma_{sat} z \tag{D.12}$$

Where γ_{sat} is the saturated unit weight of the soil and z is the depth. The pore water pressure can be considered hydrostatic, since the void spaces are continuous. The pore pressure at depth can be found by equation D.13 (Craig, 2004).

$$u = \gamma_w z \tag{D.13}$$

Where γ_w is the unit weight of water. Since Terzaghi's principle of effective stress, equation D.11, show that the total stress is equal to the sum of the effective stress and the pore water pressure, it is possible to calculate the effective vertical stress on a horizontal plane at a certain depth(Craig, 2004).

$$\sigma'_v = \sigma_v - u = (\gamma_{sat} - \gamma_w) z \tag{D.14}$$

Consolidation and undrained loading

If you have a soil that is fully saturated, and there is an increase in the total vertical stress on the soil, the grains will try to move closer together, but because water is incompressible it cannot be compressed. This is only true if the soil is laterally confined. Because the particles can't rearrange, the interparticle forces cannot increase either, that is only possible if some of the pore water can escape. The pore water resists the rearranging of the grains, and the static pore water pressure (the initial pore water pressure) increases because of this process. The increase in the pore water pressure is equal to the increase in total vertical stress. If the soil was not laterally confined, then some particle rearranging would be possible and there would be an increase in the effective stress, and the increase in the pore water pressure would be less than the increase in the total vertical stress (Craig, 2004).

Due to the increase in pore water pressure, a transient flow(unsteady) towards a free-draining boundary is created. This flow is the result of the pressure gradient created by the increase in pore water pressure. The drainage of the soil will continue until the pore water pressure in the soil is equal to the pore water pressure value for the water table in the soil. The value of the pore water pressure above the static pore water pressure is known as the excess pore water pressure. The overall pore water pressure during drainage is equal to the sum of the static and the excess pore water pressures. The reduction in pore water pressure during drainage is called dissipation, and when the excess pore water pressure is equal to zero again the soil is in a drained condition(Craig, 2004).

There can still be pore water in the soil after drainage, but there is no stress-induced pressure in the pore water, the soil can stay fully saturated during drainage. Before drainage the soil is in an undrained condition, and the excess pore water pressure has not been increased from its initial value. The solid particles can rearrange when the excess pore water pressure decreases due to drainage, so a decrease in the excess pore water pressure leads to an increase in the interparticle forces, resulting in an increase in the effective vertical stress and a reduction in volume. When

drainage is complete, the increment in total vertical stress will be carried by the soil skeleton. Permeability controls the drainage time for the soil, in low permeability soils the drainage will be slow. This process is known as consolidation (Craig, 2004).

If there is a reduction of the total normal stress, volume increase of the soil is limited because the particle rearrangement in the soil due to total stress increase is mostly irreversible. The soil skeleton can expand to a limited extent, due to small elastic strains in the solid particle contact areas, because of an increase in the interparticle forces, and clay minerals can expand due to recoverable compression for the adsorbed water surrounding the particles. Pore water pressure will therefore be reduced when the soil expands, and the excess pore water pressure will be negative. The pore water pressure will then increase back to the static value due to flow into the soil. The flow will result in a reduction in the effective normal stress and an increase in volume. This process is known as swelling and is the opposite of consolidation. If there is seepage present in the soil, the excess pore water pressure will be above or below the steady seepage pore water pressure, determined from a flow net (Craig, 2004).

Partially saturated soils

The void spaces in a partially saturated soil are occupied partially by water and partially by air. This makes calculating the effective stress in the soil much more complicated. Due to surface tension, the pore water pressure (u_w) must always be less than the pore air pressure (u_a). The pore air will produce continuous channels through the soil, while the pore water is concentrated around the interparticle contacts, unless the soil is close to being fully saturated. Bishop created in 1955 an equation for calculating the effective stress for partially saturated soils (Craig, 2004).

$$\sigma = \sigma' + u_a - \chi(u_a - u_w) \tag{D.15}$$

Where χ is a parameter that is determined experimentally, it mainly depends on the degree of saturation of the soil. $(u_a - u_w)$ is a measure of the suction in the soil. If the soil is fully saturated Sr=1 and χ=1; if the soil is completely dry Sr=0 and χ=0. When the soil is fully saturated, equation D.15 becomes equation D.11. Because equation D.15 includes a parameter that needs to be determined experimentally, the equation is not very convenient to use. It is possible to interpret χ as the average proportion of a cross sectional area A, that passes through water. By using this interpretation, equation D.16 can be used (Craig, 2004).

$$\sigma A = \sigma' A + u_w A + u_a(1 -)A \tag{D.16}$$

Seepage

When there is seepage of water in the soil, the total pressure head is dissipated when a frictional drag act on the solid particles in the direction of flow, the frictional drag is produced by viscous friction. There is a transfer of energy from the water to the solid particles, the forces created by this transfer of energy are known as seepage forces. The resultant body force on a soil mass is a combination of the seepage force and gravity. The effective normal stress on a plane within the soil mass is determined by the resultant body force if there is seepage present in the soil (Craig, 2004).

Permeability

All soils are permeable materials, this means that water can flow through the interconnected pore spaces in the soil. The three phases that a soil is built up and has been explained earlier in appendix D. Permeability is the property of the soil that allows the flow of water through the interconnected void spaces. The permeability of a soil is influenced by the particle size, void ratio, composition of the soil, fabric of the soil, and the degree of saturation. A soil that has a low permeability means that it is difficult for water to flow through the soil, and a soil that has high permeability means it is easier for the water to flow through the soil (Lambe and Whitman, 1979).

Darcy's law

To find the quantity of seepage through a soil mass given a certain condition, figure D.5 can be used.

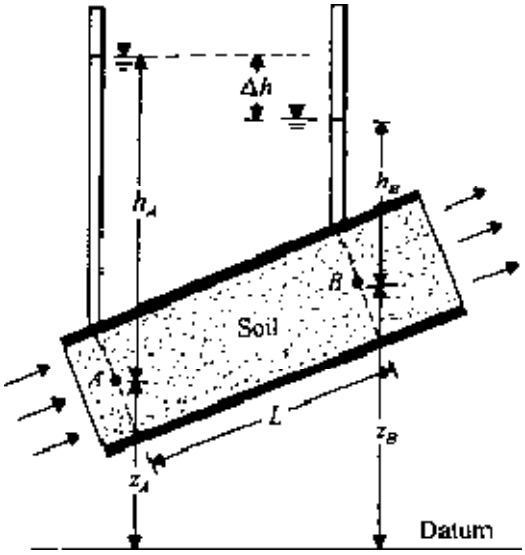

Figure D.5 The development of Darcy's law (Das, 2008). Where hA is the pressure head at location A, hB is the pressure head at location B, zA and zC is the elevation head at location A and B, L is the length between location A and B, and Δh is the difference in total head between location A and B.

Bernoulli's theorem explain that the total head for a flow in the soil is given by;

Total head= elevation head+ pressure head + velocity head (D.17)

When water flows through a soil the velocity head is so small that it can be neglected from the equation, and the total head is therefore the sum of the elevation and pressure head at the location (Das, 2008).

So for figure D.5 the equations for total head is:

Total head at A= $z_A + h_A$ (D.18)

Total head at B= $z_B + h_B$ (D.19)

The loss of head between location A and B can be found:

$$\Delta h = (z_A + h_A) - (z_B + h_B) \quad \text{(D.20)}$$

The hydraulic gradient i can be calculated as:

$$i = \Delta h / L \quad \text{(D.21)}$$

Darcy found a relationship between the discharge velocity v and the hydraulic gradient i.

$$V = ki \quad \text{(D.22)}$$

where k is the coefficient of permeability

the rate of seepage q can then be calculated:

$$q = kiA \quad \text{(D.23)}$$

where A is the cross-sectional area of the soil perpendicular to the flow of water.

The actual velocity of seepage through the soil must differ from equation D.23, because the water can only flow through the interconnected pore spaces and equation D.23 is calculated using the cross-sectional area of the soil. The actual velocity v_s can therefore be found by dividing V by the porosity n of the soil. Darcy's law is only valid for laminar flow, and the ranges for which Darcy's law is valid can be found by calculating the Reynolds number of the flow. And the calculations show that for flow through all type of soils (sand, silt, and clay) is laminar and Darcy's law is therefore valid. For coarse sand, gravel, and boulders, the water can be expected to be turbulent flow and the hydraulic gradient must therefore be calculated in another manner (Das, 2008).

Coefficient of permeability

The coefficient of permeability k is a measure of the resistance of the soil to flow of water. k can be expressed as:

$$k(cm/s) = K\rho g/\mu \quad \text{(D.24)}$$

where K is the intrinsic(or absolute) permeability, ρ is the mass density of the fluid, g is the acceleration due to gravity, and μ is the viscosity of the fluid. The coefficient of permeability depends on (Das, 2008):

- The shape and size of the soil particles present in the soil.
- The void ration in the soil. When the void ratio increases the permeability increases.
- Degree of saturation. When the degree of saturation increases the permeability increases.
- Soil particle composition. Important for clay rich soils, due to thickness of the water held to the soil particles.
- Structure of the soil. Higher coefficient of permeability for fine-grained flocculated soils.
- Permeant viscosity
- Permeant density and concentration.
- Temperature

The general thought is that the smaller the particles, the void spaces are smaller and the coefficient of the permeability is lower. If there is fine-grained material present in the soil, the coefficient of permeability will be lower than in a soil where there is no fine-grained material. For a debris flow there is normally little fine-grained material in the soil and the coefficient of permeability and therefore the seepage of water can be high. The coefficient of permeability can be found using different methods for example laboratory methods, well pumping test, or borehole test. The normal ranges for the coefficient of permeability in soils can be found in figure D.6 (Craig, 2004).

Material	*Coefficient of permeability (mm/s)*
Coarse	$10–10^3$
Fine gravel, coarse, and medium sand	$10^{-2}–10$
Fine sand, loose silt	$10^{-4}–10^{-2}$
Dense silt, clayey silt	$10^{-5}–10^{-4}$
Silty clay, clay	$10^{-9}–10^{-5}$

Figure D.6 Coefficient of permeability (m/s) Made by b found in (Das, 2008).

If the coefficient of permeability varies between each soil layer the flow in the horizontal direction can vary, in the vertical direction the flow can also vary between the layers. If a soil is undrained there is no flow out of the soil, but water must have flowed into the soil before it became undrained and water might still flow into the soil (Das, 2008).

For the study area in Veikledalen the permeability is important for the stability in the slope. Due to the last glaciations period the sediments in the area are overconsolidated at a certain depth and the permeability of the soil is therefore low. The top layer of the soil has become relatively loose due to frost and has a high permeability. This means that the water that infiltrates the soil will prefer to flow in the top layer of the soil and will have difficulties in infiltrating the overconsolidated layer of sediment. If the permeability of the overconsolidated layer is high enough so that the infiltration rate is slower that the infiltration of water into the soil the top layer can become saturated while the overconsolidated layer remains relatively dry. The flow of water can therefore flow along the boundary between the two layers or perpendicular to the boundary between the layers.

Critical Values For stability

Debris flows can only occur if several factors are present in a critical combination. Some of the main factors that the stability of a slope depends on are:

- **Material**: The availability of material is important, if there is no material present that can be eroded or slide then there is not possible to initiate a debris flow. The type of rock is important because certain materials are more unstable than other materials. Bare intact gneiss is an example of both of these phenomenon's, it is much more stable than for example volcaniclastic material, and there is very limited material available in areas where there is bare rock to initiate a debris flow (De Blasio, 2011).
- **Geometry:** The geometry of the material is important for the stability of the slope. If the layers of the material are dipping towards the slope they are more unstable than material that is dipping away from the slope. If the dipping layers have an angle that is less than the slope angle so that the dipping layers cross the surface of the slope the slope is more unstable (De Blasio, 2011).

- **Distribution of weight:** The slope angle is important to the stability of a slope because a slope can only be stable up to a certain slope angle and adding or removing weight affects the driving or resistive forces in the slope which are used to calculate the factor of safety (De Blasio, 2011). Increasing the resistive forces makes the slope more stable and decreasing the driving force makes the slope more stable. Adding weight at the toe increases the friction and therefore the resistive force of the slope. Removing weight from the top decreases the driving force of the slope by decreasing the gravity component. Adding weight to the top increase the gravity component of the slope and increases the driving force of the slope. Removing weight at the toe decrease the friction of the slope and decreases the restrictive force of the slope (Mair, 2011).
- **Water:** One of the most important factors when concerning instability is water. An increase in the water content decreases the cohesion in the soil, increases the weight of the soil, increases the pore water pressure, and increases the effective stress in the soil which decreases the soil strength. The amount of water that is needed to make a slope unstable depends on many factors, for example the material, and is therefore relatively independent for each slope (De Blasio, 2011). But the main trigger mechanism for shallow debris flows are intense rainstorms (Caine, 1980). For the stability of a slope the pore pressure is important, if the water content in an unsaturated soil changes the suction and apparent cohesion of the soil will be affected, this will affect the slope stability. If the pore pressure in the slope increases the stability of the slope will decrease, this process is explained in appendix D in the chapters on effective stress and shear strength. The same decrease in stability is true for a saturated soil where the pore pressure changes. The change in pore pressure in a saturated soil will influence the effective stress in the soil and the friction component of the shear strength in the soil due to the change in weight of the soil and particle friction. Changes in the pore pressure in a soil can induce slope deformation and failure of the slope, changes in pore pressure is often due to precipitation or by snow melting (Picarelli, 2009).
- **Vegetation:** Vegetation can influence the stability of a slope by removal of water through evapotranspiration and mechanical cohesion. Bare soil may also be more susceptible to surface water erosion than soil where there is vegetation present (De Blasio, 2011).

Appendix E Debris flow motion

Debris flow dynamics

The models for explaining momentum transport in debris flows are mostly based on Newton's second law, momentum conservation. Newton's second law states that when there is an external force acting on a particle, the time derivative of momentum is equal to the external force acting on the particle (De Blasio, 2011).

$$\vec{F} = \frac{d\vec{Q}}{dt} = m\vec{a} \text{ for constant mass.} \quad \text{(E.1)}$$

Where F is the external forces, Q if the momentum of a particle on mass m and is equal to mv if the mass is constant, where v is the velocity. a=dv/dt and is the acceleration. If there are no external forces, the particle will have a constant velocity, because the momentum of the point particle remains constant over time. The different models for explaining momentum in a debris flow differ mostly in the forces they include in the model, and how the forces are expressed. Most of the models are 2D, but 3D models also exist.

Rheological models

Rheological models for explaining the dynamics of debris flows have been the most common way for some time. The rheological models are single-phase continuum models, the mixture of particles and fluid are thought to be a continuous fluid, which in various situations behaves as a debris flow (Takahashi, 2007). The models combine the Navier Stokes equation with the relationship between shear stress and shear deformation. The Navier Stokes equation can be calculated in 3D, but will only be shown for the x-direction in this paper.

$$\rho\left(\frac{\delta u}{\delta t} + u\frac{\delta u}{\delta x} + v\frac{\delta u}{\delta y} + w\frac{\delta u}{\delta z}\right) = -\rho g \sin\beta - \frac{\delta P}{\delta x} + \frac{\delta \tau_{xx}}{\delta x} + \frac{\delta \tau_{xy}}{\delta y} + \frac{\delta \tau_{xz}}{\delta z} \quad \text{(E.2)}$$

Where ρ is density, g is gravity, t is time, P is pressure, u,v, and w are the velocity in the x, y, and z direction, and τ is the shear stress. The Navier stokes equation is divided into four parts. The momentum change per unit volume is on the left side of the equation. Then from left to right are the gravity force, Pressure force, and the last three components are the viscous forces acting in different directions (De Blasio, 2011).

The problem with the Navier Stokes equation and the different rheological models is to find the correct rheology of a debris flow. The rheology of the flow is used to calculate the viscous forces, and the rheological models differ therefore mostly in the viscosity section of the equation. The four most common rheological models, and the ones that will be covered here are the Newtonian fluid, Bingham model, Hershel-Bulkley model, and the Dilatant fluid model also called the Bagnold model.

The difference between a Newtonian and a non-Newtonian fluid in that respect is that a Newtonian fluid will start to shear immediately and at a constant rate when stress is applied to the material. The differences in the rheological models when shear stress and shear rate is applied to the fluid can be seen in figure E.1.

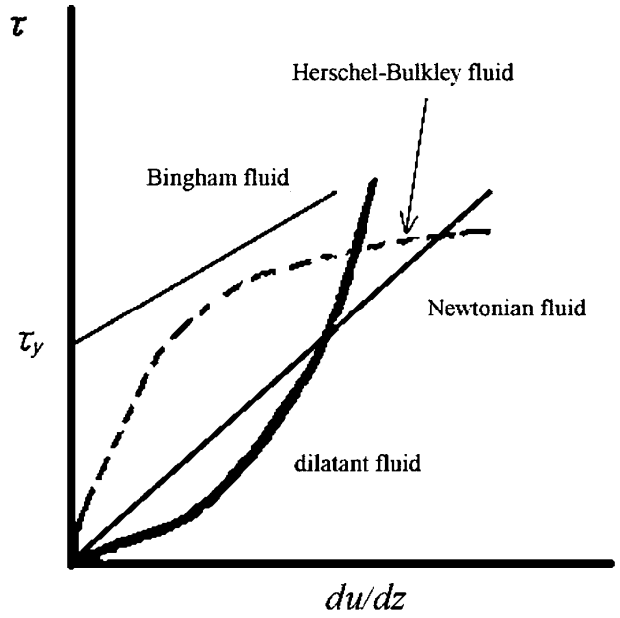

Figure E.1 Rheological behaviour of fluids when shear stress (τ) and shear rate(du/dz) is applied to the fluid (Takahashi, 2007)

Newtonian fluid

If the fluid in a debris flow is assumed to Newtonian, the viscosity can be calculated by a simple equation. The equation assume that the debris flow is an ideal Newtonian fluid, which has no marginal or terminal influences, no shear stress on the surface, no slip on the base, and that it is a laminar flow parallel to the base. Debris flows do not fit with these assumptions, which mean that it is not an ideal Newtonian fluid, and the equation is not correct (Costa, 1984).

The equation for a Newtonian fluid that is shown in figure E.1, shows that the relationship between the shear stress and shear rate is linear, and the proportional coefficient is the dynamic viscosity of the fluid. Since a debris flow contains both solids and fluid, the relationship between shear stress and shear rate is not linear. The equation is known as the Newtonian viscous flow equation(Takahashi, 2007).

$$\tau = \mu\left(\frac{du}{dz}\right) \qquad \text{(E.3)}$$

Where τ is the shear stress, μ is the viscosity, and (du/dz) is the shear rate. If the debris flow is assumed to be a Newtonian fluid, the simplification is made that the flow is laminar ,and appropriate numbers are fitted to the Navier Stoker equation, the velocity of the debris flow will become extremely high and unrealistic (De Blasio, 2011). Water acts as a Newtonian fluid until the volume sediment concentration exceeds 9% of the flow. With sediment concentrations above 9% the particle interactions alter the fluid characteristics of the water, and viscosity is no longer constant but varied with the shear rate deformation (Bagnold, 1956).

Bingham model

The Bingham model was proposed by Johnson, and (Yano and Daido, 1965) independently and have since then been used by many to explain actual debris flows. The Bingham model assume that the material is rigid until a certain threshold of shear stress has been exceeded, this threshold is known as the yield strength (Takahashi, 2007). This process can be seen in figure 8.1. Because of yield strength in the fluid, the debris flow can stop on sloping surfaces, and deposit into distinct leeves and lobes of a limited thickness(Costa, 1984). The Bingham model allow the yield strength to depend on Coulomb friction, and therefore on the mean stress, and the viscosity depend on the deformation rate (Iverson, 1997). When the Bingham model is applied to debris flows, fixed viscosities and yield strengths are assumed by most. It is also common to assume steady, uniform flow. An example of this is the yield strength found from the thickness of the deposits, see appendix D on shear strength.

The Bingham model is based on a general Hershel-Bulkley fluid.

$$\tau = \tau_y + K(\frac{\delta u}{\delta z})^a \qquad \text{(E.4)}$$

Where K is the consistency, τ is the shear stress, τ_y is the yield strength, and du/dz is the shear rate.

A Herschel-Bulkley fluid can be divided into three fluids based on the value of the exponent a.

A= 1 Bingham fluid

A>1 Shear thickening fluid

A< 1 shear thinning fluid.

The difference between these three fluids with respect to shear rate and shear stress can be seen in figure E.2 (De Blasio, 2011).

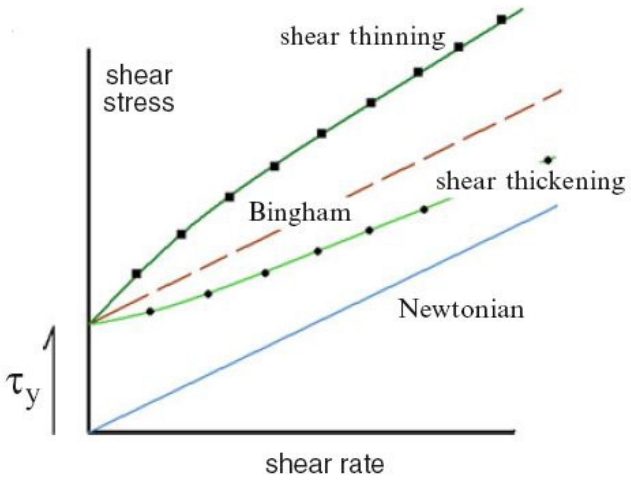

Figure E.2 Rheological behaviour for Herschel-Bulkley fluids, and a Newtonian fluid (De Blasio, 2011)

Equation E.4 with a=1 gives the equation for the shear stress in a Bingham fluid (De Blasio, 2011).

$$\tau = \tau_y + \mu_B(\frac{\delta u}{\delta z}) \quad \text{(E.5)}$$

Where μ_B is the Bingham viscosity of the fluid and can be calculated if the shear strength, maximum velocity, and the width of the plug are known (Costa, 1984). The velocity distribution in an open channel can also be calculated, this equation show that at a point in the flow the applied shear stress is equal to the yield strength. The velocity distribution in a Bingham fluid is shown in figure E.3. Above this point in the flow the shear stress is less than the yield strength and must therefore be rigid. This rigid part of the flow is called the plug of the debris flow and the thickness of the plug can be calculated (Takahashi, 1981). For debris flows that have a plug, they usually form u-shaped channels, and velocity distributions that fit with the theory of a rigid plug has been measured or observed in experimental and natural debris flows.

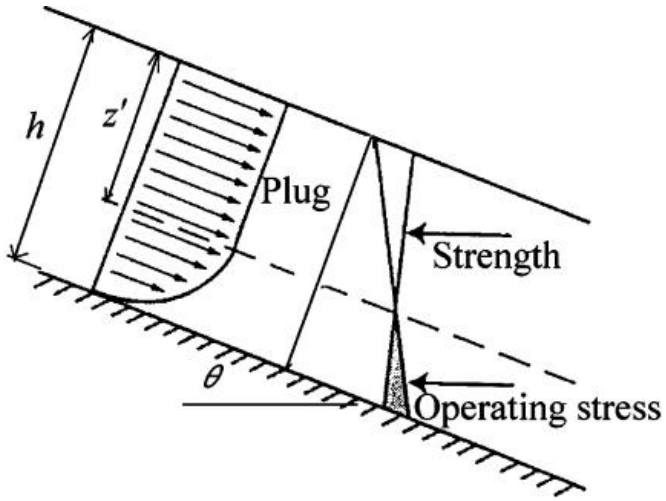

Figure E.3 Velocity distribution in a Bingham fluid (Takahashi, 2007).

Figure E.3 show the velocity distribution in a Bingham fluid that has a rigid plug in the centre of the flow, which has the depth z in the figure. Figure E.3 also show that inside the plug the operating stress is below the strength of the material, and the velocity is therefore constant. Figure E.3 can be used to find the shearing stress acting on a plane at a depth z in a Bingham fluid with a thickness h and a channel slope of θ

$$\tau_y + \mu_B(\frac{\delta u}{\delta z}) = \rho g(h - z)\sin\vartheta \quad \text{(E.6)}$$

If the fluid is assumed to be a Bingham fluid then there is a critical thickness that is needed for the material to flow. Below this critical thickness the material will remain rigid and the yield strength is not exceeded (Takahashi, 2007).

$$T_c = \frac{(\frac{c}{\gamma_m \sin\beta})}{(1-\frac{\tan\varphi}{\tan\beta})} \quad \text{(E.7)}$$

Where c is the cohesion which is equal to the yield strength, γ_m is the unit weight of the material and is equal to ρg, and β is the slope angle. If the thickness of the flow does not exceed the critical

thickness it will not flow, and if the thickness decreases to below the critical thickness the flow will stop (Johnson, 1984).

When Bingham strengths are assumed to have fixed yield strengths and viscosities, the yield strength is equal to the Coulomb strength shown in equation D.3, when the internal friction is equal to zero and only cohesion controls the yielding. If this is correct the yield strength should increase when the concentration of fine-grained material in the debris flow increases, experiments with only water and fine-grained material show this behaviour.

Large scale flume experiments with a material where the majority of the mass is a combination of sand, gravel and water, and the fine-grained material content is only a few percent, show that when the fines concentration is increased the flow thickness and apparent strength decreases. This decrease in strength and thickness is because fine-grained material help sustain high pore pressure in the material, and the pore pressure decrease the frictional resistance and this enhance lobe spreading (Major, 1997). This is a major problem of the fixed yield strength Bingham models, the models replicate the rheology of the water and fine-grained material fraction of a debris flow, but observations show that the interactions between coarse grained particles and between the particles and the fluid strongly affects debris flow behaviour (Iverson, 1997).

There are several limitations to the Bingham model, even if it is used in a very general form Johnson. The Bingham model assumes that momentum transport and energy dissipation in a debris flow only occur by viscous shearing. Rate-independent energy dissipation can occur when grains come in contact with other grains or with the flow boundaries is neglected, and fluid flow relative to the granular assemblage is also neglected. This means that the Bingham model only work for slow, creeping earth flows and similar processes, but not debris flows (Iverson, 1997).

Bingham models also assume the no-slip boundaries that fluid mechanics use. This assumption requires that a Bingham material deposits a continuous layer of material in the debris flow path, but these types of deposits are normally not found in nature. What normally occurs is that the grains slide, collide, and roll along the flow boundaries, both at the bottom of the flow and at the top. The Bingham model is therefore not an ideal model for explaining debris flow behaviour (Iverson, 1997).

The Coulomb-Viscous Model

The Bingham model does not explain debris flows all that well, so Johnson proposed a modified Bingham model, called the Coulomb-Viscous model. The main reason why Johnson modified the Bingham model was because the Bingham model made it possible for a fluid to flow in a very low slope, if the thickness of the flow was great enough, this process does not occur in actual debris flows (Takahashi, 1981). The model takes into account the lower mobility of actual debris flow, when compared to the expected mobility from rheometer tests. The model was created based on data from large-scale flume tests and observations of actual debris flows. The resistance to flow is due to the shear strength from cohesion and internal friction, and viscosity. Cohesion and internal friction can cause resistance to flow in both moving and static debris flows, and they are therefore the shear strength that must be exceeded before the material can flow. This is the yield strength of the material. The model combines the Coulomb criterion in equation D.3 with the Newtonian viscous flow equation E.3 into the Coulomb-viscous model equation E.8(Costa, 1984).

$$\tau = c + \sigma \tan \varphi + \mu \frac{\delta u}{\delta z} \quad \text{(E.8)}$$

When this equation is compared with equation E.5 in the Bingham model, τ_y is equal to (c +σ tan ϕ) (Johnson, 1970). The Bingham model and the Coulomb-Viscous model are usually called the plastic-viscous rheological models. Both models are much better at explaining debris flow than Newtonian models, but they are not without flaw.

Dilatant Model

Because of the problems with the Bingham model in regards to grain interactions a model was created by Takahashi in 1978, the model assumes the that the debris flow is a dilatant fluid (Takahashi, 1981). The model uses the concept of dispersive pressure explained in section 1.8.4. Bagnold sheared a dispersion of solid grains that were neutrally buoyant in Newtonian fluids of various viscosities. The Newtonian fluid was water and a mixture of water, glycerine and alcohol, and it was sheared in the annular space between two concentric drums (Bagnold, 1954). The grains in the fluid dilated to such a degree that they exerted a radial pressure on the vertical walls perpendicular to the flow.

The dispersive pressure is due to the momentum exchange when grains collide with each other or the walls of the container, and the dispersive pressure P is proportional to the shear stress τ (Bagnold, 1954). Bagnold found that the normal and shear stresses in the fluid varied either linearly or quadratically with the shear rate, how the stresses behaved depended on the Bagnold number, which is the ratio of inertial grain stress to viscous shear stress(Iverson, 1997). Bagnold divided the fluid into two regimes to explain how the stresses varied with shear rate, when the fluid is grain inertia it varies quadratically, and if the fluid is macroviscous it varies linearly (Bagnold, 1954).

Bagnold created an equation for the shear stress in debris flows, with the theory that when the shear rate was large the viscosity of the fluid was insignificant, and shear stress was only due to grain interactions, this is the grain inertia regime. For low shear rate, the shear stress was mixed, due to modifications in the fluid viscosity from the presence of the grain particles, this is called the macroviscous regime (Bagnold, 1954).

$$\tau = P \tan \varphi \quad \text{(E.9)}$$

Where ϕ is the dynamic internal angle of friction, and the dispersive pressure can be calculated. The dynamic internal friction angle has been shown to differ little from the static Coulomb friction angle shown in equation D.3, in rapidly shearing granular materials.

Takahashi used Bagnold's stress-strain rate relations in the grain inertia regime (Takahashi, 1981, Takahashi, 2007), while others have tried to explain debris flows using the macroviscous regime. The problem with both approaches is that Bagnold's equations are problematic because they only reflect the special conditions of his experiment. When Bagnold's equations are used as constitutive equations for general flow fields, it leads to contradictory results (Iverson, 1997).

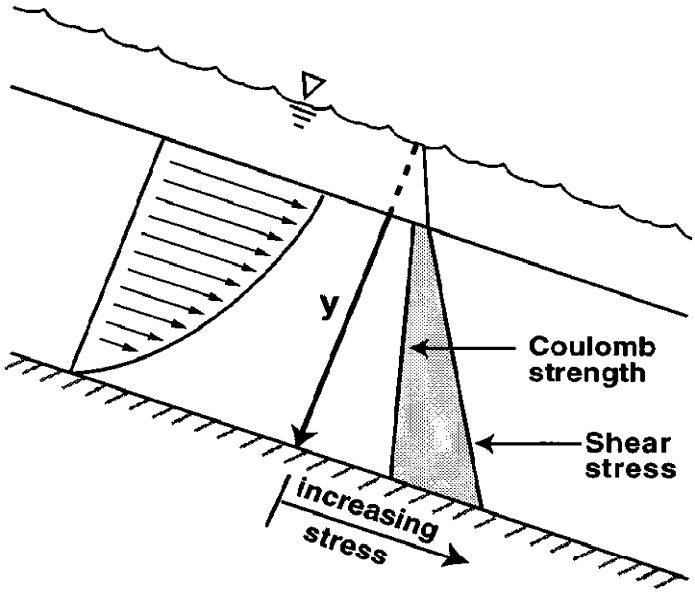

Figure E.4 Takahashi's model for mobilization of debris flows. Movement when the shear stress exceeds the coulomb strength (Iverson et al., 1997).

Takahashi assume that the Savage number, defined by the ratio of internal shear stress associated with the weight and friction of the granular mass(Iverson, 1997), moves towards infinity, that there no boundary slip, that the grains in the flow are uniformly dispersed, and that interstitial fluid sustains no excess pressure. Because of these assumptions, the stress from grain collisions mist increase linearly with depth to balance the gravitational stress(Takahashi, 1981). These assumptions mean that the shear rate distribution exclude any possibility of any debris that does not shear or are "locked", for example the plug flow (Iverson, 1997). Regions where there is no shear has been observed in actual debris flows and found using the viscoplastic model, and when the debris flow is mobilized or deposited, frictionally locked material must be present (Iverson et al., 1997).

One such contradiction can be found in a solid-fluid debris mixture flow in a channel with sides made of parallel, vertical plates. The flow is driven by longitudal body forces, for example gravity. Because of symmetry the shear rate of the flow must vanish in the centre of the flow, this must occur no matter the rheology of the material. For the Bagnold equation to be able to replicate this phenomenon, the normal and shear stress must also be zero at the centre line for both the grain inertia and the macroviscous regimes. But, if the normal and shear stress is zero at the centre line, contradicts the existence of the body force that drives the flow. When Bagnold created his experiment, granular pressure gradients from gravity or other forces, that were independent of shearing, were not present in his testing machine. Because the grains in Bagnold's experiment were neutrally buoyant they masked the effect of gravity on the grains, imposed the shear rate, and measured the stress. In an actual debris flow gravity creates a stress that increases with depth, and the shear rate responds to the increase. The granular pressure gradient can be modified by shearing by influencing the grain concentration, local granular temperature, and possibly the pore-fluid pressure. Bagnold's result were obtained using fixed concentrations and shear rates, and they are useful for understanding debris flows but they cannot be used as constitutive equations for debris flows (Iverson, 1997).

Coulomb mixture theory

Hydraulic theory models can be used to predict unsteady, nonuniform motion, which is one of debris flows obvious and easily measured characteristics. The hydraulic model uses depth-averaged equations of motion; there are some problems with these models through. Some models exclude the velocity components that are normal to the bed, and this means that they can only include solid-solid and solid-fluid interaction effects in a basic approach. The consequence of this approach is that the development of granular temperatures and nonhydrostatic pore pressure cannot be thoroughly treated by the model (Iverson, 1997).

There are several types of hydraulic models; the main difference between them is the type of slope parallel momentum balance that is used in the model. The simplest models use the kinematic wave approximation, where the steady state momentum balance is used for unsteady flow. The more elaborate models use the full momentum balance, and the difference between them is how the stresses that resist motion are represented (Iverson, 1997).

Most of the models start with the one-phase Bingham or Bagnold's Dilatant model described above, they combine the Bingham and Bagnold stresses into a resistance coefficient for bulk flow. The calibration of bulk resistance coefficients is difficult because the mechanism of momentum transport and the dissipation of energy in debris flows can differ between events. Flow resistance in the models are characterized by internal and basal friction angles, and pore fluid viscosity, which can be measured independently and does not need to be calibrated. Stress due to grain collisions are neglected by the model, while fluid effects are entered into the model by resolving the internal and basal friction(Iverson, 1997).

The coulomb mixture theory is based on the theory that debris flow do not obey any stress-strain relation, instead intergranular stresses satisfy the coulomb rule, and the variations in flow behaviour is due to varying effects of pore fluid, topography, and inertial forces (Iverson and Denlinger, 2001). The model is a generalization of the 2D grain-fluid mixture model by Iverson(Iverson, 1997), which was a generalization of the one-phase grain flow model by Savage and Hutter (Savage and Hutter, 1989, Savage and Hutter, 1991). The model gives a depth-averaged mass and momentum balance equation, which describes limited masses with changeable fluidized grain-fluid mixtures that move as an unsteady flow down a slope in 3D. The model can explain the flow from initiation and to deposition. The Savage number for natural debris flows were evaluated and the values were found to be small (Iverson and Denlinger, 2001).

The influence of Coulomb friction and grain collisions on granular flows can be found by using the Savage number, identified by Savage equation E.10. The conclusion that was drawn from this was that the Coulomb friction stress is the predominating factor in natural debris flows, rather than grain collision stress and other factors. The Savage number represent the ratio of grain collision stresses to gravitational grain contacts stress, and these stresses produce Coulomb friction (Iverson and Denlinger, 2001). Grain collisions affect flow dynamics significantly if the Savage number is above 0.1(Savage and Hutter, 1989), if the savage number is below 0,1 Coulomb friction dominates the flow (Iverson and Denlinger, 2001), this process is shown in the equation for the Savage number.

$$N_s = \frac{\rho_s \gamma^2 \delta^2}{(\rho_s - \rho_f) g H} \qquad \text{(E.10)}$$

Where ρ_s and ρ_f are the mass densities of the solid grains and pore fluid, γ is the bulk (continuum) shear rate, δ is the grain diameter, g is the gravitational acceleration, and H is the depth below the surface. The numerator represents the grain collision stress, and the denominator represent the Coulomb friction stress (Iverson and Denlinger, 2001). Iverson believes that a fixed yield strength can only occur when the flow is completely liquefied, and observations and experiments show that liquefaction, pore pressure and shear strength varies in the flow (Iverson, 2003).

The depth-averaged approach which eliminates the dependence on the coordinate normal to the bed, z. Depth averaging incorporates fundamental assumptions about stresses. The process is quite long, but it involves repeated applications of Leibniz's rule which states that mass cannot enter or leave at the free surface or the bed. The equations used in the Coulomb mixture theory to explain the behaviour of a debris flow are quite complicated and quite numerous, and will therefore not be explained here, but the equations necessitates numerical solutions (Iverson and Denlinger, 2001).

Comparison of different models

Iverson has compared the Bingham viscoplastic model (BV), Bagnold's Grain flow model (BG), and the Coulomb Grain flow with variable pore pressure model (CG) to see which of the models can explain different debris flow phenomena.

Phenomenon	Type of model		
	BV	*BG*	*CG*
Flow mobilized from rigid slope failure without changes in constitutive properties			x
Fluid pressure in flow can differ from the mean pressure and affect apparent strength or flow resistance			x
Flow can exhibit a "rigid" plug of undeforming material	X		x
Flow can lack a "rigid" plug of undeforming material		X	x
Flow is unsteady and nonuniform, with a blunt snout and tapered tail	X	X	x
Flow can transport large clasts that do not settle out	X	X	x
Flow produce grain size segregation			
Flow agitation can affect apparent strength or flow resistance		x	
Boundary slip occurs at the bed			x
Flow strengthens and halts rapidly when pore fluid is drained from beneath it			x
Deposit interior can remain weak and unable to support loads while deposit perimeter becomes rigid			x

Table E.1 Comparison of debris flow models' ability to explain physical phenomena that occur in debris flows (Iverson, 1997)

When these three models are compared, it is easy to see that almost all of the phenomena can be explained by the Coulomb mixture theory, while the other two models can explain fewer phenomenons. But the Coulomb mixture theory is 3D and the other two are a one-phase model, so the Coulomb mixture theory is much more complicated and there is a need for more input data. Many will therefore still use Bagnold's Grain flow model and the Bingham model, and they can explain debris flow motion in a better way than Newtonian models.

Undrained loading of torrent deposits

When a debris flow travels over torrent deposits, the loading is rapid. The saturated torrent deposits will therefore experience undrained loading, the concept of undrained loading was explained briefly in appendix D, but will now be explained more detailed.

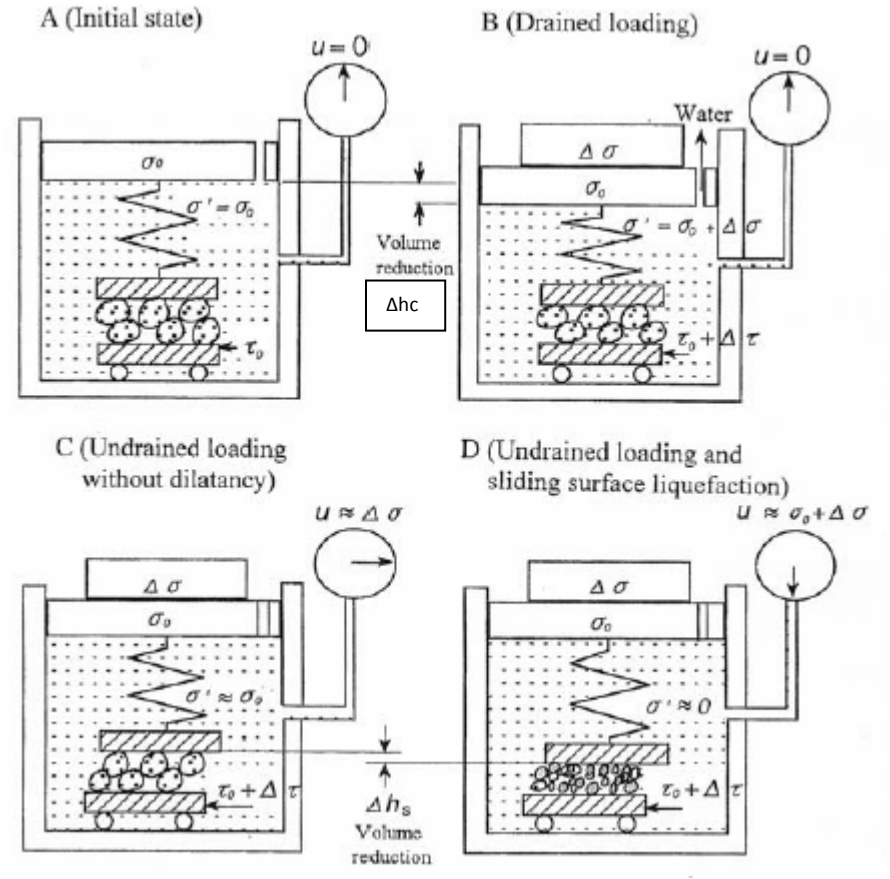

Figure E.5 Consolidation-shear model by (Sassa, 2000) found in, but slightly changed to correct error (Sassa and Wang, 2005). U is the water pressure inside the box, Δhc is the change in the consolidation model height (here represented by the spring), Δhs is the change in the shear model height, σ' is the normal stress on the spring, Δσ is the added normal stress, and Δτ is the added shear stress.

Undrained loading by normal stress was proposed by Terzaghi and Peck in 1948. The soil skeleton is represented in the model by an elastic spring in figure E.5. The elastic spring is in a box filled with water that has a small drainage hole on the side of the box. In loose sands contraction, especially shear loading is accompanied by grain crushing will result in excess pore-water pressure in the box. When trying to model undrained shearing on torrent deposits it is necessary to combine the two models in figure E.5. Peck and Terzaghi created a model that had normal stress, but no shear stress,

the pore water pressure increase due to the increase in normal stress could then be calculated (Sassa and Wang, 2005).

Normal stress and shear stress are applied at the same time to a saturated sand illustrated in figure 8.5, and there are then four different situations to explain (Sassa and Wang, 2005).

- ***Initial state*** The initial normal stress σ_0 and the initial shear stress τ_0 are applied to the sand, the pore water pressure in the box is zero.
- ***Drained loading*** The water can drain from the open valve at the top of the box and the excess pore pressure is therefore zero. The excess pore pressure is zero regardless of the presence of shear failure or grain crushing in the sand. The increase in effective normal stress is therefore equal to the added normal stress $\Delta\sigma$. The spring is compressed due to consolidation and this means that the change in the consolidation model height Δhc is < 0.
- ***Undrained loading without dilatancy*** For cases where there is no volume change in the soil during shearing, the change in shear model height Δhs and the change in the consolidation model height Δhc sum up to zero. The increase in normal stress is transferred into the pore-water pressure, due to inability of the soil skeleton to compress. The effective normal stress is equal to the initial value.
- ***Undrained loading and sliding surface liquefaction*** Due to contraction during shearing the box undergoes volume changes, the change in shear model height Δhs is greater than zero. The box is still under undrained conditions and $\Delta hs + \Delta hc = 0$, this means that $\Delta hc > 0$, and the initial effective normal stress decreases. If the soil structure collapses and there is grain crushing present in the sample, the initial normal stress can be balanced by the excess pore-water pressure ($u \cong \sigma_0 + \Delta\sigma$), and the effective normal stress is reduced to a very low value.

For drained conditions the increase in normal stress will be carried by the soil skeleton, here represented by an elastic spring, for undrained conditions and increase in normal stress will lead to an increase in the pore-water pressure where the increase in the pore-water pressure is equal to the increase in normal stress. If there is contraction in the sand-grain model due to shearing, the spring can compress further and the effective normal stress will be reduced. It is then possible to achieve full liquefaction (Sassa and Wang, 2005).

A debris flow moving in a channel or slope covered with debris is illustrated in figure E.6(a), while the stresses acting on the base of the column with weight W_0 is demonstrated in figure E.6(b). Points A, B, C, and D represent the four consolidation states in figure E.5, but the stresses are on the sliding surface due to the sliding mass. Point A represent the initial stress due to W_0. Point B represent drained conditions where no excess pore pressure were generated when the material slides over the deposits the stress point would move to point B, this is due to the adding of static normal and shear stress from the weight of the mass (ΔW) of a column of the slide. The change in normal stress and shear stresses are calculated as ($\Delta\sigma = \Delta W \cos\theta$ and $\Delta\tau = \Delta W \sin\theta$). The stress path for the situation is then from point A to point B. In general the slope angle is smaller than the internal friction angle of the soil grains, and shear failure will therefore not occur. It is possible for a short-lived impact load to temporarily bring the stress path up to the failure point F, but it will disappear quickly. The apparent friction angle (ϕ_a) during shearing can be found, and this means that if there is no cohesion in the soil the apparent friction angle is equal to the internal friction angle of the soil grains that are in motion(ϕ_m)(Sassa and Wang, 2005).

For undrained conditions with no dilatancy there was no change in the effective normal stress, and the stress path will therefore be vertical to point C. If the stress is great enough so that point C reaches the failure envelope, shear failure will occur. This is the same principle that was explained in appendix D. If there were no dilatancy in the soil after the shear failure and the shear strength after during motion would not change and remain the same as the shear strength of point C. This shear strength can be calculated and also defines the apparent friction angle for point C. For undrained loading and sliding-surface liquefaction the shear resistance decrease to a very low value at point D. The shear resistance is much smaller than the shear strength at the initial normal stress and the apparent friction angle will therefore also be very small when it is compared with the internal friction angle of the soil grains and the apparent friction angle for undrained loading with no dilatancy (Sassa and Wang, 2005).

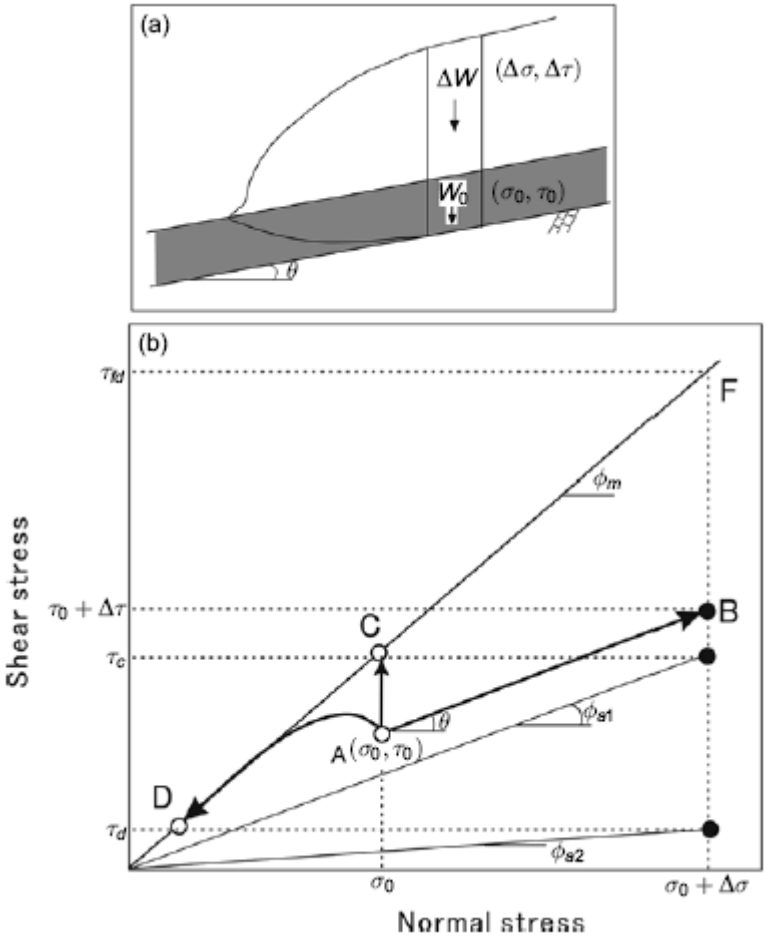

Figure E.6 Drained or undrained loading of a soil sample (Sassa and Wang, 2005).

Liquefaction and Sliding surface liquefaction

Liquefaction initiation of debris flows under undrained conditions have been observed in real life and has also been filmed in 1984 by Costa and Williams. Undrained load-controlled triaxial tests has been performed on soil samples from debris flows in Japan. The tests show that not all the tests show excess pore pressure, while other tests had a sudden liquefaction failure followed by a rapid decrease in the effective normal stress. Liquefaction occurred if the effective normal stress decreased to 1/10 of the initial stress. It was therefore possible to create a boundary between

liquefaction and non-liquefaction, shown in figure E.7. The void ratios measured in the samples were close to the boundary between liquefaction and non-liquefaction, and the samples where the torrent deposits liquefied then would rapidly transform into debris flows , this process is shown in figure E.8 (Sassa and Wang, 2005). Figure E.7 show that the void ratio needs to be high for the soil to liquefy, and that the void ratio needed for liquefaction decreases when the degree of saturation in the soil increases. Since a void ration of 0 is a completely dense soil without any voids and a void ratio of 1 are only voids figure E.7 shows that the soil needs to be loose for the soil to liquefy, the denser soil samples do not liquefy, unless the degree of saturation is sufficiently increased.

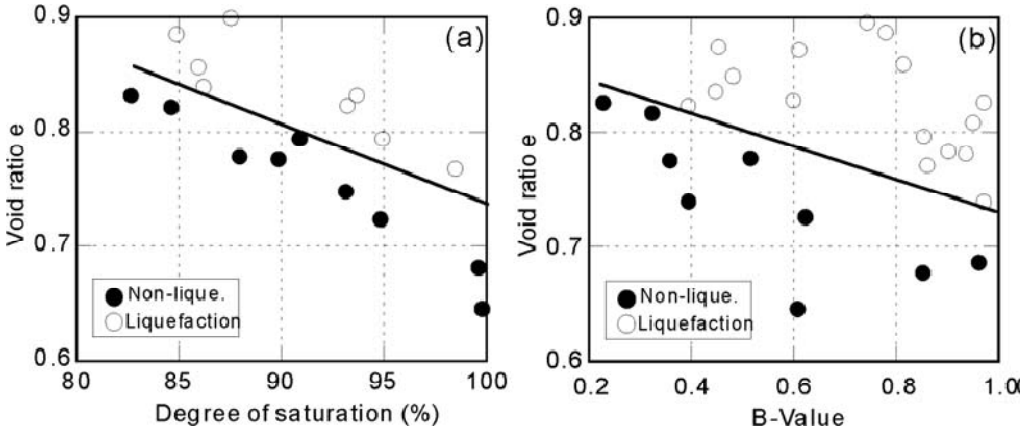

Figure E.7 triggering liquefaction boundaries for deposits from Mount Usu (Sassa and Wang, 2005). The boundary is defined by the void ratio, the degree of saturation in the soil which is expressed by the pore pressure coefficient B defined by Skempton in 1954.

Figure E.8 show the initiation of a debris flow, part a and b have torrent deposits that has a loose and unstable structure, and the torrent deposits can therefore collapse under rapid loading, by for example a debris flow moving over the deposits. The debris flow material is therefore seated on a liquefied layer. Part c and d show when the torrent deposits start to flow, this causes liquefaction in front of the flow and increases the volume of the flow. Liquefaction can occur in granular soils when the soil structure collapses, this collapse causes a reduction in the volume of the soil and creates an excess pore-water pressure in the soil. Sliding-surface liquefaction has been found, these are cases where it is the sliding that trigger liquefaction not liquefaction causing debris flows and mobile debris flows were created. Liquefaction can only take place in soils that has a very loose meta-stable structure, but sliding-surface liquefaction can occur in dense soils, all that is needed is that grain crushing and a volume reduction takes place in the soil due to the overburden pressure. When a debris flow mass slides over torrent deposits or on a slope either drained or undrained loading can occur, which means that either liquefaction or sliding-surface liquefaction can occur in the soil (Sassa and Wang, 2005). Sliding-surface liquefaction due to crushing of the soil grains results in rapid movement and a long runout distance for the debris flow, high pore pressure is generated because of shearing along the sliding surface (Wang and Sassa, 2003).

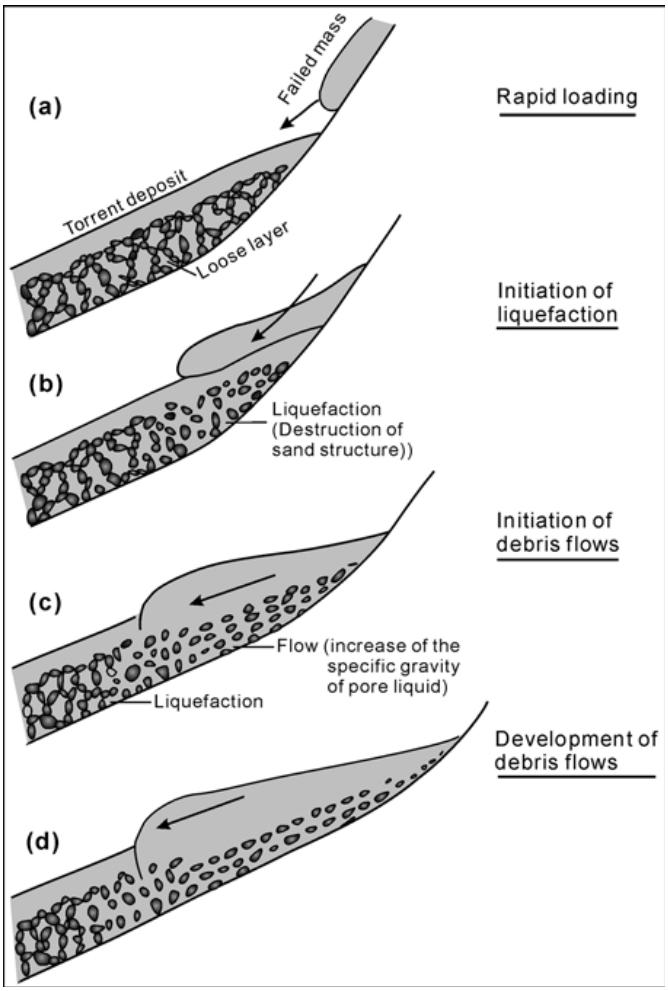

Figure E.8 Initiation of a debris flow due to liquefaction of the torrent bed materials (Sassa, 1985) found in (Sassa and Wang, 2005).

Several scientists believe that flow slides are slope movement that have been induced by the liquefaction of soil, liquefaction often occurs in loose saturated granular soils for example sands and as previously explained is due to the generation of excess pore pressure in the sand. Complete saturation of a soil is rare in steep slopes, and they are normally unsaturated because of a high permeability which do not allow the formation of an aquifer. These slopes have a slope angle that is steeper than that of the friction angle due to cohesion in the slope because of suction. Theory therefore tells us that in steep slopes liquefaction is not a common triggering mechanism for flow slides on steep slopes, but excess pore pressure as a triggering mechanism for flow-like debris flows has been found in actual cases and there must therefore be something wrong with the theory. The debris flows are triggered when precipitation increase the water content in the soil, this causes the suction in the slope to decrease until the slope fails. The soil can either be fully saturated or unsaturated at the point of failure depending on the slope angle and the shear strength of the soil (Picarelli, 2009).

For an infinite slope, as explained in chapter 1.7.1, for a soil that is uniform and cohesionless the soil can only be fully saturated at the point of failure when the slope angle is less or equal to the friction angle. Excess for pressure can be built up in the soil if the degree of saturation in the soil is high enough at the point of failure and that the rupture or the movement after failure is rapid enough (Picarelli, 2009). It is therefore possible to divide the soils into deposits that can liquefy and deposits

that cannot liquefy after failure of the slope. If the slope is steep failure of the slope will take place before the slope can become fully saturated, and the debris flow will therefore start as a slide or a debris avalanche instead of a flow slide. The slide can later transform into a debris flow. The soil cannot liquefy unless the excess pore water generation mechanism is induced by progressive failure in the soil downslope as explained earlier in this chapter(Picarelli, 2009).

Excess pore pressure can be generated by other mechanisms , for example by a collapse in the volume because of a decrease in suction, by impacts, or by progressive failure. For volumetric collapse and impacts the excess pore pressure build up is the reason for the slope failure, while progressive failure is normally a process in drained conditions that in theory should also be possible for undrained conditions. Progressive failure begins in the part of the slope that has the highest stresses and spreads throughout the slope because of the drop in strength due to induced plastic strains that redistribute the stress in the slope, and this can generate excess pore pressure but the excess pore pressure is not the reason for the soil to fail (Picarelli, 2009). Liquefaction can trigger a mechanism of complete fluidization (Iverson, 1997), which means that the material can move without any resistance at the base, this increase the velocity by a tens of meters per second.

Large scale flume experiments show that there is a delay in the generation of excess pore pressure in different parts of a slope when the flow moves down the slope. If the slope is concave the progressive failure will start in the steepest parts and positive excess pore pressure will be generated down slope as the flow moves. If there is retrogressive progressive failure in the slope a negative excess pore pressure will be generated. For debris flows that occur in soils that are more fine grained the excess pore pressure will take much longer to drain and the consolidation process is very low because of the low permeability of the soil, this means that for fine-grained flows the velocities will be higher. The mechanisms that causes excess pore pressure and flow-like movements in fine-grained soils are that the debris that is removed from the scar must accumulate rapidly, which means that excess pore pressure can build up in the debris, the stress in the soil increases because of surges moving in the flow, and finally the stress is redistributed in the debris flow because the track narrows or other local topography changes. Seismic loading can also be a mechanism that can induce excess pore pressure in a soil (Picarelli, 2009).

Debris flow-triggered debris flow examples

Wang and Sassa did flume experiments to study rainfall induced debris flows and the effects of grain size and fine-grained material content on the pore pressure generation and the movement of the debris flow. They showed that the debris flow movement depended on the soil, flow slides were initiated for samples that were more fine-grained, but not for the one sample that was fine silica sand (S7) with a mean grain size of 0.13mm. All other samples had a mean grain size that was less than 0.05mm. The movement of the debris flow was affected by the initial density of the soil, the failure process is illustrated by figure E.9 (Wang and Sassa, 2003).

The failure modes in figure E.9 was divided into four time periods (Wang and Sassa, 2003):

- **Wetting**: sprinkling of water is completed and the water flows from the surface of the sample down towards the base. The wetting front is parallel to the base. Normal displacement was visible in the test on S7 of failure type A, and in the test of extremely loose sample S8 of failure type C, there was no visible displacement in any other tests.

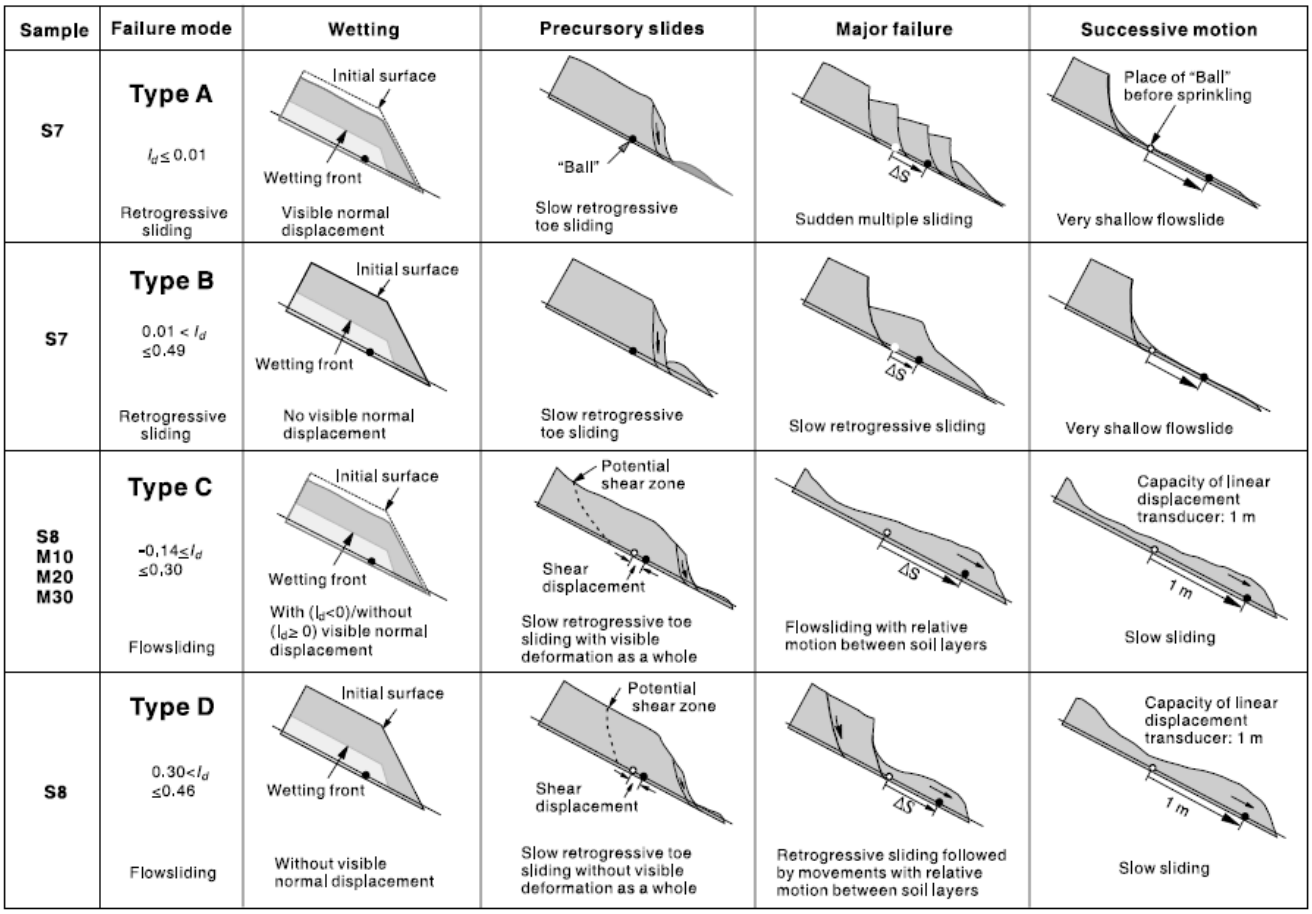

Figure E.9 Failure modes for five different soil samples after a flume test (Wang and Sassa, 2003). Id is the density index and has the following values. Extremely loose, Id<0; very loose, 0 ≤ id< 0,15; loose, 0,15 ≤ id < 0,35; medium, 0,35 ≤ id < 0,65; dense, 0,65 ≤ id < 0.85; very dense, 0.85 ≤ id ≤ 1. Rainfall intensity is 1,7mm/min and the slope angle was constant at 30°.

- **Precursory slides:** The wetting front has reached the base, and the degree of saturation in the soil was rising. Retrogressive compound shallow sliding occurred in the toe portion of the slope for all tests. After the material slid from the toe it became very thin and flowed down the slope. There was shear deformation within the entire layer for Type C, but no visible deformation in any of the other types.
- **Major failure:** Major failure occurred after the retrogressive compound shallow sliding. The material displaced a distance ΔS from its original position and then it stopped. The sliding behaviour of the four types are clearly different, as shown in figure E.9. For type A and B there was only retrogressive sliding, while type C and D had flow slide motion. For type C the surface movement were faster than at the base of the flume, which means that there was relative motion inside the failed soil at different depth which is a characteristic of flows. Type D had slow retrogressive sliding. One block failed and slid down the slope, and then the next block failed and pushed the previously failed block in front of itself. Two or three blocks were created and they combined in the final stages of the period and moved as one large block.
- **Successive movement:** After the major failure, if the material was under continuous sprinkling of water the soil could start to slowly move again downslope. For type A and B the soil was so thin that the displacement was not possible to measure with the instruments.

Type C and D was measured as 1 m at the maximum capacity due to the rated capacity of the measuring device of 100cm.

The high pore pressure was found to build up after the initiation of failure, and this can clearly be seen in figure E.10 that shows the build up of pore pressure in a S8 sample test. The failure of the soil begins before the rapid increase in pore pressure, the increase in pore pressure before failure is probably due to the rise of the water surface in the soil. Excess pore pressure was generated after failure and the pore pressure in the soil increased swiftly. The pore pressure is then shown to fall and this was probably due to the soil moving down the slope which resulted in a decrease in the mass height that decreased the pore pressure (Wang and Sassa, 2003).

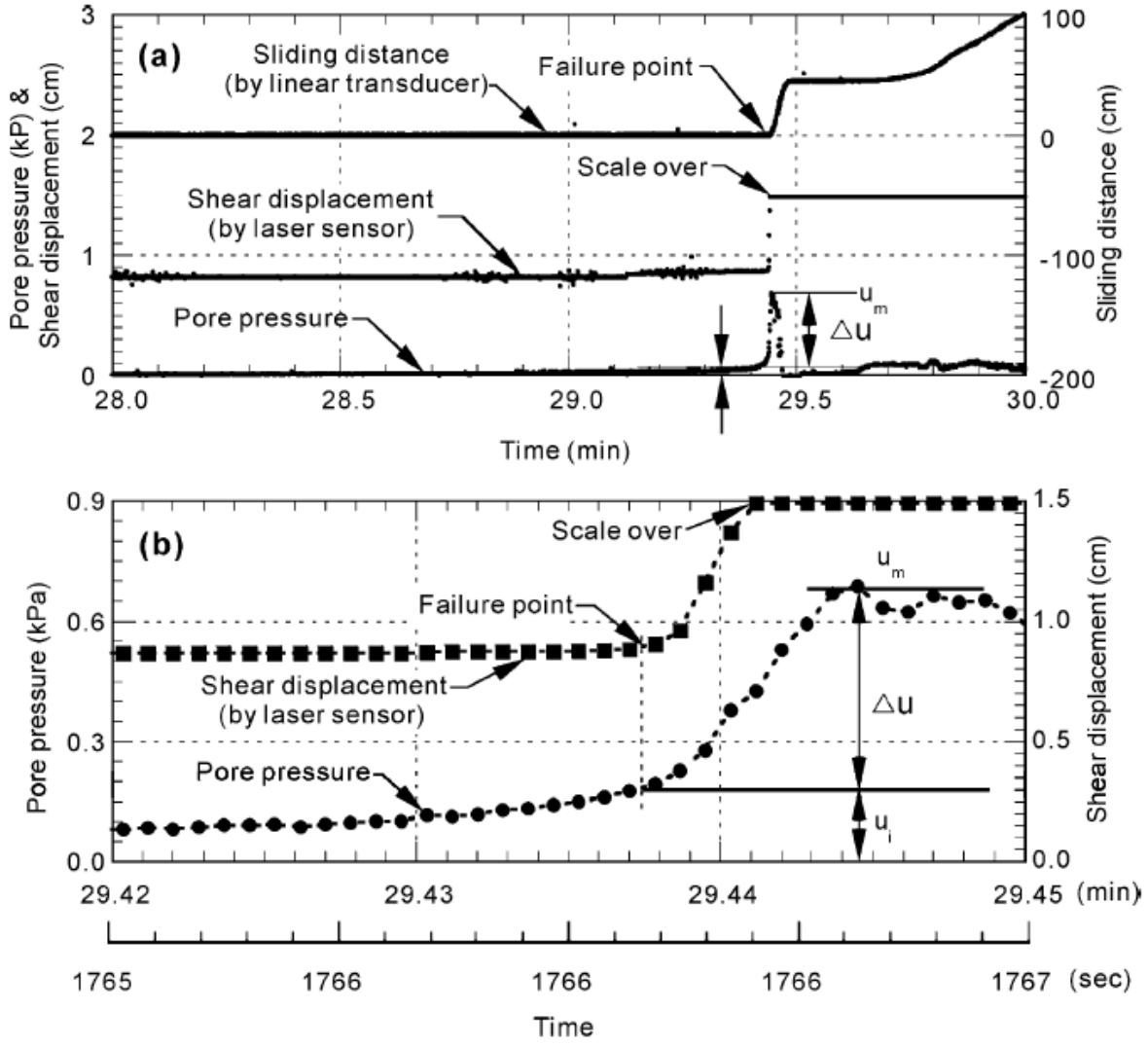

Figure E.10 Pore pressure build up, shear displacement, and sliding distance for test $S8_{11.8}$. The capacities of the linear transducer to measure displacement is 100cm while the capacity for the laser is 15mm, displacements that were greater than these numbers could not be determined by the equipment. A, Pore pressure and sliding distance before and after failure, b, an enlargement of a that shows the exact time of failure in the soil (Wang and Sassa, 2003).

The initial density and thickness of the soil layer is important for the generation of pore-water pressure as seen in figure E.10. There is an optimal density for when the pore-pressure build up after failure Δu reaches its maximum and it has been plotted for samples S7 and S8. Δu increases with increased density index up to the optimal density index before it decreases after with increased

density index. For sample S7 the ideal density index is approximately -0,03 and for S8 it is 0,19, the curve for S7 is much less steep and the pore pressure built up after failure will therefore not vary as much with the density index as for sample S8 which does not create any pore pressure after failure for density indexes below -0,17 and above 0,5. The pore pressure built up in sample S8 was greater than the pore pressure in sample S7, this indicates that it was easier to build up higher pore pressures in finer soils, and could be a result of the higher permeability in sample S7. (Wang and Sassa, 2003). The pore pressure build up depends on the rate of debris flow motion, soil deformation, and the permeability of the soil. Soil which has a higher permeability will have a faster dissipation of pore pressure, and therefore a lower pore pressure generated in the soil if the velocity for the debris flow mass is the same (Iverson et al., 1997).

The reasons for the differences in failure modes for samples S7 and S8 are that the pore pressure build-up in S7 is smaller than for sample S8, and the pore pressure that is generated in S7 dissipates very quickly because of the higher permeability in sample S7, and finally sample S8 is more likely to float during movement than sample S7 because sample S8 has smaller grains. Increase in pore pressure is due to the floating of grains in the fluid, with the weight of the suspended grains being supported by the fluid. If every grain in the soil is floating in water the soil is completely liquefied. The finer the grains are the easier they are to float, this means that the samples with the highest percentage of fine-grained material should have more grains that float and therefore also a higher pore pressure. The dissipation time of the pore pressure in the samples increased with increased fine-grained material percentage in the sample. For sample S7 which is the coarsest grained sample the dissipation took 27 seconds, while for the most fine-grained sample M30 the dissipation took approximately 24 hours. This show how important fine-grained material is in the dissipation of pore pressure in a soil, and how the generated pore pressure is maintained in the material during flow and after deposition (Wang and Sassa, 2003).

Appendix F GPS data from august 2011.

204	**18-AUG-11 3:43:50AM**	**Skredløp**	**N61 41.359 E9 41.500**	**439 m**
205	18-AUG-11 3:44:23AM	Skredløp	N61 41.374 E9 41.486	441 m
206	18-AUG-11 3:45:13AM	Skredløp	N61 41.392 E9 41.485	447 m
207	18-AUG-11 3:45:38AM	Skredløp	N61 41.399 E9 41.476	452 m
208	18-AUG-11 3:46:06AM	Skredløp	N61 41.387 E9 41.463	455 m
209	18-AUG-11 3:47:06AM	Skredløp	N61 41.371 E9 41.442	462 m
210	18-AUG-11 3:57:02AM	Skredløp	N61 41.367 E9 41.427	463 m
211	18-AUG-11 4:04:55AM	Skredløp	N61 41.363 E9 41.408	468 m
212	18-AUG-11 4:11:08AM	Skredløp	N61 41.365 E9 41.394	477 m
213	18-AUG-11 4:11:13AM	Prøve 1	N61 41.364 E9 41.396	477 m
214	18-AUG-11 4:43:47AM	Skredløp	N61 41.396 E9 41.313	516 m
215	18-AUG-11 4:46:53AM	Skredløp	N61 41.398 E9 41.288	533 m
216			N61 41.398 E9 41.288	533 m
217	18-AUG-11 4:47:17AM	Skredløp	N61 41.406 E9 41.279	532 m
218	18-AUG-11 4:59:57AM	Skredløp	N61 41.405 E9 41.214	565 m
219	18-AUG-11 5:04:59AM	Skredløp	N61 41.401 E9 41.191	585 m
220	18-AUG-11 5:36:25AM	Skredløp	N61 41.437 E9 41.108	647 m
221	18-AUG-11 5:41:36AM	Løsneområde	N61 41.430 E9 41.044	674 m
222	18-AUG-11 6:06:45AM	Øvre løsneområde	N61 41.436 E9 41.007	696 m
223	18-AUG-11 6:35:34AM	Løsneområde	N61 41.457 E9 41.018	695 m
224	18-AUG-11 7:01:34AM	Løsneområde	N61 41.425 E9 41.047	672 m
225	18-AUG-11 7:02:51AM	Skredløp	N61 41.423 E9 41.046	673 m
226	18-AUG-11 7:05:37AM	Løsneområde	N61 41.421 E9 41.018	685 m
227	18-AUG-11 7:32:01AM	Blokk i skredløp	N61 41.416 E9 41.066	662 m

Table F.1 GPS measurements taken from mainly the track of landslide five on the 18th of august, 2011 (Bargel, 2011).

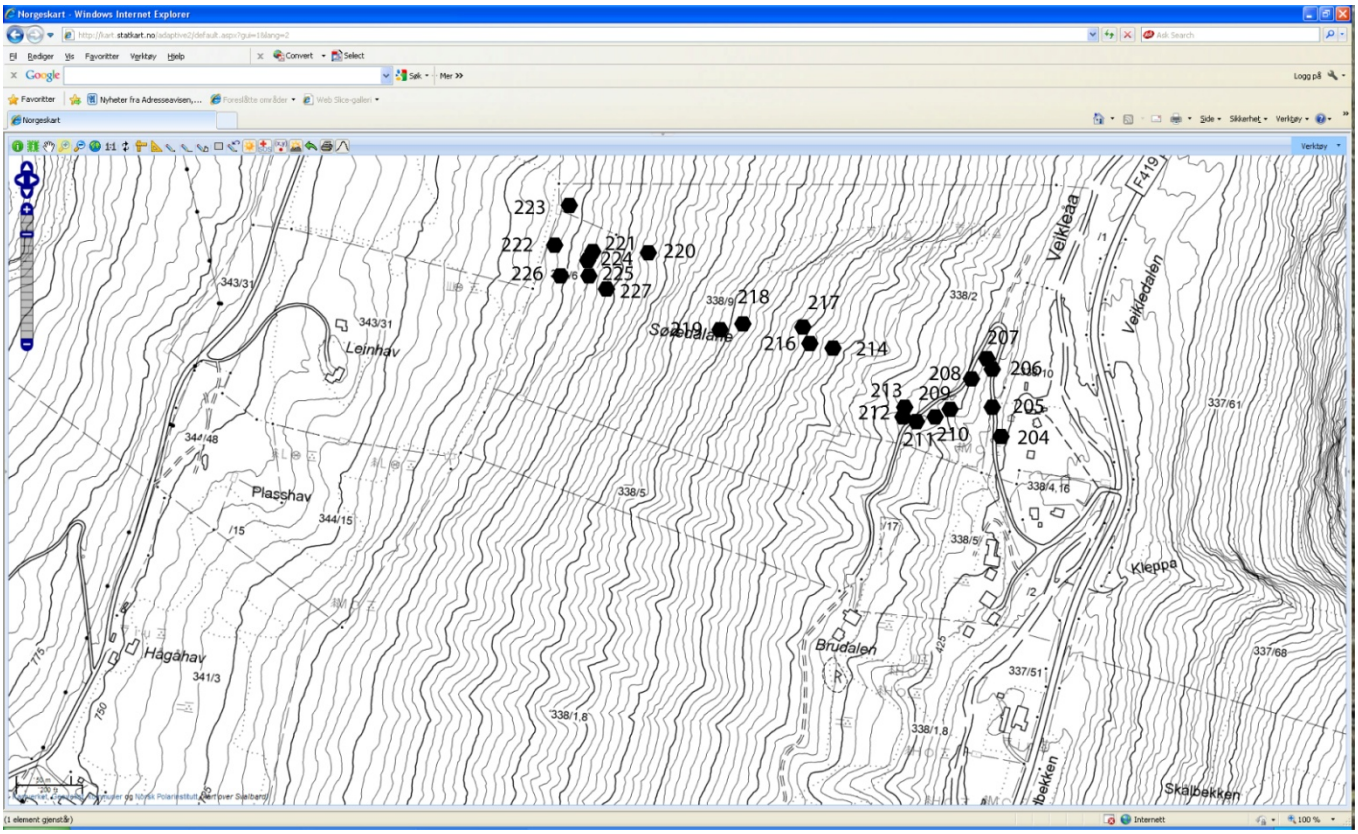

Figure F.1 GPS measurements from table F.1 presented in a map of the study area (Bargel, 2011).